HANDBOOK ON AEROSOLS

ATOMIC ENERGY COMMISSION

HANDBOOK ON *Aerosols*

Chapters from the SUMMARY TECHNICAL REPORT OF DIVISION 10, NATIONAL DEFENSE RESEARCH COMMITTEE, *selected and published by the* UNITED STATES ATOMIC ENERGY COMMISSION

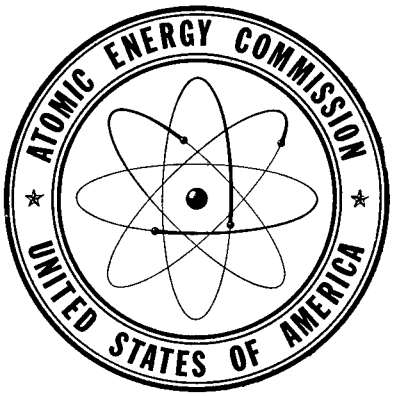

Washington, D C., 1950

A NOTE ON THE PREPARATION OF THIS VOLUME

In anticipation of possible declassification and wider publication of the Summary Technical Reports of the National Defense Research Committee, the Office of Scientific Research and Development secured reproduction proofs of all the Summary Technical Reports. A set of reproduction proofs for the report of Division 10, NDRC, was made available to the Atomic Energy Commission for use in its program of issuing and stimulating the publication of technical reports on the problem of radioactive wastes.

Since some of the material in the original volume had no bearing on this problem, a selection of relevant pages was made from the reproduction proofs. The pages selected were renumbered consecutively and grouped in chapters which were also renumbered consecutively. All references in the bibliographies which follow each chapter, which are not relevant to the material selected, were eliminated. Plates for printing the volume were then prepared photographically from this material.

Because of this method of publication, it has not been feasible to change the numbering of the chapter sections, and the reader will notice that these sections still retain the original numbers of the chapters from which they were selected. Further, although we have attempted, as far as practicable, to eliminate all references in the text to omitted materials and to numbers which were not used, some such references may still be found.

The foresight of the Office of Scientific Research and Development in arranging for the printing of reproduction proofs enabled the Atomic Energy Commission to save a considerable amount of time and money in the preparation and publication of this volume.

PREFACE

MANY OF THE PROBLEMS in the atomic energy program involve the handling of small particles. Some of the operations produce radioactive wastes in the form of dust, fume, and mist which would create hazards if considerable quantities were released in or near the installations. Methods of treating these materials to prevent the contamination of the atmosphere have been developed, but much more needs to be learned about finely divided matter suspended in gases and the practical application of this field of science to industrial problems. The problem of waste disposal is not unique to the atomic energy industry. Many large industries must dispose of obnoxious gases and aerosols created in the course of their operations. This industry differs from others, however, in that permitted tolerances must be lower when the waste materials are radioactive. Careful monitoring must be maintained at all times to cope with accidental releases, and operations can be carried on only with the full realization of the effect of the meteorological conditions in the dispersion of stack discharges.

Realizing the importance of these problems, in June 1948 the AEC Division of Engineering appointed in Advisory Stack Gas Problem Working Group under the chairmanship of Dr. Abel Wolman, of Johns Hopkins University. After studying the conditions in the various installations, the Group recommended that special research investigations be initiated in certain fields with the objectives of improving existing methods and developing new equipment for dealing with the radioactive wastes. It is also recommended that, wherever possible, information on aerosols be compiled and published so that it would be readily available to workers in the field.

Some of the greatest advances in the science of aerosols were made during the recent war, when problems on the formation and behavior of smoke clouds, analysis, assessment of particle size, protection against toxic agents, and the dispersal of insecticides had important military implications. Much of the research work was done under the auspices of the National Defense Research Committee. The work was started in section L–1 (later sec. B–5), which was organized during the summer of 1940 under the chairmanship of Prof. W. H. Rodebush, of the University of Illinois. When the Office of Scientific Research and Development was reorganized in December 1942, the work on aerosols was incorporated in division 10 of NDRC under the direction of Prof. W. Albert Noyes, Jr., of the University of Rochester. After the war, a technical report was prepared by division 10, summarizing the information that had been gathered for the use of the military agencies as a guide for further research. At the request of the Atomic Energy Commission, portions of this report have now been declassified and are being published by the Commission so that the methods developed may find their greatest use. It is gratifying to know that this work, which occupied the attention of many men for several years, will now be available to all scientists.

In a field of science which has been as active as this, there have, of course, been many developments, even in the few years since the war, especially in the aspects related to air pollution. The reader will find that this volume contains basic discussions and descriptions of theoretical and experimental importance in the field of aerosols. To supplement the information contained in this volume, the reader may refer to two recent symposia of the American Chemical Society—one on "Aerosols," which was published in Chemical Reviews in April 1949, and the other on "Atmospheric Contamination and Purification" which was published in Industrial and Engineering Chemistry in November 1949. An excellent review of the theory and performance of industrial equipment for the removal of dust and fumes from gases appears in the Third Edition of Perry's "Chemical Engineers' Handbook," published in March 1950 by McGraw-Hill Book Co.

H. F. JOHNSTONE
Stack Gas Working Group
Atomic Energy Commission

TABLE OF CONTENTS

Chapter 1

THE ADSORPTION WAVE

By *Irving M. Klotz*

8.1 INTRODUCTION

THE GENERAL OBJECT in the study of the adsorption wave has been to obtain an understanding of the various factors which determine the variation in concentration of a toxic gas effluent from a bed of charcoal. The study of the adsorption wave includes the consideration, from an experimental and theoretical point of view, of the distribution of toxic gas throughout a bed both on the adsorbent and in the air above the adsorbent.

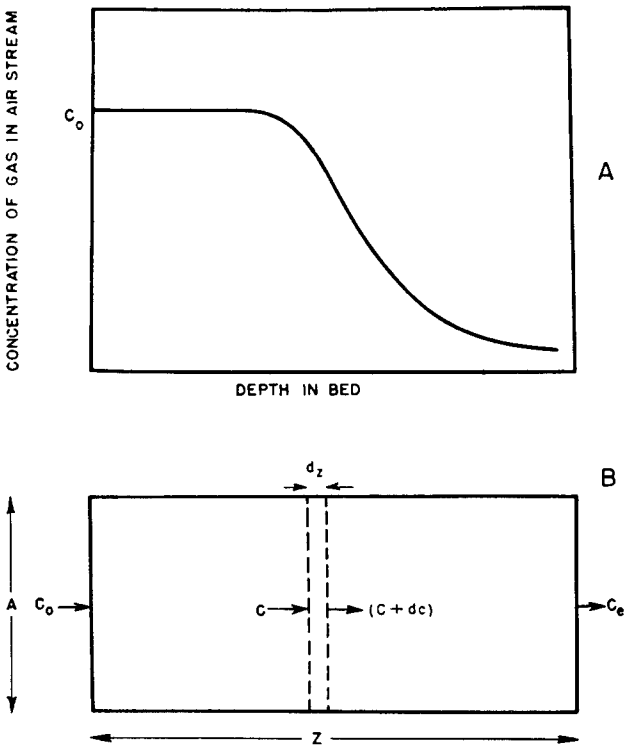

FIGURE 1. A. Distribution curve for the concentration of air above various points in the bed of adsorbent. B. Flow of gas through an adsorbent.

A typical distribution curve showing the concentration of gas in the air above various points in the bed of adsorbent is shown in Figure 1A. The curve for the concentrations which would be in equilibrium with the adsorbed gas at various points in the bed would be similar in shape but displaced slightly to the left. The term *adsorption wave* is generally applied to the movement of these distribution curves (to the right in Figure 1A) during the continuous passage of gas-laden air through the bed of adsorbents.

A complete mathematical description of the wave would effect a number of important consequences. It would be possible to predict the performance of a particular canister from a minimum of experimental data and without exhaustive tests on the canister itself. It would also be possible to devise the best test procedures from which to obtain the information necessary for the prediction and evaluation of canister behavior. A complete understanding of the adsorption wave would lead also to the design of the most efficient type of canister. Equally important would be the elucidation of the mechanism of the adsorption process for various gases on different types of charcoal. Such an understanding would suggest additional treatments for the improvement of the adsorbent and would also indicate when the natural limit to such improvement had been attained.

The problem of the adsorption wave has not been solved in its most general form, primarily because of the prodigious mathematical difficulties entailed. In connection with a similar problem of correlating the performance of small-scale and large-scale reactors in chemical engineering processes, the opinion has been expressed [6] that the correlation is impossible to attain in a truly rigorous manner. Nevertheless, a number of simplified special cases of the adsorption wave have been considered and, with these results as guides, it has been possible to develop several semi-empirical approaches to the problems of performance and mechanism of reaction.

It is recognized generally that the removal of a toxic gas from air by a porous adsorbent may involve one or more of the following steps:

1. Diffusion (mass transfer) of the gas from the air to the gross surface of the granule.
2. Diffusion of the molecules of gas into (or along the surface of) the large pores of the adsorbing particle.
3. Adsorption of the molecules on the interior surface of the granule.
4. Chemical reaction between the adsorbed gas and the charcoal or adsorbed oxygen, water, or impregnant.

The relative importance of each of these four steps may vary widely with the particular conditions under which the removal is taking place. The rate of mass transfer is influenced strongly by the flow rate of the gas stream, by the diffusion coefficient of the gas, and by the particle size of the adsorbent, but is relatively unaffected by temperature. The importance of diffusion in the pores is determined by such factors as the particle size, the structural characteristics of the pores, certain diffusional properties of the system, and the rate of reaction at the internal surface. The speed of adsorption at the interface depends on the nature and extent of the surface as well as on the activation energy for the adsorption of the particular gas under consideration. Chemical reaction is also determined by the properties of the surface, but much more specific effects will be obtained than in adsorption. Since large activation energies may be expected in steps (3) and (4), these processes will be highly sensitive to temperature.

Usually, all four steps in the removal process may proceed with rates of approximately the same magnitude, and hence a problem of extreme mathematical difficulty is presented. On the other hand, in many situations one particular step may be much slower than the others, and hence it may be considered the rate-controlling process. For a single rate-controlling process, a number of mathematical approaches have been developed. A few attempts have also been made to treat situations with more than one rate-controlling step, and for certain special circumstances, partial success has been attained.

8.2 THEORIES PREDICTING EFFLUENT CONCENTRATION AS A FUNCTION OF TIME

The ultimate aim of the mathematical analysis is an expression for the dependence of the effluent concentration on time. Even without such an expression, however, some qualitative description of the shape of an effluent-time curve can be given. Figure 2 illustrates a number of interesting cases. If the reaction on the charcoal were instantaneous and if the adsorbent were infinitely fine-grained, none of the adsorbable gas would penetrate until some time t, when the charcoal would be saturated, and then the gas would penetrate at full influent concentration.

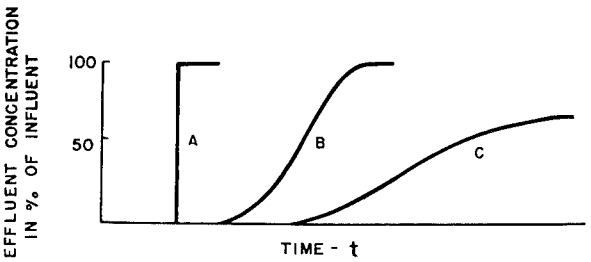

FIGURE 2. Transmission of a gas by an adsorbent.

Such an adsorbent would exhibit a transmission curve such as A in Figure 2. On the other hand, if the reaction is not instantaneous, a curve such as B would be exhibited. This curve would be symmetrical only for certain simple rates of adsorption. In addition to these two examples, cases may be encountered (for example, in the removal of carbon monoxide) where the charcoal, or its impregnant, acts as catalyst for a reaction involving the toxic gas. As a result, the effluent-concentration curve C may rise very slowly; and if the catalyst remains at least partially unpoisoned, the transmission of gas may never reach the full influent value. It is also conceivable, although no such case has been yet encountered, that the rate of catalysis may be very high compared to the rate of supply of gas. In such circumstances the transmission curve would be the time axis, that is, none of the gas would penetrate.

8.2.1 Theories in Which One Step is Rate-Controlling

THE GENERAL DIFFERENTIAL EQUATION

Consider a stream of gas and air flowing through a bed of adsorbent as indicated in Figure 1B. Each layer of the adsorbent removes a portion of the gas from the air, and hence the concentration of gas drops from an influent value of c_0 to an effluent value of c_e. A cross section of infinitesimal thickness dz will reduce the concentration from c to $c + dc$

(dc is negative). From the principle of conservation of mass it follows that:

Quantity of gas entering = quantity of gas picked up by charcoal + quantity of gas leaving. (1)

The quantity of gas entering the infinitesimal section of bed will be equal to the concentration c times the volume rate of flow L times the interval of flow dt:

$$\text{Quantity of gas entering} = cLdt. \tag{2}$$

The amount of gas picked up by the charcoal will be given by the rate of pickup per unit volume $\partial n/\partial t$ times the volume of the infinitesimal section of the bed (area $A \times$ depth), multiplied by the interval of exposure:

$$\text{Quantity picked up by the charcoal} = \frac{\partial n}{\partial t}(Adz)dt. \tag{3}$$

The quantity of gas leaving the section dz will be given by:

$$\text{Quantity leaving} = (c + dc)Ldt. \tag{4}$$

Setting up the equality demanded by the conservation principle, one obtains:

$$cLdt = \frac{\partial n}{\partial t}(Adz)dt + (c + dc)Ldt, \tag{5}$$

which can be rearranged to give:

$$-dc = \frac{A}{L}\frac{\partial n}{\partial t}dz. \tag{6}$$

Since c is a function of the variables z and t, the total differential is:

$$dc = \left(\frac{\partial c}{\partial z}\right)_t dz + \left(\frac{\partial c}{\partial t}\right)_z dt, \tag{7}$$

and since

$$\partial z/\partial t = V \tag{8}$$

and

$$L = VA\alpha \tag{9}$$

where V is the linear velocity through the interstices between the particles of the adsorbent, and α is the porosity (that is, the fraction of voids per unit gross volume of bed) one obtains:

$$-\left(\frac{\partial c}{\partial z}dz + \frac{\partial c}{\partial t}dt\right) = \frac{1}{\alpha V}\frac{\partial n}{\partial t}dz \tag{10}$$

which can be rearranged to give

$$-\frac{1}{\alpha}\frac{\partial n}{\partial t} = \frac{\partial c}{\partial t} + V\frac{\partial c}{\partial z} \tag{11}$$

It is implicitly assumed in the derivation of this equation that the concentration of gas is small and that diffusion in the direction of flow is negligible.

The solution to equation (11) depends on the mathematical relation one assumes for $\partial n/\partial t$, the local rate of removal of the toxic gas by the granules. The particular mathematical form to be chosen depends on the mechanism of the removal process. No matter which mechanism is visualized, the local rate of removal would be dependent in general on the following variables:

1. The nature of the adsorbent.
2. The nature of the gas to be removed.
3. The geometrical state of the adsorbent.
4. The temperature.
5. The local concentration of the toxic gas, as well as of other gases in the air.
6. The relative amount of the toxic and other gases already adsorbed by the granules.
7. The velocity of the gas-air stream.

In all cases which have been considered, it has been assumed that the first four variables are maintained constant, but that $\partial n/\partial t$ may depend on one or more of the remaining three.

Diffusion as the Rate-Controlling Step

Case A. In some cases, one may encounter a gas which has no back pressure on charcoal, but which ceases to be removed by the granules when the moles of gas on the granules n approaches N_0, the saturation capacity of a unit gross volume of adsorbent for the toxic gas. Under these conditions the local rate of removal would be given by the relation:

$$\frac{1}{\alpha}\frac{\partial n}{\partial t} = \frac{Fac}{\alpha\rho}, \tag{12}$$

where F is the mass transfer coefficient, a the superficial surface per unit volume of granules, and ρ the density of the air-gas mixture.

The solution of the differential equation may be resolved into two cases. For all times up to t_0 when $n = N_0$ at the entrance face, the concentration at a given point in the bed is given by the equation:

$$\frac{c}{c_0} = \exp\left[-\frac{Fa}{\alpha\rho}\frac{z}{V}\right]. \tag{13}$$

For times greater than t_0, the following relation holds:

$$\frac{c}{c_0} = \exp\left[-\frac{Fa}{\alpha\rho}\left(\frac{z}{V} - \frac{c_0 t}{N_0}\right) - 1\right]. \tag{14}$$

Case B. If a gas is adsorbed reversibly on charcoal, the equation obtained for c/c_0 depends on the character of the adsorption isotherm. One of the simplest

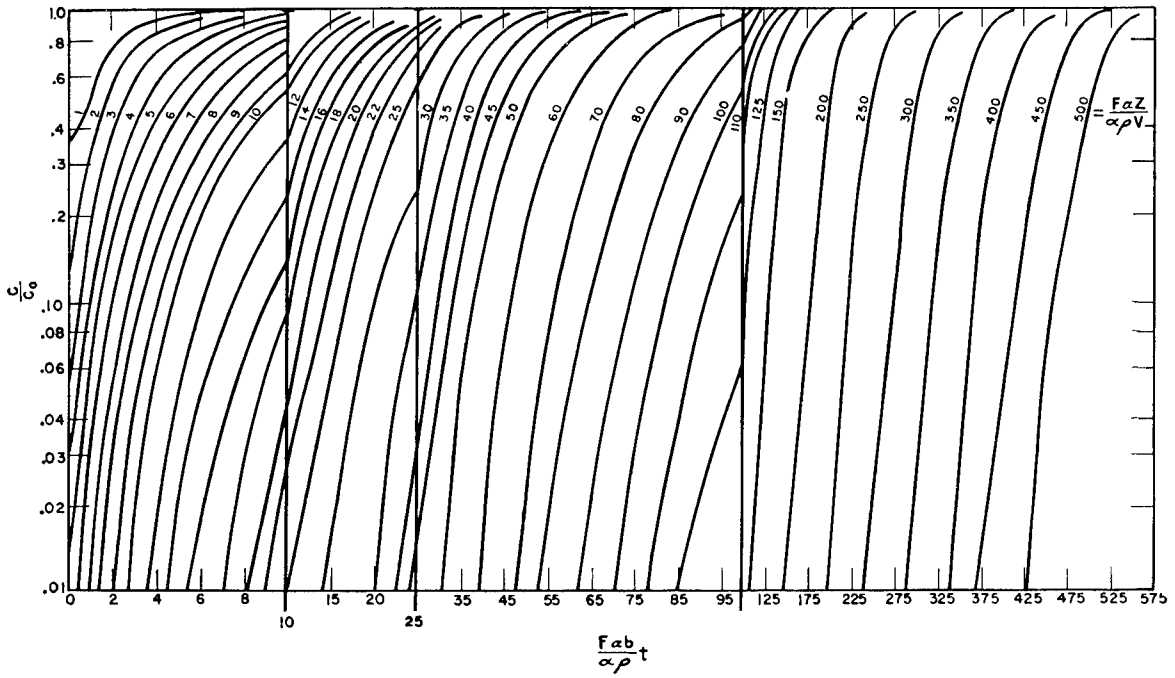

FIGURE 3. Relation of gas unremoved to time and position.

cases that has been considered is that of the linear isotherm, for which

$$c^* = bn \tag{15}$$

where c^* is the concentration of the gas in air stream at a given point in the bed in equilibrium with the charcoal at that point, and b is a constant. With a linear isotherm governing the back pressure of the gas, the equation for the local rate of removal becomes:

$$\frac{1}{\alpha}\frac{\partial n}{\partial t} = \frac{Fa}{\alpha\rho}(c - c^*)\,. \tag{16}$$

The solutions of the differential equations, for the boundary conditions encountered in charcoal, are well known because completely analogous equations have been encountered in the problem of heat exchange in granular beds. Analytical expressions, in terms of Bessel functions, for the solutions are cumbersome to handle, and hence the results are given best in the form of reference curves of c/c_0 as a function of the important variables. The curves worked out by Furnas [14] are very incomplete in regions of low concentrations, the regions of great interest in work on gas transmission. Consequently a semi-logarithmic plot taken from a report by Hougen and Dodge [17] is given in Figure 3. For values of c/c_0 below 0.01 see reference 10.

Case C. Most gases do not exhibit a linear isotherm on charcoal. A better approximation is the Langmuir isotherm which may be expanded in a power series of the form

$$c^* = \frac{K}{N_0}n + \frac{K}{N_0^2}n^2 + \cdots \tag{17}$$

where K is a constant. Using the first two terms in equation (17) as a parabolic approximation to the isotherm, one may substitute for c^* in equation (16). The solutions of the resultant equations in terms of standard graphical procedures have been worked out.[10]

ADSORPTION OR REACTION ON THE SURFACE AS THE RATE-CONTROLLING STEP

Case A. The earliest analysis of the adsorption wave was made by Bohart and Adams [4] on the assumption that the toxic gas is adsorbed irreversibly and at a local rate of removal governed by the equation:

$$\frac{1}{\alpha}\frac{\partial n}{\partial t} = k_1 c(N_0 - n), \tag{18}$$

where k_1 is a constant.

A similar treatment has been carried out more recently.[7] Both groups of investigators have derived the following expression for the variation of the concentration of gas in the air stream:

$$\frac{c_0}{c} = 1 + [\exp(-k_1 c_0 t)]\left[\exp\left(\frac{k_1 N_0 z}{V}\right) - 1\right]. \tag{19}$$

This equation in its various forms has been used very widely to interpret and to interpolate data on the performance of various charcoals. Unfortunately, present indications are that there are few cases where the rate of removal of a gas by charcoal is governed primarily by adsorption or reaction at the surface. Diffusion, or mass transfer, seems to make some contribution to the slowness of removal of almost all gases by charcoal, and hence equation (19) is not strictly applicable.

Case B. An attempt has been made by Lister to consider the relations obtained when adsorption on the surface is the rate-controlling step but for the special case where the adsorption is reversible and the adsorbed gas exerts a back pressure. For such conditions, the equation for the local rate of adsorption becomes

$$\frac{1}{\alpha}\frac{\partial n}{\partial t} = k_1 c(N_0 - n) - k_2 n, \qquad (20)$$

where k_1 and k_2 are constants.

No complete solution of the resultant differential equations has been given. Approximations have been given for the conditions obtained with fresh charcoal, but the general validity of these has been questioned.[10]

8.2.2 Theories in Which More Than One Step Contributes to Rate of Removal

DIFFUSION IN AIR AND DEPOSITION ON SURFACE CONTRIBUTING

It has been possible to construct [10] a differential equation for the local rate of removal on the assumption that the diffusion of the toxic molecule from the air to the charcoal and the subsequent deposition process, whether chemical or adsorptive in nature, both contribute to the slowness of removal. The general equation for this process has not been solved. Nevertheless, certain special cases have been considered, but each of them reduces to one of the single-step processes discussed in the preceding text and hence does not warrant further elaboration.

DIFFUSION IN AIR AND PROCESSES WITHIN THE GRANULE CONTRIBUTING

A very detailed consideration of the nature of the processes involved in the removal of gases by adsorbents has been made.[37] Emphasis has been given particularly to diffusion within the pores and to the various factors which influence the cross-sectional and longitudinal mixing in the intergranular spaces. Where the equilibrium adsorption of a gas follows a linear isotherm, the differential equations have been solved and have been shown to be applicable to the experimental data on the removal of CO_2 at 100 C. For gases with curved isotherms, however, the general solution to the differential equation has not been obtained though certain special cases have been considered.

8.2.3 Comparison of Theories with Experiment

None of the theoretical approaches gives a satisfactory correlation of the experimental data on the removal of a toxic gas by charcoal. Even with gases such as chloropicrin, where (as is shown later) mass transfer seems to be the rate-controlling step, the observed dependence of effluent concentration on time does not agree over any appreciable range with the curves given in Figure 3. The primary cause of the deviation, for other gases as well as for chloropicrin, is the curvature of the adsorption isotherm, a condition which so far has not been incorporated into the wave equations, except in an approximate, empirical manner.[29] In addition to the curvature of the isotherm, a further difficulty that arises with most other toxic gases of interest is the combination of mass transfer with one or more of the succeeding steps in controlling the rate of removal of the gas by the adsorbent. Minor discrepancies may also arise from thermal factors. Temperature changes in the removal process, which in some cases are many degrees, may raise the back pressure of the adsorbed gas or may affect the rate of mass transfer in the carrier stream.

Sufficiently fundamental differences exist in the differential equations for the local rate of removal in the mass-transfer and surface adsorption mechanism so that one can determine the presence or absence of a slow, diffusion step. In equation (18), based on surface adsorption as the rate-controlling step, the velocity V does not appear, and hence, in the integrated equation for c/c_0, V will enter only as z/V as can be verified by glancing at equation (19). Similarly, on expanding and rearranging (19) to obtain an equation for the instantaneous break time, t_b, an expression is obtained in which V enters only as z/V. In contrast, when mass-transfer (diffusion) is the controlling step, the velocity of flow enters the equation for the local rate of removal, inasmuch as F, the mass-transfer coefficient, depends on the rate of flow. In consequence, the instantaneous break

time depends on V as well as on z/V, and a plot of t_b vs z/V gives different curves for different rates of flow. (It should be emphasized that the cumulative break time, that is, the time in which a total quantity of gas sufficient to produce a change in some indicator has escaped from the bed, depends on V and z/V whether or not V enters the expression for the local rate of removal. Therefore, the cumulative break time cannot be used to distinguish between mechanisms of removal.) Thus, a criterion has been established for detecting the presence of a slow diffusional step. In Figure 4, this criterion is applied

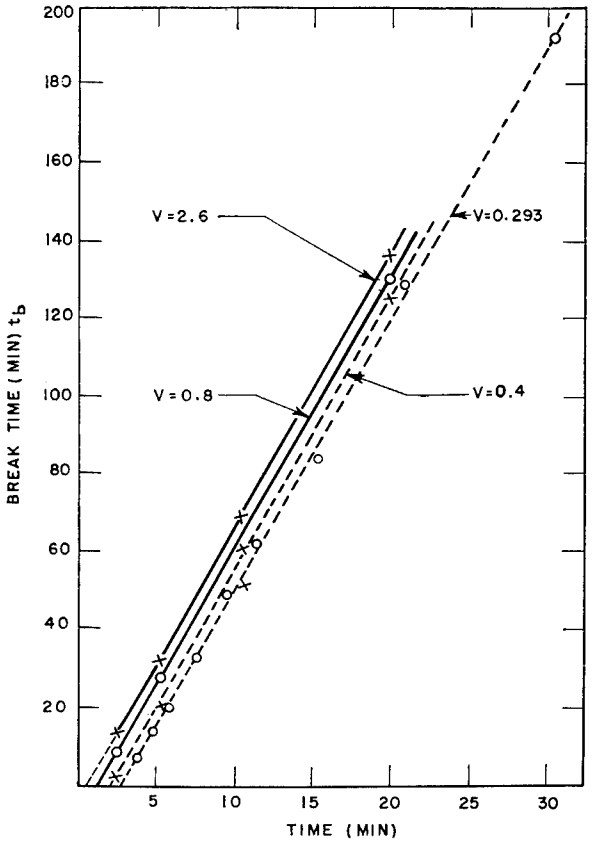

FIGURE 4. Effect of rate of flow on rate of removal of chloropicrin. Time (of contact) = $z/V \times 10^3$ min.

to some data on chloropicrin. It is obvious from the graph that t_b depends on V as well as on z/V, and in consequence, that diffusion contributes to the slowness of removal of chloropicrin by charcoal. Consequently, it is unlikely that the theories based on surface adsorption or surface reaction as the rate-controlling process will be applicable to any charcoal which has sufficient activity to make it useful in protection against toxic gases.

Unfortunately, these relationships were not realized in much of the early work and many extrapolations were made on the basis of the Bohart-Adams-Hinshelwood equation,[4,7] which is based on a surface-deposition, rate-controlling mechanism. The particularly misleading fact is the observation that in many circumstances a plot of log $(c_0/c - 1)$ is linear with time, a necessary condition derivable from equation (19). Unfortunately, such linearity is not a reliable test of the applicability of equation (19), for all the other mechanisms will also lead to such linear equations over wide ranges if suitable values are chosen for the constants. When constants for equation (19) are determined from plots of log $(c_0/c - 1)$ vs time, one finds that both k_1 and N_0 vary with the rate of flow of the air stream. Such behavior is completely at variance with the postulates of the mechanism and illustrates the inapplicability of the equation to the removal of gases by the usual charcoal adsorbents.

8.3 SEMI-EMPIRICAL TREATMENTS

In the absence of a satisfactory comprehensive theory of the adsorption wave, investigators have been forced to develop semi-empirical methods of treating data. Primary emphasis has been given to equations which relate break time to the common variables such as bed depth, rate of flow, particle size, and concentration of influent gas. With the accumulation of results from different modes of approach, it has also been possible to correlate certain relations with particular mechanisms of removal.

8.3.1 Factors Affecting Break Time

Nature of Flow in Charcoal

The flow of fluids through beds of granular solids is very complicated in nature because the channels are very tortuous and nonuniform. It is impossible to fix the dimensions or number of channels, as two streams may frequently merge or a single stream may redistribute itself into several new paths of flow. Since sudden contractions or enlargements in the intergranular spaces may occur, it is quite possible to have both streamlined and turbulent flow occurring simultaneously in different portions of a granular bed. In consequence, there is a much slower transition from conditions of laminar flow to those of turbulent flow in the passage of gas through an adsorbent bed than there is in the flow of fluid through pipes.

Usually the nature of the flow of fluids is studied by measuring the pressure drop in the bed or pipe. Correlations are then made with the dimensionless parameter known as the Reynolds number, $D_pV\rho/\mu$. When a graph of a function of the pressure drop known as the friction factor[15, 16] is plotted against the Reynolds number, two linear portions are observed which intersect at the *critical* Reynolds number, a value corresponding to conditions under which laminar flow is transformed into turbulent flow.

In studies made of the flow of fluids through porous carbon,[16] a critical Reynolds number of about 4 has been found. Extensive work has also been carried out on the flow of gases through beds of charcoal. Two representative curves are shown in Figure 5.

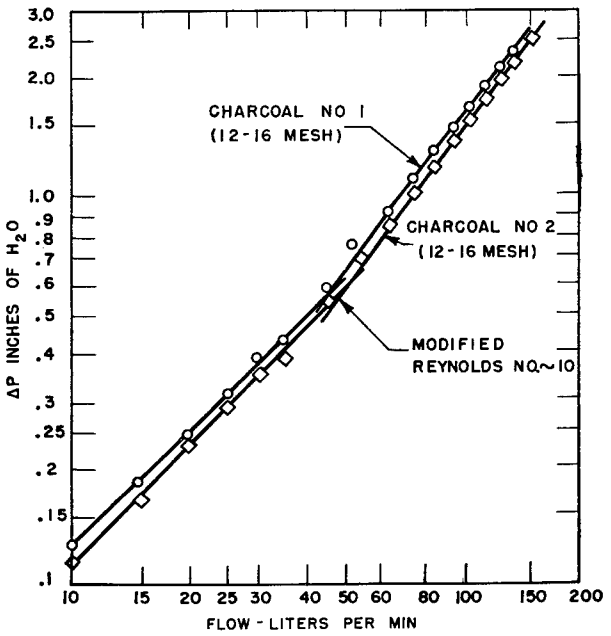

FIGURE 5. Relation of flow rate to pressure drop in charcoal beds.

From these curves and other data, it has been concluded that the critical Reynolds number is about 10 in the charcoals investigated. The Service laboratories[33] and two English workers[20] have found a transition in the same region. But it cannot be certain that the same critical value will be observed with all charcoals of any possible shape since it is quite conceivable that curious shape factors may occasionally be encountered in view of the rather arbitrary use of particle diameter D_p in place of pore size in the Reynolds number. In all the work described here, however, it has been assumed that the critical region is in the neighborhood of a Reynolds number of 10.

THE EFFECT OF BED DEPTH

The dependence of canister or tube life on the depth of charcoal has been investigated more widely than has the dependence on any other variable. The reason for such emphasis is perhaps obvious, for the amount of adsorbent necessary determines very largely the bulk of the canister. Life-thickness curves have become, therefore, the most common method of representing the performance of a charcoal. In consequence, the interpretation of performance in terms of the mechanisms of removal has revolved around the elucidation of life-thickness curves.

General Character of Life-Thickness Curves. A survey of performance data shows that two types of life-thickness curves are encountered. The simplest case is a linear relation such as is shown in curve A of Figure 6. Most organic gases when tested in a dry

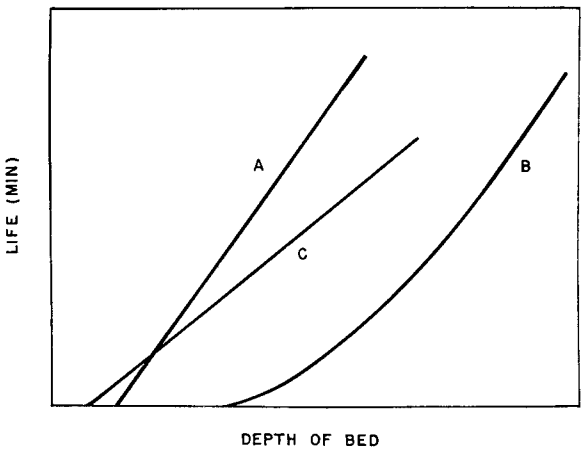

FIGURE 6. Life-thickness curves.

condition against dry charcoal exhibit linear life-thickness curves. In principle, a break-time test using a cumulative indicator should not show a linear relation with bed depth, at least not at small depths, but this lack of linearity is frequently overlooked because few tests are carried out at very small depths. Curve B exhibits a very common observation of curvature at low lives with a tendency to linearity at high break times. Such behavior should always be encountered in cumulative tests of the break time. It is also usually observed when tests are carried out with humidified gases and charcoal, and in some cases occurs in tests under dry conditions.

Whether or not curvature occurs, the life-thickness curve intersects the bed-depth axis at a finite value. It follows then that there exists a critical bed depth below which the life is zero. This critical length varies with the conditions of flow, concentration, mesh size, sensitivity of the detector, and the nature of the charcoal. It is this manifold dependence which has engaged much attention. Numerous attempts have been made to correlate these variables in some convenient analytic expression, for in small beds as in canisters, it is the critical bed depth which primarily determines the degree of protection.

The Mecklenburg Equation. A very convenient expression for the linear life-thickness curve has been derived by Mecklenburg [28] from elementary considerations of conservation of mass. At the break time a negligible portion of the toxic gas has penetrated the bed, and hence one can assume that:

Weight of gas supplied = Weight of gas picked up by adsorbent. (21)

The weight of gas supplied by the air stream is equal to the time of flow (the break time in minutes) times the rate of flow L (in liters per minute) times the concentration (in grams per liter). In turn, the pickup by the charcoal may be *arbitrarily* considered as occurring in a certain portion of the bed instantaneously and up to the saturation value, while the remainder of the bed, defined by Mecklenburg as the *dead layer*, remains completely free of gas. As was emphasized by Mecklenburg, the dead layer is a purely fictional concept devised merely to facilitate the derivation of the following equation and to obviate the necessity of considering in detail the distribution of gas in the bed of adsorbent. With this arbitrary division it follows that the amount picked up by the charcoal is equal to the saturation value per unit volume times the area, times the difference between the bed depth and the depth of the dead layer h. In algebraic terms the equality in (21) may be expressed as follows:

$$t_b L c_0 = N_0 A (z - h). \tag{22}$$

This equation may be rearranged readily to give an expression for the break time,

$$t_b = \frac{N_0 A}{L c_0} (z - h). \tag{23}$$

As has been pointed out previously (Chapter 2), the slope of the life-thickness curve for a fixed rate of flow, input concentration, and bed cross-section is a measure of the capacity (N_0) of the charcoal. For a system which obeys this equation throughout the complete life-thickness curve, the dead layer h and critical bed depth I must be equal, so that

$$t_b = \frac{N_0 A}{L c_0} (z - I). \tag{24}$$

The great deficiency of equation (24) is that it cannot be used to extrapolate information from one set of flow or concentration conditions without further information on the dependence of the critical bed depth on these variables. The wave theories discussed in preceding paragraphs set certain requirements for the variation of critical bed depth, and where these theories are applicable they may be used to extend equation (24). Further details are considered in a subsequent section.

Curvature Due to Cumulative Method of Test. If the break time is defined in terms of the period necessary for a total cumulative amount of gas to penetrate the bed, it can be shown that the life-thickness curve, even in the simplest mechanism of removal, would obey an expression of the form

$$t_c = \frac{N_0 A}{L c_0} k_3 V^{k_4} \ln \left[\frac{k_5 \exp (z/k_3 V^{k_4})}{N_0 A k_3 V^{k_4}} + 1 \right]. \tag{25}$$

In general, equation (25) would not be linear; however, for large bed depths, the first term inside the brackets becomes large in comparison to the second term and the equation as a whole approaches the linear relation:

$$t_c = \frac{N_0 A z}{L c_0} + k_6. \tag{26}$$

These predictions are in agreement with the behavior observed in cumulative tests.

The Effects of Velocity of Flow, Concentration, and Particle Size

It can be shown from considerations similar to those discussed by Hurt [19] for the design of catalytic reactors, that if more than one step contributes to the rate of removal of a gas from the carrier stream, the critical bed depth I will be the sum of two terms I_t and I_r. I_t represents the portion of the critical bed depth due to the slowness of diffusion of gas from the air stream to the surface of the charcoal, whereas I_r represents the fraction due to processes occurring within a charcoal granule. Since the critical bed depth can be thought of as the distance which the gas may penetrate the bed before its concentration is reduced to the break value, it seems reasonable to expect a certain minimum value of I for a fixed set

of conditions, which would represent the smallest penetrable depth possible, even if every process in the granule were instantaneous and the rate were determined entirely by the speed with which the gas diffuses to the particle. This limiting value of I for a fixed set of conditions would be I_t. Any critical bed depth above I_t must be the contribution of the processes within the granule. That this contribution should be an additive term, rather than a multiplicative factor, has been shown in principle by Hurt.[19]

The critical bed depth due to diffusion, I_t, can be expressed in terms of a number of familiar parameters, independent of the nature of the charcoal, but dependent on the properties of the air-gas mixture and on the granular characteristics of the bed. Considerations of dimensional analysis lead to the conclusion that at a fixed ratio of influent to effluent concentration, I_t should be a function of the particle size of the granules, and of two dimensionless parameters D_pG/μ and $\mu/\rho D_v$, the Reynolds number and Schmidt number, respectively. The specific function which has been adopted is essentially that of Gamson, Thodos, and Hougen:

$$I_t = \frac{2.303}{a}\left(\frac{D_pG}{\mu}\right)^{0.41}\left(\frac{\mu}{\rho D_v}\right)^{0.67}\log\frac{c_0}{c_b}. \qquad (27)$$

In the derivation of this equation, it is assumed that c_0/c_b is very large. Strictly speaking, this equation should be applicable only in cases of turbulent flow, but it has been found that in the region of laminar flow in charcoal, I_t is approximated satisfactorily by equation (27). For a fixed ratio of influent to effluent concentration, the equation expresses the variation of the critical bed depth with particle size D_p, rate of flow G, and diffusion coefficient of the gas D_v. The factor a, the superficial surface of the granule (ignoring pore structure), depends on the particle size and on the percentage of voids in the bed. Values of a have been calculated and are tabulated.[15] Where the absolute value of I_t is not desired but only the form of the equation is necessary, one can substitute the following approximate equation:

$$a = \text{Constant} \times D_p^s. \qquad (28)$$

The power s takes into account the variation of percentage voids with particle size and generally has a value slightly less than 1.

For convenience in comparing data on critical bed depths with analogous performance data in chemical engineering processes, the following transformation is useful:

$$H_t = \frac{I_t}{2.303\log c_0/c_b} = \frac{1}{a}\left(\frac{D_pG}{\mu}\right)^{0.41}\left(\frac{\mu}{\rho D_v}\right)^{0.67}. \qquad (29)$$

H_t is called the *height of a transfer unit.*

In contrast to I_t, I_r would be a complex function of the structure and nature of the charcoal and would be specific for the particular gas being removed. While it would be independent of the Reynolds number, it should [judging from consequences of equation (19)] vary directly with the rate of flow of the gas-air stream, and it may be quite sensitive to temperature. Since many of these variables cannot be estimated in any general way, it is only possible to suggest the following relation for I_r (on the assumption that c_0/c_b is large and that the reaction is first order):

$$I_r = k_8 V \ln\frac{c_0}{c_b}. \qquad (30)$$

The total critical bed depth, therefore, should be given by the expression

$$I = I_t + I_r = \frac{1}{a}\left(\frac{D_pV\rho}{\mu}\right)^{0.41}\left(\frac{\mu}{\rho D_v}\right)^{0.67}\ln\frac{c_0}{c_b} + k_8 V\ln\frac{c_0}{c_b}. \qquad (31)$$

To determine the relative contributions of I_t and I_r, one may proceed in at least two ways. One approach would be to calculate I_t from equation (27) and obtain I_r by difference from the total critical bed depth. To facilitate these calculations a series of graphs has been prepared in which I_t is plotted as a function of the common variables.[22] A second approach is to obtain data on I as a function of the linear velocity V, and then to plot the data against $V^{-0.59}$. It is obvious from equation (31) that for all conditions, except flow rate, fixed, I/V may be expressed as

$$\frac{I}{V} = k_9 V^{-0.59} + k_{10}, \qquad (32)$$

where k_9 and k_{10} are constants. The intercept of the line obtained is a relative measure of I_r and the value of the first term in equation (32) at any particular linear velocity is a relative measure of I_t.

The variation of the critical bed depth with particle size depends on the relative importance of the two terms in equation (31), that is, on the mechanism of the removal process. If the slow step in the granule

is some surface reaction, I_r will be independent of particle size, whereas I_t will vary as some power of D_p, usually near 1.4. If diffusion in air and surface reaction contribute about equally, a plot of I against D_p will approach a finite limiting value as D_p approaches zero. This is illustrated by curve A in Figure 8. If mass transfer alone is rate-controlling, one obtains a similar curve (B in Figure 8) but with an intercept at the origin. In contrast, if the surface reaction were rate-controlling, I would be independent of granule size, as is illustrated in curve C of Figure 8.

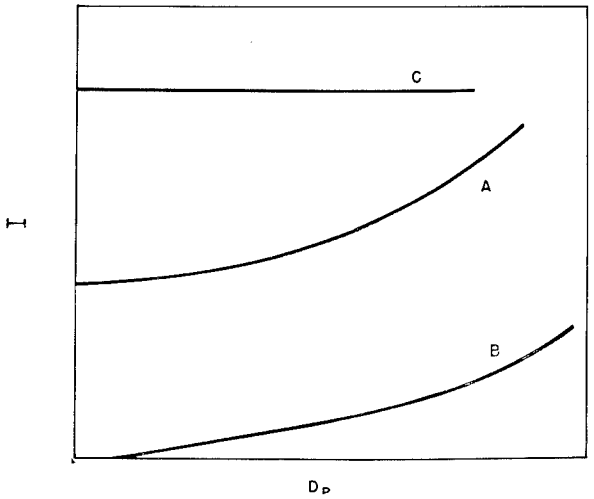

FIGURE 8. Effect of mesh size on critical bed depth, for various mechanisms of gas removal.

Where both terms contribute appreciably to the critical bed depth, one obtains an interesting graph in a plot of break time versus particle size. For large sizes, the life is less than that for small particles, but as the granule size decreases the life rises and approaches a limiting value, corresponding to conditions where the surface reaction becomes the important factor and mass transfer has been effectively eliminated. A typical curve is shown in Figure 9.

The variation of the critical bed depth with velocity of flow also depends on the relative importance of the two terms in equation (31). If the slow step is a reaction in the granule, I will vary directly with the velocity. In contrast, if mass transfer is rate-controlling I will vary with the 0.4 power of the velocity. Where the two processes contribute, I can usually be expressed in terms of some power of the velocity between 0.4 and 1.0, although it must be realized that such a function would be merely an approximation to the fundamental one of equation (31).

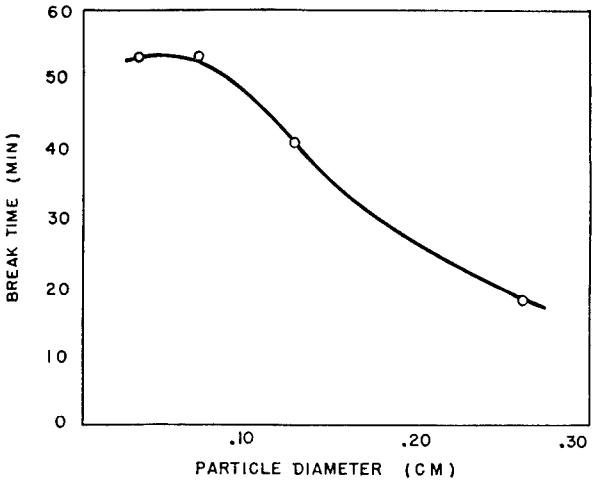

FIGURE 9. Dependence of break time on particle size (for phosgene).

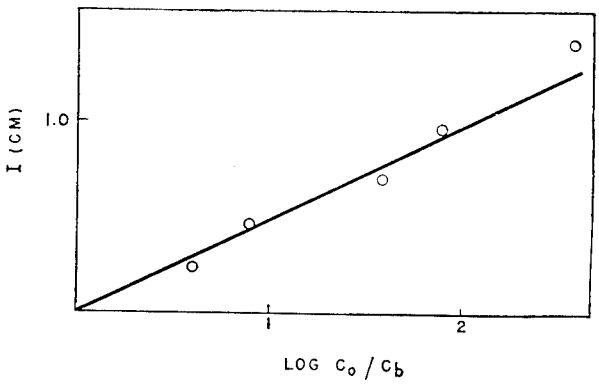

FIGURE 10. Dependence of critical bed depth on ratio of influent to effluent concentration.

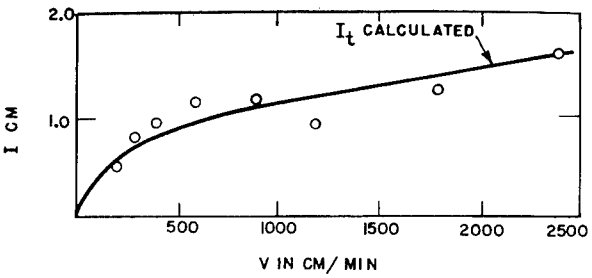

FIGURE 11. Critical bed depths for chloropicrin.

The available evidence indicates that the critical bed depth is a logarithmic function of c_0/c_b. According to equation (31), the logarithmic relation should hold for any mechanism of removal. Sufficient data on effluent concentration as a function of time are available only for a few gases, so that the predicted relation has not been tested adequately. That it does hold for chloropicrin is shown in Figure 10.

Mechanism of Removal of Some Gases. The criteria described for estimating the relative contributions of diffusion in air and physical or chemical reactions in the charcoal to the critical bed depth have been applied to a number of gases with the aim of elucidating the mechanism of their removal.

Chloropicrin is an example of a gas whose rate of removal is governed primarily by the rate of diffusion to the particle surface. In Figure 11 the observed values of the critical bed depth are plotted as a function of the linear velocity, and for comparison the curve calculated for I_t is also shown. The observed values do not deviate significantly from the calculated curve. Such behavior indicates no appreciable contribution of any factors other than mass transfer (diffusion in air) to the removal of chloropicrin, at least not in the initial stages of the process.

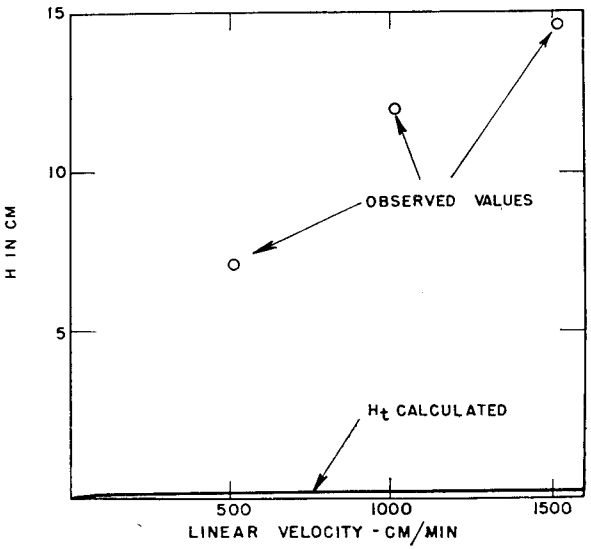

FIGURE 12. Water removal by charcoal. Deviation of observed from computed values of H.

In direct contrast to chloropicrin is water, whose rate of removal seems to be governed primarily by some slow surface process. Experimental data on the rate of removal of H_2O have been expressed in terms of a quantity H which may be defined by the equation

$$H = \frac{I}{\ln c_0/c_b}. \qquad (33)$$

Values of H on a sample charcoal are shown in Figure 12. In comparison to the values to be expected if diffusion in air were the controlling process, the observed values are very high and indicate the large contribution that is made by factors which appear within or on the granule.

Dependence of Critical Bed Depth on Nature of Adsorbent. It must be realized that the relative contributions of various steps to the rate of removal will be very sensitive to the nature of the adsorbent. This dependence is well illustrated in the case of water where different base charcoals, having different pore structures and surface complexes, can react with water with different speeds and hence strikingly influence the critical bed depth or the value of H. Similarly, charcoals treated with impregnants usually react more rapidly with water, apparently because of their ability to form hydrates, and hence the magnitude of H is reduced considerably. In adsorbents such as silica gel, where the combination with water vapor at low pressures is probably due to hydrogen-bonding rather than primarily to van der Waals' forces, the removal reaction is extremely rapid and H approaches the limiting value due to diffusion in air alone. These factors are illustrated by the values of H listed in Table 1.

TABLE 1. Dependence of H on adsorbent.

Adsorbent	H (in cm)
Charcoal, base, CWSN–19	38–64
Charcoal, base, CWSC–11	20–30
Charcoal, impregnated, CWSE1–TE1	7–15
Silica gel	0.5–2.5

The measurement of critical bed depths for charcoals which have been subjected to various treatments is a useful method of analyzing the results obtained. For gases such as chloropicrin, at least some of the available charcoals can react so rapidly that the limiting factor in the removal of gas (the rate of diffusion to the granule) has been reached, and it is futile to attempt to improve the adsorbent any further toward these particular toxic materials. On the other hand, toward most possible toxic agents there is still sufficient room for additional treatments or impregnations which may speed up processes which occur within the granule.

THE EFFECT OF THE CAPACITY OF THE CHARCOAL

A clear statement of what is meant by *capacity* of a charcoal is not as readily available in a flow type of experiment as it is in the static case. In the latter situation, capacity refers to the amount of gas picked up by a unit weight of charcoal after sufficient time has elapsed for equilibrium to have been attained.

879245 O - 50 - 2

The primary value of a measure of capacity is in the prediction of the dependence of life on bed depth. Consequently, it is customary to define N_0 in terms of the slope of a life-thickness curve [see equation (23)]. In this manner, two samples which show linear life-thickness curves can be compared reliably in their performance under a set of conditions requiring a slight extrapolation from the measured ones. It is realized of course that such a capacity may be far different from the final equilibrium value, even for gases removed by adsorption alone. Nevertheless, it is more useful than a definition based on a static experiment.

For small bed depths, the break time is determined primarily by the critical bed depth of the adsorbent, inasmuch as the critical bed depth is a large fraction of the total bed. On the other hand, as the bed is made deeper, the critical bed depth becomes less important, whereas the capacity becomes increasingly significant and in large depths is the determining factor. These relations became evident in a comparison of the lines A and C in Figure 6.

The capacity is also a useful function for estimating the maximum possible life one can obtain from a sample. By assuming a critical bed depth of zero, one can calculate the total amount of gas that could be picked up by the bed and, from the flow conditions, the maximum limit for the break time (see "Efficiency of Canister," Chapter 2).

8.3.2 Equations for Canister Life

To predict the performance of canisters under any set of conditions other than those used in routine tests, it is necessary to have convenient analytic relations for life as a function of the common variables. This problem has not been solved satisfactorily except in a few special cases. Where the life-thickness relations show distinct curvature, no suitable analytical method has been evolved for extrapolating data. Since many tests are carried out under humid conditions, in which curvature is generally observed, this large field of testing still remains to be considered. However, in testing under dry conditions, where linear life-thickness curves are obtained, useful equations for the break time have been developed.

Cases in which Diffusion in Air is the Rate-Controlling Step

Under these conditions it is a simple matter to combine the Mecklenburg relation for t_b and equation (27) for I_t. The result is the expression:

$$t_b = \frac{N_0 A}{L c_0}\left[z - \frac{1}{a}\left(\frac{D_p G}{\mu}\right)^{0.41}\left(\frac{\mu}{\rho D_v}\right)^{0.67} \ln\frac{c_0}{c_b}\right]. \quad (34)$$

It allows the prediction of the complete break-time history for any gas whose removal is controlled by mass transfer after the determination of one constant N_0, the capacity of the charcoal for the particular toxic material. The diffusion coefficient D_v of the gas can be estimated readily from relations available in the literature, or in most cases can be estimated sufficiently from the molecular weight curve illustrated in Figure 13. Tables of a, the superficial area, for various particle sizes and percentage of void spaces are listed.[15] All other constants may be evaluated from the conditions of flow and from the dimensions of the adsorbent bed.

Cases in which More Than One Step Contributes to Rate

It has been shown that under these conditions the critical bed depth may be expressed as a sum of two terms, each of which contains the linear velocity V to a different power. Equation (31) for I could be inserted into the Mecklenburg relation but the resultant expression is not as convenient for manipulation as an alternative developed.

It has been observed in most experiments that a plot of the critical bed depth versus the logarithm of the rate of flow can be approximated sufficiently well by a straight line. Because of the large errors

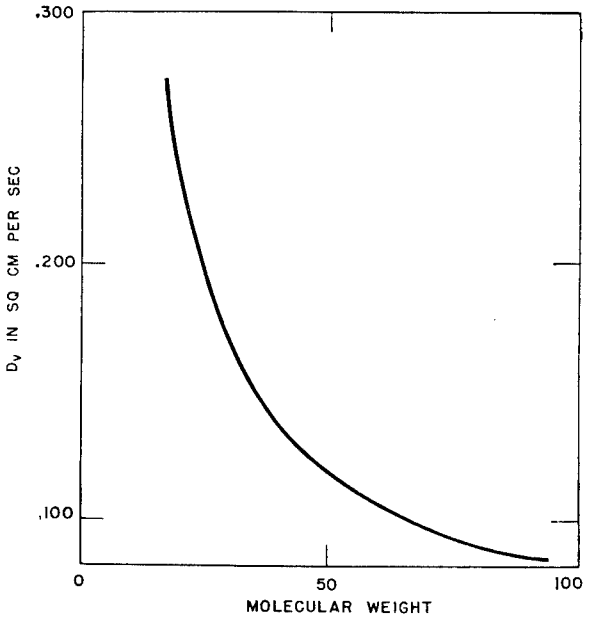

Figure 13. Relation between diffusion coefficient and molecular weight.

inherent in the determination of the critical bed depth, the relation

$$I = \text{Constant} \times V^d, \qquad (35)$$

where d is a constant, can be used in place of the two-term expression of equation (31). The insertion of this simple relation into the Mecklenburg equation gives:

$$t_b = \frac{N_0 A}{L c_0}\left[z - g\left(\frac{L_e}{A_b}\right)^d \log \frac{c_0}{c_b}\right], \qquad (36)$$

in which g is a constant which depends on the mesh size of the charcoal and the particular gas being removed, d is a constant determined by the test gas, A_b is the open area of the baffle at the effluent end of the canister and L_e is the steady flow rate equivalent to the pulsating rate of flow actually used. As has been described in a previous chapter, canister tests are made with a *breather* apparatus, designed to simulate respiratory conditions, in which the flow may vary from a high peak rate down to zero. The equivalent steady flow may be determined by measuring critical bed depths for a series of different constant flow rates and plotting I vs V. Then in a subsequent experiment with pulsating flow, the value of I is determined and from the reference graph a corresponding equivalent steady flow is read off. The reference curve may vary with the test gas as well as with large changes in the shape factor of the charcoal.

The use of equation (36) requires the evaluation of three constants, N_0, g, and d. The other parameters would be fixed by the conditions of flow and the geometric properties of the bed.

The equation has been applied [33] to five test gases (arsine, chloropicrin, cyanogen chloride, hydrogen cyanide, and phosgene) and to a number of different charcoals and found to be reliable within the precision of the experimental data. Thus, it affords a very convenient interpolation formula for the prediction of the performance of axial-flow canisters.

The principles used in the derivation of equation (36) have been applied to the radial-flow canister also. The result depends on the geometrical configuration of the canister.[33]

8.4 CONCLUSIONS

In examining the whole of the theoretical and experimental results of the work on the adsorption wave, it is seen that progress has been attained in the following respects. The nature of the steps involved in the removal of a toxic gas from air by a granular adsorbent has been clearly stated. Where the rate-controlling process is a single one of these steps, it has been possible within recognized restrictions to develop a complete analytical expression for the adsorption wave. Where two steps contribute to the rate of removal, a complete theory is still lacking, but it has been possible to develop criteria for the evaluation of the relative importance of diffusion in air and reactions in the granule in the removal process. These criteria have been applied to a number of different gases and the mechanism of their removal has been elucidated. From the general nature of the various equations for the adsorption wave it has been possible to develop semi-empirical relations for the prediction of canister lives under dry conditions and to predict qualitatively the effects of mesh size, flow rate, and concentration under dry or wet conditions.

The great gap in the present work is a suitable analytical treatment of results obtained under humid conditions or in other cases where non-linear life-thickness relations are obtained. Related to this is the absence of a complete treatment of the adsorption wave where many steps contribute to the rate of removal. These failures, however, are bound very closely to the general obscurity of the structural characteristics of granular adsorbents and of the nature of catalytic reactions. As fundamental relations in these latter fields are gradually evolved, one may anticipate further progress in the treatment of the adsorption wave and in canister design.

SYMBOLS

- a superficial surface of the granule (ignoring pore structure) per unit volume of bed
- A cross section of adsorbent bed
- A_b open area of the baffle at the effluent end of the canister
- b constant in equation for linear adsorption isotherm
- c concentration of toxic gas in air stream at any point in bed of adsorbent
- c^* concentration of toxic gas in air stream at any point in the bed in equilibrium with the charcoal at that point
- c_b concentration of toxic gas in air stream chosen as the *break* value
- c_e concentration of toxic gas in air stream at exit face of bed
- c_0 concentration of toxic gas in air stream at entrance face of bed
- d constant in equation for critical bed depth
- D_p diameter of granule
- D_v diffusion coefficient of the toxic gas (units of area per unit time)
- exp notation for the exponential e
- F mass transfer coefficient
- g constant in equation for canister life
- G mass velocity, that is, weight per unit time per unit cross section of bed

h depth of the "dead layer"
H height of a removal unit; $I/\ln c_0/c_b$
H_t height of a transfer unit; $I_t/\ln c_0/c_b$
I critical bed depth, that is, the actual intercept of a life-thickness curve on the thickness axis
I_r fraction of critical bed depth due to slowness of processes occurring within a charcoal granule
I_t fraction of critical bed depth due to slowness of diffusion of gas from air stream to the surface of the charcoal
k_1 constant in rate equation
k_2 constant in rate equation
k_3 constant in equation for t_c
k_4 constant in equation for t_c
k_5 constant in equation for t_c
k_6 constant in equation for t_c
k_7 constant in equation for critical bed depth
k_8 constant in equation for critical bed depth
K constant in the expanded form of the Langmuir isotherm
L rate of flow in liters per minute
L_e rate of steady flow equivalent to rate of pulsating flow
n moles of toxic gas on or in the granules contained in a unit volume of bed
N_0 saturation capacity of a unit gross volume of adsorbent for the toxic gas
s constant in equation for superficial area
t time
t_b *instantaneous* break time, that is, the time at which the effluent concentration reaches a value specified as the break concentration
t_c *cumulative* break time, that is, the time necessary for a given total amount of gas to penetrate the adsorbent
V linear velocity through the interstices between the particles of the adsorbent; $G/\alpha\rho$
z distance from the entrance face of the bed
α porosity, that is, the volume of intergranular voids per unit gross volume of bed
μ viscosity of gas-air stream
ρ density of gas-air stream

Chapter 2

GENERAL METEOROLOGICAL PRINCIPLES

By *Wendell M. Latimer*

14.1 ATMOSPHERIC STABILITY

14.1.1 General Principles

Air is in a stable state of equilibrium when a volume of the air, which is displaced a small distance up or down, tends to return to its original position. Unstable air, when displaced upward, is acted upon by forces which tend to accelerate it in the direction of the impulse, while stable air is decelerated. The acceleration, which acts upon a volume of unstable air, depends upon the difference in density between it and its surrounding air; but since air is a compressible medium, changes in pressure and temperature occur, so that the difference in density of both the displaced volume and its surrounding air vary from the initial conditions. When resulting temperature changes cause condensation of aqueous vapor, the heat of vaporization is liberated and the density changes are further complicated by this heat.

Atmospheric pressure decreases with increasing elevation and from the first law of thermodynamics

$$dT = \frac{dQ}{C_p} + \frac{RT}{C_p}\frac{dp}{p}, \qquad (1)$$

where T is absolute temperature, Q the heat added to the system, R the gas constant, C_p the specific heat of the air at constant pressure, and p is the air pressure. If no heat flows in or out of the system, $dQ = 0$ and the process is called *adiabatic*. Then

$$T = T_0\left(\frac{p}{p_0}\right)^{(C_p - C_v)/C_p}, \qquad (2)$$

where C_v is the specific heat at constant volume. From the average decrease of pressure with altitude, the rate of change of temperature for the adiabatic transfer of air from low levels to higher levels is about 1 degree C per 100 m or 5.4 degrees F per 1,000 ft. This is known as the *adiabatic lapse rate.*

The condition for the stability of dry air is not that the density must decrease and the temperature increase with altitude, but that the temperature shall not decrease more rapidly than the dry adiabatic lapse rate.

The normal lapse rate, that is, the normal decrease of temperature with altitude, is about 3.3 degrees F per 1,000 ft. An air mass with this lapse is stable, as is indicated in Figure 1.

To interpret Figure 1, let a volume of air be taken from the level k to the level l. If it is dry air (or air which will not become saturated in the process) its temperature decreases by the adiabatic rate, that is, line lk is parallel to line CD. Its temperature at l is less than that of the surrounding air which has a temperature corresponding to m. Therefore its density is greater than that of the surrounding air, and

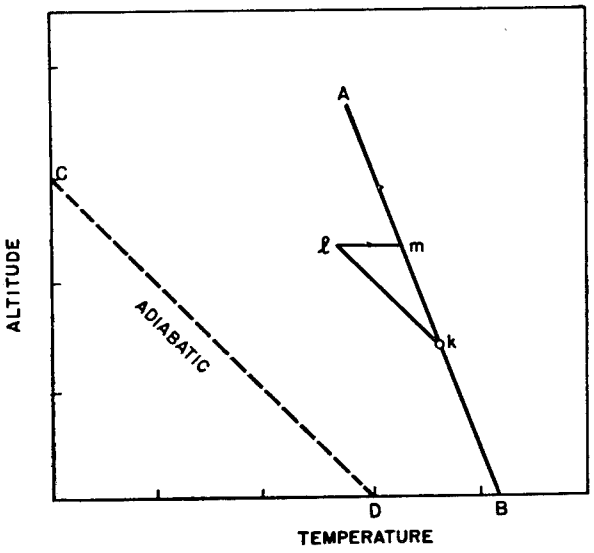

Figure 1. Relation of stability to lapse rate.

the displaced mass tends to return to its original level. If the rate of decrease of temperature with increase in altitude for AB had been greater than for CD, the temperature at l would have been warmer than that of its environment and the air mass would have been unstable.

The dependence of the lapse rate upon the rate of fall of pressure has been indicated in the last paragraph. However, there is an interdependence of the two factors as indicated by the following argument.

The rate of fall of pressure with height is proportional to the density d.

$$\frac{dp}{dz} = -gd, \qquad (3)$$

where g is the acceleration due to gravity. But for a

gas $d = p/RT$, and if the temperature were constant at all heights, by integration

$$\log \frac{p}{p_0} = \frac{gz}{RT} . \tag{4}$$

Actually, however, temperature falls off and may be represented usually by a straight line function

$$T = T_0 - az, \tag{5}$$

where T_0 is the ground temperature (absolute). Hence

$$\log \frac{p}{p_0} = \frac{g}{aR} \log \frac{T - az}{T_0} = \frac{g}{aR} \log \frac{T}{T_0} . \tag{6}$$

In dealing with air masses which are subject to changes in both temperature and pressure, it is convenient to have some standard reference condition for the sake of comparisons. Such a factor is the *potential temperature* Θ, which is defined as the temperature the air would have if brought adiabatically to a standard pressure (1,000 millibars). From equation (2)

$$\Theta = T\left(\frac{1000}{p}\right)^{(C_p - C_v)/C_p} . \tag{7}$$

At 25 C the specific heats of dry air are $C_p = 0.2396$ and $C_v = 0.1707$ cal per g. Hence

$$\frac{C_p - C_v}{C_p} = 0.288. \tag{8}$$

Atmospheric stability may be defined in terms of potential temperature.

For stability, the potential temperature must decrease with height. For instability, the potential temperature must increase with height.

14.1.2 Moist Air Stability

The criteria for the stability of dry air apply with sufficient accuracy to moist air, even though there is a slight difference in the specific heat values, as long as the movement of the air fails to produce saturation. The value for the saturated adiabatic lapse rate depends upon the temperature and pressure of the air but is not simply related to the altitude. A number of graphical thermodynamical methods are in use for solving problems involving ascending saturated air. An example of such is the aerogram. In this method $\log T$ as abscissa is plotted against $T \log p$ as ordinate. Isotherms are shown as vertical lines and isobars as nearly horizontal lines. The graph has three sets of lines: (1) constant, maximum, specific humidity (dew point lines), (2) dry adiabatic, and (3) moist adiabatic. At low temperatures and low pressures, lines (2) and (3) are nearly parallel but they diverge greatly at high temperatures and pressures.

By means of such a diagram measurements of temperature and relative humidity permit the calculation of the level at which ascending moist air will form a cloud and also the thickness of the cloud. Since the purpose of this discussion is to give a foundation for consideration of problems on the earth's surface, it is not necessary to amplify the problem of saturated air and cloud formation. Reference should be made to a standard text.[12]

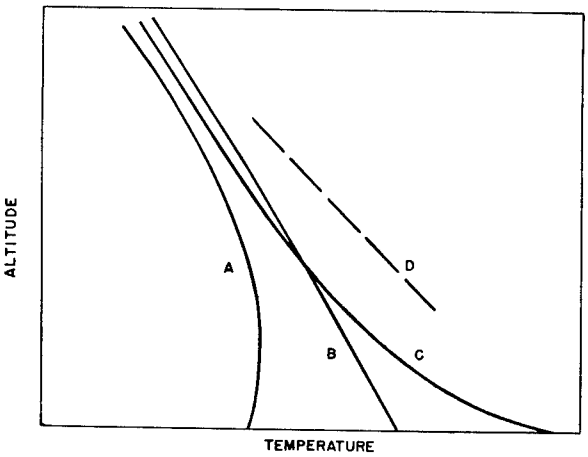

FIGURE 2. Diurnal variation in air temperature near the ground; (A) night; (B) evening; (C) midday; (D) day-adiabatic.

The arguments in the previous paragraphs have assumed that a volume of air could be displaced vertically without disturbing its environment. Actually an ascending current is normally balanced by a descending current. The coexistence of such adjacent currents modify somewhat the conditions for stability. They give rise to *solenoid-producing* terms. These do not greatly affect dry air problems but do lead to slight changes in the criteria for the stability of saturated air.

14.2 METEOROLOGY OF THE GROUND LAYER

The layer of air near the ground tends to assume the ground temperature. The large diurnal heating and cooling of the earth's surface is thus accompanied by corresponding changes in the air next to the surface. These effects are illustrated in Figure 2 and Figure 3.

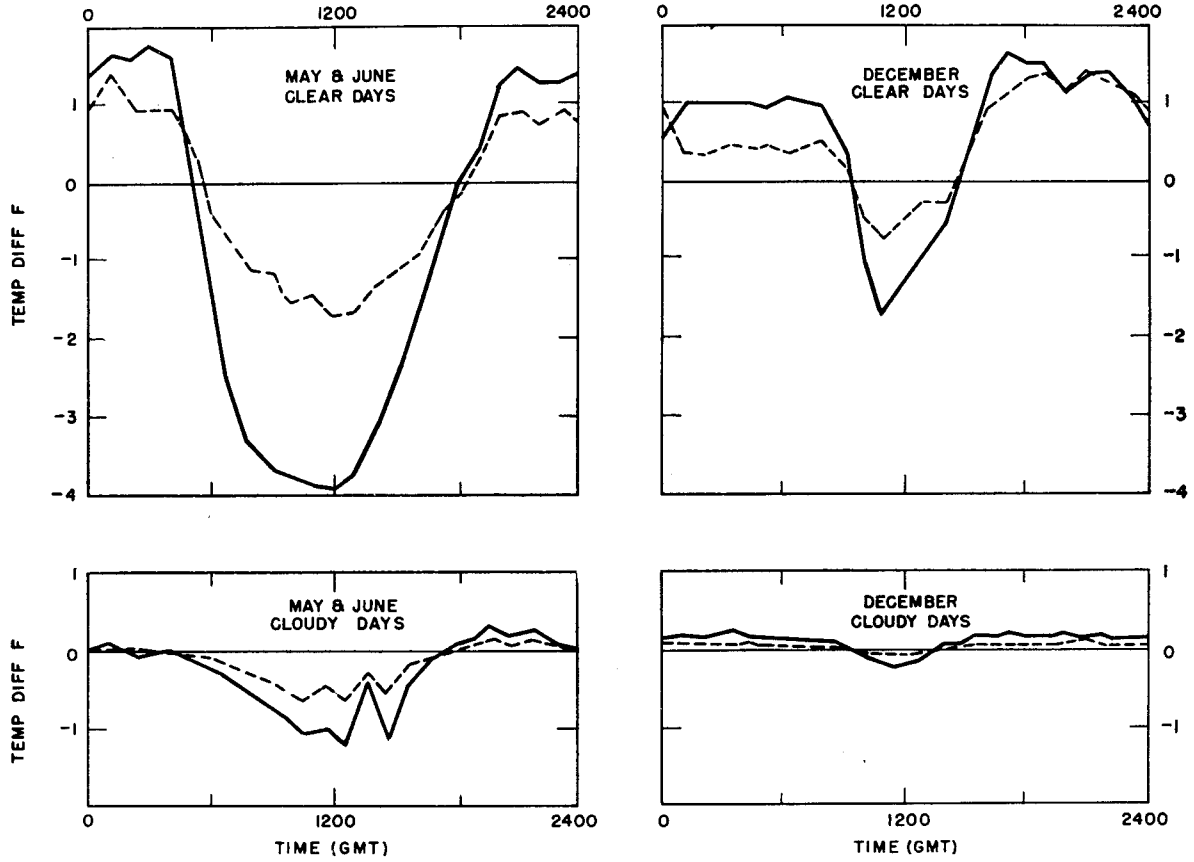

FIGURE 3. Mean diurnal curves showing temperature differences over the height intervals 2.5 to 30 cm (full line) and 30 cm to 1.2 m (dashed line) on clear and cloudy days in summer and winter (after Best).

The very high ground temperatures in midday and early afternoon give rise to temperature gradients in the air which are in excess of the dry-adiabatic lapse rate. These conditions are referred to as *superadiabatic lapse* or often as high lapse or strong lapse. As the ground cools at night the temperature gradient of the air near the ground inverts from the normal decrease with height to an increase with height. This condition is referred to as *inversion*. A cross-over occurs in the morning and evening where there are zero or normal lapse gradients; these are known as *neutral conditions*.

14.3 FACTORS INFLUENCING TEMPERATURE GRADIENTS NEAR THE GROUND

14.3.1 Radiation Effects

The mean energy of solar radiation just outside the earth's atmosphere is given as 1.93 cal per min per sq cm. On the average, 38% of the incoming radiation is scattered or reflected back into space. This reflection is due to such surfaces as dust clouds or earth's surface and for any region is subject to considerable variation. Thus, clouds and snow-covered ground may reflect 80% of the radiation, and the reflection from water surfaces is much greater than from the ground.

Most of the sun's radiation lies within the limits of wavelengths 0.2 to 3 μ, about half within the visible range 0.4 to 0.7 μ and half on the infrared side of the visible. The absorption by oxygen and nitrogen molecules is negligible except in the ultraviolet below 0.3 μ. Most of this appears to be due to atomic oxygen at 100-km levels and to ozone around the 40-km level. Carbon dioxide absorbs in a narrow band around 15 μ. The absorption of water vapor lies in the region 5 to 8 μ and 15 μ to longer wavelengths.

Since both the CO_2 and H_2O vapor absorption regions are so far out in the infrared, these absorptions do not remove an appreciable amount of energy from

the direct solar radiation, but they do play an important part in both the emission and absorption of atmospheric-temperature radiation.

Because the average yearly temperature of the earth is fairly constant and the amount of solar energy absorbed by vegetation is a small fraction, it follows that the energy of the temperature (black body) radiation of the earth's surface and atmosphere must be approximately equal to the amount of solar radiant energy.

From the Stefan-Boltzmann equation,

$$E = 8.22 \times 10^{-11} T^4, \tag{9}$$

the effective black-body temperature of the earth as a radiator to space may be calculated. Using 38% as the loss of solar energy by reflection and dividing by 4, the ratio of the area of the surface of a sphere to the area of a circle, we have

$$\frac{0.62 \times 1.93}{4} = 8.22 \times 10^{-11} T^4$$

or

$$T = 246 \text{ K}.$$

This value is too low by about 40 degrees C. The assumption that the earth radiates as a black body is far from exact, and the actual value of the temperature should be higher than that calculated. Moreover,

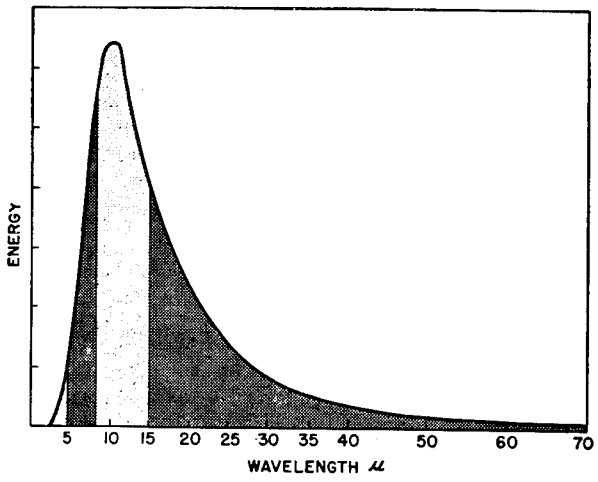

FIGURE 4. Energy distribution in black-body radiation at 300 K. Shaded portions are regions of water-vapor absorption.

the earth's temperature is dependent upon evaporation, condensation, and turbulent wind convection; these factors are also involved in the departure from black-body conditions.

Since the wavelength of maximum energy in black-body radiation is inversely proportional to the absolute temperature, and since the ratio of the temperatures of the sun and earth is about 20 (that is, 6,000/300), the maximum energy of the earth's black-body radiation lies around 10 μ. This is in the region of the water vapor bands and much of the outward radiation from the earth's surface is therefore absorbed by the atmospheric water vapor (see Figure 4). However, it is noted that there is a transparent region in water vapor between 8 and 15 μ, and it follows that an appreciable fraction of the radiation is transmitted.

The water vapor and carbon dioxide of the atmosphere emit radiation in the same regions in which they absorb. This gives rise to an atmospheric radiation back to the earth's surface which is highly important. If the temperature of the atmosphere is much colder than the earth's surface, the atmospheric radiation is small in comparison to that of the surface because of the T^4 dependence of the energy, but if the temperatures are nearly the same, as they normally are, they differ only by the amount of radiation transmitted by the water vapor in the 8 to 15 μ region.

With clear skies the incoming atmospheric radiation (sky radiation) is between 50 and 85% of the black-body value corresponding to the temperature of the air near the ground. The variations are largely due to changes in the relative humidity or weight of water in the air, but the total pressure and temperature differences in the upper atmosphere are also factors.

Various formulas have been proposed to calculate the sky radiation. Angstrom gave

$$\frac{R}{F_b} = 0.806 - 0.236 \times 10^{-0.052e}, \tag{10}$$

where R is the incoming radiation, F_b the black-body radiation at the temperature of the air near the ground, and e is water vapor pressure in millibars. Brunt found that the experimental data are quite accurately expressed by the equation

$$\frac{R}{F_b} = 0.526 + 0.065\sqrt{e}.$$

Rabitzsch wrote

$$\frac{R}{F_b} = \frac{0.135p + 6.0e}{T}, \tag{11}$$

where p is air pressure in millibars and T is absolute temperature.

Taking as an example the set of conditions, $p = 1{,}000$, $e = 15$, and $T = 300$, one may calculate from equation (11) $R/F_b = 0.75$. F_b at 300 K is 0.60

cal per cm per min. Hence R, the sky radiation, is 0.45 cal per min per sq cm and the effective outward radiation of a black body on the earth's surface would be 0.60 − 0.45 = 0.15 cal per min per sq cm.

For the same set of data, Brunt's equation would give:

$$\frac{R}{F_b} = 0.526 + 0.065\sqrt{15} = 0.78 .$$

Angstrom and Asklof have shown that there is a simple linear relation between the effective outward radiation when the sky is clear, R_0, and when the fraction $w/10$ of the sky is overcast, R_w;

$$R_w = R_0\left(1 - \frac{kw}{10}\right). \qquad (12)$$

The value of k depends upon the type of cloud: for low clouds 1 to 2 km above the ground (stratus, nimbus, stratocumulus) $k = 0.9$; middle clouds (altostratus at 3 km) $k = 0.7$; very high clouds (cirrostratus and cirrus, at about 7 km) $k = 0.2$.

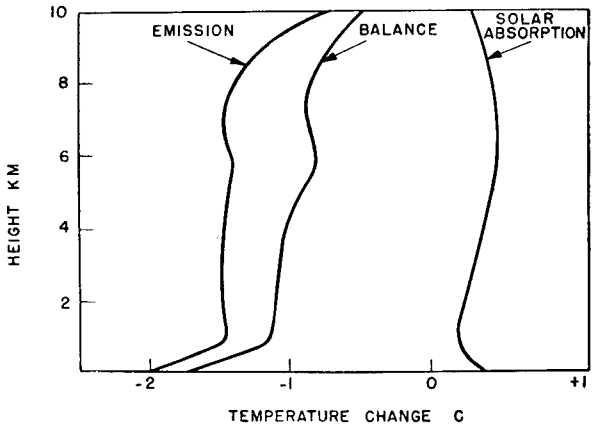

FIGURE 5. Heat balance of the free air over Ludenberg in June, clear sky (after Möller).

The atmospheric counterradiation must depend upon the mass of the atmosphere and therefore decrease with elevation. Angstrom gave the following data, but it should be kept in mind that they represent average conditions and are subject to variation with changes in temperature and humidity.

Elevation, meters	0	1,000	2,000	3,000	4,000	5,000
Counterradiation, cal per min per sq cm	0.44	0.37	0.31	0.25	0.21	0.18

The net outward radiation also depends upon elevation. Absorption diminishes as the amount of water vapor in the atmosphere (above) decreases, but at the same time the outward radiation decreases as the water vapor decreases, and also as the temperature

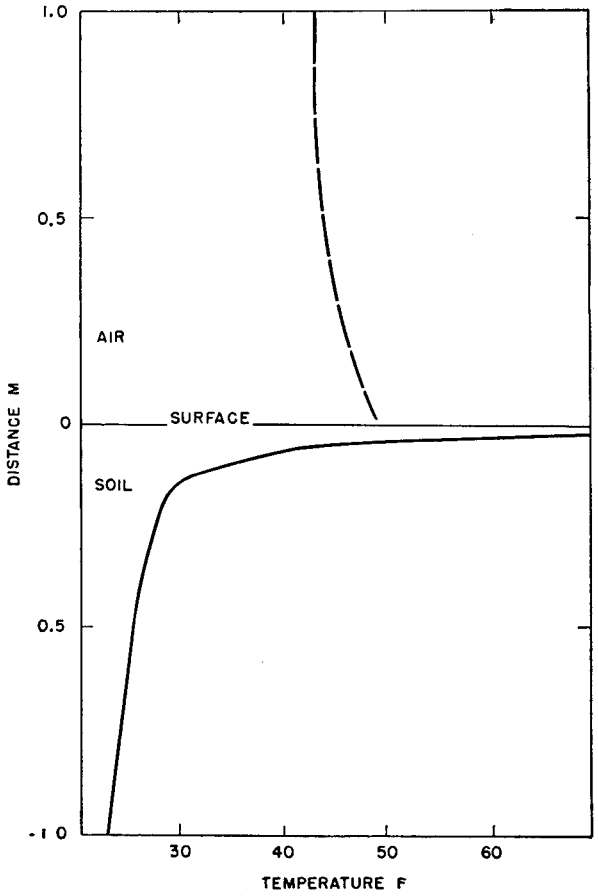

FIGURE 6. Vertical distribution of temperature in air and soil (midday).

falls with elevation. As a result of these opposing factors, there is a maximum in the effective outward radiation at elevations around 2,000 to 3,000 meters above sea level. The ground surface gains energy from the solar radiation, but the net effect of radiation on the atmosphere is always cooling.

Figure 5 (from Möller) indicates the radiation balance on a clear day. With clouds present, the situation is markedly altered as water particles check the outward flow of radiation and increases the counterradiation of the atmosphere.

14.4 GROUND TEMPERATURES

The black-body temperature corresponding to maximum energy density of the solar rays on the earth's surface, 0.62 × 1.93 cal per min per sq cm (that is, sun directly overhead and corrections made for scattering), is 347 K or 74 C. The theoretic maximum may exceed this value as a clear dustless sky may transmit more than the assumed 62%. Maxi-

mum ground surface temperatures have been reported of 71.5 C at the Desert Laboratory, Tucson, Arizona, and 69 C in Agra, India.

Results of Sinclair at the Desert Laboratory in Tucson, Arizona, are given in Figure 6 to illustrate air and earth gradients with respect to the ground surface.

It is observed that the temperature falls rapidly in the soil below the surface. In fact this rapid falling off makes it very difficult to measure surface temperature accurately. At the surface there is a discontinuity between the air temperature and the surface temperature. At least there is a region in which no accurate measurements of the air gradient have been made, and from the very nature of the problems the convection air currents must be such as to render the temperature indefinite.

The surface temperature is obviously a function of the rate of transfer of heat to the air and the conductivity of heat down into the soil. The first of these depends upon the velocity of the air and its turbulence. The conductivity of the soil and other surface materials varies greatly. Values for various substances are given in Table 1.

TABLE 1. Heat conductivity (cal per cm sec C).

Air 0 C	5.6×10^{-5}
Basalt	5.2×10^{-3}
Clay	2×10^{-3}
Concrete	2.2×10^{-3}
Diatomaceous earth	0.13×10^{-3}
Brick	1.1×10^{-3}
Granite	8.2×10^{-3}
Gypsum	3.1×10^{-3}
Paper	0.3×10^{-3}
Peat	0.4×10^{-3}
Snow	0.1×10^{-3}
Soil (heavy)	1.5×10^{-3}
Soil (light)	0.7×10^{-3}
Water	1.3×10^{-3}
Wood	$0.4 - 0.8 \times 10^{-3}$

Because of the low conductivity of air, types of ground which contain high proportions of air show low heat conductivity. The conductivity of grass and other vegetation is also low and it is noted from the table that the value for snow is the lowest listed.

If two substances have the same albedo but differ in thermal conductivity, the substance with poor conductivity will be heated to a higher temperature by the solar radiation in the day time and will be cooled to a greater degree by the thermal radiation at night. Thus the diurnal variation in temperature will increase in the following order: granite, concrete, clay, heavy soil, light soil.

The variation will be greater over grass than over bare soil. Snow forms a highly insulating blanket, but at night the surface temperature of the snow will fall more rapidly than ordinary ground. In the daytime, snow reflects such a high fraction of the sun's radiation that it does not show an abnormal heating. The effect of the low conductivity of wood is noticeable on frosty mornings when the coating of frost will be much heavier on a board walk than on a concrete walk.

The presence of moisture on the surface greatly reduces the diurnal temperature variations. If the soil is moist, part of the energy which would otherwise heat the soil will be expended in vaporizing the water. This effect increases with the porosity or water content of the surface material. Thus, for granite the effect is slight, for moist sand, half of the radiant energy may be so expended, and for peat as high as 80% of the energy may be used up in this way. The process of vaporization essentially transfers the energy to the atmosphere as the subsequent condensation of the water vapor will again release the equivalent energy.

The effect upon night radiation cooling is not so direct, since a moist surface may be an effective black-body radiator. However, if the atmosphere is near saturation, the cooling of the surface results in the formation of dew or frost and the heat liberated on condensation will increase the surface temperature.

Diurnal temperature variations of the ocean's surface are small, about 1 degree C being the maximum change between day and night. The solar radiation is not absorbed on the surface as in the soil, but penetrates to a considerable depth before the absorption is complete. Thus the heat is distributed over a large volume of water with a correspondingly small rise in temperature. However, in very shallow pools, the sand on the bottom will absorb the radiation and transmit it to the water so that in this case appreciable temperature rise may result.

At night, the surface radiates its corresponding temperature radiation but as the temperature of the surface decreases, the increase in density causes the surface water to sink, and thus again, the total heat change is distributed over a large column.

14.4.1 Albedo Effect

An average value for the solar radiation reflected and scattered by the earth's surface has been given

as 38%. The specific effect for various types of substances is obviously an important factor in determining the surface temperatures and accounting for thermal differences which exist along the horizontal. The albedo (ratio of reflected to incident radiation) for a number of substances is given in Table 2.

TABLE 2. Albedo values for various materials.

Material	Dry	Wet
Black soil	0.14	0.08
Granite	0.14	...
Sand	0.18	0.09
Short grass	0.25	...
Tall grass	0.32	0.22
Old snow	0.70	...
New snow	0.81	...

14.5 CONVECTION, TURBULENCE, AND GUSTINESS

Turbulence and convection are more important in the transfer of heat in the atmosphere than is radiation. Petterssen estimates that, under normal conditions, eddy transfer of heat is about 100 times as large as the radiative transfer. Most of this eddy transfer occurs in the daytime under high lapse conditions.

The vertical movement of unstable air is called convection. Whenever the temperature gradient exceeds the dry adiabatic lapse rate, the air is unstable and should rise, but actually no overturning occurs unless a considerable impulse is applied. Thus, very near the ground, the lapse rate may be 800 to 900 times the adiabatic.

Geiger gives the following calculation of the acceleration of a parcel of air which has a temperature gradient of 0.84 degree between the heights 5 and 10 cm. Expressing g, the acceleration of gravity in meters per square second and t, the time in seconds, the acceleration in meters per square second is:

$$\frac{d^2z}{dt^2} = g\frac{T - T'}{T} . \qquad (13)$$

If the particle is lifted from the 5-cm level to the 10-cm level and T is 300 K,

$$\frac{d^2z}{dt^2} = 980\frac{0.84}{300} = 2.8 \text{ cm per sec}^2 . \qquad (14)$$

The particle, displaced only 5 cm from its original position, would move 1.4 cm in the first second and after 4 seconds would be 0.25 m above its original position. The acceleration would increase so that these values are too small. At these velocities an adjustment to the temperature of the surroundings is not probable with parcels of any considerable volume. However, the very existence of superadiabatic lapse rates argues that an initial impulse must be given to start the upward movement.

The initial impulses may be regarded as due to (1) unequal heating, and (2) wind. Natural surfaces are neither smooth nor homogeneous in material. Differences in reflectivity, radiation, blackness, and heat conductivity, as well as sunny and shady sides of surfaces, will give rise to temperature differences, and gravity differences in the horizontal will be converted into up and down movement. These differences in density may be observed visually over heated ground in the middle of the day as the familiar shimmering of the air.

Air is seldom at rest and the friction and roughness of the earth's surface tend to convert any horizontal motion along the surface into turbulent motion. Under lapse conditions, these impulses provide the initial displacements necessary to set up convection currents, and thus break down the high superadiabatic lapse rates. At high wind speeds on a clear afternoon the lapse rate will tend to approach the adiabatic rate. Under inversion conditions the stability of the air tends to damp out vertical displacements, but if the wind is high much irregular movement will be present. This is frequently referred to as *turbulent motion.* The effect of turbulence is to carry the slower moving air upward and to replace it by faster moving air from above. In this way the ground speed is maintained. As indicated, turbulence is at a minimum with low wind velocity under inversion conditions.

Taylor sought to express the power of eddies for the diffusion of heat as a constant K, the eddy diffusivity which is roughly proportional to $0.5wd$, where w is the vertical component of velocity in the eddy and d the mean diameter of the eddy. K varies from 10^3 to 10^5 cgs units, depending upon the nature of the surface and the atmospheric stability.

Schmidt introduced the idea of the Austausch coefficient, A, to represent the behavior of groups of turbulence bodies. From a consideration of the turbulent convection of heat, the coefficient is seen to be analogous to k/σ, the ratio of the heat conductivity to the specific heat. Its magnitude may be evaluated from the change of temperature with height.

$$A = \frac{\pi\rho}{T}\frac{\ln(x_2 - x_1)^2}{\ln \delta_1 - \ln \delta_2} , \qquad (15)$$

where x is height, δ temperature, and ρ density. Geiger gave the following values for A from observations at Schleissheim in the middle of the day.

Height (cm)	A
140	0.015
100	0.010
50	0.0028
20	0.0005
10	0.0002
0	0.000

For pure heat conductivity

$$\frac{k}{\sigma} = \frac{0.000048}{0.238} = 0.0002 \cdot \qquad (16)$$

Thus, at the ground, A is zero because there is no vertical turbulence. Just above the surface it is the same magnitude as k/σ and it increases with height.

Components of gustiness are defined in a Cartesian coordinate system as

$$G_x = \frac{|\overline{u'}|}{\bar{u}}, \quad G_y = \frac{|\overline{v'}|}{\bar{v}}, \quad G_z = \frac{|\overline{w'}|}{\bar{w}}, \qquad (17)$$

where $\bar{u}$ is the average x component of the wind velocity, the direction of x being the mean wind direction, and u', v', and w' are the differences between the instantaneous and average values of the x, y, and z components of the velocity, respectively.

The vertical component of gustiness is obviously significant in the transfer of momentum, or heat, or dust and smoke particles from the lower to the higher altitudes; experimental observations confirm this correlation. However, the measurement of these components involves peculiar difficulties. A bilateral vane described by Best gives a fair approximation to the relative values of the horizontal and vertical components.

Best has discussed the effect of stability and wind speed upon gustiness. For low wind speeds (0.5 to 1.0 m per sec) gustiness is much less during inversions than during heavy lapses, and the same is true for speeds between 1.0 and 1.5 m per sec. For speeds between 1.5 and 4 m per sec the effect is much smaller, and for higher speeds there appears to be no variation with changing temperature gradient. For lapses less than 0.9 degree F and for inversion, the gustiness in both lateral and vertical directions increases with wind speed. The small gustiness is maintained for higher speeds in the greater inversions. The ratio G_y/G_z appears to be independent of temperature gradient but decreases slightly with increasing speeds. Best gave a value of 1.81 as an average for this ratio. Additional data on the correlation of gustiness with wind and temperature gradients are given in Table 3.

14.6 WIND FLUCTUATIONS

A fluctuation or eddy velocity may be defined by the equation

$$u' = u - \bar{u}, \qquad (18)$$

where u is the instantaneous velocity and $\bar{u}$ the average velocity. Best has studied the mean value of the fluctuation ratio

$$\bar{g} = 100\,\frac{|\overline{u'}|}{\bar{u}}, \qquad (19)$$

which is the ratio of mean eddy velocity to mean velocity, expressed on a percentage basis. His data indicate that $\bar{g}$ decreases as the temperature gradient changes from lapse to inversion and the effect is more marked at low velocities than at high velocities.

14.6.1 Wind

Gradient wind is defined as the speed of the air at which the deflective force, due to the rotation of the earth, and the centrifugal force jointly balance the horizontal pressure gradient. The direction of the gradient wind is along the isobars and, at heights sufficiently great to be unaffected by surface friction (2,000 ft), its value may be calculated with considerable accuracy from the pressure gradient and the latitude of the station. For a general equation, see any standard text on meteorology.

Closer to the ground, frictional forces cause the *surface wind* to blow between 20 and 30 degrees across the isobars toward the low pressure center. The speed at 30 ft will be about half the gradient wind, depending upon the stability of the air, roughness of the surface, and local topography.

At heights between 10 and 400 m, the variation of wind speed with height is given fairly accurately by the equation of Chapman

$$u = a \log h + b, \qquad (20)$$

where a and b are constants dependent upon a given time and place.

For speeds near the ground, Sutton derived the expression

$$\frac{u}{u_1} = \left(\frac{h}{h_1}\right)^{n/(2-n)}, \qquad (21)$$

in which n is a constant varying from 0 to 1 with an average value about 0.25. The value of n depends upon the stability of the atmosphere and the roughness of the surface. Best states that a power law can be used provided only a shallow layer is considered,

TABLE 3. Correlation of temperature gradient, velocity gradient, and gustiness components over long grass in Sacramento Valley.

u_{2m}	$\frac{u_{2m}}{u_{1m}}$	$\frac{u_{4m}}{u_{1m}}$	ΔT,F		G_y	G_z	Time
mph			2m–1m	6m–3.5m			
4.5	1.12	1.29	−0.4	−0.2	0.67	0.43	7:18 p.m.
5.5	1.13	1.43	−0.4	...	0.57	0.38	7:44 a.m.
5.6	1.16	1.44	−0.3	−0.2	0.70	0.46	7:19 a.m.
6.7	1.17	1.37	−0.4	−0.2	0.90	0.45	3:00 p.m.
5.2	1.17	1.42	−0.8	−0.6	0.52	0.42	3:40 p.m.
5.9	1.19	1.33	−0.4	−0.4	0.66	0.43	7:49 a.m.
5.6	1.23	1.23	0.0	0.0	0.58	0.43	6:53 a.m.
6.2	1.24	1.55	0.5	0.3	0.70	0.52	8:45 p.m.
9.3	1.25	1.54	0.3	0.2	0.63	0.48	8:45 p.m.
4.3	1.25	1.53	0.6	0.3	0.58	0.36	10:23 p.m.
5.3	1.25	1.59	0.4	0.3	0.60	0.44	8:18 p.m.
5.9	1.29	1.63	0.6	0.5	0.58	0.40	8:48 p.m.
4.3	1.31	1.74	0.5	0.6	0.50	0.40	9:43 p.m.
3.5	1.35	1.91	0.5	0.8	0.41	0.27	5:48 a.m.
3.5	1.39	1.73	1.0	0.6	0.59	0.24	11:04 p.m.
3.4	1.43	1.98	1.0	1.1	0.32	0.23	10:00 p.m.
4.0	1.45	...	0.9	2.6	0.28	0.16	10:45 p.m.
3.2	1.50	2.08	0.9	0.7	0.32	0.23	9:46 p.m.
3.0	1.53	2.32	1.6	2.3	0.32	0.22	9:20 p.m.
3.2	1.66	2.78	1.8	2.7	0.21	0.15	9:56 p.m.
3.0	1.68	2.54	1.8	2.0	0.18	0.08	10:24 p.m.
3.5	>1.8	...	>5.0	1.5	0.08	0.0	9:58 p.m.
1.9	1.95	3.61	1.0	1.5	0.25	0.17	11:14 p.m.
4.0	2.2	4.6	..	..	0.07	0.06	9:26 p.m.

and that the index for zero temperature gradient may vary from about 0.43 in the lowest layers to 0.13 at greater heights. This index can increase considerably during light winds and big inversions.

If the wind at two levels is different, a frictional stress, τ, which is a function of the velocity gradient, is set up.

$$\tau = \nu \frac{du}{dz}, \tag{22}$$

where ν is the eddy viscosity of the air. For neutral conditions Rossby defines ν by the equation

$$\nu = 0.02\,(z + z_0), \tag{23}$$

where z_0 is the roughness coefficient, approximately one-thirtieth of the height of the roughness elements of the ground. The value of ν also varies with atmospheric stability and becomes smaller with inversion conditions.

Extensive investigations have been made of the dependence of the velocity gradient upon atmospheric stability. In many of these measurements the wind speeds have been determined at heights of *two* and *one* meters and the ratio determines the so-called *R value*,

$$R = \frac{u_2}{u_1}. \tag{24}$$

The effects of temperature gradient upon the R value over short grass at Leifield were summarized by Best.

1. For light winds (less than 1.5 m per sec), R is about 1.06 for lapses of 1 degree C per m or greater; R is about 1.35 for inversions of 1 degree C per m, and R varies linearly for lapse rates between −1 degree C per m and +1 degree C per m.

2. For moderate winds (1.5 m per sec to 4.0 m per sec) R varies from about 1.08 to 1.16 from lapse to inversion conditions.

3. For strong winds (4.0 to 8.0 m per sec) R is approximately constant at about 1.11.

It should be emphasized that this summary applies to short grass and level surfaces. The R values increase with the roughness of the surface and will increase by some 0.05 unit as the grass length changes from 2.0 to 4.5 cm.

An extensive study of R values, temperature coefficients, and gustiness was made in the Sacramento Valley. The surface was flat and covered with high dry grass which was bent over. The data are summarized in Table 3. The following points will be noted. High values for R occur with high inversion. High inversion existed only at wind speeds of 4 mph or under. Both G_y and G_z decrease with inversion conditions. The correlation of R values and temperature gradients is shown graphically in Figure 7.

TABLE 4. Wind speed at various heights over flat open country of different surface roughness. (In all cases wind speed is 1.00 in arbitrary units at 30 ft.)

Surface roughness	High lapse low or moderate wind				Neutral or very high wind				High inversion low wind			
Height in ft	20	10	6	3	20	10	6	3	20	10	6	3
Smooth snow field					0.99	0.94	0.89	0.81	0.97	0.87	0.81	0.69
Close cropped grass	0.97	0.90	0.86	0.80	0.95	0.84	0.77	0.68	0.88	0.68	0.53	0.44
Grass 12 to 24 in. high	0.93	0.79	0.68	0.50	0.92	0.75	0.65	0.48	0.86	0.63	0.50	0.32
Desert brush 2½ ft high and 4 ft diameter covers 10 — 20% of ground					0.90	0.71	0.60	0.43				

Best found that, for low lapse and inversion, R increased with decreasing wind speeds, but for lapses greater than 0.9 degree F per m the velocity gradient increased with increasing velocity. He concluded, "The chief factor which tends to minimize velocity gradients is mixing due to turbulence and it appears that mixing accompanying high lapse rate is greatest when there is little or no wind."

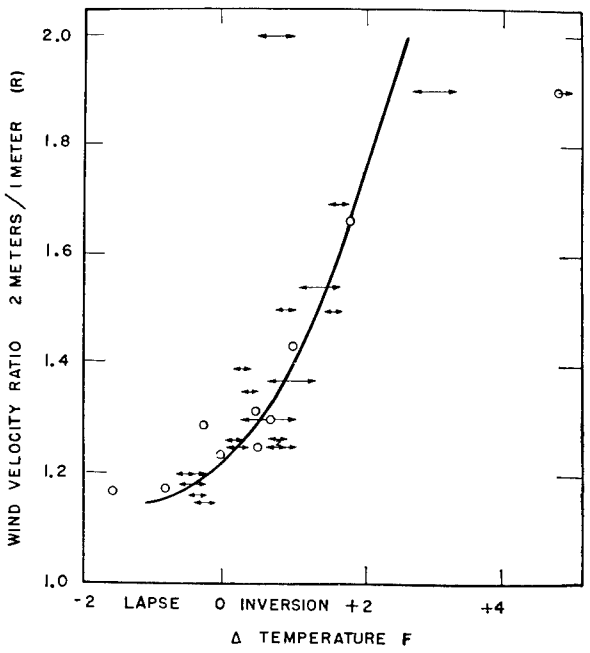

FIGURE 7. Wind velocity ratio versus temperature gradient.

Dickinson, Gilman, and Johnston have given a table[6] of factors by which the wind speed at heights of 20, 10, 6, and 3 ft over various surfaces and under lapse, neutral, and inversion conditions may be predicted from the value at 30 ft. This table is useful since the speed at 30 ft is normally given by the Air Corps forecast. The influence of the various factors are in agreement with principles already discussed.

14.6.2

Gravity Winds

Under inversion conditions, the surface layer of air on a slope is colder and heavier than the air on the same level away from the surface. The surface air then tends to flow down the slope under a force,

$$f = gw \sin \theta, \tag{25}$$

where g is the acceleration of gravity, θ the angle of slope, and w a factor that depends upon the difference in density between the air in the surface layer and that of the free atmosphere at the same level. A steady state is usually reached in which

$$gw \sin \theta = kv^n, \tag{26}$$

in which k is the coefficient of friction as the surface air moves with the velocity v, and n is a numerical exponent. This gravity flow is also known as mountain wind, canyon wind, or *katabatic wind.* These winds show their greatest development over high snow-covered mountains or gently sloping plateaus such as exist in Greenland or the Antarctic Continent. In these regions katabatic wind speeds of 100 to 200 mph occur. However, on most slopes these flows are normally only a few miles per hour and the air currents quite shallow. Latimer, Ruben, Gwinn, and Norris studied the katabatic currents which exist on clear nights on the slope of Mt. Shasta at a distance about ten miles from the summit. The slope at the site was approximately 2%. The data in Table 5 illustrate the type of velocity and temperature gradients which normally existed.

TABLE 5. Temperature gradient and wind speed at base of Mt. Shasta 11:27 p.m., August 27, 1943.

Temperature gradient	Wind speed at various heights	
	Height, m.	Miles per hour
$T_{2m} - T_{1m} = 1.5$ (inversion)	1	1.69
$T_{3.5m} - T_{2m} = 1.3$	2	1.55
$T_{6m} - T_{3.5m} = 1.9$	4	1.32
$T_{9.4m} - T_{6m} = 0.7$	8	1.08
		$R_{2m/1m} = 0.92$

It will be observed that the air next to the ground is moving more rapidly than at higher levels and that the R value is less than unity. This occurred in spite of the inversion present, so it is obvious that R cannot be used as a measure of stability under these conditions.

Light gravity winds may occur on the shaded side of a mountain in the afternoon. In general, it may be stated that gravity flow of air under inversion conditions tends to follow the natural water flow from the area. Both the depth and speed of the stream will be greater down ravines, canyons, and river beds. An example of aerial drainage down a narrow canyon is the fierce wind which sometimes develops in Santa Ana Canyon in Southern California during a high-pressure area over the mountains. At night, level valleys surrounded by high mountains tend to fill with cold air, often up to well-defined levels which are known as *thermal belts.*

In the daytime, high lapse conditions on mountain slopes give rise to upward surface convection currents or *anabatic winds.* The following effects were described by Jelinek from experiments with theodolite balloons on the slope winds of a mountain 1,100 m high near Innsbruck, Germany.

1. Upslope winds developed from 15 to 45 min after sunrise.

2. Speeds were greatest (max 3.7 m per sec) and depth of upslope wind layer highest (max 280 m) on the south slope. The north slope also showed the least development both in speed (max 1.6 m per sec) and depth of layer (max 170 m).

3. The speed and depth of layer of the upslope winds increased steadily during the morning to a maximum before noon, decreased toward noon with the development of cumulus clouds on the top of the mountain, increased in the afternoon when the clouds drifted away and decreased to zero near sunset.

4. Both uphill and downhill winds are best defined when the pressure gradient over the area is small.

Wexler has given the following examples of valley winds in the region around Dugway Proving Ground.

1. Dugway Proving Ground has a general drainage from the mountains to the east and southeast. During the early morning the winds are prevailingly from the southeast. During the afternoon the winds are from the northwest direction up the area toward the mountains. A tendency has been observed for the direction of the wind to follow the sun in the morning. This can be explained by the fact that the slopes facing the sun receive more heat than other slopes, causing a rising air from the slopes and a thrust of air from the valley toward these slopes. The southeast winds in the morning are light, averaging less than 5 mph.

2. During the afternoon, the northwest winds are slightly stronger, averaging about 8 mph during the summer months. With cloudiness during the morning, the shift from southeast to northwest may be delayed. Strong pressure gradient or storms in the vicinity will overcome the diurnal cycle of winds. The depth of these local winds are in the vicinity of 2,000 ft.

14.6.3 Land and Sea Breezes

As a result of the comparative constancy of the ocean temperature, it can happen that during the day the air over the land heats above the temperature of the air over the ocean, and during the night cools below it. In daytime the hot air over the land may rise and be replaced by air flowing in from the sea. Such a wind blowing *from* the *sea* is called a *sea breeze*; the wind that blows similarly *from* the *land* at night is called a *land breeze.*

Both land and sea breezes are shallow and do not extend many miles from the shore. The sea breeze is likely to be rather stronger than the land breeze. The former generally reaches 10 to 25 miles inland but the latter seldom extends more than 5 to 6 miles to sea. If hills come near the shore line, the land and sea breeze effect can combine with the mountain and valley effect. Land and sea breezes are most prominent when strong radiation effects occur along with weak general winds; they are often important in the tropics.

The thermal stability of the air near a coast line needs special consideration. The ocean surface is much more constant in temperature than the land surface. When air flows landward or seaward it may flow from a region where one stability condition prevails to a region where there is a different stability condition. For example, if approximately neutral air from the ocean moves inland over a sunny beach, a short travel (for instance, 50 ft) may suffice for the development of a distinct lapse in the lowest foot or two of the air. If a very small flat island is being considered, air may move entirely across the island, retaining its neutral structure in all but the lowest levels. Even if the air is moving in over a large land surface, an examination of the temperature gradient

in the lowest levels alone will give misleading information concerning the thermal stability unless the air has moved a sufficient distance over land to modify all the levels of interest. Similar remarks apply to air moving out from land over water.

A small island can modify the turbulence and the thermal stability of the lowest layers of air; but the land and sea breeze effect may be unimportant even on larger islands. On a wooded tropical island 5x7 miles, the land and sea breeze effect was difficult to detect; and this was in the region of the doldrums. The size that an island must have in order to show land and sea breeze effects evidently depends on the magnitude of the general wind and on radiation conditions as well as on the mountainous or flat character of the topography.

14.7 THE EFFECT OF AIR MASS CHARACTERISTICS

An air mass which has moved from a cold area to a warmer area will be heated from below and thus become unstable. This instability will be a maximum

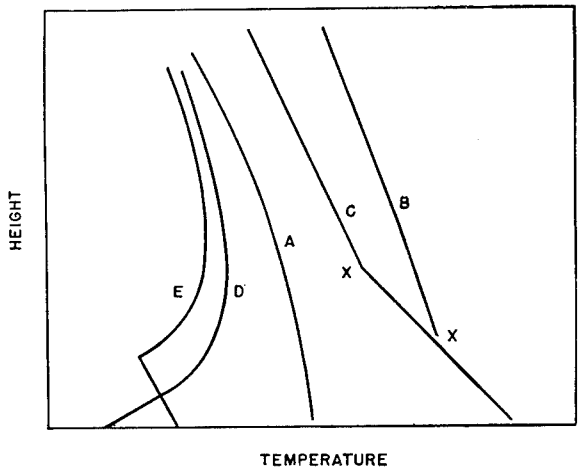

FIGURE 8. Types of temperature-height curves in traveling air masses. A, initial curve; B, after travel over warmer ocean; C, after travel over warmer continent; X, condensation level; D, after travel over a colder surface, slight wind velocity (slight turbulence); E, after travel over a colder surface, high wind velocity (strong turbulence).

in the afternoon and a minimum at night, when a radiation inversion may be set up if the area is land. Over ocean the diurnal effects will be slight.

Conversely, an air mass which travels toward a colder area will be cooled from below and develop stability in the surface layers. Since turbulence will be a minimum, convection will be small and the effects of cooling will be confined to the lower levels.

Petterssen,[12] in discussing Figure 8, notes that "the development from A to B results in numerous convective clouds and a low condensation level, whereas the development from A to C results in a smaller number of convective clouds at a considerably higher level. The development from A to D usually results in formation of fog, whereas the development A to E results in formation of stratus or strato-cumulus below the base of the inversion." It should also be noted that case E is important in smoke screening as the smoke will tend to rise and level off at the base of the inversion.

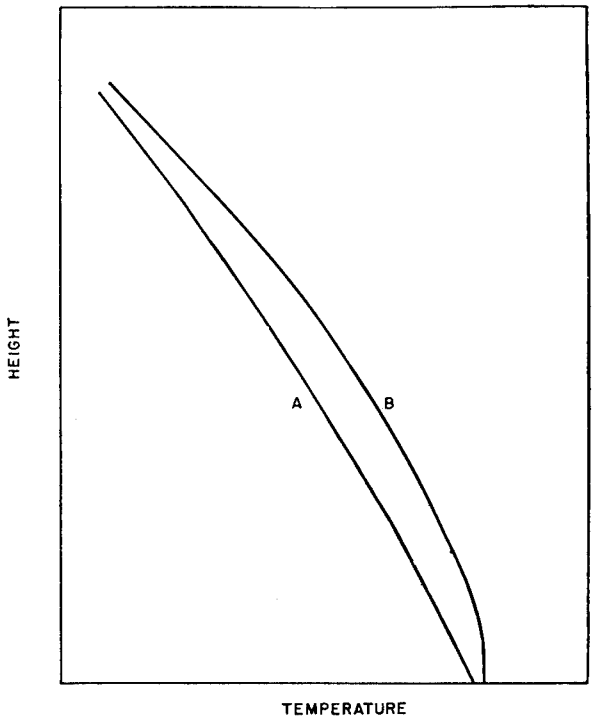

FIGURE 9. The diurnal variation in stability over oceans: A, night; B, day.

Subsidence in high pressure areas may produce inversions and intensify existing inversions. These effects are often difficult to recognize from temperature measurements alone but are disclosed by the vertical distribution of humidity. Petterssen has given the data in Figure 10.

The relative humidity in the inversion layer near the ground is always high. If the inversion is produced by surface radiation alone, there is no rapid decrease in the humidity above the inversion layer.

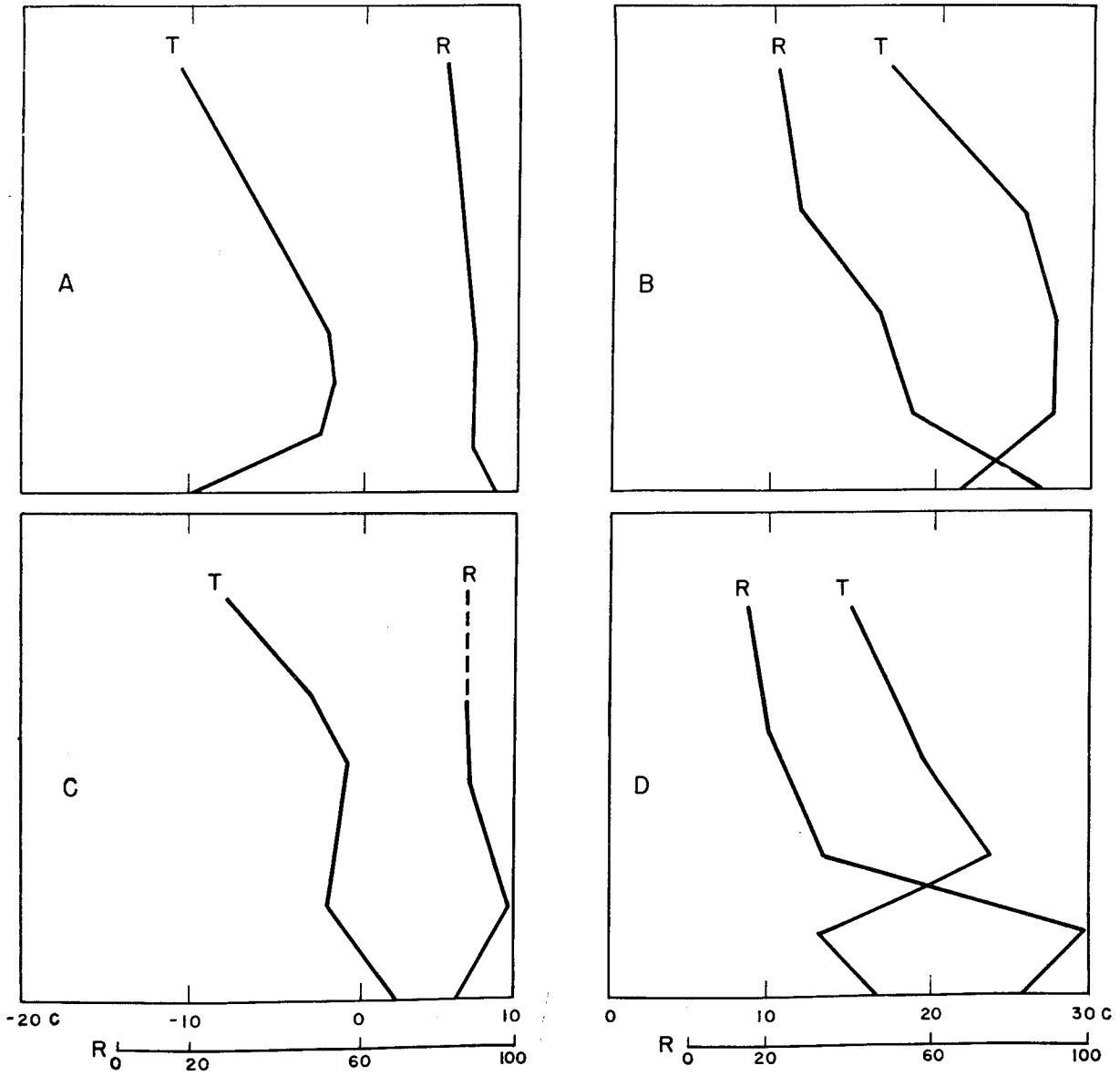

FIGURE 10. Types of inversions. A, Kjeller, 21 Feb. 1938, inversion produced by cooling from below; B, Fargo, 27 July 1938, inversion produced by subsidence aloft and cooling from below; C, Mildenhall, 17 Dec. 1938, inversion produced mainly by cooling and turbulent mixing; D, San Diego, 6 Oct. 1938, inversion produced by subsidence aloft and heating and turbulent mixing below.

In the case where subsidence is a factor the descending cold air is dry and the humidity will fall rapidly with increasing altitude.

Since the wind normally increases with elevation, advection of air aloft may alter the stability of the atmosphere over an area. However, conditions are rarely favorable for potentially colder air to overrun potentially warmer air, but, if the air temperature decreases in the direction opposite to that of the wind, this type of instability may be produced. In cold fronts, cold air may overrun warmer air largely owing to the friction of the ground layer. Such conditions result in great instability and high turbulent winds.

14.8 CORRELATION OF CONTINUOUS MICROMETEOROLOGICAL OBSERVATIONS

Probably the most complete micrometeorological measurements in America have been made by Dr. M. D. Thomas of Salt Lake City, Utah, in connection

879245 O - 50 - 3

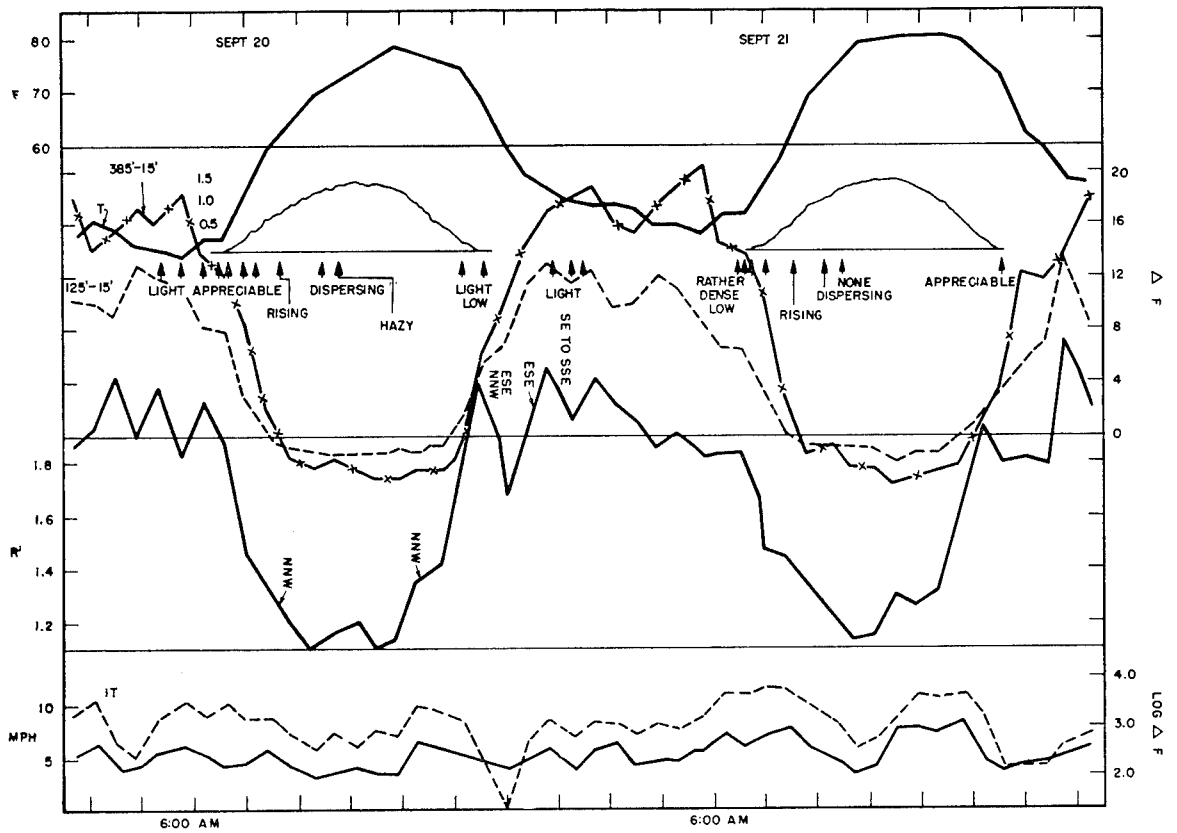

FIGURE 11. Typical daily recordings of meteorological data.

with smoke problems in that region. The work was undertaken by the American Smelting and Refining Company and was supported in part by Division 10, NDRC. A discussion of these measurements will be given as an illustration of the principles presented in this chapter. Some of the conclusions are based upon a study of the Thomas data.[20]

The data consist of the following elements.

1. Continuous temperature records (10 ft above ground).
2. Temperature differences for the intervals: 110 to 10 ft, 220 to 10 ft, 330 to 10 ft, 440 to 10 ft. (After August 1943 the intervals were for the heights: 15, 125, 255, and 385 ft.)
3. Wind direction.
4. Wind speeds at 7 m, 2 m, and 1 m.
5. Pyroheliometer traces.
6. Degree of turbulence.

The above measurements are automatically recorded throughout the 24 hr of the day. Observations are also made on the density of smoke in the valley. From the data, continuous plots have been made of the various elements. Figure 11 is given as an example of this record. The items included on this chart are:

1. Temperature at 10 ft (top curve).
2. Intake of solar radiation in cal per min per sq cm (inserted curves).
3. Temperature differences for the height intervals 385 to 15 ft and 125 to 15 ft (second and third curves).
4. R' values. The ratio of the wind speed at 7 m to that at 1 m. R (2 m to 1 m) given in some instances (fourth curve).
5. Index of turbulence of the wind. Defined as the logarithm of the number of degrees per hour through which the wind vane rotates in one direction (fifth curve).
6. Wind speed (mph) at 7 m (sixth curve).
7. Smoke observations (noted on line below solar radiation).

A study of Figure 11 discloses the diurnal variations in temperature, temperature gradient, and wind gradient previously discussed in this chapter. In general ΔT and R' are high at night, due to the stability set up by radiation cooling, and are low in the

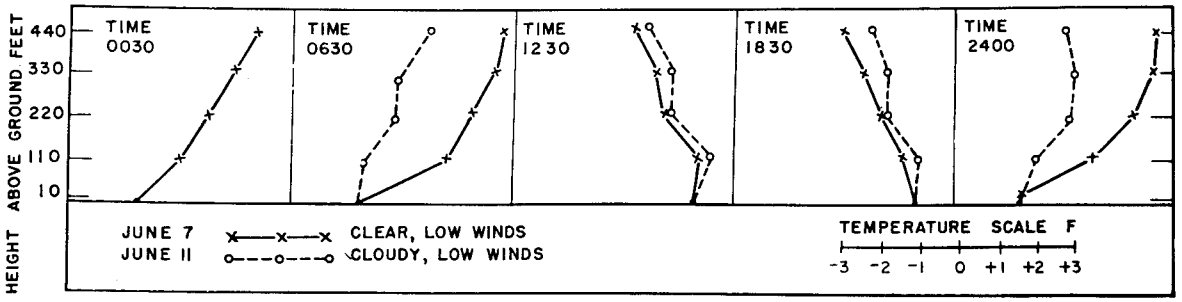

FIGURE 12. Temperature profiles for days in June.

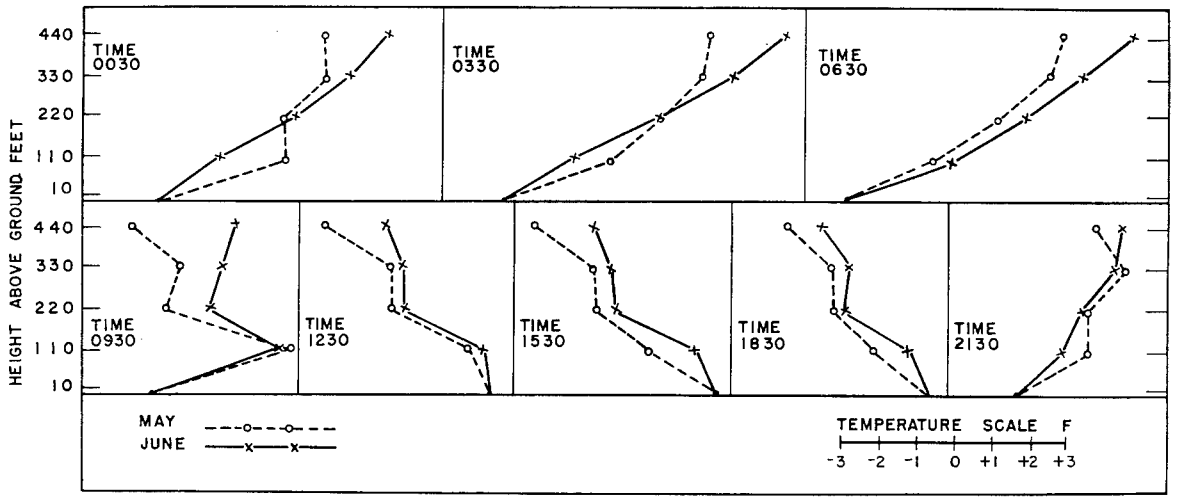

FIGURE 13. Temperature profiles for May and June, all weather.

daytime under the convection currents of high lapse conditions. The curves at ΔT and R' are roughly similar but there are certain interesting divergencies. Thus about 8 p.m. there is a sudden drop in R' without a corresponding large drop in ΔT. This appears to be due to a very shallow katabatic wind flowing down from the mountains and occurs with a change of the wind direction from northwest to southeast. In general, there is a close correlation between the wind speed and the index of turbulence; high turbulence is associated with high wind speed. A remarkable drop in the values of the index of turbulence is also associated with the shallow katabat, but as the katabat deepens and develops into a valley wind, the values of both the index of turbulence and R' again rise. An inverse relationship exists between R' and the index of turbulence but it is often masked by the effect of the wind speed upon both of these quantities.

The effect of clouds upon the temperature profile is illustrated in Figure 12. It will be observed that both the night inversion and the day lapse were greater on a clear day (June 7) than on a cloudy day (June 11). On foggy days ΔT is mainly lapse.

Figure 13 summarizes the average temperature profiles for the months of May and June 1943. May inversions terminated rather sharply at the 330-ft level, and the June inversions were stronger in general than those of May. On the other hand, the intensity of the lapse was greater in May than in June, which is not to be expected, but these data include all weather and the normal trends will be influenced by the wind velocity and number of cloudy days.

In Figure 14, the difference in the maximum temperature on the preceding afternoon and the minimum temperature before sunrise is plotted against the maximum inversion. It will be observed that the two quantities are roughly proportional; this is to be interpreted as the effect of temperature on the net nocturnal radiation loss. Thus, when the ground surface is hot, the radiation loss will be proportionally larger and the resulting inversion greater. The rate of cooling is probably the most important factor in

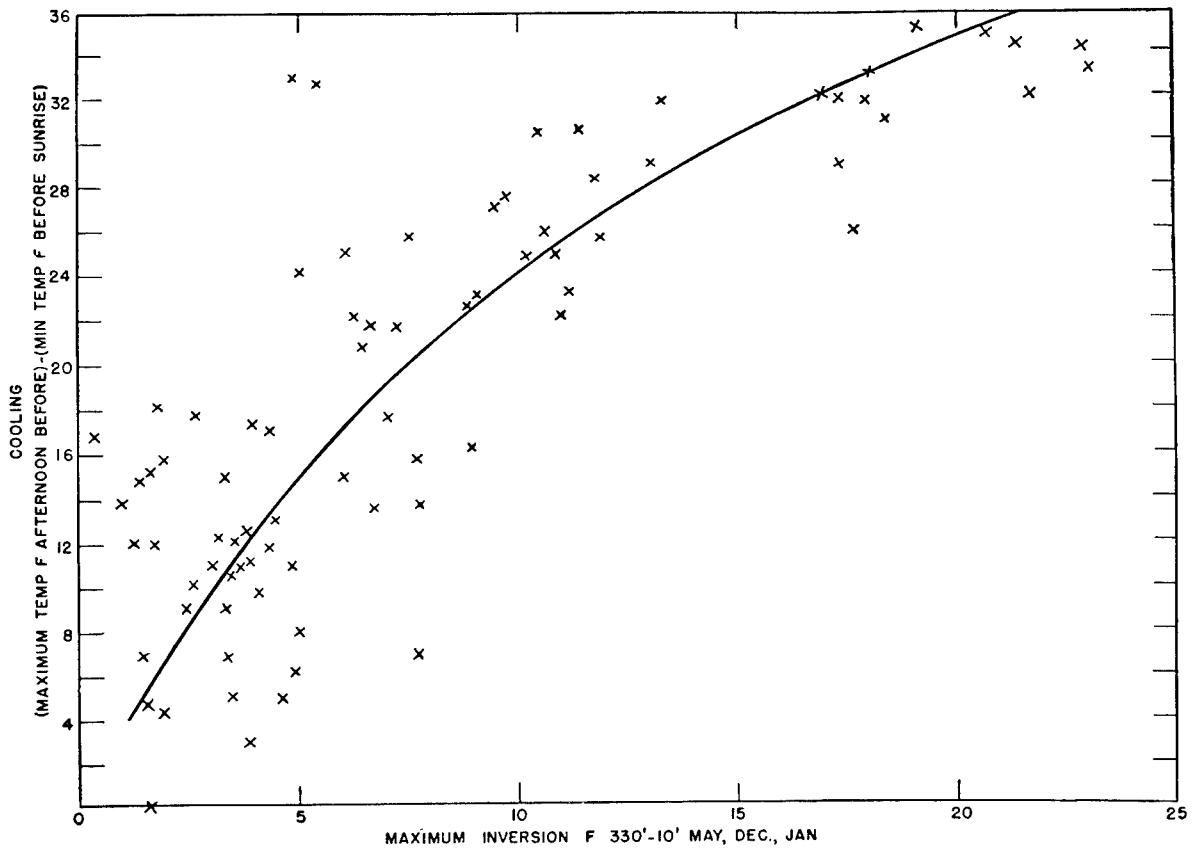

FIGURE 14. Plot of difference in maximum and minimum temperature against maximum inversion.

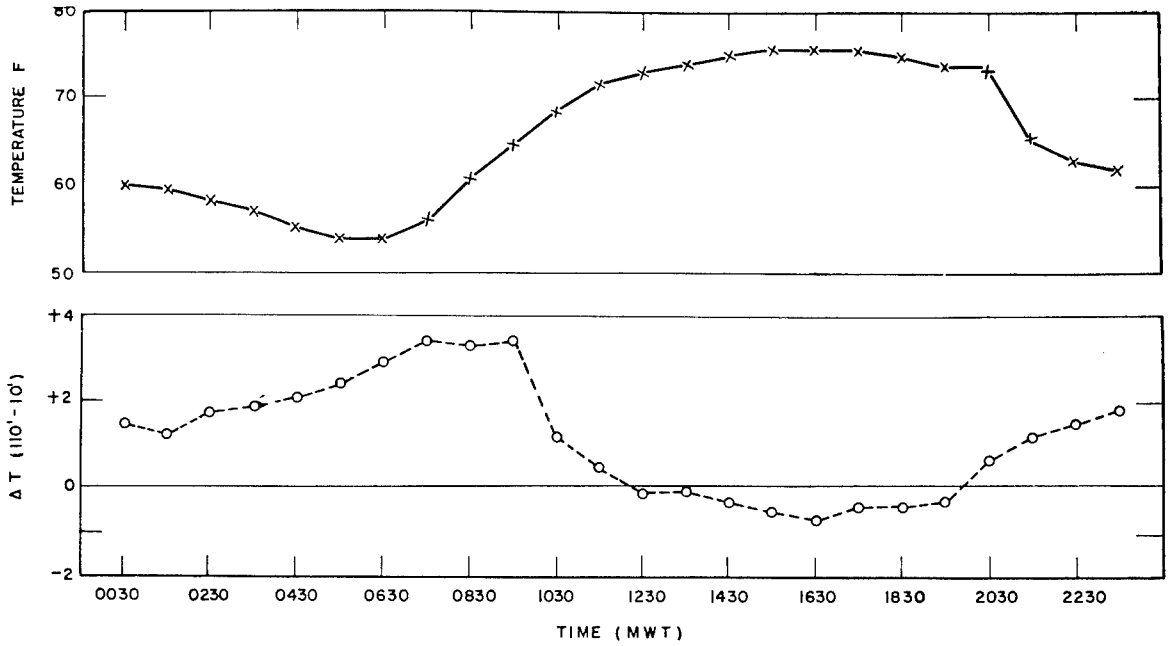

FIGURE 15. Diurnal temperature variations.

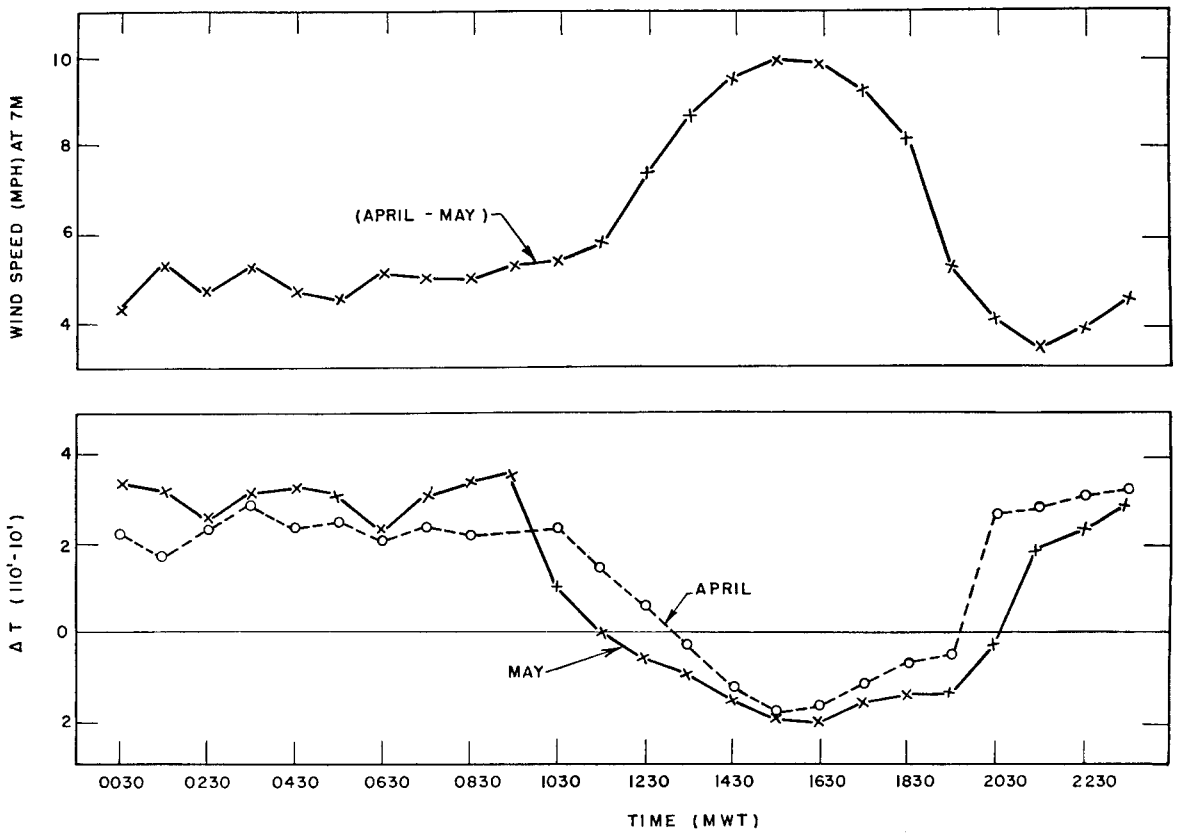

FIGURE 16. Wind velocity at ΔT on clear days.

determining the extent of inversion. The time of maximum inversion for small heights is generally after the period of most rapid cooling but for gradients over several hundred feet inversion may occur after the time of minimum temperature. The time of maximum lapse generally follows the time of maximum temperature closely. Figure 15 gives a comparison for T and ΔT curves for June.

Figure 16 is a plot of monthly average values of ΔT for hourly recording throughout the day and, for comparison, a plot of the corresponding hourly averages of the wind velocity. Figure 17 gives similar plots of R' and velocity. The conclusion might be drawn that inversion produces low winds and lapse high winds. While of course there are effects in these directions, it must be kept in mind that high winds tend to break down both inversion and lapse conditions to neutral. If the higher wind velocities had not existed during the day, the lapse values would have been considerably larger. The effect of wind speed upon stability is so great that it is frequently difficult to differentiate between the wind factor and radiation factor. This is illustrated in Figure 18, which gives R' values for a clear day with low winds in each of the months of April, May, and June. The inversions at night intensify as the days get hotter and the humidity of the desert region decreases. However, for the days chosen, the R' values under lapse conditions do not show the expected order.

The region around Salt Lake is so mountainous that orographic factors are usually more important than frontal activity or cyclonic convergencies. However, the air mass characteristics play an important role in determining the ground conditions. In the wintertime, high-pressure areas of stable marine polar air, or even continental polar air, prevail over Utah; subsidence occurs, wind velocities are low and smoke tends to accumulate in the valley in spite of the fact that nocturnal inversions are not so great as in the summer months.

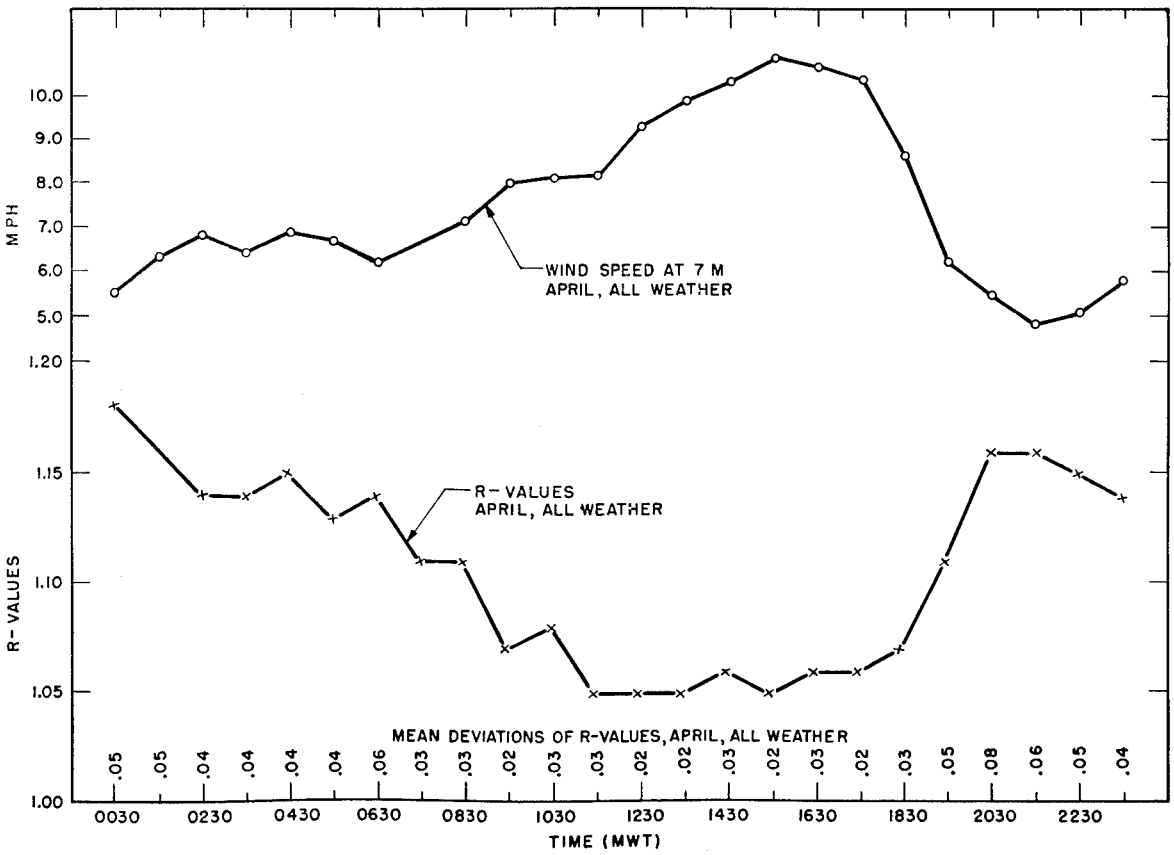

FIGURE 17. Diurnal variation in R values and wind velocities.

14.9 MICROMETEOROLOGY IN WOODED AREAS

14.9.1 General Considerations

For the sake of simplicity, wooded areas are treated here as distinct from open country. Actually there is no sharp demarcation between open and wooded terrain. There is, in reality, a continuous gradation in vegetation from close-cut grass to dense jungle. And there is also a continuous gradation in the complexity of meteorological factors. The same general principles apply to the air over and in a forest as do in the open. In the forest, however, emphasis has to be placed on the character of the vegetation and the effects it imparts.

The types and characteristics of wooded areas and their relation to climatic conditions will not be discussed in this report. In this section, the role played by meteorology is treated in relation to wooded areas in general. It must be left to the individual to apply the principles stated in the following text to the particular type of forest where operations are planned. Furthermore, the following sections dealing with wind, turbulence, and temperature are intended to apply to forests on level terrain. Important effects of topography have been treated elsewhere.

A great variety of vegetative covers can occur. For definiteness, remarks will be made with a particular type in mind; the effect of departures from this type can then be discussed. Consider a fairly dense jungle with a canopy of irregular height; the tops of the trees may be mostly at, for example, 30 to 50 ft. Suppose that there is a moderate amount of undergrowth and that little direct sun reaches the forest floor even at midday.

14.9.2 Wind Speed

WIND ABOVE AND IN CANOPY

The wind in the free air above a forest canopy has a somewhat reduced velocity because of the drag

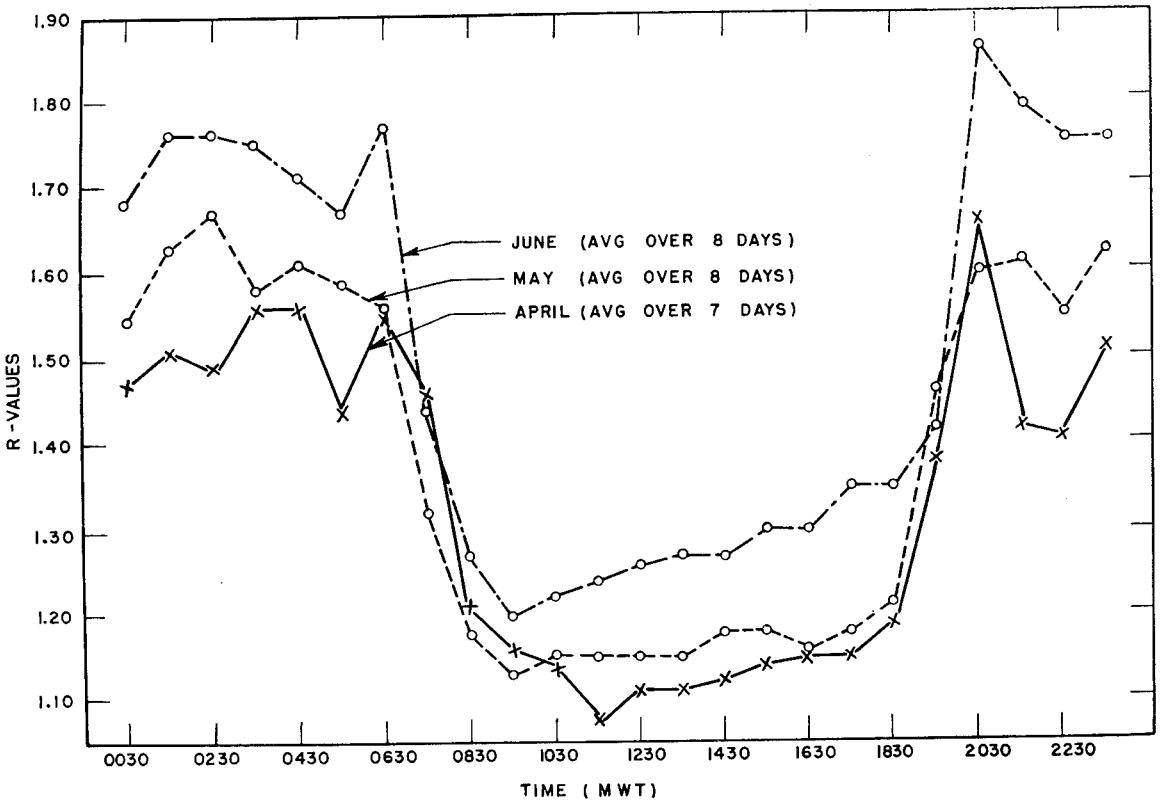

FIGURE 18. Diurnal variations in R' values.

effect of the comparatively rough surface offered by the canopy. On passing from the free air down into the tops of the tree-crowns, there is a large and sudden decrease in wind velocity. The heavier the forest growth, the greater is the magnitude of this decrease. Some typical wind profiles in a forest are shown in Figure 19.

WIND UNDER THE CANOPY

The winds below the tree-crowns are usually induced by the overhead wind. Under given thermal conditions the relation between the forest wind speed and that of the overhead wind is controlled by the thickness of the canopy and the development of the undergrowth. Speeds of greater than 2 mph below a moderate to heavy forest-cover are relatively infrequent. In fact, it is not uncommon to encounter speeds below ½ mph, particularly at night time.

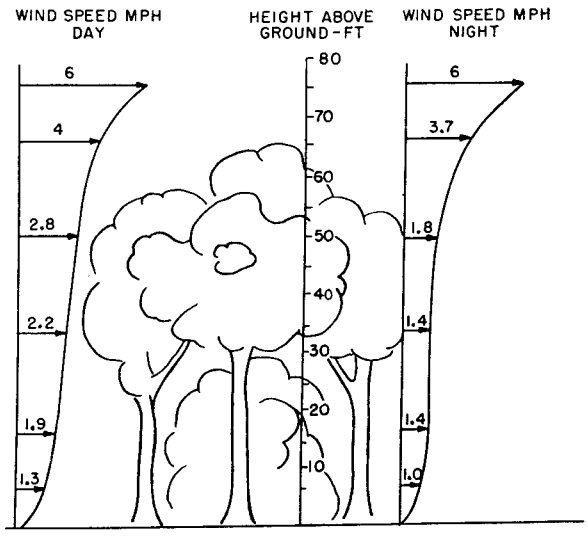

FIGURE 19. Wind speed at various heights in forest.

RELATION BETWEEN WINDS ABOVE AND BELOW A FOREST CANOPY

The wind near the floor of a forest (say at 2 m above the ground) is generally caused by the motion of the air above the trees. As the horizontal motion is transported downward through turbulence, most of the energy of the wind is dissipated by the stationary obstacles in its path so that the speed near the ground is much less than that above. The thicker the foliage, the greater will be the difference in speeds.

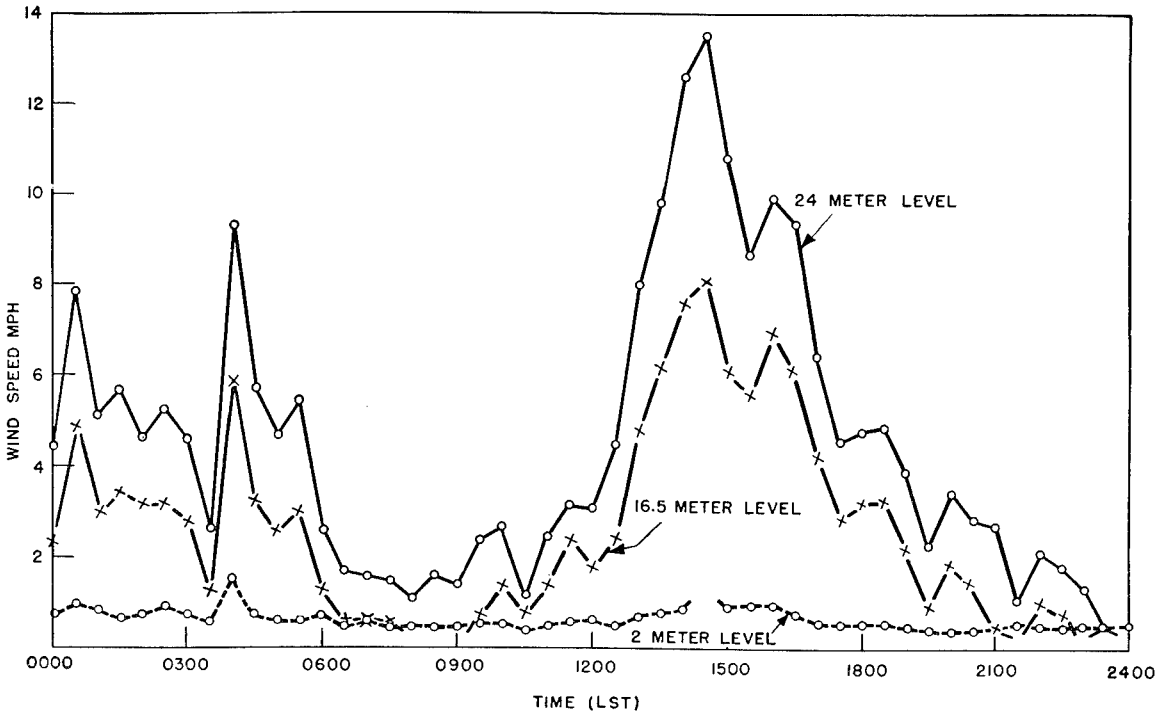

FIGURE 20. Wind profile record.

In addition, this downward transfer of motion from above is affected by the thermal structure of the air in and over the trees. The question of air stability in a forest will be taken up later. It is sufficient to say that when the air is stable, the transfer of motion is curtailed. For a given overhead wind, the wind speed at 2 m will be less under stable conditions than under unstable conditions. When the air is unstable, vertical mixing is enhanced; hence, there is less tendency for the existence of a large vertical velocity gradient. Thus, if the wind overhead is constant day and night, it is to be expected that the winds in the woods will be generally lower at night than during the daytime.

Under given stability conditions the wind speed in a moderately heavy jungle is nearly independent of the wind speed over the canopy if the latter is not over 5 mph. With higher wind speeds overhead, those in the woods increase and become more nearly proportional to those overhead. The jungle speeds are then roughly one-eighth of those overhead.

The wind profile of a typical day in the San José Forest is illustrated in Figure 20. The heights are 2 m in the jungle, 16.5 m at the top of the canopy, and 24 m above the canopy. Throughout the day the speed at 16.5 m closely follows the speed at 24 m. The speed at 2 m hardly follows even the peaks and troughs. Worth noting is the fact that while the wind speed above the jungle is greater than 10 mph, the speed in the jungle is only about 1 mph. In contrast, while the speed above the jungle is about 0.5 mph near midnight, the speed in the jungle is also 0.5 mph.

Figure 21 is a plot of the ratio: wind speed at 24 m divided by wind speed at 2 m vs the wind speed at 24 m. It is apparent that the ratios measured with inversion conditions are well enough separated from those measured under lapse so that separate curves for average values may be drawn. The implication here is that the speed in the jungle is more dependent on the speed above the jungle under lapse conditions than under inversion conditions. Since there is more downward transfer of momentum under lapse, greater turbulence will also result under these conditions.

14.9.3 Wind Direction

The wind direction above a wooded area is generally the same as in open terrain.

Insofar as the wind below the canopy is caused by the overhead wind, the average wind direction inside a forest coincides with that above. The air movement, however, as a rule is much more irregular than that above. Hence, at any given instant the direction

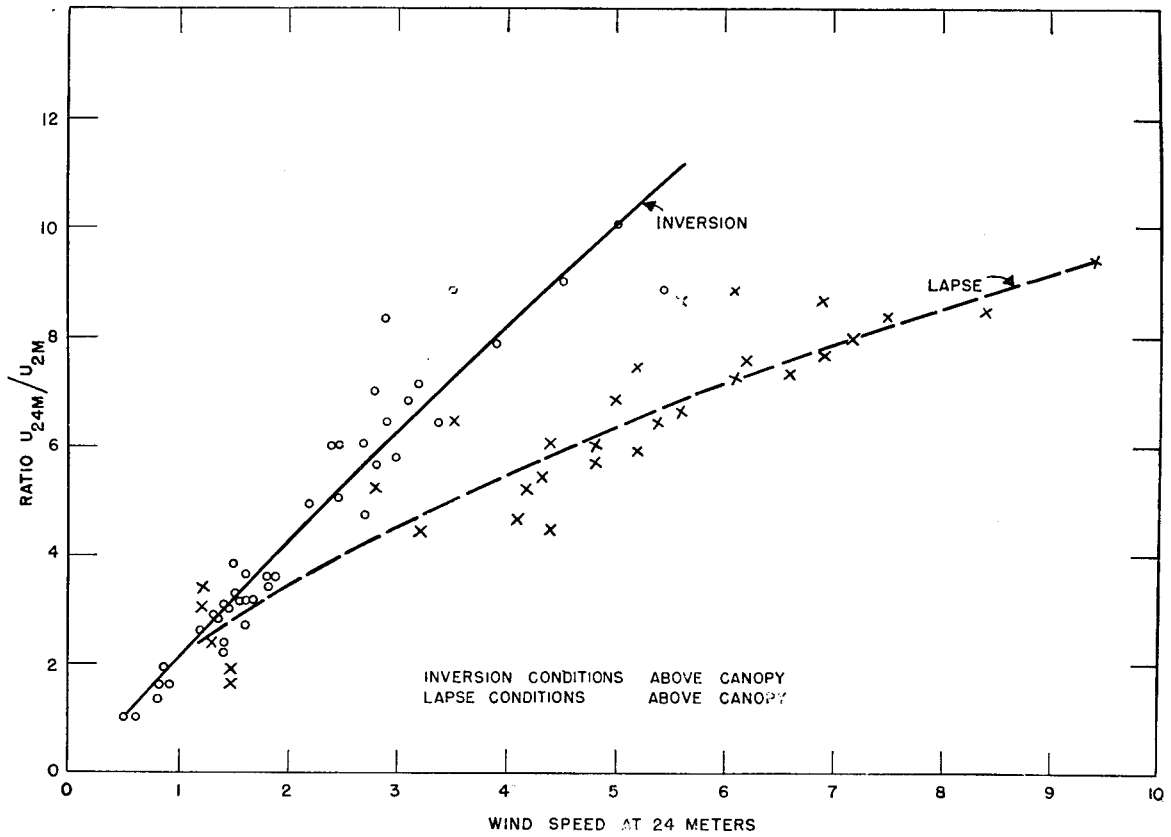

FIGURE 21. Effect of wind speed on R' for lapse and inversion.

near the ground may be considerably different from the average. It is not uncommon for the slowly moving air in a wooded area to execute two complete 360-degree changes in direction in the space of one minute. Moreover, at any moment the direction of winds at two points at the same level in a forest usually differ considerably.

On clear days or on cloudy days with moderate to high overhead wind speeds, the wind directions in a forest fluctuate rapidly over a wide range because of the turbulent condition of the air. When there is a heavy overcast and low winds during the daytime, the fluctuations are more subdued. At night, especially with clear skies and a low overhead wind, turbulence is at a minimum, and the direction observed at one point in the woods usually exhibits slow and random changes.

This last mentioned situation seems to result from the wind in the woods being relatively independent of the wind above. It is presumed that the stability of the air under these conditions makes this possible. Apparently the air movement below the canopy is caused not so much by the transfer of motion from above as by effects such as the settling of cold air and uneven radiational cooling whose origins are purely local. There results, therefore, a low local wind which does not fluctuate rapidly and which is not necessarily in the same direction as the wind above the trees, but which gradually shifts as one local effect becomes more predominant than another.

These effects are further indicated by Figure 22, which compares the frequency of the wind direction at 24 m (above the canopy) to that observed in the jungle. The fact that the daytime data show larger deviations in the directions than do the night data is consistent with the greater turbulence under lapse conditions.

A comparison of the low- and high-wind speed traces from a hot wire anemometer is given in Figure 23. Again, greater turbulence is to be noted for lapse conditions.

An important exception to the above remarks about wind directions in woods at night is found in the remarkably steady winds on slopes. These katabatic winds have been discussed in preceding text in some detail.

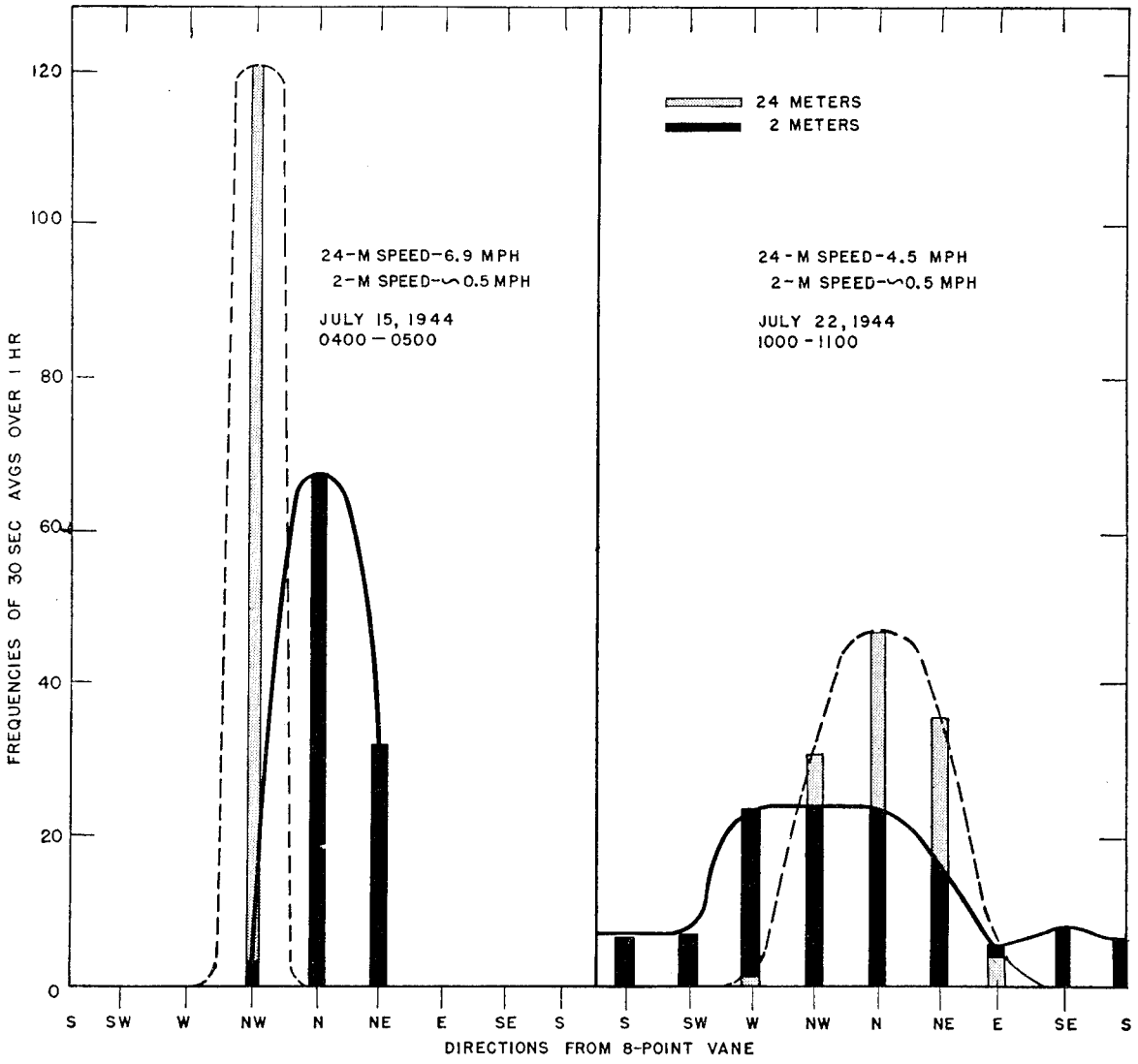

FIGURE 22. Wind direction frequency in San José jungle.

14.9.4 Forest Temperatures

TEMPERATURES IN AND ABOVE THE CANOPY

In the free air above the tree tops, conditions are much the same as over open ground with the tree tops taking the place of the ground surface for radiation purposes. The surface temperatures of living leaves in the sun are often 10 degrees F, or hotter than the surrounding air; and dried leaves can give larger differences. Accordingly, the canopy and the air above it undergo a diurnal variation with a maximum in the afternoon and a minimum before sunrise. Furthermore, above the canopy, lapse conditions develop in the sunshine, and inversion conditions develop on clear nights just as they do over open ground. Some difference arises from the fact that the canopy does not show nearly so well defined a surface as the open ground; the temperature gradients are consequently not so large in the air over the tree tops as over an open field. Again, the ground of an open field presents a solid obstruction while the canopy of a forest does not; air, cooled by open ground during an inversion, pools on the ground but when cooled by the cold leaves of a canopy it sinks down through the canopy.

TEMPERATURES BELOW THE CANOPY

If the surface of the ground or of some low vegetation lies under a heavy forest canopy and has little or no direct exposure to the sun or sky, then the surface temperature undergoes a smaller diurnal varia-

DATE	TIME	AVERAGE WIND SPEED (2 METERS)	GUSTINESS CHARACTERISTIC	TEMPERATURE DIFFERENCE °C	
				$T_{24M} - T_{12M}$ (ABOVE CANOPY)	$T_{12M} - T_{1.0M}$ (BELOW CANOPY)
8-24-44	1000	0.5 M P H	HIGH	-0.9° (LAPSE)	1.2° (INVERSION)
8-25-44	0100	0.5 M P H	LOW	2.1° (INVERSION)	-0.4° (LAPSE)

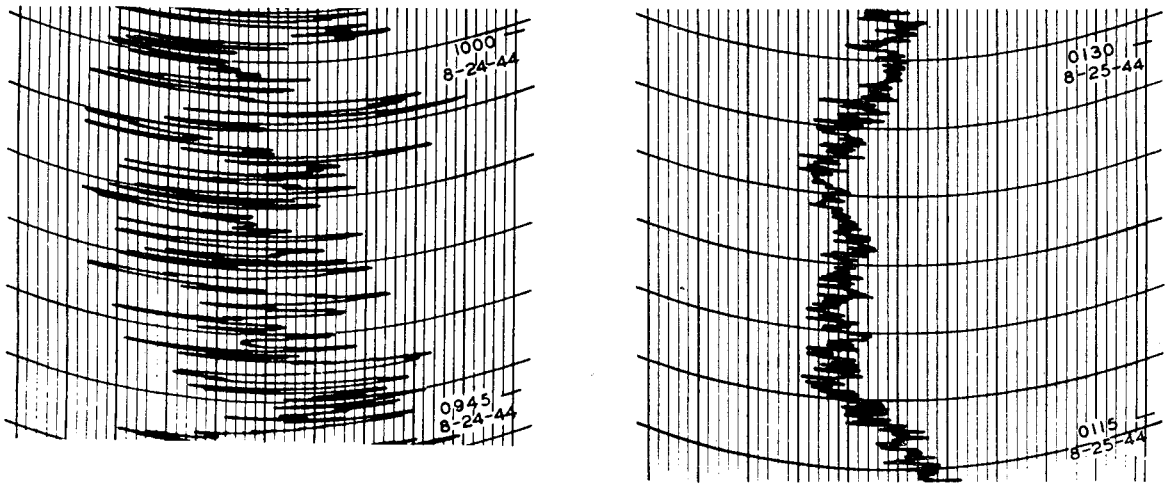

FIGURE 23. Low and high gustiness wind-speed traces.

tion than it would if the surface were exposed. In woods in Florida during May and June, the average daily range in ground surface temperature on clear days was only 16 degrees F while that of the grass in a nearly open area was 40 degrees F. A range of only 5 degrees F has been found in the jungle on a tropical island.

Also, the temperature of a well-shaded surface does not depart greatly from that of the nearby air. For the Florida woods, the air was usually cooler than the ground surface at night and warmer in the middle of the day; but the difference was usually less than 2 degrees F.

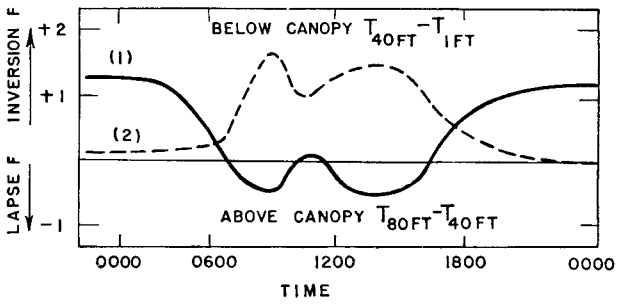

FIGURE 24. Temperature differences in jungle between air above and in canopy; and between air in canopy and near ground.

LAPSES AND INVERSIONS UNDER THE CANOPY

In the open, inversions usually develop at night and lapses occur in the day. Under a fairly heavy canopy the reverse occurs; lapses develop at night and inversions occur in the day. This is illustrated by Figure 24 drawn from observations in a jungle on a small tropical island. For various times of the day and night there are shown two temperature differences: one, $T_{80\text{ ft}} - T_{40\text{ ft}}$, is the temperature of the free air well above the crown minus that of the air in the crown; the other, $T_{40\text{ ft}} - T_{1\text{ ft}}$, is that in the crown minus that of the air near the ground. Positive differences indicate inversions.

Rapid changes in the temperature profile occur rather frequently under the jungle canopy. These are illustrated [23] in Figures 25 and 26. Thus, in Figure 25, a change from inversion to lapse occurs between 10 and 13 m in a few minutes. These rapid changes are indicative of the vertical and horizontal motions of the air due to heating and cooling of the vegetation and it may be concluded that any single measurement of the temperature profile during the day may not be representative of the average condition.

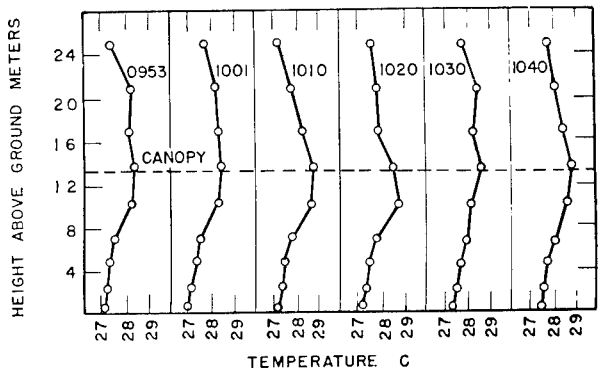

FIGURE 25. Variation of jungle temperature profiles under uniform cloud cover.

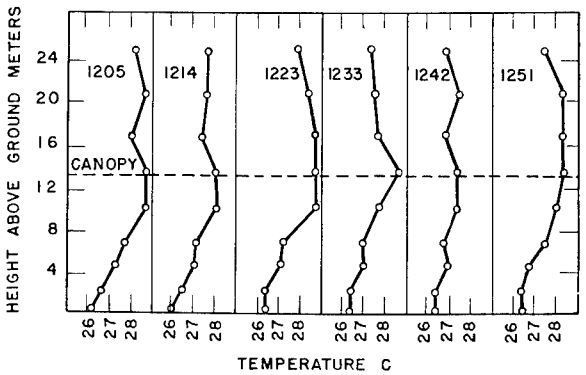

FIGURE 26. Modification of jungle temperature profile by passing small clouds.

THERMAL INSTABILITY IN THE FOREST

Although the inversions under a heavy canopy occur in the daytime, it is not to be concluded from this that day is the time of air stability in the woods; for at any one height in the crown, horizontal temperature differences with consequent circulation doubtlessly exist.

To understand this daytime inversion, consider that when the sun strikes a forest canopy many leaves at the tree tops receive direct sunshine and are heated to temperatures distinctly greater than of the surrounding air. The leaves then warm this air. Below the tree tops, fewer leaves are exposed to the sun; if the canopy is fairly heavy, very few spots receive direct sunlight at the lowest levels. From the ground on upward into the canopy there is, then, an increasing number of hot spots with the result that the average air temperature increases from the ground well into the canopy. Although this is an average temperature distribution corresponding to an inversion, its manner of production by hot spots results in convective turbulence.

Similarly, on clear nights many leaves at the top are exposed to the sky; they radiate freely and become cooler than the surrounding air which is then cooled by the leaves. At lower levels, fewer leaves are exposed so that, on the whole, the air is cooler in the canopy than somewhat below it, that is, the temperature distribution here is that of a lapse.

This simple picture requires modification in a less dense forest. If considerable sun is able to reach the forest floor at midday but not in the morning or afternoon, it can happen that there is a lapse near the ground at midday but an inversion morning and afternoon. If the forest is very thin, lapses by day and inversions by night may be expected somewhat as in the open. Evidently, within the woods, the knowledge that a lapse or inversion exists is of no value alone.

14.9.5 Turbulence in the Forest

From what has been said it is clear that thermal stability and turbulence in the woods cannot be estimated simply from average temperature gradients. However, a good idea of the turbulence in the woods can be formed from a knowledge of the wind speed and temperature gradient *above* the canopy.

If lapse conditions exist above the canopy, a turbulence of convective origin is present in addition to that due to canopy roughness. But, if an inversion exists above the canopy, even the turbulence of mechanical origin tends to be damped out. Accordingly, with a lapse over the canopy, much turbulence is present which can, to a greater or lesser extent, be communicated through the canopy to the air below. With an inversion over the canopy there is relatively little turbulence present for communication to lower levels.

The turbulence in the forest also depends on the speed of the wind. With a given size of lapse or inversion over the canopy, the turbulence below is least when the magnitude of the wind speed over the canopy is least.

These relations are illustrated by Figure 27, which shows qualitatively the amount of turbulence (low, medium, or high) in the jungle of a tropical island under various conditions over the canopy. The turbulence was estimated from the fluctuations of a hot wire anemometer 6 ft from the ground.

The figure shows that low turbulence in the woods is favored by low winds aloft (5 mph or less) and an inversion above the canopy. These conditions are

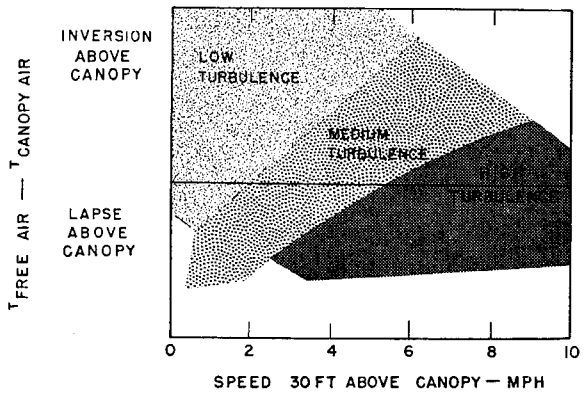

FIGURE 27. Turbulence under canopy.

most apt to be found in the very late afternoon, night, or early morning.

If it is not possible to estimate the temperature gradient and wind velocity over the canopy, the same quantities estimated for a near-by open field may be used with some success.

14.9.6 Low Canopy Jungle or Heavy Brush

The San José project investigated the condition inside a heavy, low-canopy jungle. Measurements were made of wind speed at heights of 5 m (above the canopy) and 2 m (inside the canopy). The following text is quoted from their results.

The relationship between the winds at the 5- and 2-m levels and the temperature profiles showed that the same general effects occur in a low- as in a high-canopy jungle, except that the effects are concentrated over a much smaller height interval. In fact, the effects are intensified by the extremely heavy cover which at times produces effectively a second ground surface at the top of the jungle in typical areas. For example, between the free air and the jungle floor (a height interval of roughly 20 m in high-canopy terrain) a ratio of 8/1 is common for the wind speeds when the overhead wind is 6 mph. In a heavy, low-canopy jungle this ratio would be 12/1 or 15/1 and the height interval would be only 3 to 5 m. Whereas a lapse or inversion of 1 degree C might be found in a layer 10 m deep over a high canopy, the same temperature difference is possible in only 1 m over a low canopy because of the compactness which makes the top akin to a ground surface.

A further similarity between the high- and low-canopy jungles was found in the comparable situations which exist in each at night with low overhead wind. This is the condition most favorable for the formation of inversions (provided it is not too cloudy). On a calm night, it is found that the air underneath the canopy is relatively independent of the air above. Its movement is not caused so much by the downward transfer of momentum from the air above the jungle as by the existence of drainage or gravity wind currents inside the jungle. Under such conditions, the ratio of the wind speeds can fall below unity. This effect was undoubtedly enhanced by the location of the low jungle station on a slope, where drainage winds are most likely to occur. On a flat region, it would be expected that, with a strong inversion above the canopy, the air underneath a low canopy would be stagnant.

Chapter 3

MICROMETEOROLOGICAL INSTRUMENTS

By *Wendell M. Latimer*

15.1 INTRODUCTION

THE VARIOUS micrometeorological instruments employed on Division 10 and CWS field projects are described in this chapter. While, in general, they proved adequate for the acquisition of the desired data, it is realized that many of them were developed rapidly under the stress of an emergency and can be further improved. In some cases it would have been desirable to make the instruments self-recording. This may be accomplished readily for permanent locations but is difficult for portable field equipment. The following instruments are described in this chapter.

1. Anemometers.
   a. Magnetic cup anemometer.
   b. Mercury cup anemometer.
   c. British anemometer.
   d. Hot wire anemometer.
2. Wind direction recorder.
   a. CIT-type vane.
   b. Commercial eight-point vane.
3. Temperature apparatus.
   a. Aspirated thermocouple system.
   b. Aspirated resistance thermometer system.
   c. Surface thermometer system.
4. Vanes for gustiness.
5. Miscellaneous.
   a. Smoke puffer.
   b. Photocell illumination recorder.
   c. Humidity measurement.
6. Dugway portable recording system.

15.2 ANEMOMETERS

15.2.1 Magnetic Cup Anemometer [a]

The anemometer is of the cup type with three cups rotating about a vertical axis (see Figure 1). The rate of rotation of the cups depends on the wind speed

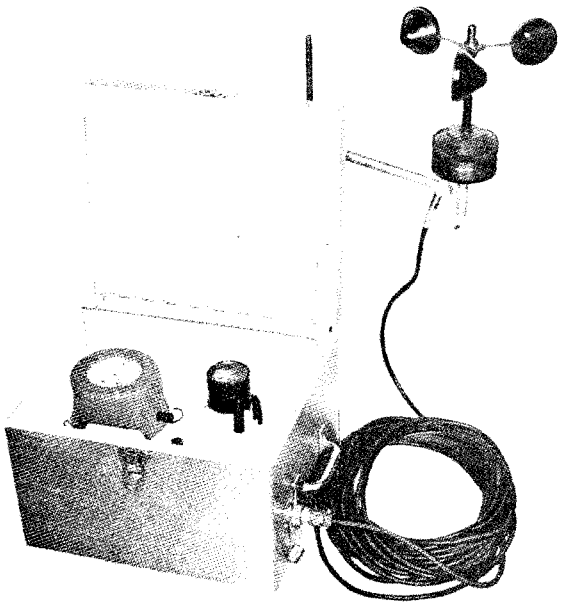

FIGURE 1. Anemometer and box ready for use. The cable from the anemometer is attached to the box through a weatherproof fitting.

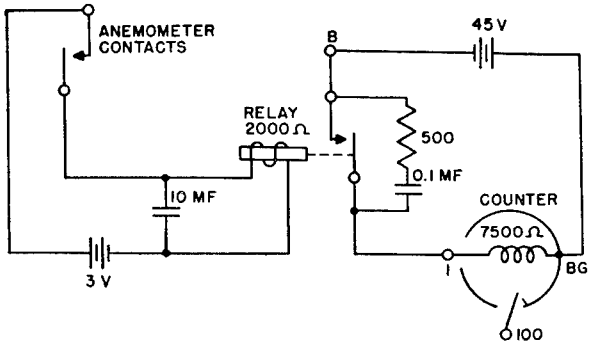

FIGURE 2. Diagram of wiring of anemometer, relay, and counter.

but is independent of direction for horizontal winds. For each rotation of the cup system, a set of small electric contacts close and open a circuit once (see Figure 2). Through a relay, one count is registered on a counter for each rotation of the cup assembly.

[a] This anemometer was developed by the Lane-Wells Company of Los Angeles in accordance with requirements set forth by Contract OEMsr-861. Since it was the anemometer most widely used in the field experiments, it will be described in some detail.

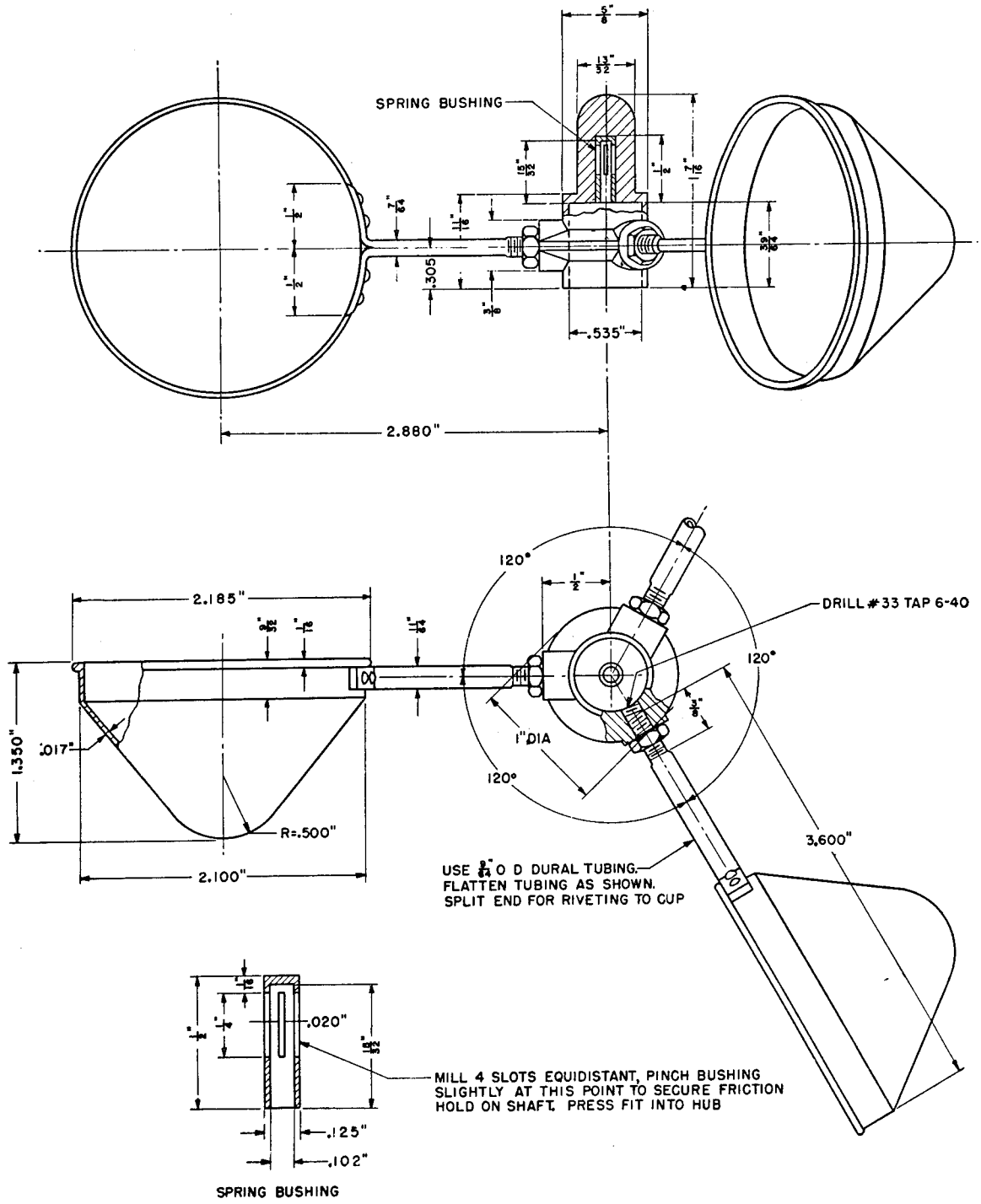

FIGURE 3. Cup and hub sub-assembly.

By observing the number of counts recorded in a calibrated instrument in a measured lapse of time, the average wind speed over a given time interval is obtained. The instrument will operate at wind speeds varying from a little less than 0.5 mph to perhaps 30 mph. The instrument has been left in the rain for days without having water reach the internal working parts.

The cup assembly rides on a jeweled bearing at the bottom and is guided by a circular Phosphor-bronze bearing near the top. The coupling between the rotor and the electric contacts is magnetic. The rotor shaft carries a horizontal semicircular segment of iron which moves under one pole of a permanent U-shaped magnet once for each rotation. In the field of the magnet is an armature supported in jeweled bearings. The armature carries one of the electric contacts and is moved a small amount on each approach of the iron semicircular segment. The armature is restored by a hairspring.

If it is desired to record the indications of the anemometer, an appropriate chronograph pen may be connected in place of the counter.

Since the cup assembly gives about 20 rotations per min per mph of wind (fewer at low speeds), direct counting by a chronograph pen may often be inconvenient. An auxiliary contact built into the counter makes it possible to record every hundred rotations instead of single rotations.

Details of the Anemometer

Cup System. The cup system is held on the rotor shaft by a spring bushing and is simply lifted off when the instrument is to be packed away. The cups are matched by weighing before assembling so that the rotor is carefully balanced. From one instrument to another the rotor dimensions are held closely similar; except at the lowest wind speeds, the calibration curves should be substantially the same for all instruments.

The cups (Figure 3) are somewhat deeper than those of the British anemometer Meteor No. 4 but are otherwise the same and will interchange with the cup system of the British instrument.

Rotor. Figure 4 shows the semicircular iron piece which is carried by the vertical rotor shaft. This drawing also shows the pivot point of the bearing on which the rotor stands.

Upper Bearing. The shaft housing carries a circular Phosphor-bronze bearing near the top. If this bearing is made too tight, the low-speed sensitivity of the anemometer is seriously impaired. The design of the instrument is such that dirt should not collect in this bearing too readily; but experience on this point is not extensive. The bearing is readily removable for cleaning; the bearing retainer at the top may be unscrewed and the bearing shaken out.

Inner Case. This is a small housing which carries the shaft housing. The inner case is cut away on one side to permit interaction of the soft iron segment with the armature, and on the other side to permit the introduction of a compensating magnet. A rubber packing ring is placed on the beveled top of this housing for waterproofing purposes.

Compensating Magnet. There is, naturally, a force between the U-shaped magnet and the semicircular iron piece which is carried by the rotor. This force might be expected to have some influence on the starting wind speed. With the idea of compensating it, a bar magnet has been mounted on a post on the opposite side of the rotor from the U-shaped magnet. Care must be exercised in selecting and placing this bar magnet; if the field from it is too strong, it can easily do more harm than good.

Electric Contacts Subassembly. This assembly is shown in Figure 5. The base (1) carries the subassembly and is fastened by two screws to the outer case bottom. The upright piece (3) is screwed to the base (1) and carries the moving parts of the subassembly. The permanent U-shaped magnet is (4). The armature (11) is mounted on an axis (7) and rocks slightly when the soft iron swings under it. This axis moves in jeweled bearings; one of these bearings is rigid in the upright (3) and the other bearing (12) is adjustable. A restoring force is exerted on the armature by a hairspring (13); tension on this spring may easily be altered somewhat by rotating (8) about the axis. The purpose of all this is to move an electric contact; this is carried by the right-angled piece (10) which is rigidly attached to the armature axis. The stationary contact is carried on the upright (5) which is electrically insulated from the base by the bakelite piece (2). The upright (5) carries two screws which limit the motion of the contact carried by (10). One of these two screws is tipped with a platinum contact; the other screw is insulated from the upright and is simply a stop. (In later instruments these two screws have been interchanged from the positions shown in the working drawing. In these instruments the hairspring closes the circuit and the magnetic effect opens it.)

External Electrical Connection. Within the instrument the electric circuit, when made, passes through the base, the hairspring, the contact, the upright (5), and a wire from (5). The circuit is brought to the outside of the outer case through an Amphenol part No. CL-PCLM. This can be connected to the cable by an Amphenol part No. MC1F on the end of the cable. The other end of the cable attaches to a receptacle in the carrying case.

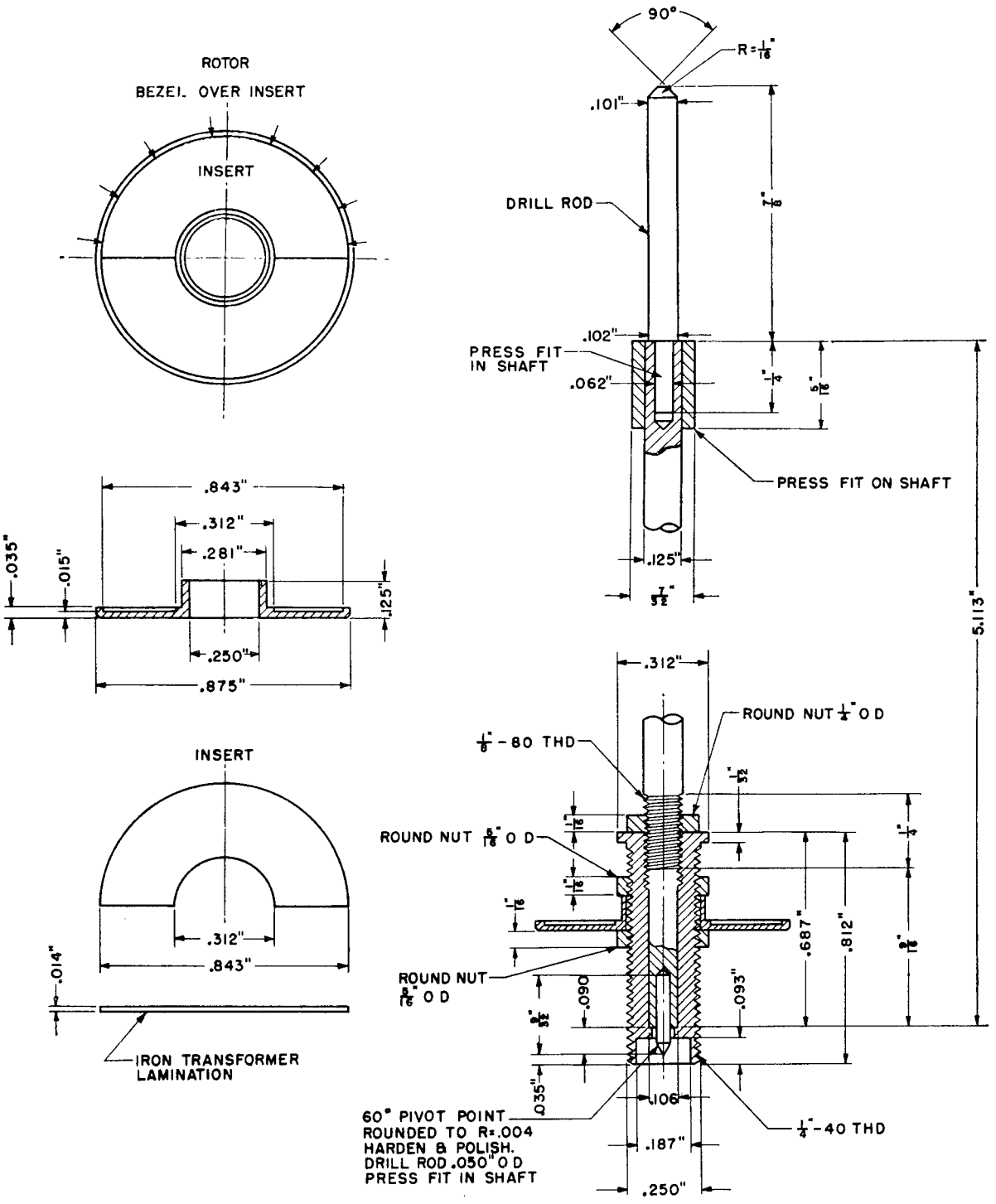

FIGURE 4. Shaft and rotor sub-assembl.

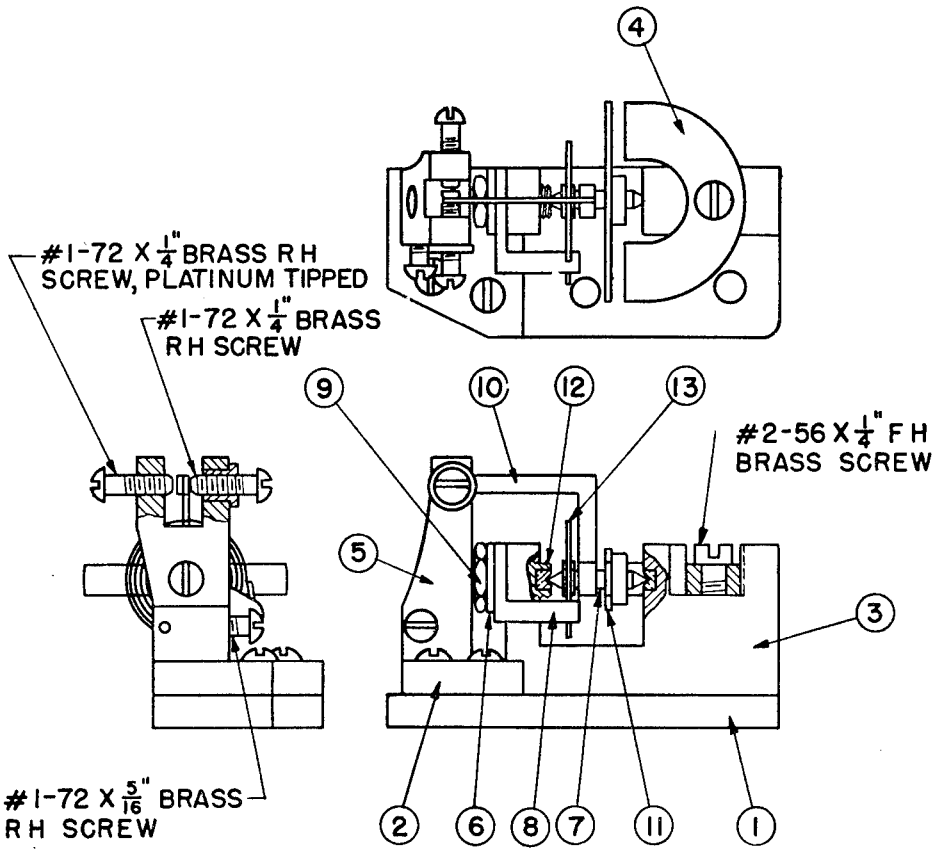

NOTE: TO FASTEN 5 ON TO 2 USE 1 #1-72 X 3/16" F H BRASS SCREW
TO FASTEN 2 ON TO 1 USE 2 #1-72 X 3/16" R H BRASS SCREWS
TO FASTEN 3 ON TO 1 USE 2 # 2-56 X 3/16" F H BRASS SCREWS

FIGURE 5. Contact sub-assembly.

ACCESSORIES

A wiring diagram showing the connections of the anemometer to relay, batteries, and counter is shown in Figure 2.

The anemometer is connected through a small 3-v dry battery to the coil of a 2,000-ohm relay. Under these operating conditions the relay is extremely critical in its behavior toward adjustment; a small fraction of a turn of the screw controlling the relay hairspring makes the difference between operating satisfactorily and not operating at all.

Across the coil of the relay is placed a 10-μf electrolytic condenser. Without a large condenser, the contacts of the anemometer are very apt to stick and thus cause the instrument to cease indicating.

The counter is one made by the Cyclotron Specialties Co. It has a resistance of about 7,500 ohms and is actuated by a 45-v B battery. Although not imperative, a small condenser (0.1 μf) has been connected across the relay contacts through a 500-ohm resistance to reduce sparking. The carrying box is built to receive a standard-size B battery but not a heavy-duty battery. One end of the counter coil has been connected to the counter case and to the binding post marked *BG*.

An auxiliary contact has been built into the counter which allows a second independent circuit to be closed every 100 counts. The terminals for this circuit are the posts marked 100 and *BG*. Any apparatus employing this feature is additional to that shown in the photographs.

The box, which has been designed as a carrying case, in addition to holding the anemometer, relay, and counter, has compartments for the batteries, a

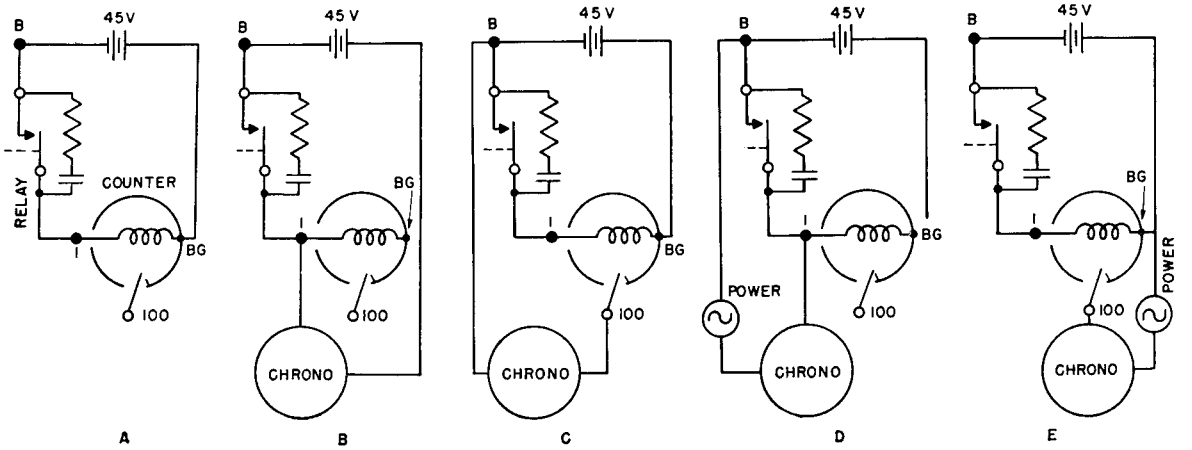

FIGURE 6. Diagram of alternative wiring arrangements.

cable, and calibrations. The outer dimensions of the box exclusive of handle and clasps are $12\frac{1}{2} \times 10\frac{3}{4} \times 8\frac{1}{4}$ in. The weight of the complete outfit including batteries is about 25 lb.

WIRING ARRANGEMENTS FOR RECORDING

In the wiring diagram of Figure 2, the apparatus is arranged to give one count on the counter for each rotation of the cup system (case *A* of Figure 6). If it is desired to record by using a chronograph pen on a moving paper the connections may be made in any of the several ways shown in Figure 6. In these diagrams the anemometer circuit is like that of Figure 2 and has been omitted. The points labeled *B*, 1, 100, and *BG* are the similarly labeled binding posts. The necessary connections may all be made at the binding posts or at the wires connected to them without removing the panel on which the counter is mounted.

In case *B* the chronograph pen is arranged to be actuated by the B battery of the anemometer and receives one impulse per rotation of the rotor. The counter is shown disconnected. The chronograph pen of some Esterline-Angus milliammeters can be actuated by 45 v; but this power supply may not be appropriate in all cases.

In case *C* the B battery is again used for the chronograph but the chronograph receives only one impulse for each 100 rotations of the rotor. The counter is actuated once per rotation. If a chronograph is used with any except very low winds this arrangement or case *E* is desirable.

Case *D* is similar to *B* except that an external power supply is used for the chronograph.

Case *E* is similar to *C* but has an external power supply.

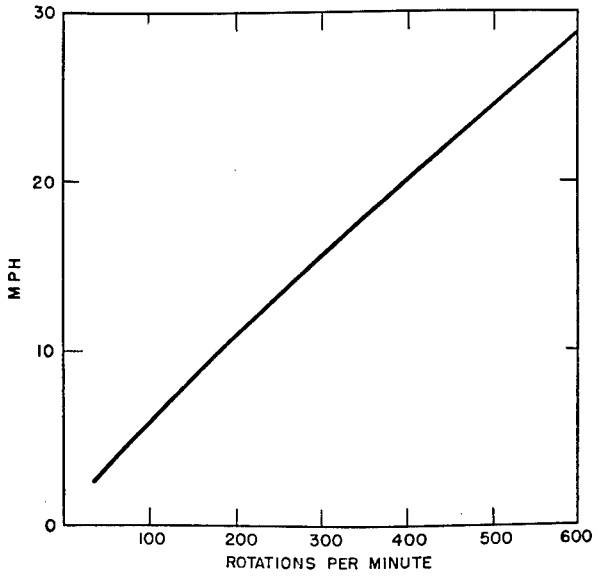

FIGURE 7. Anemometer calibration for higher speeds.

CALIBRATION CURVES

Calibration curves which are typical of all instruments are shown in Figures 7 and 8.

15.2.2 Mercury Cup Anemometer

Another anemometer which is capable of measuring wind speed as low as 0.5 mph is the mercury cup instrument.[b] This principle is quite simple. With each revolution, two small curved stainless steel knife edges attached to the cup arms make contact with two mercury surfaces contained in small iron

[b] This anemometer was designed and constructed on NDRC Contract 126, University of California.

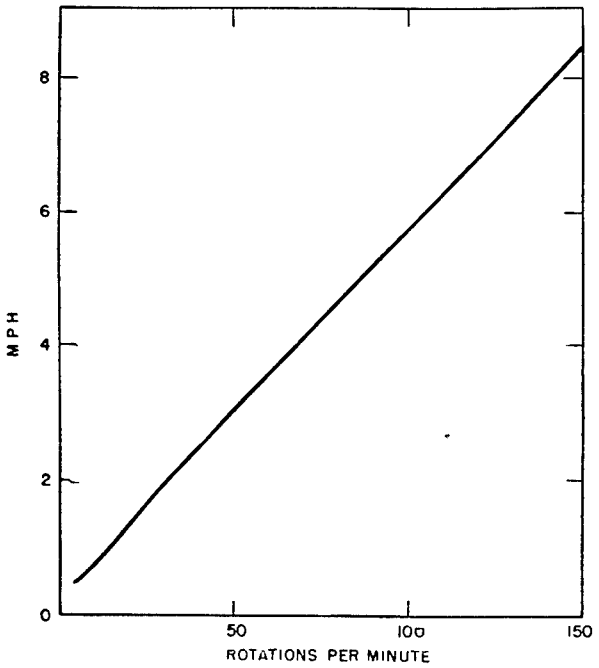

FIGURE 8. Anemometer calibration for low speeds.

cups attached to, but insulated from, the shaft. The current from a 45-v dry battery actuates the mechanical register. A schematic diagram is shown in Figure 9. The mercury contacts offer no detectable resistance to the rotation of the cups. This method was employed to replace a photoelectric counter and had the advantages of (1) simplicity, (2) no required vacuum tubes or amplifiers, (3) low voltage and current consumption, thereby making it independent of 110-v power supply.

15.2.3 British Anemometer

This instrument is the 3-cup type, the cups being 5.4 cm in diameter and the centers of the cups being at a distance of 7.0 cm from the axis of rotation. In early models the counting mechanism consists of a high-grade stop watch, the lever escapement of which is operated indirectly by the rotation of the anemometer spindle. The train of wheels is driven by the spring of the watch and thus imposes no frictional load upon the anemometer. As a result, this anemometer will function accurately to wind velocities as low as 1 mph. The provision of a beaded edge to the cups ensures a nearly constant factor for the instrument.[c] In later models the stop watch mechanism has been replaced by the more orthodox

[c] The design of this anemometer is due to P. A. Sheppard.

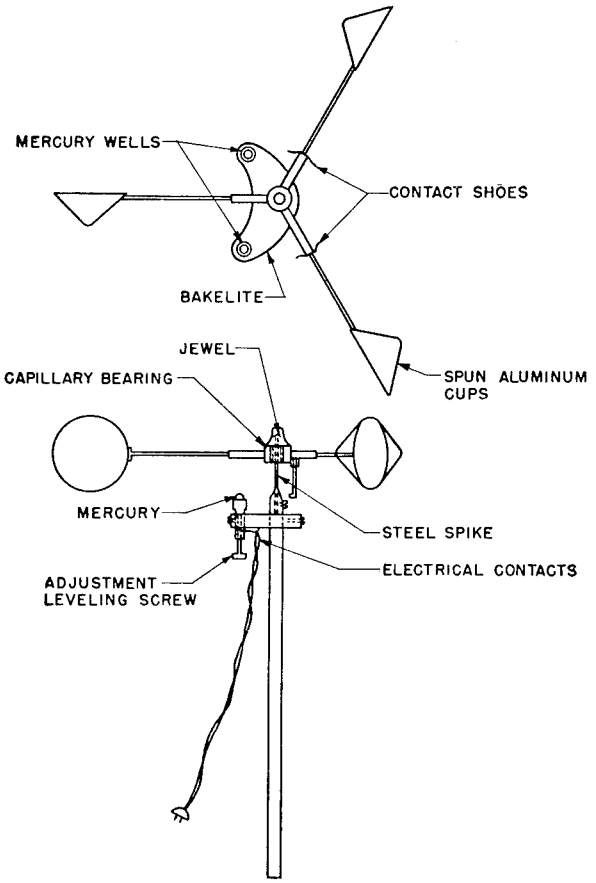

FIGURE 9. Schematic diagram of mercury cup anemometer.

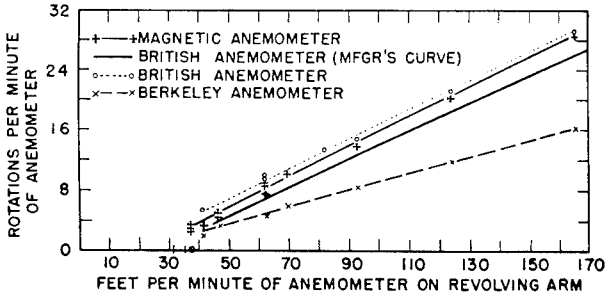

FIGURE 10. Comparison of magnetic, mercury (Berkeley), and British anemometer.

direct drive to a train of gears, but careful design of the bearings has resulted in this instrument being practically as sensitive at low wind speeds as the earlier model.

A comparison of the three anemometers was made [d] and is shown in Figure 10. The starting velocities of all three ranges between 30 and 40 fpm and the run-over or coasting rates are also comparable.

[d] Contract NDCrc-137.

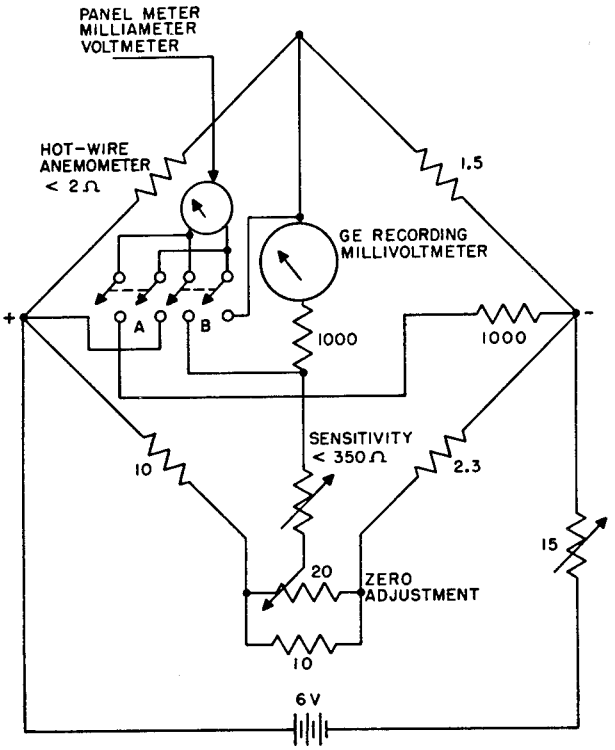

FIGURE 11. Diagram of recording-type hot wire anemometer.

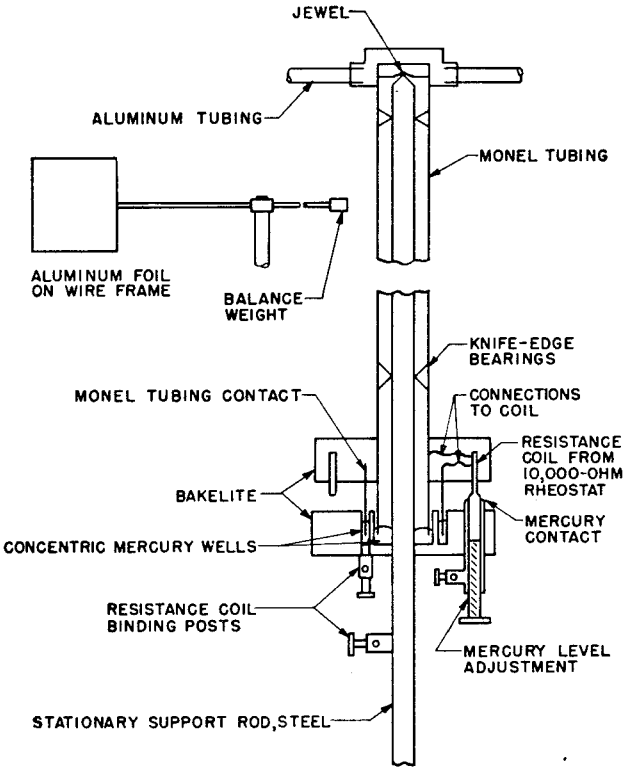

FIGURE 12. Diagram of CIT-type vane for wind recording.

15.2.4 The Hot Wire Anemometer

The hot wire anemometer, because its sensitivity is greatest at very low wind speeds, was found to be the most useful instrument in the jungle where winds of less than 0.5 mph (the starting velocity for the cup anemometers) are common.

The electrical circuit of the anemometer consists of a Wheatstone bridge, one arm of which is a short, fine wire (usually 50 in. of 0.003-in. Pt wire in the form of a bird cage) which is exposed to the wind. Through this wire is passed a given current, supplied by a storage battery, which causes the wire to heat. The wire will assume a certain temperature (and hence a certain resistance) when wind of a given speed blows by. The bridge is balanced with the anemometer covered; when the cover is removed, the resistance of the platinum wire will change by an amount corresponding to the wind speed. This causes the bridge circuit to be out of balance. The amount of this unbalance is measured by observing the reading of a milliammeter or by a suitable recording meter. A General Electric recording millivoltmeter was used for this purpose. A diagram of the circuit used in the San José work is given in Figure 11.

15.3 WIND DIRECTION RECORDERS

15.3.1 The CIT-Type Vane

This vane was designed and built at the California Institute of Technology [CIT] for the specific purpose of enabling the recording of wind directions at speeds of a few tenths of a mile per hour. This high sensitivity was made possible by the use of (1) lightweight materials, (2) circular knife edge and jeweled bearings, and (3) mercury contacts for the electric circuit. A diagram of the working parts of the vane is given in Figure 12. Omitted from the figure are the brass cover and collar which slip over the electrical part and protect it from the weather. A schematic circuit diagram is given in Figure 13.

The electrical circuit of the vane is essentially that of a potentiometer. By means of a B battery, a potential difference is applied across the 10,000-ohm coil in the vane. A certain fraction of this difference, which depends on the orientation of the vane, is tapped off by a small drop of mercury which touches the coil, and which in turn is connected with the recording meter. The current passing through the meter, then, is a function of the direction in which the

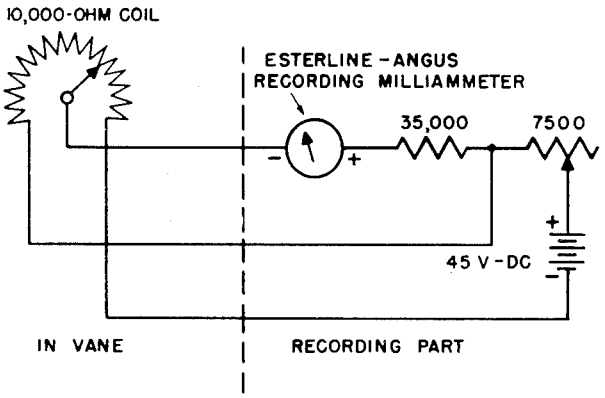

FIGURE 13. Diagram of electrical circuit of continuous recording vane.

vane is pointing. By having a high resistance in series with the meter, the current is made practically linear with the direction. Thus, if south is selected as zero, then east will read 0.2, north 0.4, and west 0.6 ma. The variable 7,500-ohm resistor in the circuit is used to adjust the proper maximum current which can flow through the meter. Since there is of necessity a gap of 15 to 20° in the vicinity of the switch-over direction (that direction corresponding to zero or the maximum current) the vane is set up so that the switch-over occurs at the direction, if any, which is least likely to be recorded. This keeps the record obtained from being confused and readings are kept away from that part of the scale which is least linear.

This type of recording vane was used in the winds normally encountered in the open, with just as satisfactory results as in the light jungle winds. A smaller tail was generally installed when higher wind speeds were encountered.

15.3.2 The Eight-Point Commercial Vane

At more or less permanent installations, the wind directions at the 2-m height were recorded by means of two eight-point vanes. As originally constructed, the vanes were designed merely to indicate direction by causing lights to go on inside a panel. They were not at all sensitive to low winds because of the heaviness and poor balance of the vane assembly. However, by devising a lighter assembly quite similar in its dimensions and construction to the CIT-type vane (the CIT tails were used), it was found that these vanes could be made adequately sensitive to winds as low as ½ mph. Instead of indicating directions on a lighted panel, the nine leads from each vane (see diagram) were wired to eight coils of a

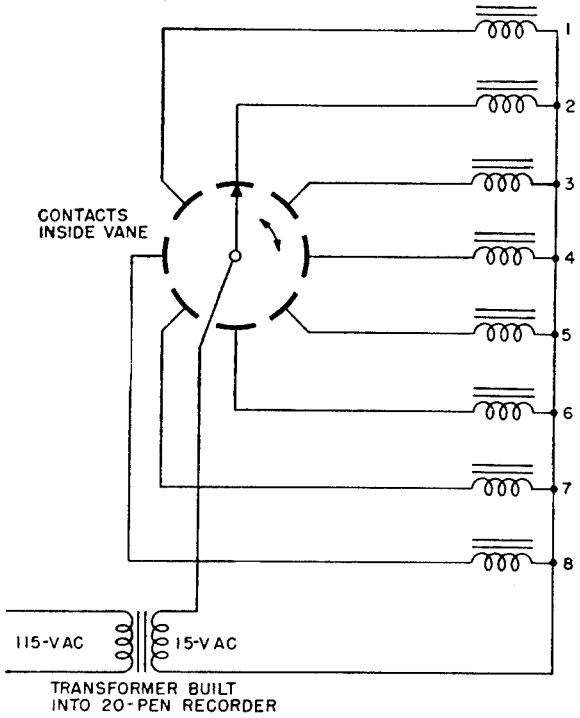

FIGURE 14. Diagram of eight-point vane.

twenty-pen recorder. A diagram of the electrical circuit is presented in Figure 14. These vanes were in operation for over two months without requiring any attention; the performance has been most satisfactory.

15.4 TEMPERATURE APPARATUS

15.4.1 Aspirated Thermocouple Systems

The apparatus consists essentially of a hollow mast carrying the radiation shields, aspiration occurring through the mast itself. With it, temperature differences between various thermoelements are read on a sensitive portable galvanometer. The apparatus is not recording but could be so modified. It was not designed for quantity production (only four have been made) nor for rough handling, although it is reasonably sturdy. It is, however, believed to give reliable results when properly used.

RADIATION SHIELDS

The radiation shields are the right-angled pieces attached to the mast as shown in Figure 15. They consist simply of the elbow (see Figure 16) of thin-walled tubing of 1-in. OD with an $1\frac{1}{16}$-in. inner tube of the same material held in the vertical part of the

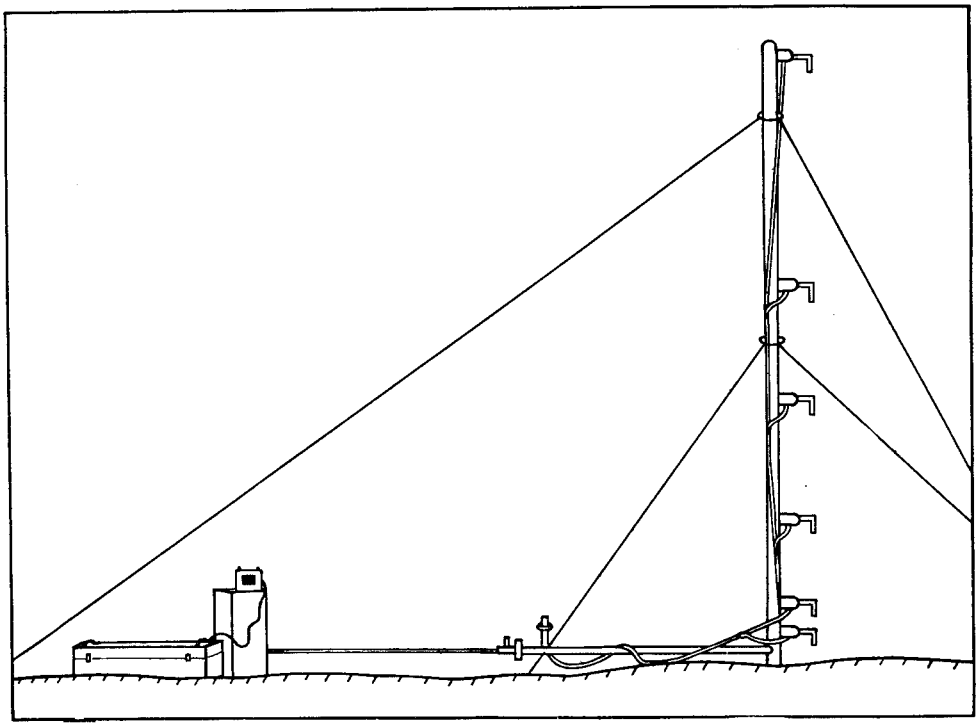

FIGURE 15. Diagram of mast with thermocouple system.

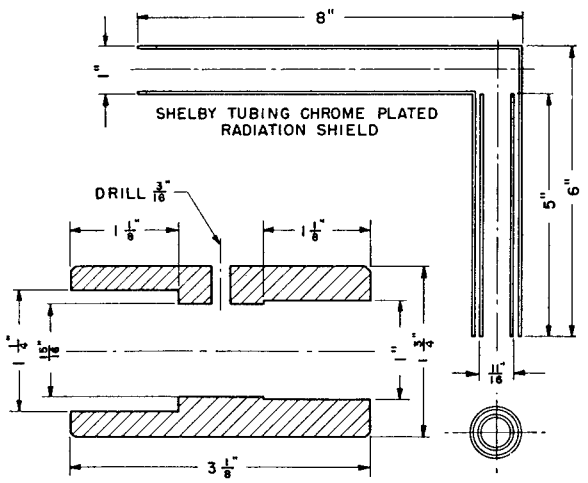

FIGURE 16. Diagram of radiation shield.

elbow by small pieces of rubber. The exposed thermoelement is placed just inside the outer opening of this inner tube and is held in the center by light pieces of wood. These various pieces of rubber and wood must not be so large as to impede aspiration.

The shields fit tightly into hardwood adapters which, in turn, slip over short open tubes protruding from the mast at appropriate levels. These adapters would be better if made of plastic.

The wires from the thermoelement continue through the length of the shield into the adapter and emerge from a hole in its side.

The type of shield shown here is a simplification of that used by A. C. Best.[1] The principal disadvantage compared with that of Best is the slight uncertainty as to the exact level at which air is being taken in; experiments with smoke suggest that the uncertainty is not more than 2 or 3 cm. In addition to simplicity, the present shield has the advantage that the air examined strikes the thermoelement before striking any part of the shield.

THE MAST

The free opening of the highest radiation shield is 5 m from the ground. (Higher masts with the same construction could doubtlessly be used.) The mast is made of 3-in. No. 18 Shelby steel tubing (cadmium plated). To give portability, it is made in five sections (see Figure 17); these fit together with the aid of end sleeves of 3-in. ID. The top section is closed at the top. The top section and the middle section are each provided with a loose ring carrying three eyes

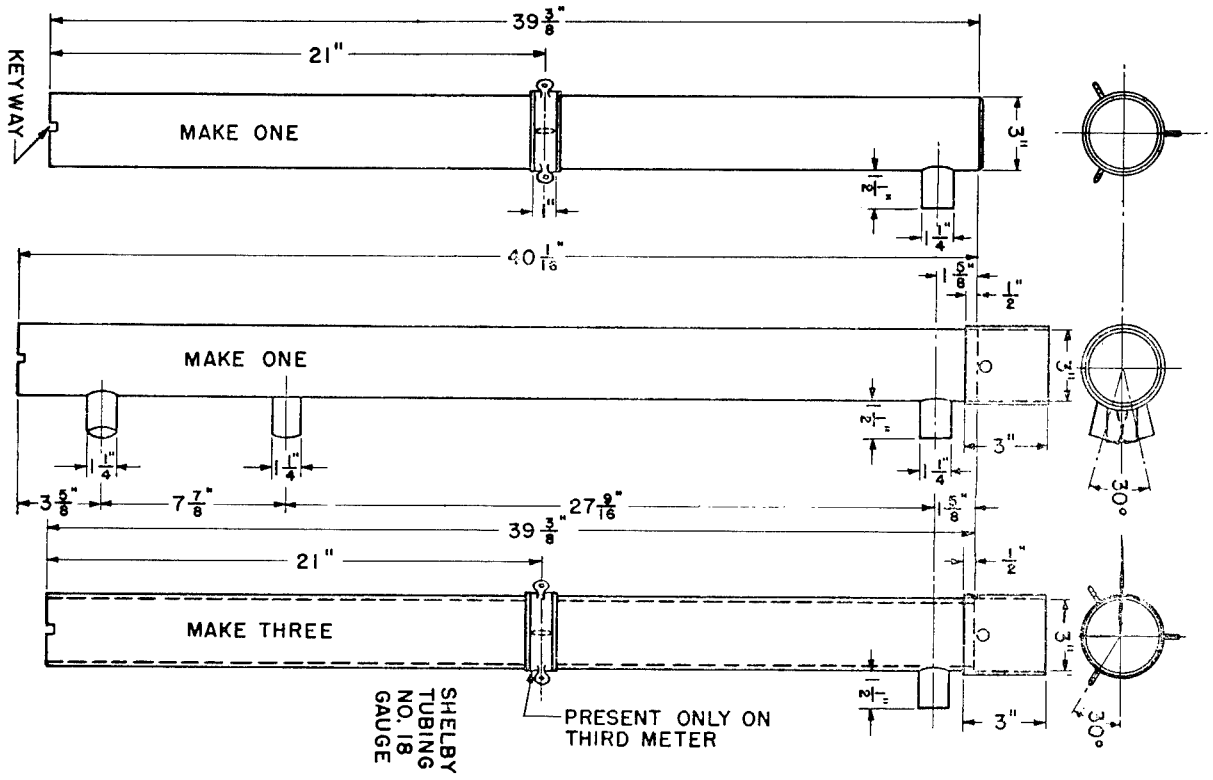

FIGURE 17. Diagram of 5-meter mast sections.

for light guy ropes. The various sections are provided with short side tubes to receive the radiation shield adapters. The heights provided by the mast are 5, 4, 3, 2, 1, 0.3, and 0.1 m; however, the side tube for a 4-m shield has never been used and might well be omitted. The bottom section of the mast fits into an L joint mounted on a base plate (Figure 18). The base plate is designed to assist in erecting the mast. The L joint receives a horizontal stretch of Shelby tubing leading to the aspirator. This horizontal member consists of two plain 1-m sections (not shown in the drawings); it is necessary that the aspirator be somewhat removed from any of the shields so as not to disturb the air around them.

The base plate carries a hinged flap with two $\frac{3}{8}$-in. holes, shown at the top of Figure 18. Before the mast is erected, this flap is pinned to the ground through these two holes. After the entire mast with shields is assembled on the ground, it is erected by rotation about the horizontal axis of the hinge; a third pin is then placed in the ground through the base plate and the mast is guyed.

Without moving the guys or base plate, the mast and the horizontal section leading to the aspirator may be rotated about the vertical axis of the mast. This is necessary so that the radiation shields may be kept up-wind of the mast, auxiliary apparatus, and observer in case the wind shifts.

The Aspirator

An ordinary aluminum household vacuum-cleaner blower has been found satisfactory for aspiration. To drive it, a 6-volt model locomotive motor No. 117-4 was used, made by Kendrick and Davis Co. of Lebanon, New Hampshire. A blower with its motor is indicated in Figure 15 at the left end of the horizontal 3-in. tube. The motor was operated from a storage battery, but alternating current may be used if available.

With the arrangement described, the radiation shields are found to be adequately and substantially equally aspirated. The air flow past the thermoelement is 1,200 fpm or more. The shields and their aspiration have been considered adequate if no significant temperature difference developed when two shields were placed side by side in the sun and a shadow was thrown on one shield.

A squirrel-cage blower, No. 3, made by the L-R Manufacturing Co. of Torrington, Connecticut, can

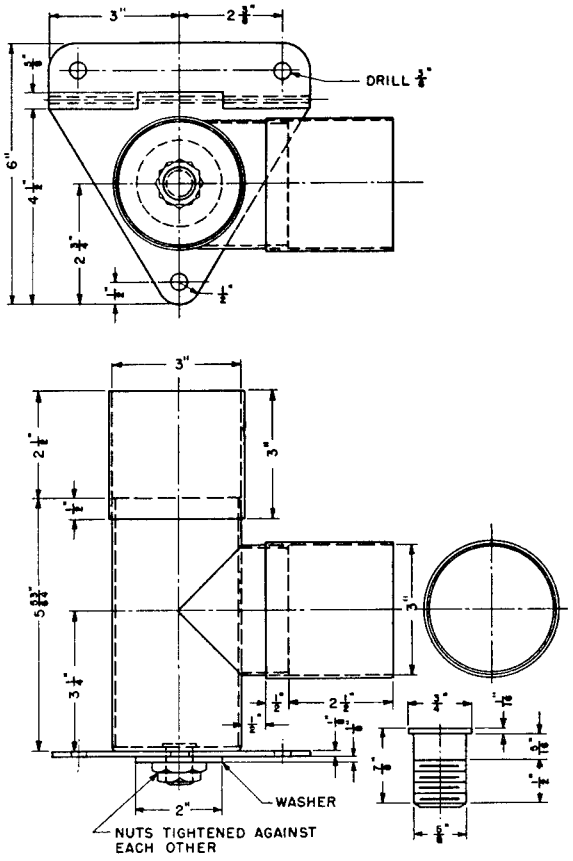

FIGURE 18. Diagram of base plate and L joint.

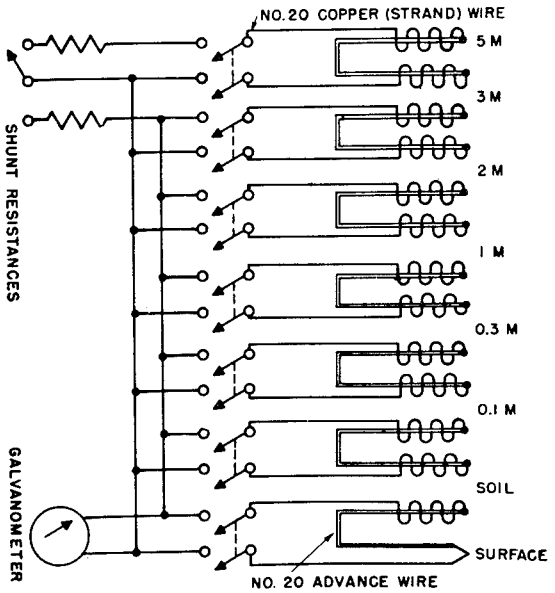

FIGURE 19. Diagram of thermocouple system.

easily be mounted so as to be used instead of the vacuum-cleaner blower. Although the squirrel cage blower would appear to be satisfactory, field trials have not been made with one.

If it is desired to measure profiles through heights of more than 5 to 10 m, such as is the case if a profile is desired from the ground up through the tree crowns in a forest, it may be more convenient to dispense with aspiration through a mast and provide each junction with an aspirator at its own level.

THE ELECTRICAL SYSTEM

Single-junction copper Advance thermoelements were used. Number 20 wire was employed; and, at the junction, several turns of one wire were wound closely around the other and the whole soldered. This gave a junction of moderate heat capacity, which was desired since it was not the intention to follow momentary temperature fluctuations. The arrangement of the various junctions is shown in Figure 19. Thus, there was one junction in the top radiation shield and two junctions in each of the other shields, so that temperature differences between adjacent levels were measurable.

In order to obtain temperatures as well as differences, one thermocouple had one junction in an aspirated shield (that at 0.1 m) and the other in a pointed copper piece inserted about 2 in. into the ground. In the copper piece was also placed a mercury thermometer graduated to 0.1 C and with its bulb in good thermal contact with the thermoelement. The *soil temperature* as given by this mercury thermometer was relatively steady. Aside from its own interest it afforded the basis of determination of the air temperatures.

In the soil thermometer there was also one junction of a couple, the other junction of which was in a device to measure surface temperatures. This was a piece of heavy felt with a fine wire junction in its surface. The felt was mounted in a convenient handle. In use, the junction is pressed against the ground for a second or two and then moved to a new spot presumed to be similar to the first. This is repeated as many times as may be necessary to obtain a constant reading. This procedure appears to give intelligible results in case the ground presents a reasonably well-defined surface on which to make measurements.

Although not imperative, it is highly convenient to

have all thermocouples built with the same resistance so that deflections on a galvanometer may be converted to temperature differences, using the same calibration for each couple. It was found convenient to build all thermocouples into a single waterproof rubber-covered cable with appropriate taps leading to each shield. (Thus, the top section of cable between 3 and 5 m contains only two wires, one copper and one Advance, with increasing numbers of wires at lower levels. The wires in the part of the cable leading to the galvanometer are all copper.)

The electromotive force given by a copper Advance thermocouple is only 40×10^{-6} v per centigrade degree of temperature difference. Consequently, care must be exercised with the insulation to avoid the introduction of extraneous electromotive forces; and precautions must be taken to eliminate thermoelectromotive forces other than those due to the couples.

The thermocouple cable leads to a set of switches; these are contained in the upright box at the left of Figure 15. (This box serves as a carrying case for all parts except the mast, which packs in the horizontal box.) Ordinary copper knife switches are used; attempts to replace these by a compact multiselector switch have been unsuccessful because of the introduction of spurious electromotive forces presumably originating at the silvered switch contacts. With the aid of double-pole single-throw switches any desired couple may be connected to the galvanometer.

The galvanometer should be a low-resistance instrument with as high sensitivity as is compatible with ready portability. A Leeds and Northrup galvanometer No. 2420B with enclosed lamp and scale has been found convenient. A galvanometer chosen to have adequate sensitivity for small temperature differences may give too large deflections with large temperature differences. Therefore, it is convenient to provide one or two shunts which may be quickly thrown in if desired; these may be chosen so that the factor for converting deflections into temperature differences is made a small integer and thus the apparatus is made substantially direct reading.

Observational Procedure

With the apparatus set up in the desired location, and with the radiation shields up-wind from the mast and the rest of the apparatus, the blower is started 2 or 3 minutes before observations are to start. The zero position of the galvanometer is read with the instrument shorted through a resistor; this observation is repeated frequently. A series of deflections is then read, starting with the 5- and 3-m junctions and proceeding down the mast, ending with the 0.1-m soil thermocouple. Because of fluctuations in the individual temperatures, the series is immediately repeated. About 5 min are required to make four series of readings; thus any one temperature difference is measured four times at intervals of a little over one minute and the results averaged. Along with this group of observations, the mercury soil thermometer is read and, if desired, the soil-surface difference.

15.4.2 Recording Resistance Thermometers

A convenient method of measuring and recording a series of temperatures in order to establish the gradient in the atmosphere is by means of resistance thermometers. The temperature difference between two thermometers at different levels may be measured by placing the resistance coils in the arms of a Wheatstone bridge. The unbalanced bridge circuit may be employed to operate a Leeds and Northrup Micromax, or the unbalanced potential may be registered directly on a recording General Electric millivoltmeter. The following is a description of the system employed on the San José program. Figure 20 is a diagram of the circuit. There are ten pairs of arms, any two pairs of which can be connected by means of automatic rotor and base selector switches to form a bridge. T_1 through T_9 are the arms whose resistance indicates the desired temperatures. They are coils of fine copper wire inserted in the aspirated shields at various levels from 0.3 to 24 m on the tower. When two of these arms form part of a bridge, a temperature difference between them will cause the bridge to be out of balance, and a potential difference proportional to the unbalance will be set up across the meter and recorded. T_{10} is a coil of Manganin wire. Because of the low temperature coefficient of resistance of Manganin, a bridge formed with this arm and the one selected for the reference temperature will be out of balance by an amount indicative of the actual temperature of the base thermometer. Either of the bottom two thermometers is used for the reference because the short period temperature fluctuations are smallest at these points.

When in operation, the rotor switch is actuated by a synchronous motor in such a way that the bridge

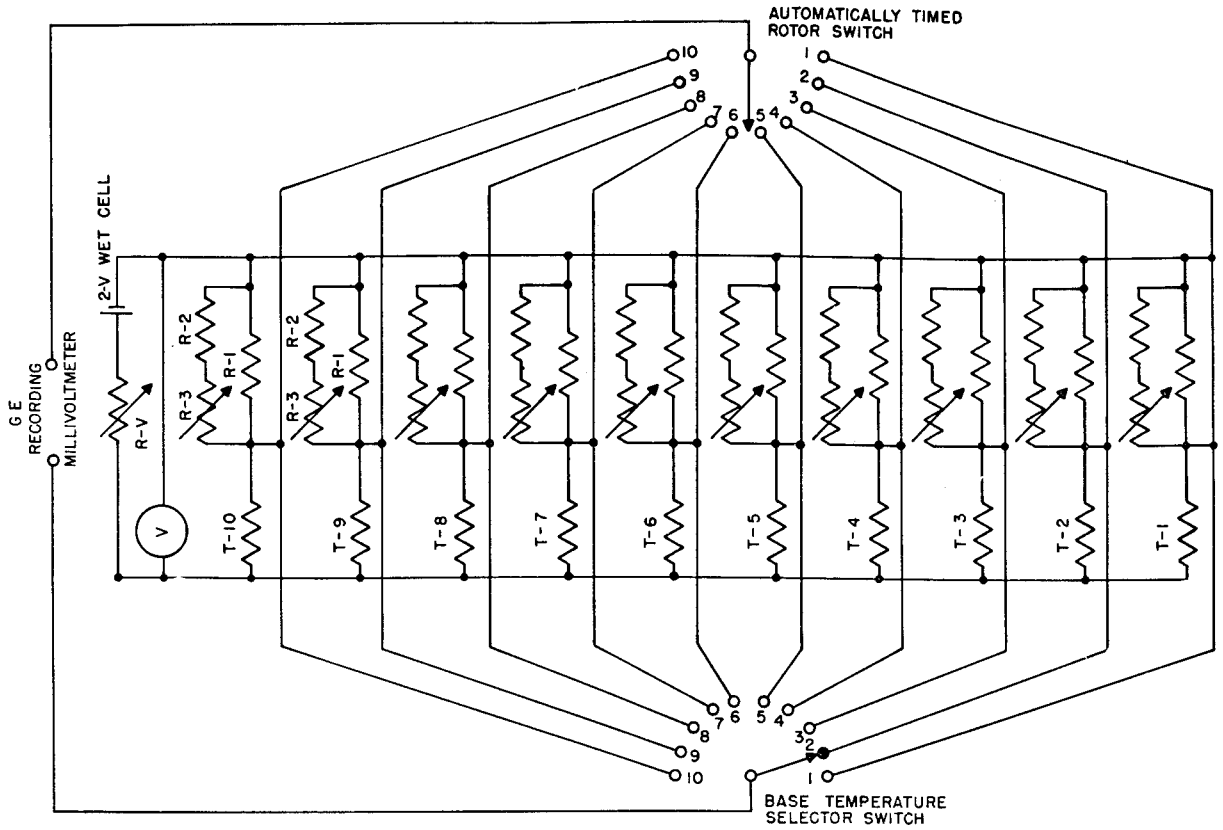

FIGURE 20. Diagram of resistance thermometer system.

circuit is changed every minute. A complete cycle, then, is made every 10 min. Each time a new circuit is made, the synchronous motor also causes the meter to make a mark on the record roll, thus permitting the separate temperature differences to be distinguished readily. A sample record is given in Figure 21. A typical cycle with T_1 as the reference thermometer will have the following sequences. First, when T_1 is in the circuit, the meter records the zero reading, because there is no potential difference across the meter. Then, with T_2 through T_9 succeeding one another, the temperature differences between each thermometer and T_1 are recorded. Readings to the right of the zero indicate that that thermometer is warmer than T_1; to the left, cooler. Finally, when T_{10} is in the circuit, the actual temperature of T_1 is recorded. After an open circuit, the cycle repeats itself.

Certain of the important details of the electrical circuit will be mentioned below. Reference is made to Figure 20. The thermometers T_1 through T_9 are wound with No. 38 copper wire and have a resistance of exactly 5 ohms. Since the nine arms containing these thermometers must all have the same resistance, the leads to them are all of the same length. (At the tower station 40-m lengths were used.)

The T_{10} is a 3-ohm Manganin coil. The ten resistors R_1 are Manganin coils each with a resistance equal to the total resistance of its opposite arm. R_2 and R_3 are fixed and variable 500-ohm resistors, respectively. The resistances of the 10 arms on the left-hand side of Figure 20 are adjusted by means of the variable resistors to be exactly equal to one another and as close to 5 ohms as possible. The variable resistor R_v is used to adjust the voltage applied across the bridge and the sensitivity of the scale.

15.4.3 Surface Thermometers

In general, the moving felt-pad method of measuring surface temperatures was employed with either a thermometer or a thermocouple junction in the pad.

A description of the San José project thermocouple system follows.

An Advance copper couple of No. 32 wire was used. One junction was fixed on the bottom of a rubber

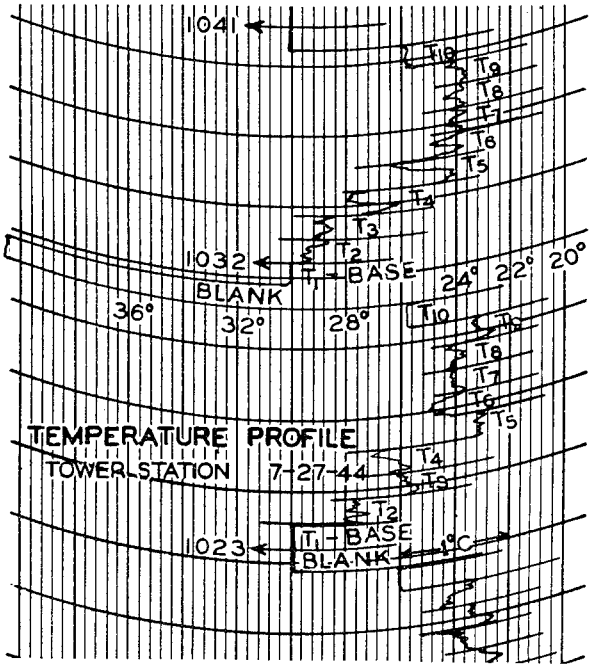

FIGURE 21. Diagram of a thermometer profile recording.

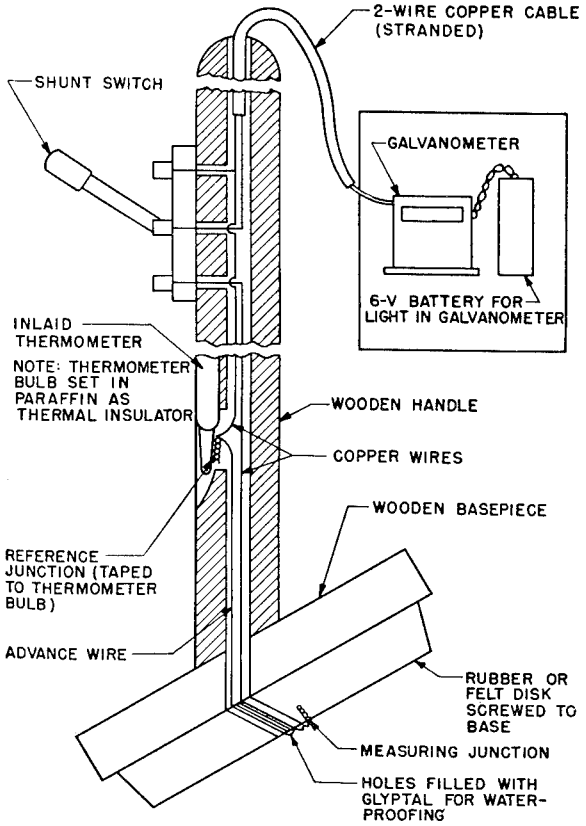

FIGURE 22. Diagram of a surface temperature measuring device.

disk which was attached to a wooden handle 4 ft long. The other junction was set in the handle of a thermometer which gave its temperature. A Leeds and Northrup low-resistance (25-ohm), high-sensitivity galvanometer was mounted on a portable stand and connected to the circuit at the end of 20-ft leads. Thus, while one operator recorded the galvanometer reading, another would apply the junction to various surfaces, reading the reference temperature occasionally. A schematic diagram of the assembly is given in Figure 22.

15.5 VANES FOR GUSTINESS

The British bidirectional vane is probably the most satisfactory instrument used to obtain gustiness factors. However, two other instruments were developed and employed to a limited extent. One, designed at Berkeley, was a vane which consisted of a single lightweight weathervane with a single turn of No. 40 Chromel wire mounted on the rim of a bakelite disk attached to the stationary shaft. A brush is attached to and rotates with the vane. A suitable potential difference (depending on the desired sensitivity) is applied along the full length of the Chromel wire and as the brush rotates with the vane, the difference in voltage between the brush and one end of the Chromel wire is recorded on the moving chart of an Esterline-Angus recording milliammeter.

The other, developed at CIT, is a bidirectional vane whose movements are registered by Cenco electric impulse counters. The shaft of the vane is mounted in brass gimbals, and on each of the two axes of the gimbals, brass wheels are mounted which turn with the axes. These contact wheels are slotted around the periphery, and the slots are filled with an insulating material. As the wheel turns, a sliding contact alternately makes and breaks an electric circuit and records on the counters the magnitude of movement of the wheel, and, hence, of the vane itself. One wheel registers lateral movements of the vane and the other vertical movements. Each is slotted over one-half its circumference to make contacts so spaced that the attached counter registers once for each 3° movement of the wheel. A single slot is cut in the center of the unslotted portion of each wheel, and the orientation of the wheel and sliding contact is made in such a way that this slot breaks the contact whenever the vane is in a mean position.

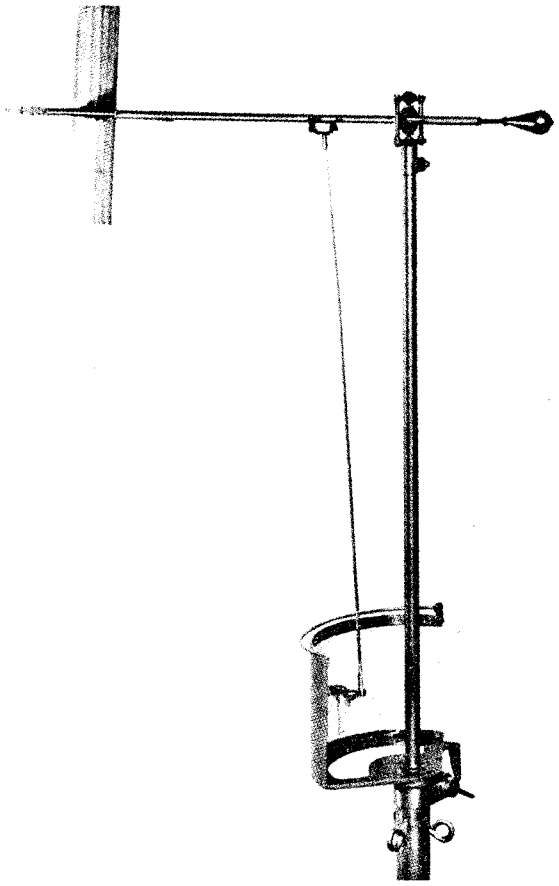

FIGURE 23. Photograph of British bidirectional vane.

Two sliding contacts are mounted 180° apart on each wheel, and each registers on a separate counter. One measures the total amount of deflection which the vane experiences and the other records the number of times that the mean position is crossed. The four counters required are mounted in a conveniently transportable box. The gimbals are mounted on a brass tube which can be supported by a surveyor's tripod, and from the tube a cable connects the contact points in the gimbals with the counter box.

The British bidirectional vane was constructed after the design by Best. In his original paper Best gives the following discussion.

The bidirectional vanes were constructed for this particular investigation and in their construction, special attention was paid to the following points:

1. The vanes should be as sensitive as possible to light winds.

2. The sensitivities in horizontal and vertical directions should be as nearly equal as possible.

3. The supports and chart holders should be arranged to cause the least possible interference with the vane.

4. The two vanes should possess similar characteristics.

5. The vanes should be fairly robust in order to prevent accidental damage.

The first two points were satisfied by making the vanes light, reducing the friction at the bearings to a minimum, making the moment of the pressure due to the wind about the axis as large as possible, and making the vanes symmetrical about their axes. Allowance was made for the third point by ensuring that the center of the vane should be at least five times the height of the chart holder above the base of the chart holder.

A photograph of one of the vanes is shown in Figure 23. As may be seen, the actual vane was constructed of stiff wire and balsa with a brass balance weight at the nose. The bearings were all point bearings, and stops were provided to prevent the vanes from being deflected too far in either direction. Suspended from the framework of the vane was a wire pen arm to the end of which was attached a small glass pen. Every movement of the point of suspension of the pen on the vane arm was reproduced, to a close approximation on the same scale, on a chart which formed part of a cylinder having the same vertical axis as the vane. The glass pen was made by drawing out a piece of glass tubing and bending the fine end suitably.

15.6 MISCELLANEOUS

15.6.1 Smoke Puffer

A simple and practical means for estimating wind speed and direction in the jungle without the use of elaborate recording instruments is by observing the travel of a small smoke cloud. The smoke from an H–C mixture is fairly satisfactory, but because of its heat, this smoke tends to tower in low winds. On mixing with moist air, titanium tetrachloride ($TiCl_4$) forms a cool white smoke. Figure 24 gives the essential features of a simple device which employs this material to produce puffs of smoke which can be followed with ease for distances of 10 to 20 ft through the jungle. A rubber tube of suitable length permits the operator to generate the smoke by "remote control."

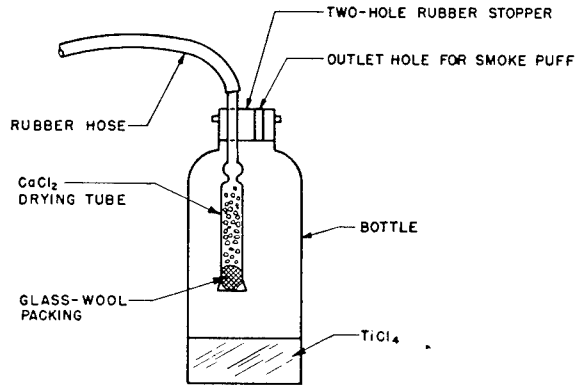

FIGURE 24. Diagram of a smoke puffer bottle.

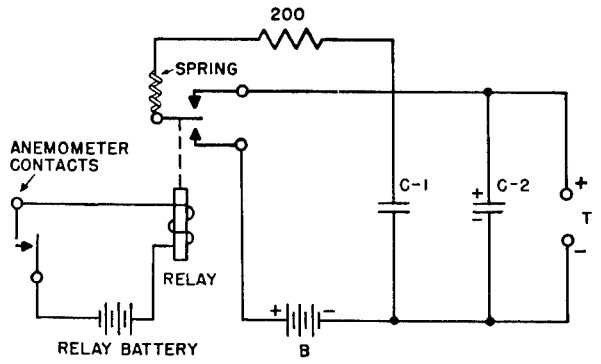

FIGURE 25. Circuit diagram of a relay-type frequency meter.

15.6.2 Photocell Illumination Recorder

The primary factors influencing the magnitude of the daytime lapse in a given area are: (1) the altitude of the sun, (2) the wind speed, and (3) the amount of cloud cover. The first two factors can be ascertained readily by direct measurement and from knowledge of the time of day, time of year, and the approximate latitude of the area under consideration. The amount of cloud cover, however, is a different quantity to handle, especially in a jungle, and when more or less continuous observations are necessary. An instrument which records a quantity related to the intensity of the solar radiation should yield data varying with cloud cover. Such an instrument was designed and constructed at San José and installed at the tower station. It was essentially an electronic circuit which amplified the current of a photocell.

The cell with vacuum tube and batteries was mounted in a waterproof box at the top of the tower, one side of the box being made of Plexiglas, a transparent plastic. A sheet of white celluloid, fixed in the horizontal plane, reflected the light from the sun, sky, and clouds through the window to the photocell. The current induced in the cell was amplified by the vacuum tube and then passed through long leads to a recording milliammeter at the instrument shack.

15.6.3 Humidity Measurements

Sling psychrometers were generally used to measure relative humidity. A hygrograph may frequently be employed to follow general diurnal trends in the forest, although it is not accurate in detail because of shifting of the zero point. The dry bulb of the sling psychrometer was used regularly in some projects as a check against the temperature profile apparatus.

15.7.3 The Relay-Type Frequency Meter

The most satisfactory means found for recording wind velocity from a rotating anemometer consists of an Esterline-Angus milliammeter used with a relay-type frequency meter. This system presents the advantages that (1) the record is immediately available without further treatment, (2) the record is not far from linear in calibration, (3) there is a choice of paper speeds ranging from $\frac{3}{4}$ in. per hr to 3 in. per min depending on the purpose for which the record is required, and (4) that the records may be preserved in compact form in such a way that although any portion may be intensively studied, there is no further measuring or computation to be done.

This type of circuit, shown in Figure 25, is referred to [14] as a condenser discharge anemometer. It operates as follows:

When the anemometer contacts are closed, the relay (see Figure 25) is energized and C_1 is charged through the lower relay contact to essentially the full voltage of battery B. When the anemometer contacts are opened, condenser C_1 discharges almost completely into the smoothing condenser C_2 (much larger than C_1) and eventually the charge passes through the milliammeter. This process is repeated for every make and break of the anemometer contacts, the quantity of electricity transferred each time being equal to the $V_b \times C_1$, where V_b is the battery voltage and C_1 is in farads. The current through the milliammeter is then equal to $F \times V_b \times C_1$, where F is the number of anemometer contacts per second.

Since the resistance of the milliammeter is fairly high, the voltage drop across the terminals T is an appreciable fraction of V_b, and C_1 will not be completely discharged when the milliammeter shows a

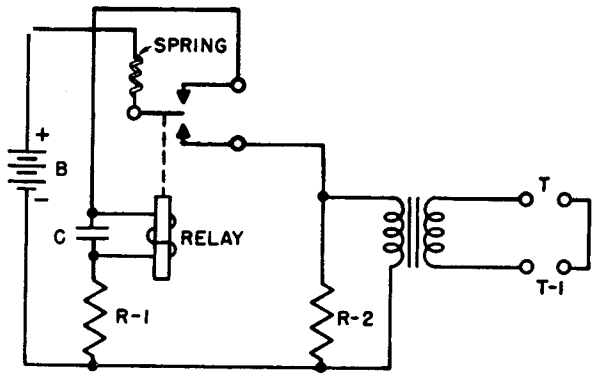

FIGURE 26. Circuit diagram of a keep-alive relay oscillator.

deflection. The exact formula relating I_m, the current in milliamperes passing through the recording meter, to F is given below:

$$I_m = \frac{1{,}000\, C_1\, F\, V_b}{1 + C_1\, F\, R_m}$$

where R_m is the meter resistance.

The number of contacts per second corresponding to each successive mile per hour of wind speed can be obtained from the anemometer calibration curve; V_b and C_1 can then be so chosen that the resultant calibration curve (milliamperes against wind speed) is nearly linear and corresponds in some way to the lines on the chart paper. Since the anemometer will not turn at all below a threshold of ½ to 1 mph, the zero of the milliammeter may be intentionally set a little to the right of the first chart line and then the uniformly spaced chart divisions will correspond quite well over the whole range to uniform steps of miles per hour.

The smoothing condenser C_2 is chosen to be large enough so that each individual pulse from C_1 will cause, even at the lowest wind speeds, only a tolerable wavering of the recording pen. A larger value of C_2 will unnecessarily reduce the speed of response of the system, tending to give a weighted time average of the wind velocity over the past period of time. The overall speed of response of the system then depends on the response time of the milliammeter, the introduced time delay, and hence the number of contacts per revolution of the anemometer, and the relation between the moment of inertia of the anemometer cups and their effective area which is exposed to the force of the wind.

Both the CIT model of the Lane-Wells anemometer and the Friez 339-L anemometer (preferably modified so that it gives two contacts per revolution) have proven satisfactory; the use of photocells with a faster-acting similar type of vacuum-tube frequency meter has also been used with the Biram anemometer with good field results and a somewhat faster speed of response. In practice, the Lane-Wells anemometer with its recording circuit will in a few seconds (depending on the wind speed) give a 50% response to an abrupt change in wind speed.

15.7.4 The Keep-Alive Circuit

Experience with the Esterline-Angus meters in the field has indicated that far more satisfactory records are obtained with them if, in addition to the measuring current, a small low-frequency alternating current is passed through the moving coil. This "keep-alive" current, just enough to cause the pen to tremble visibly, serves to make the pen continually assume its true equilibrium position; if it is not present the pen will not follow rapid fluctuations in the measuring current with a high degree of accuracy, and particularly at low paper speeds the pen will tend to move in jumps.

The most economical way of obtaining this small alternating current, of a frequency of about 10 c, is by the use of a relay oscillator together with a small transformer, condenser system, or pair of batteries controlled by the relay contacts. A simplified diagram of the shunt-type relay oscillator with transformer is given in Figure 26, and the explanation is as follows.

When the battery B is first connected, condenser C is charged through resistance R_1 and as soon as the voltage across C becomes high enough, the relay armature is pulled down and a pulse of current is sent through the transformer. When the connection at the upper contact is broken, however, the relay armature is not released immediately because the current stored in C continues to flow through the relay coil. Since the air gap in the magnetic circuit is reduced when the armature is held down, the armature can be held down by a current considerably smaller than that required to pull it down initially. Finally the condenser current through the relay coil decreases sufficiently to allow the spring tension to release the armature, and the cycle can then be repeated.

In practice it has been found that considerable experimentation is required to get a given type of relay to function dependably over long periods of time; the exact analysis of the action is complicated and there are numerous possible variations of the

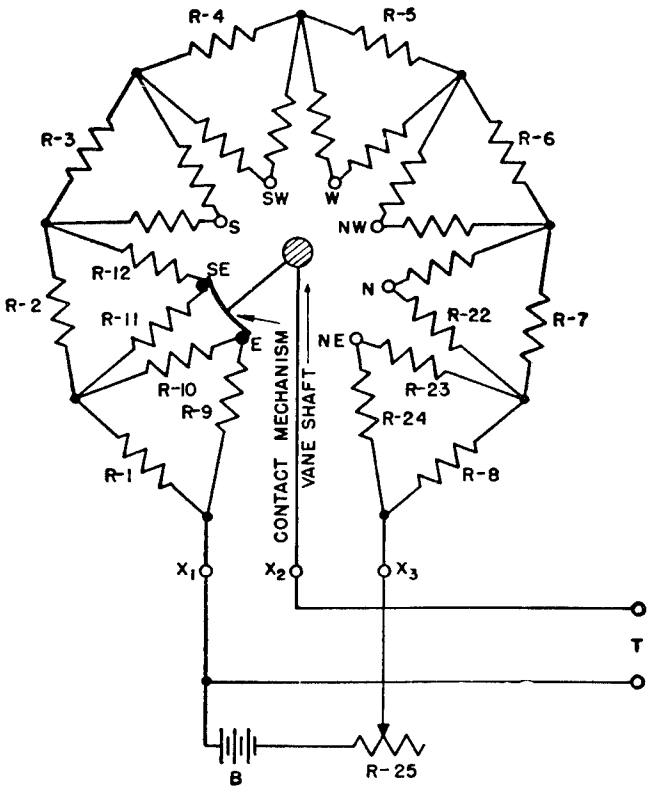

Parts List for Recording Wind Vane Circuit

12 Volt Model:

R_1 to R_8	75 ohm 1 watt carbon resistors (selected for uniform resistance).
R_9 to R_{24}	1000 ohm ½ watt carbon resistors (selected for uniform resistance).
R_{25}	200 ohm 4 watt rheostat.
B	Two 6 volt dry batteries in series (Burgess Uniplex No. 4F4H).
T	Terminals to Esterline-Angus recording milliammeter connected in series with 12,000 ohms or more.

2 Volt Model:

R_1 to R_8	5 ohms each (see above).
R_9 to R_{24}	200 ohms each.
R_{25}	15 ohm rheostat.
B	2 volt charge-retaining storage battery.
T	Terminals to E–A meter connected in series with 800 ohm wire wound resistor.

FIGURE 27. Diagram of a resistor assembly with Friez 363–C wind vane.

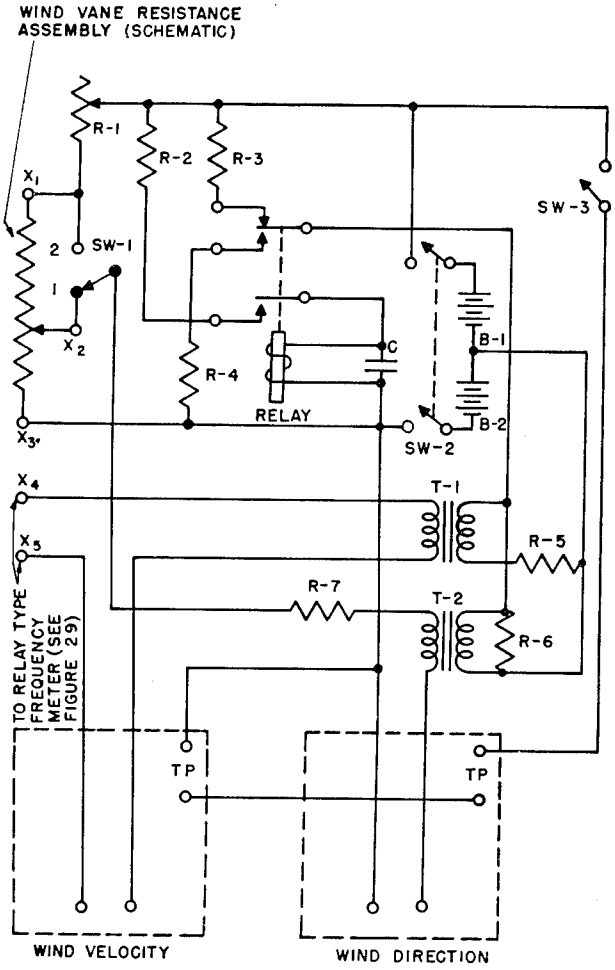

Parts List for 12-Volt Wind Direction and Velocity Recorder.

B_1,B_2	Burgess Uniplex No. 4F4H dry batteries.
C	150 mfd 50 volt electrolytic condenser.
Relay	Advance No. 500 DPDT 6 volt, 1000 ohm coil.
R_1	200 ohm rheostat.
R_2	450 ohm 1 watt carbon resistor.
R_3R_4	10 ohm 1 watt carbon resistor.
R_5	5000 ohm 1 watt carbon resistor.
R_6	1500 ohm 1 watt carbon resistor.
R_7	13,500 ohms total, wire wound.
SW_1	SPDT toggle switch (ordinarily in position 1; for adjusting R_1 to give standard deflection of wind direction meter, switch to position 2).
SW_2	DPST toggle switch.
SW_3	Push-button type microswitch [for simultaneous actuation of chronograph pens (TP)].
T_1,T_2	Doorbell transformers, 110 volt to 10 volt, 60 c.

FIGURE 28. Diagram of a circuit for 12-volt wind direction and velocity recorder.

circuit. The time the relay remains in the open and closed positions depends on the capacity of C, the battery voltage, the relay resistance, and the adjustment of the spring and relay contacts. The inertia of the armature and the resonant frequency of the condenser-resistance-inductance combination appear to have quite an effect on the stability of operation. When properly designed, however, the circuit appears capable of giving year-long uninterrupted service from a dry cell.

15.7.5 The Recording of Wind Direction

Figure 27 shows a means of obtaining an indication of wind direction by a resistor assembly attached to a standard Friez 363–C wind vane. The eight contacts of the vane are made to indicate 16 steps of

direction, 15 of them as successive steps in the milliammeter, and one as a single position about midway in the deflection. It has been found in practice that the latter indication, although nearly the same as one of the other steps, causes no confusion in interpretation because the vane will not ordinarily turn abruptly through an angle of 180° without leaving an indication of the intervening directions, and this anomalous position can in any case be oriented away from the prevailing directions.

Since the circuit is a modified potentiometric circuit, the resistance of the contacts is unimportant, and a completely open contact will show zero voltage on the milliammeter; this indication is different from that of any wind direction. The use of a specially designed wind vane would reduce the bulk and weight of the apparatus, and light-friction units are now commercially available for changing a circular indication into linear meter indication, with a negligible transition interval from low-scale to high-scale readings.

15.7.6 Examples of Complete Circuits as Used in the Field

Figures 28 and 29 show the complete diagrams with circuit constants of two field sets for recording wind direction and velocity. The 12-v model, containing two recording meters in one case, is too heavy for convenient transportation away from a vehicle, but has the advantage of being self-contained. It will record for a week without attention to the meters, and the self-contained batteries will give about 1,500 hr of service before it is necessary to replace them.

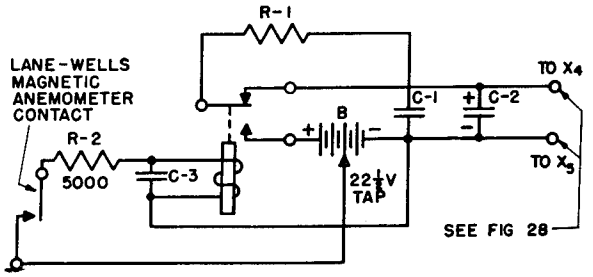

FIGURE 29. Diagram of a frequency meter circuit for 12-volt recorder.

The 2-v model, using a charge-retaining lead-acid storage battery, will withstand temperatures far below 20 F, where dry cells would freeze and become unreliable, and contains only the recording meter for wind velocity; the wind-direction recording milliammeter can be easily carried separately and attached. In all cases the milliammeters must be properly shock-mounted to withstand transportation.

Chapter 4

GENERAL PROPERTIES OF AEROSOLS

By *W. H. Rodebush*

18.1 INTRODUCTION

THE TERM *aerosol* is used to designate particles dispersed in a gaseous medium. The term *particulate* is preferred in Great Britain and more specific and familiar terms such as *smoke*, *fog*, and *dust* should be used whenever applicable. For example, an aerosol of particles of diameter less than about one micron will exhibit the characteristic behavior of a smoke and may be properly so designated. The particles of which the aerosol is composed may be either solid or liquid. If liquid the particles will be spherical, but solid particles will usually behave approximately as spheres.

18.2 STABILITY

Aerosols, like most colloidal forms of matter, are essentially unstable, and will usually disappear with the passage of time either by evaporation or precipitation. Evaporation will occur if the substance of which the aerosol is composed has an appreciable vapor pressure at room temperature. The vapor pressure of a small drop is larger than that from a large mass of substance, but this effect is not important for a drop diameter greater than 0.01 micron.[1]

Precipitation may occur as a result of diffusion or settling. The diffusion constant varies inversely as the particle diameter, and the rate of diffusion to a wall depends upon the concentration of aerosol in the surface layer. Unless the surface layer is constantly renewed the concentration quickly falls to zero, and only by very violent stirring can the surface layer be kept moving with sufficient velocity to maintain the diffusion process.

These statements concern ordinary or kinetic diffusion. Thermal diffusion is the process by which an aerosol is deposited on cold surfaces. It is a much more effective process in the precipitation of aerosols but the theory of thermal diffusion is not in very good agreement with the observed facts.

Settling, ordinarily, accounts for the precipitation of aerosols of diameter 1 micron or greater. According to Stokes' law a particle falls with a steady velocity which is proportional to the square of the diameter. The instantaneous rate of precipitation is independent of the amount of stirring (within limits) because the layer of air in contact with the surface remains stationary and the particles fall through this layer at constant velocity.

It follows, therefore, that aerosols of large particle diameter disappear by settling, and those of very small particle diameter by diffusion. For particles in the range of 0.1 to 1.0 micron diameter, the diffusion constant is small and the Stokes' law rate-of-fall is small. Smokes, which are usually composed of particles in this size range, therefore, are remarkably stable, and remain dispersed for long periods of time. The foregoing statements apply to aerosols which do not carry electrical charges. The behavior of charged aerosols will be discussed later.

18.3 COAGULATION

When a particle of small diameter collides with a surface it adheres because of surface forces. Large dust particles may be dislodged by a strong blast of air so that air cleaners are often coated with a film of oil or sticky liquid, but small particles will adhere regardless of the surface. Similarly, the collision is inelastic and a single particle is the result when two particles collide. If the particles are liquid they coalesce to a single drop whereas solid particles form aggregates which often take the form of chains and resemble fibers on casual inspection. This coagulation resembles a bimolecular mechanism, and is described by the equation for a second order reaction. Table 1 gives the approximate times necessary to reduce the number of particles to one-tenth of the original number [computed on the basis of equation (19), Chapter 19].

TABLE 1. Rates of coagulation (t_0) equals time required to reduce the number of particles to one-tenth of the initial number. W equals mg per l, assuming diameter equals 1μ, and density equals 1.

No. per cm^3	W mg per l	t_0 sec
10^{10}	5,236	3
10^9	523.6	30
10^8	52.36	300
10^7	5.236	3,000

As a result of this coagulation a smoke of uniform small particle size will become heterogeneous, and the larger particles will settle out. It follows, therefore, that a smoke with a concentration of particles greater than 10^7 per cubic centimeter will not be stable. There is no method known for preventing the coagulation of aerosols. The stabilizers which are effective for preventing the coagulation of solids or liquids dispersed in a liquid medium are completely ineffective with aerosols.

18.4 FORMATION OF AEROSOLS

Natural-occurring fogs are of relatively large particle size, 10 to 50 microns diameter, and of relatively low concentrations, a few droplets per cubic centimeter. Each droplet is formed by the condensation of water on a nucleus, which in the neighborhood of cities may be a particle of dust or soot. Near the ocean, minute salt crystals, which are thrown into the air by spray, serve as nuclei, and the water collected always contains dissolved salt. Therefore, fogs are more common near the ocean, or in the neighborhood of large cities, or industrial areas.

Because of the large particle size, fogs tend to fall out as a fine mist or rain, and this process is accelerated by the tendency of the small drops to evaporate; the vapor condensing on the larger drops. Thus, fogs will only persist if meteorological conditions are such that new drops are constantly forming to replace those that fall.

The droplets of natural fogs often carry considerable electrical charges and the accumulation of these charges accounts for the electrical effects that occur in thunderstorms when the small drops coalesce rapidly to form larger drops. It may be remarked that the conditions which produce rapid coalescence and the heavy downfall of rain are not compatible with the conditions that produce fog, and vice versa.

The methods of producing aerosols artificially fall into two categories: mechanical dispersion, and vapor condensation. Mechanical dispersion appears at first thought to offer the most promise. The work required to break up a liquid into drops of 1 micron diameter is negligible when compared to the heat of vaporization. There are two difficulties. The first is that the only method for bringing about this breakup is that of turbulent flow through a nozzle which is, of course, a very inefficient process mechanically. An even more fundamental difficulty, however, is that the concentration of drops leaving the nozzle is so high that most of the small drops coagulate before leaving the immediate vicinity of the nozzle. This difficulty can be avoided only by using an aspirator nozzle, and maintaining a very high air velocity to scatter the drops before they can coalesce. One hundred and fifty cubic feet of air at 50 lb pressure per gallon of liquid will give only a fair dispersion. The dispersion of solids is even more difficult. The solids must be ground to the required particle size, which is a very inefficient process mechanically, and then dispersed in an air jet. It has been pointed out earlier that the surface forces which cause particles to adhere are relatively very strong so that it is difficult to bring a sufficient shearing force to overcome them by a blast of air. The operation of grinding and dispersal may be combined in one operation by the use of a *micronizer* but the process remains an inefficient one.

The most satisfactory way to produce an aerosol is to imitate the process by which natural fogs are produced. Any substance which can be vaporized without decomposition can be converted to an aerosol by blowing a jet of the vapor into cool air. When the degree of supersaturation is small, drops will not form by condensation except on nuclei which may be present in the form of ions, dust particles, etc. When the degree of supersaturation is great, as when the vapor of a high boiling oil escapes into the atmosphere at high velocity, an enormous number of very small droplets will be formed. It is difficult to see what sort of nuclei can be present in such enormous numbers but it cannot be stated categorically that nuclei are not present. It may be in the case of the oil that the larger molecules behave as nuclei. Coagulation takes place very rapidly as described in Chapter 22 but the size range remains narrow as the process

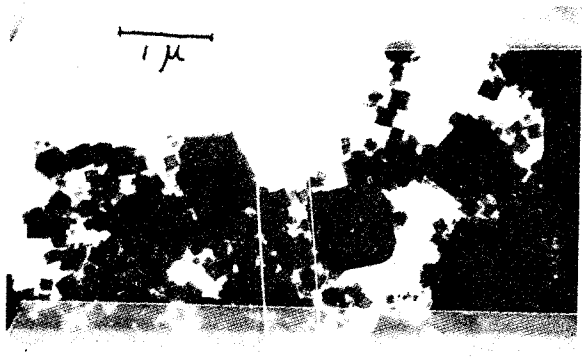

FIGURE 1. Electron microscope picture of magnesium oxide smoke particles.

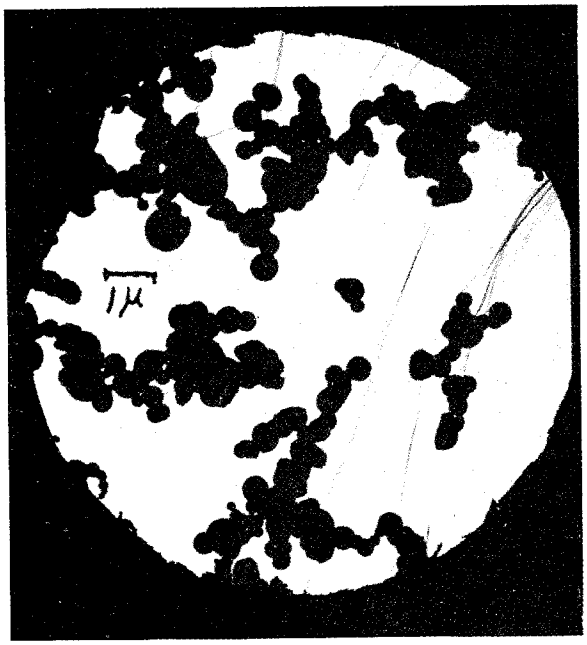

FIGURE 2. Electron microscope picture of titanium oxide smoke particles.

goes on, so that it is possible to control the size of droplets quite precisely by regulating the rate of vapor flow.

A modification of the vapor condensation process is used when smokes are produced by combustion. When magnesium ribbon is burned, the ultimate particles produced are nearly perfect crystals of magnesium oxide which are too small to be seen by the ordinary microscope, but are revealed by the electron microscope as shown in Figure 1. These submicroscopic crystals agglomerate into chains and clusters of fantastic shape and structure, which appear under the microscope as though they were solid particles. Figure 2 is an electron microscope photograph of titanium particles produced by thermal dispersion. When carbon smoke is produced by incomplete combustion the small crystals of graphite tend to form filaments that resemble a string of beads (see Figure 3). This tendency of soot and dust particles to form filaments often deceives the housewife who supposes these "cobwebs" to be produced by spiders.

18.5 ELECTRICAL PROPERTIES OF AEROSOLS

Except for special cases, which will be discussed later, electrical charges are of minor importance. Most of the particles produced are uncharged, particularly if the concentration of the aerosol is high, since normally there are only a few ions present per cubic centimeter. Even in the case where ions are produced by special means to serve as nuclei, the resulting aerosol will contain many uncharged particles, since the positively and negatively charged particles have a tendency to neutralize each other by agglomeration. If it is desired to precipitate aerosols in a uniform field, it is necessary to charge the aerosol before the process will be effective.

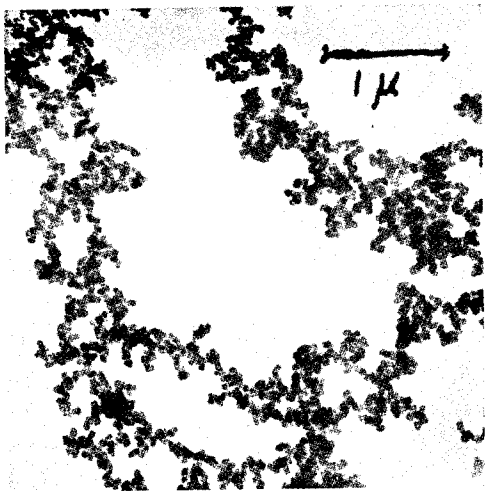

FIGURE 3. Electron microscope pictures of carbon particles from camphor smoke.

18.6 FILTRATION

Neither electrical nor thermal precipitation have proved in the past to be practical for the rapid removal of aerosols. Filtration appears to be, by long odds, the most satisfactory method of precipitation. Aerosol filters consist of loosely aggregated fibers, and, in order to avoid excessive resistance to the flow of air, the mesh of the filter must be large compared to the size of the particle to be removed. There is therefore no screening action; the removal of a particle depends entirely upon a chance collision of the particle with a fiber of the filter. Once having collided, the particle adheres by the natural forces which are always operative.

Very large particles can be precipitated by centrifugal action as in a cyclone separator. For smaller particles whose diameter is in the neighborhood of 1 micron the centrifugal action is no longer effective since the inertia of the particle is not sufficient to overcome the resistance of the air. Thus the air flows

around the fibers of a filter in stream lines and the particles are carried around with the stream lines. There is a range of particle sizes for which a higher velocity will improve the operation of the filter since the inertial effects will carry the particles across the stream lines into collision with the fibers of the filter. For particles smaller than 1 micron diameter no inertial effects exist, but the kinetic diffusion becomes of greater importance in the smaller particle. Very small particles($\approx$ 0.01 micron) are precipitated very rapidly by diffusion. The process is analogous to the condensation of a vapor on a cold surface. The particles most difficult to remove by filtration are those in the range 0.1 to 1.0 micron, i.e., smokes. In order to obtain efficient filtration without excessive resistance the filter must contain fibers of small diameter approaching that of the particles themselves.

18.7 BULK DENSITY OF AEROSOLS

It will be apparent from reference to Table 1 that the increase in density of the air due to the presence of an aerosol cannot be very great unless (1) the number of particles per cubic centimeter is very large, or (2) the particle size is very large. If the number of particles per cubic centimeter is large, however, the particle size will increase rapidly so that the second condition is actually the only one under which a considerable mass of aerosol can be present. If the particle size is very large, the particles will fall so rapidly under the force of gravity that the aerosol concentration cannot persist. If a high concentration of aerosol particles of 10 microns diameter could be produced, a very great increase in the bulk density of the air would result, but there is no simple method of doing this. In general, therefore, the density of an aerosol cloud does not differ greatly from that of the air itself.

18.8 OPTICAL PROPERTIES

Lord Rayleigh called attention to the very important optical properties of finely dispersed particles in his theory of the blue color of the sky. The theory of optical behavior is still obscure for opaque or reflecting particles but for transparent spheres such as oil drops the behavior is now well understood (see Chapter 21). The maximum scattering effects are obtained when the particle size approximates the wavelength of the light being scattered. The greatest scattering is in the forward direction and the maximum polarization is at right angles to the incident light. It is entirely a coincidence that the particle size which gives the greatest stability against precipitation and filtration lies in the range which gives the maximum scattering for visible light.

18.9 SMOKE SCREENS

Smoke screens composed of small drops of transparent liquids actually have greater obscuring power than those of opaque particles. The reason for this is that the transparent drop transmits a background of light which makes it difficult for the observer to distinguish inconspicuous objects. This effect is particularly important when the observer is facing the sun so that the forward scattering causes a glare.

Chapter 5

STABILITY OF AEROSOLS AND BEHAVIOR OF AEROSOL PARTICLES

By *David Sinclair*

19.1 DEFINITIONS

An AEROSOL is an assemblage of small particles, solid or liquid, suspended in air. By small particle is meant a particle with a radius less than about 50 microns. The usual range of particle radii in aerosols is from 0.1 to 10 microns, although particles as small as 0.01 micron may be encountered.

Aerosol is the generic term for dust, smoke, fog, and haze. Dust is commonly thought of as solid particles of any material blown up by the wind, smoke as solid particles of ash or carbon resulting from fires, and fog as water droplets. These definitions are satisfactory for natural aerosols. For artificial aerosols, a smoke is defined as an aerosol of solid particles, and fog is defined to include droplets of any liquid such as water, oil or acid.

The different types of aerosol frequently overlap. Carbon may produce a smoke or a dust. Tobacco smoke is very hygroscopic and consists chiefly of water droplets. When fresh, stearic acid aerosol is a fog of supercooled droplets, which slowly change to a smoke of crystal particles. Haze may be composed of fine particles from any source.

19.2 RANGE OF PARTICLE SIZE

The range of particle sizes in the various types of aerosol is considerable. Dust may range from fine particles of 0.1 micron radius or less, which produce haze, to sandstorms having large particles beyond the range considered to be aerosols. Smoke is often composed of extremely fine primary particles which have coagulated to form groups (see Figures 1 and 2 in Chapter 18, 1 and 2 in Chapter 22). Carbon smoke is composed of small primaries about 0.01 micron radius which coagulate into long irregular filaments that may reach several microns in length (see Figure 3, Chapter 18). Screening oil for droplets should be about 0.3 micron radius for maximum screening. Water fog droplets are much larger, ranging from 4 to 40 microns in radius.

19.3 STABILITY

The stability of an aerosol is determined by a number of factors. The individual particles may move about under the influence of several different forces: (1) Brownian movement, which consists of random oscillations and rotations causing coagulation, accompanied by drift which results in diffusion to any solid object such as the walls of a containing vessel or the ground; (2) settling under gravity; (3) thermal forces, causing movement of the particles toward any object colder than its surroundings; (4) electrical forces; (5) acoustical forces; and (6) centrifugal forces.

In addition, convection currents are usually present which consist of motion of large or small regions of the aerosol relative to other regions.

Finally, there may be evaporation, causing the particles to decrease in size and even disappear, and condensation which may cause the particles to increase in size until they fall out very rapidly.

Under ordinary conditions the stability of an aerosol is chiefly affected by the Brownian oscillations and by gravity settling. Owing to the Brownian oscillations the particles collide and either adhere or coalesce. If the particles are solid they adhere to form more or less loose aggregates which may be roughly spherical in shape as those for ZnO or albumin, or filamentary like carbon. If the particles are spherical droplets such as oil or water fog, they coalesce to form larger spherical droplets. As a result of this coagulation process, the number of particles per unit volume of aerosol and the number concentration decreases, and the average size of the particles increases.

Filtration of fine particles is largely a diffusion process (see Chapter 23). Otherwise, except for an aerosol of very fine and highly concentrated particles in a small containing vessel,[1] diffusion is unimportant.

The question often arises as to the efficiency of collision, i.e., what proportion of the colliding particles will adhere rather than rebound. It would be difficult to observe the process directly under the microscope, but indirect experiments indicate that the collision process is 100% efficient. In most experiments, the observed coagulation of solid particles is greater than that calculated from the simple theory, and not less, as it would be if the efficiency of collision were appreciably less than 100%. In the case of

liquid droplets it can be safely assumed that all droplets will coalesce on collision. Whytlaw-Gray [2] finds that his experiments on coagulation justify the assumption of 100% efficiency. We know of no experiments to contradict it.

Numerous attempts have been made to surface-treat solid particles,[3] or charge them electrically so that they would be less likely to adhere on collision, but no significant effect has as yet been observed. The only observed effect has been either to cause aerosol particles to disappear more rapidly, or to cause the particles in powder form to adhere less tightly, thus making them more easily dispersed in an air jet or by explosion. In the aerosol state, the forces of adhesion are always greater than any ordinary forces of separation.

Under the force of gravity, aerosol particles settle onto any surface having a horizontal component. The large particles settle out faster than the small particles, the rate of settling being proportional to the cross-sectional area of the particle. As a result, both the number concentration and the average particle size decrease.

Because of their comparatively small size, the particles adhere to whatever type of surface they settle upon, and the efficiency is again 100% as in the case of coagulation. The forces of adhesion are greater than the ordinary forces tending to pull the particle away from the surface.

Whenever aerosol particles are found adhering to vertical or inverted surfaces, forces other than gravity must be present.

Thermal and electrical forces are more common than generally realized. Dust near steam pipes or other hot bodies is precipitated onto the neighboring walls or ceiling. Ink fog in printing plants or dust in textile mills is precipitated onto the walls or ceiling by static electrification from the rollers or other machinery. Filtration is in some cases due largely to static electrification.

Acoustical forces are also fairly common. Sound vibrations above a certain minimum frequency, depending on the particle size, increase the rate of coagulation. Intense vibrations in factory buildings may cause precipitation, particularly in pipes. Thunder claps and explosions are known to precipitate rain and dust. Air raid sirens and similar sound sources will precipitate natural and artificial water fog.

Centrifugal forces large enough to cause coagulation or precipitation are less common. Small particle aerosols will travel around bends in pipes or through constrictions (provided they are free of sharp edges) without serious precipitation. For example, a particle of 0.1 micron radius requires a centrifugal acceleration of one million times gravity to precipitate it in a centrifugal separator.[4] Much of the coagulation of small particle aerosols in pipes and ducts is attributable to thermal, electrical, or acoustical forces rather than to centrifugal forces. This is not true, however, for aerosols of large particles, i.e., radii above a few microns.

One or the other of these factors may dominate in determining the stability of an aerosol. In a natural water fog, settling is the predominant factor, as it usually is in large particle aerosols. In flue gases, which contain very large numbers of very fine particles, coagulation is very rapid at first. Later, settling becomes more important, usually after emission into the atmosphere. In the case of screening oil fogs, evaporation and wind are the important factors.

Dilute aerosols of fine solid particles that neither coagulate nor evaporate may be so stable as to persist almost indefinitely. For example, volcanic dust, which may be expelled into the air several miles above sea level and which has a particle radius of 0.3 micron, falls at the velocity of about one mile per year. This is the size of the droplets of a screening oil fog. It is the slow rate of fall of fine particles that makes it possible to maintain a smoke screen for long periods.

19.4 SETTLING OF AIRBORNE PARTICLES UNDER GRAVITY

19.4.1 Uniform Particle Size or Homogeneous Aerosols

In aerosols of uniform particle size, which may be produced in the laboratory by a method described in Chapter 20, two cases may be distinguished: (1) settling when the aerosol is completely free from convection currents, called tranquil settling, and (2) settling when the aerosol is kept stirred so that the concentration throughout the containing vessel is uniform at all times.

Tranquil Settling

In tranquil settling all the particles fall with the same velocity. The cloud will have a well-defined flat top which will be observed to fall with a constant velocity equal to that of a single particle. This is the basis of a method of measurement of the particle radius of a uniform aerosol, described in Chapter 22.

The velocity of fall in centimeters per second is given by Stokes' law [5] of fall of small spheres in a continuous viscous medium. In air

$$v = \frac{2}{9}\frac{r^2\rho g}{\eta} = 1.2 \times 10^6 \rho r^2, \qquad (1)$$

where r is the particle radius in centimeters, ρ the particle density, η the coefficient of viscosity of the air, and g the acceleration of gravity.

This law is correct to 5% or better for spherical particles between 1 and 50 microns radius. The particles fall with a velocity less than that given by Stokes' law when they are so large [6] that $vr = \eta/\rho_1$, where ρ_1 is the density of the air. For air $\eta/\rho_1 = 0.15$ and when $r = 50\mu$, $vr = 0.15$ for particles of unit density. For such particles the velocity becomes so large that turbulence occurs, decreasing the velocity more than does the viscous drag alone.

For smaller particles whose size is comparable with the mean free path of the air molecules, a correction must be applied to compensate for the tendency of the particles to "slip" between the air molecules, and thus move faster than predicted by Stokes' law. This correction has been calculated from Cunningham's equation [5] and it was found that the true radius is given quite accurately by subtracting 0.04 micron from the Stokes radius (in microns), for all radii between 2 and 0.1 microns.

For still smaller particles the correction is much larger. However, the velocity of fall of particles below 0.1 micron is so small that it is extremely difficult if not impossible to make observations of their settling velocity.

Stokes' law applies strictly only to spherical particles. Millikan [7] has shown, however, that the law holds quite well for particles whose shape is somewhat different from spherical.

Stirred Settling

In stirred settling the motion of the particles is complicated by random convection currents. Except for very large particles or violent stirring there is little or no impingement on the walls or ceiling. Nearly all the particles eventually settle on the floor.

The horizontal components of convection current have no effect on the velocity of fall. Since the upward convection currents will, on the average, exactly compensate for the downward convection currents they also have no effect on the velocity of fall. The convection currents merely serve to keep the concentration uniform throughout the containing vessel. The result is that the concentration continuously decreases as the settling continues so that the amount of aerosol settling out per unit of time continuously decreases.

The number of particles dn that settle out during a small interval of time dt is proportional to the number concentration n at the time t. The fraction of particles having velocity of fall v that settle out of a rectangular box of height h in time dt is

$$\frac{v}{h}dt = -\frac{dn}{n}.$$

By integrating this equation we find that

$$n = n_0 e^{-vt/h}, \qquad (2)$$

where n_0 is the initial concentration in the box. Thus the rate of settling (in terms of the number of particles per second), as well as the number concentration, decreases exponentially with time.

19.4.2 Heterogeneous Aerosols

In ordinary aerosols, composed of particles of many sizes, the settling process is more difficult to analyze. Again the two cases of tranquil and stirred settling will be considered separately.

Tranquil Settling

In tranquil settling, a differential separation according to size will occur, which may be analyzed as follows. Suppose at time $t = 0$ the concentration is uniform throughout the containing vessel and no convection currents are present. The particles of radius r will begin falling with the constant velocity v_r corresponding to that radius, and will continue to fall with that velocity independent of larger or smaller particles.

Consider a layer in the aerosol at a height x below the top of a containing vessel. At a time $t_1 = x/v_1$ there will be no particles in or above this layer, of radius greater than r_1. At a greater time $t_2 = x/v_2$, there will be no particles in or above this layer of radius greater than r_2, where r_2 is less than r_1. Consequently, observation of the decrease in number concentration at a height x, during the time interval $t_2 - t_1$ will give the number of particles having velocities of fall between v_2 and v_1, or radii between r_2 and r_1, given by Stokes' law.

This is the principle of the differential settler, described in Chapter 22, in which the decrease in number concentration is measured by the decrease in scattered light.

STIRRED SETTLING

The analysis of stirred settling of heterogeneous aerosols is more complicated. Each group of particles of radius r will settle exponentially, at a rate given by equation (2). The following discussion is based on the assumption that the particles have a logarithmic probability distribution.

Most natural distribution curves are found to be skewed from the symmetrical probability distribution. The number at larger sizes decreases more slowly than at smaller sizes in such a way that the distribution curve is made symmetrical when the number at a given size is plotted against the logarithm of the size.[8,9] This type of distribution has been found approximately in the thermally generated smokes produced in the laboratory (see Chapter 20).

One can characterize a given physical property of a heterogeneous aerosol, such as particulate volume or cross-sectional area, by an average diameter. For example, the total cross-sectional area of N spherical particles is $\frac{1}{4}\pi N d_2^2$, where

$$d_2 = \sqrt{\sum(nd^2)/\sum n}$$

is the diameter of the sphere having the average area; and the total volume of these N particles is $\frac{1}{6}\pi N d_3^3$, where

$$d_3 = \sqrt[3]{\sum(nd^3)/\sum n}$$

is the diameter of the sphere having the average volume.

If the aerosol has a logarithmic probability distribution of sizes, the number of particles per cubic centimeter having diameter d is:

$$n_d = \frac{N}{\log \sigma_g \sqrt{2\pi}} \exp\left[-\frac{(\log d - \log d_g)^2}{2 \log^2 \sigma_g}\right]. \quad (3)$$

Here N is the total number per cubic centimeter of particles of all sizes, d_g is the geometric mean diameter, i.e.,

$$\log d_g = \frac{\sum(n \log d)}{N},$$

which is equal to the number median diameter in this type of distribution and σ_g is the geometric standard deviation, i.e.,

$$\log \sigma_g = \sqrt{\frac{\sum(n \log d - n \log d_g)^2}{N}}.$$

It follows that

$$d_2^2 = \frac{\sum(n_d d^2)}{N} = \frac{1}{\log \sigma_g \sqrt{2\pi}} \int_0^\infty d^2 \exp\left[-\frac{(\log d - \log d_g)^2}{2 \log^2 \sigma_g}\right] \delta \log d, \quad (4)$$

with similar expressions for d_3, d_4, d_m. These equations have been integrated[9] and it is found that, in general,

$$\log d_m^n = n \log d_g + 2.303 \frac{nm}{2} \log^2 \sigma_g. \quad (5)$$

At time $t = 0$, when the aerosol is formed, the number of particles per cubic centimeter having diameters between $\log d$ and $\log d + \delta \log d$ is $n_d \delta \log d$. Therefore the initial total cross-sectional area per cubic centimeter of particles is:

$$C_0 = \frac{\pi}{4} \int_0^\infty d^2 n_d \delta \log d = \frac{\pi}{4} N_0 d_2^2. \quad (6)$$

Similarly the initial mass concentration in grams per cubic centimeter is:

$$M_0 = \frac{\pi}{6} \rho \int_0^\infty d^3 n_d \delta \log d = \frac{\pi}{6} N_0 \rho d_3^3. \quad (7)$$

Due to stirred settling, the mass concentration and cross section per cubic centimeter decrease exponentially with time according to equation (2). Therefore, at time t:

$$C_t = \frac{\pi}{4} \int_0^\infty d^2 n_d \exp\left(-\frac{v_d t}{h}\right) \delta \log d, \quad (8)$$

and

$$M_t = \frac{\pi}{6} \rho \int_0^\infty d^3 n_d \exp\left(-\frac{v_d t}{h}\right) \delta \log d. \quad (9)$$

In Stokes, settling [equation (1)] the velocity v_d in centimeters per second is

$$v_d = 3.0 \times 10^5 \rho d^2. \quad (10)$$

Taking the logarithm (to the base 10) of C and differentiating with respect to t, we obtain on substituting the value of v_d given by equation (10):

$$-\frac{d}{dt} \log C_t = 1.3 \times 10^5 \frac{\rho}{h} \cdot \frac{\int_0^\infty d^4 n_d \exp\left(-\frac{v_d t}{h}\right) \delta \log d}{\int_0^\infty d^2 n_d \exp\left(-\frac{v_d t}{h}\right) \delta \log d}. \quad (11)$$

For time t, small compared to h/v, equation (11) becomes:

$$-\frac{d}{dt} \log C_t = 1.3 \times 10^5 \frac{\rho}{h} \frac{\int_0^\infty d^4 n_d \delta \log d}{\int_0^\infty d^2 n_d \delta \log d}, \quad (12)$$

or

$$-\frac{d}{dt} \log C_t = 1.3 \times 10^5 \frac{\rho}{h} \frac{d_4^4}{d_2^2}. \quad (13)$$

Similarly:

$$-\frac{d}{dt}\log M_t = 1.3 \times 10^5 \frac{\rho}{h}\frac{d_5^5}{d_3^3}. \qquad (14)$$

Making use of equation (5), we find that equations (13) and (14) become:

$$-\frac{d}{dt}\log C_t = 1.3 \times 10^5 \frac{\rho}{h} d_6^2, \qquad (15)$$

and

$$-\frac{d}{dt}\log M_t = 1.3 \times 10^5 \frac{\rho}{h} d_8^2. \qquad (16)$$

It can be readily shown [10] that d_6 is the median weight diameter, which is equal to the geometric mean weight diameter in a logarithmic probability distribution. Consequently, when the particle density is known, the median weight diameter can be obtained by measurement of the decrease in cross section per cubic centimeter. Measurement of the decrease of mass concentration will yield d_8.

By substituting the values of d_6 and d_8 into equation (5), the number median diameter d_g, and the geometric standard deviation σ_g, may be calculated. By substituting the values of d_g and σ_g into equation (3), the particle size number distribution curve may be calculated.

This is the basis of a method of particle size distribution measurement described in Chapter 22, in which the geometric cross section is obtained by measuring the scattering cross section.

19.5 BROWNIAN MOTION. COAGULATION

19.5.1 Brownian Motion

In the preceding discussion it was assumed that coagulation and the other effects of Brownian motion were negligible. Due to the random Brownian motion, the top of a tranquil settling cloud of uniform particles will become blurred. Similarly, the upper boundary of the region of occurrence of particles of radius r in differential settling of nonuniform smoke will be spread vertically. This effect is unimportant except for very small particle sizes.

According to Einstein's [11] and Smoluchowski's equation of Brownian movement, the average displacement $\bar{x}$, in a given direction of a spherical particle of radius r in air in the time t, is

$$x = \sqrt{\frac{RT}{N}\frac{t}{3\pi\eta r}} = 4.8 \times 10^{-6}\sqrt{\frac{t}{r}}\ \text{cm} \qquad (17)$$

at $T = 293$ K. For a particle of radius 0.2 micron, in 1 hr $\bar{x} = 6.4 \times 10^{-2}$ cm, or slightly over ½ mm.

If this displacement is taken to be upward, then during the same time other particles will move an equal distance downward, so that after 1 hr the top of a cloud of uniform particles falling in still air will be spread vertically over a distance of about 1¼ mm. During this same time the whole cloud would have fallen through a distance, given by the Stokes-Cunningham equation of fall, of 2.5 cm.

The spread of 1¼ mm in 2.5 cm corresponds to a particle size spread of 2½%. This is considerably less than the spread of particle size in the most uniform aerosols.

19.5.2 Law of Atmosphere

Since the particles of an aerosol are in constant random motion, they exert a pressure just as do the molecules of a gas. Due to gravity, the pressure and particle concentration, i.e., the density of the aerosol, will ultimately vary with height according to the law of atmosphere: [12]

$$n_h = ne^{-mgh/KT} = ne^{-mh \times 2.46 \times 10^{16}}, \qquad (18)$$

when $T = 293$ K. Here n_h is the number concentration at a height h above the region where the concentration is n, and m is the mass of a particle.

As the aerosol particles fall under the action of gravity, and diffuse due to Brownian motion, the cloud approaches a concentration gradient given by equation (18). The time required to reach this concentration gradient decreases with the size of the particle, according to equation (17). Due to the settling and adhering of the particles onto the floor, the magnitude of the concentration at any point will finally decrease to zero, although the rate of disappearance is retarded by the Brownian movement.

It is seen that the concentration gradient increases rapidly with particle size. For example, particles of unit density of 0.01 micron radius will approach a concentration gradient of 10% per centimeter. For such particles the rate of diffusion is approximately equal to the rate of fall. For particles of 0.03 micron the final gradient is 90% per centimeter.

Above this size the final gradient is so large as to be practically equivalent to complete settling. Such sizes are well below the limit of usefulness of settling methods. Thus the law of atmosphere has no practical significance in aerosols of particle size greater than 0.05 micron in radius.

Perrin [12] found considerable effect in hydrosols for

particles of about 0.5 micron radius. Due to the buoyancy of the water, the concentration gradient is much less than in air.

19.5.3 Coagulation in a Homogeneous Aerosol

It has been found experimentally that due to coagulation alone the particle concentration in a uniform aerosol varies inversely with the time [13] that is:

$$\frac{1}{n} - \frac{1}{n_0} = \mathcal{K}t, \tag{19}$$

where n_0 is the initial particle concentration, and $\mathcal{K}$ is the coagulation constant. The differential equation of this process is evidently:

$$-\frac{dn}{dt} = \mathcal{K}n^2 \tag{20}$$

showing that the rate of coagulation is proportional to the square of the concentration.

According to the theory of Smoluchowski [13] $\mathcal{K}$ is equal to $4kT/3\eta = 3.0 \times 10^{-10}$ cc per sec in air at $T = 293$ K. Thus the rate of coagulation is independent of particle size. The equation is, of course, true only during the initial stages of coagulation before the process has introduced appreciable nonuniformity of particle size.

The coagulation equation has been tested experimentally by Whytlaw-Gray [13] who obtained good agreement with the theory when using approximately uniform particle size aerosols.

This equation holds only for particles that are large compared to the mean free path l. For smaller particles, the Cunningham correction must be applied. Equation (20) then becomes [13]

$$-\frac{dn}{dt} = \mathcal{K}\left(1 + \frac{0.9l}{r}\right)n^2 . \tag{21}$$

In air at room temperature, the mean free path $l = 10^{-5}$ cm. Consequently, due to the Cunningham correction 1 micron radius particles coagulate 8% faster, and 0.1 micron radius particles 88% faster than 10 micron radius particles.

The rate of coagulation at ordinary concentrations is quite low. For example, rewriting equation (20) in terms of the per cent coagulation per hour, gives:

$$-100\frac{dn}{n} = 1.08 \times 10^{-4}n . \tag{22}$$

Taking $n = 10^5$ (the concentration of a screening oil fog of 133-ft visibility) it is seen that approximately 11% of the particles coagulate per hour. A concentration of 10^5 particles per cubic centimeter is also frequently encountered in the laboratory. Due to the Cunningham correction, the rate for 1 and 0.1 micron particles would be increased to 12 and 21% respectively.

19.5.4 Coagulation and Stirred Settling Combined

Elementary Theory

The calculation of the rate of disappearance of particles due to both coagulation and settling is more complicated.

In the early stages of the life of a stirred uniform particle size aerosol the decrease of particle concentration is given approximately by adding equation (20) to the differential equation of equation (2). That is:

$$-\frac{dn}{dt} = \mathcal{K}n^2 + \frac{v}{h}n . \tag{23}$$

The solution of this equation is

$$\frac{1}{n} = -\frac{\mathcal{K}h}{v} + \left(\frac{\mathcal{K}h}{v} + \frac{1}{n_0}\right)e^{-vt/h} . \tag{24}$$

For times short compared to h/v, $e^{-vt/h} = 1 + vt/h$ so that equation (24) becomes

$$\frac{1}{n} = \frac{1}{n_0} + \left(\mathcal{K} + \frac{v}{h}\right)t . \tag{25}$$

For particles of 1 μ radius when $h = 100$ cm, $h/v = 10^4$ sec. Therefore equation (25) is reasonably correct for a period of about 15 min provided the concentration is not much over 10^5 per cubic centimeter.

If $1/n$ is plotted against time a straight line will be obtained having the slope $\mathcal{K} + v/h$ and the intercept $1/n_0$. Thus if $\mathcal{K}$ is known r may be calculated, and conversely.

This is the basis of a method of particle size measurement, described in Chapter 22, in which n is measured by measuring the intensity of light transmitted by the aerosol.

General Equation

The general equation of coagulation of a heterogeneous aerosol in stirred settling was derived by Goldman.[14] It was assumed that the aerosol is composed of spherical fog droplets which coalesce on collision to form larger spherical fog droplets.

Let the distribution of particle size be given by $dn(r) = n(r)dr$ = number of particles between r and $r + dr$. Then $\int_0^\infty n(r)dr = N$ = total concentration.

Since the distribution changes with time, $n(r) = n(r,t)$. The total concentration N does not depend upon r, so that $N = N(t)$.

The Smoluchowski expression for the number of collisions per second between particles of radius r_1 and r_2 in a heterogeneous smoke is:

$$\nu(r_1,r_2) = 4\pi kT[w(r_1) + w(r_2)](r_1+r_2)\cdot n(r_1)dr_1n(r_2)dr_2 \quad (26)$$

$w(r)$ is the mobility of the particle, given by the Stokes-Cunningham law, as:

$$w(r) = \frac{r+\alpha}{6\pi\eta r^2}, \quad (27)$$

where: $\alpha = Al$; A = constant; l = mean free path of air molecule; η = viscosity of air.

Let $\mathcal{K}_0 = (4/3)(kT/\eta)$, the coagulation constant

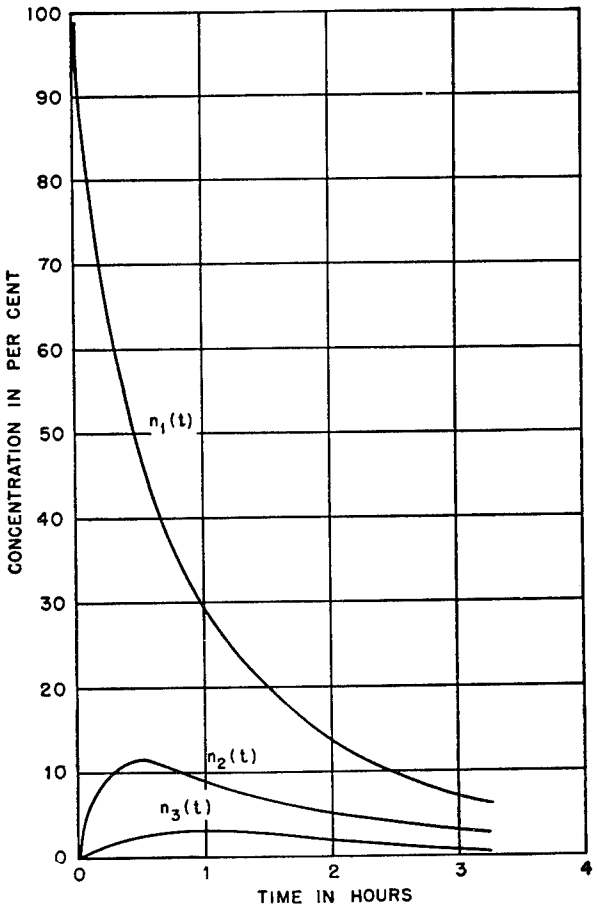

FIGURE 1. Coagulation and settling in stirred homogeneous aerosol.

for large particles, and let

$$\phi(r_1,r_2) = \left(\frac{r_1+\alpha}{r_1^2} + \frac{r_2+\alpha}{r_2^2}\right)(r_1 + r_2). \quad (28)$$

Then

$$\nu(r_1,r_2) = \frac{\mathcal{K}_0}{2}\phi(r_1,r_2)n(r_1)dr_1n(r_2)dr_2. \quad (29)$$

This is the general equation of coagulation[15] of which equation (21) is a special case.

The number of particles of radius r settling out onto the floor per second [see equation (2)] is

$$\nu(r) = \frac{v}{h}n(r)dr. \quad (30)$$

h is the height of a rectangular box, or the ratio of the volume to the floor area, v is the Stokes-Cunningham velocity of fall:

$$v = mgw(r), \quad (31)$$

where

$$m = \frac{4}{3}\pi r^3\rho.$$

Let

$$u = \frac{2\rho gr}{9\eta h}(r + \alpha). \quad (32)$$

Then

$$\nu(r) = u(r)n(r)dr. \quad (33)$$

At each collision with one another the particles are destroyed as such, but a new particle is formed by coalescence having a radius corresponding to the sum of the masses of the two original particles. Hence the total rate of change of particles of radius r is:

$$\frac{\partial}{\partial t}n(r)dr = -\int_{x=0}^{\infty}\nu(r,x) + \frac{1}{2}\int_{x^3+y^3=r^3}^{\infty}\nu(x,y) - u(r)n(r)dr, \quad (34)$$

or

$$\frac{\partial n(r,t)}{\partial t} = -\frac{\mathcal{K}_0}{2}\int_0^\infty \phi(r,x)n(r,t)n(x,t)dx + \frac{\mathcal{K}_0}{4}\int_{x^3+y^3=r^3}^{\infty}\phi(x,y)n(x,t)n(y,t)\frac{dy}{dr}dx - u(r)n(r,t). \quad (35)$$

In the second integral the range of x is from 0 to r, and y is determined by the equation $y^3 = r^3 - x^3$. This equation expresses the fact that, in coalescence, the volumes add.

The above is the fundamental equation whose solution gives the number of particles of any size at any time when a given initial distribution is placed in the box.

This is a nonlinear integro-differential equation whose solution has been obtained in certain special cases,[16] namely: in an initially homogeneous aerosol when either the coagulation or the settling is predominant. Since the equations are rather complicated they will not be given here.

Figure 1 shows a numerical solution for a particular case of the differential equations derived from equation (35). The smoke was initially homogeneous, of radius $r_1 = 0.83$ micron, and concentration $n_1 = 5.8 \times 10^5$ per cubic centimeter. Terms $n_1(t)$, $n_2(t)$, and $n_3(t)$ are the relative number of particles of radii r_1, $\sqrt[3]{2}r_1$, and $\sqrt[3]{3}r_1$ present after time t.

19.6 DEPOSITION IN CENTRIFUGAL FIELDS

A particle in a field of force of acceleration a, will move with a terminal velocity v given by Stokes' law [equation (1)] as follows:

$$v = \frac{2}{9}\frac{r^2\rho a}{\eta}. \tag{36}$$

As stated in Section 19.4.1, this equation will hold as long as $vr < \eta/\rho_1 = 0.15$ for air.

When $vr \gg 0.15$ the motion becomes turbulent and the terminal velocity of the particle (relative to the air) is given by Newton's law for bodies in turbulent motion:

$$v = \sqrt{\frac{8r\rho a}{3\rho_1}}. \tag{37}$$

Here ρ is the density of the particle and ρ_1 is the density of the air. It is seen that the velocity is no longer dependent upon the viscosity of air. Allen [17] found that this equation holds when vr is about 100 times greater than η/ρ_1.

If aerosol particles are given a sufficiently high centrifugal acceleration by causing a sudden change in the direction of flow, they can be precipitated out of the aerosol. Various forms of such precipitators have been constructed, such as centrifugal separators, impingers or impactors. They may be very effective for large particles but are frequently ineffective for small particles.

The particles may be precipitated by directing a jet of aerosol against a collecting surface. In this type of precipitator the jet must have a high velocity and the change of direction must take place in a small distance in order that the acceleration may be high. Consequently the length of time during which the particle is in the high centrifugal field must of necessity be very small.

The centrifugal acceleration $a = V^2/R$, where R is the radius of curvature of the path of the particle, and V is the jet velocity.

Substituting the value of the acceleration a, into equation (37) yields the following value for r, the minimum radius of the particle which will be precipitated:

$$r = \frac{3}{8}\frac{\rho_1}{\rho}\frac{v^2}{V^2}R$$

$$= 4.5 \times 10^{-4}\left(\frac{v}{V}\right)^2 R \tag{38}$$

for a particle of unit density in air.

If we replace v by d_p/t, where d_p is the distance the particle must travel *relative to the jet of aerosol* in order to reach the collector during the time t, and if we replace V by d_a/t, where d_a is the distance traveled by the jet of aerosol during the same time, we obtain:

$$r = 4.5 \times 10^{-4}\left(\frac{d_p}{d_a}\right)^2 R. \tag{39}$$

Consequently, if R or the ratio d_p/d_a or both are small, small particles will be precipitated.

In the impinger or impactor, R is made small by placing the end of the jet tube near the collecting plate.

The ratio d_p/d_a may be made small by passing the aerosol through a long spiral tube of moderately small radius. This results in a considerable separation of the particles according to size, the larger particles being, of course, deposited first. The use of this type of separator is described by Abramson.[18]

19.7 ELECTRICAL EFFECTS. PRECIPITATION

19.7.1 Charge on Homogeneous Smoke Particles

The electrical charge on the particles of homogeneous smoke was investigated. The homogeneous oleic acid fog produced in the usual way with electric spark (Chapter 20) is electrically almost neutral. Only 5% of the particles are charged, mainly positive, and with small numbers of electronic charges (1 to 4) per particle. These observations were made in a Millikan oil drop apparatus using an electrical intensity of 500 v per cm.

19.7.2 Unipolar Smoke

Unipolar charged smokes are produced by a direct current corona discharge from a needle point at a potential of 10,000 v. This potential is obtainable from a 2V3G RCA rectifier tube. The needle point was placed in the center of a 2-l, three-neck flask through which the electrically neutral homogeneous smoke was passed. The other electrode consisted of an aluminum strip placed inside on the bottom of the flask. The characteristics of the negative unipolar charged smoke, obtained when the needle point was negative, are as follows:

1. About 99% of the droplets are charged.
2. Droplet charges are high, 25 to 50 electrons per droplet. These charges were observed in a Millikan oil drop apparatus using an electrical intensity of 90 v per cm.
3. Dilution with air from 1,000 to 32 μg per l has no significant effect on the droplet charge.
4. High humidities have no effect on the droplet charge.
5. The mass concentration of the neutral smoke may be decreased by as much as 65% due to passage through the corona discharge.
6. The number of spectra (Chapter 21) in the Tyndall beam as counted by the naked eye may be decreased by ½ to 1 spectrum on passage between the electrodes.
7. This smoke disappears with great rapidity when introduced into a flask or other chamber.

19.8 MOVEMENT OF PARTICLES IN A THERMAL GRADIENT

Aerosol particles in a temperature gradient are acted on by a force directly proportional to the temperature gradient,[20] and inversely proportional to the absolute temperature. When introduced into a region between two bodies at different temperatures, particles will move toward the colder body and deposit on it.

The method of calculation of the force acting upon a spherical particle in a thermal force field depends upon the relative values of the particle radius r, and the mean free path l of the gas molecules. When $r \gg l$ the force is proportional to $(l^2rp/T)(dT/dx)$, and when $r \leq l$ the force is proportional to $(lr^2p/T) \cdot (dT/dx)$, where p is the pressure and T the absolute temperature.

It was found that when $r > 0.5$ micron the velocity is independent of particle size. In the region between 0.05 micron and 0.5 micron, there is a twofold decrease in velocity with increasing particle radius (Figure 2). Hence there exists a definite possibility in this range of using a thermal gradient for the separation of smoke particles according to size, and thence obtaining the size distribution.

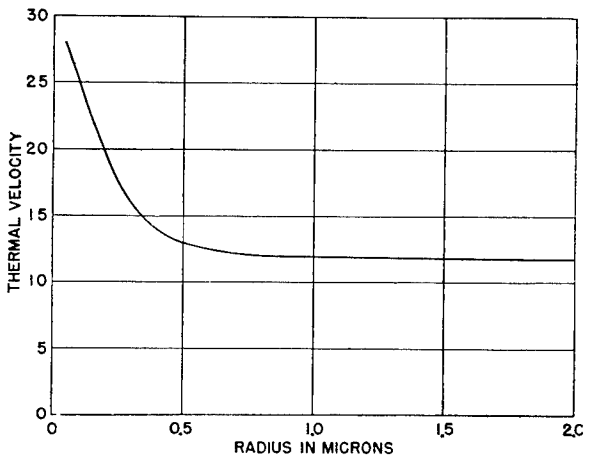

FIGURE 2. Thermal velocity vs particle radius.

Various types of thermal separators have been discussed elsewhere. Because of the limited size range of applicability, this method of size distribution measurement has not as yet been developed experimentally.

A method of sampling smoke particles without separation according to size is described in Chapter 22.

19.9 COAGULATION BY SONIC AND SUPERSONIC VIBRATIONS

It is well known that sound of supersonic frequency and high intensity will cause the rapid coagulation of smoke. For example, Andrade [23] and Parker [24] observed the coagulation of magnesium oxide smoke using frequencies of 22,000 c, and Brandt and Hiedemann [25] coagulated tobacco and ammonium chloride smoke using frequencies of 10,000 to 20,000 c. St. Clair [26] found that a frequency as low as 4,000 c at an intensity of 0.2 w per sq cm (153 db) caused rapid coagulation of ammonium chloride smoke of 1 micron radius.

Large particle aerosols, including natural and artificial water fogs of droplet radii from 4 to 16 microns, can be coagulated by sound of 250 to 1,000 c provided sufficient energy is generated. The available

theory of the phenomenon indicates that sound of 350 c should cause nearly as rapid coagulation of natural water fog as any higher frequency.

At such frequencies, the absorption of sound in air is negligible. At a frequency of 10,000 c, however, the sound intensity is reduced 10 db (a factor of 10) every 150 ft. At higher frequencies, the adsorption is much greater.

19.9.1 Theory

The coagulation of an aerosol by sound vibrations is due to at least three effects: (1) the motion of different sized particles relative to each other, (2) attractive forces set up between particles by the air vibrating between them, and (3) vortex motion which occurs around large particles.

These effects vary in different ways with the size and density of the particle and the frequency and intensity of the sound.

1. For supersonic frequencies in small particle aerosols and for audible frequencies in large particle aerosols, the different size particles will vibrate with different amplitudes, the smaller particles having the larger amplitude. The largest particles will have practically zero amplitude. Consequently, the velocities of the particles relative to one another will be increased and the probability of collision thereby increased.

In order to determine the dependence of the particle velocity upon frequency and particle size it is necessary to assume some law for the force on the particle moving through the gas. In an intense sound field the velocities vary from about 7 cm per sec at 120 db (10^{-4} w per sq cm) to about 2,000 cm per sec at 170 db (10 w per sq cm).

As stated above, Stokes' law holds only when $vr < \eta/\rho_1$. In a sound field, v is the velocity of vibration of the air relative to the particle. For air, $\eta = 1.81 \times 10^{-4}$ poise and $\rho_1 = 1.2 \times 10^{-3}$ g per cu m, so that $\eta/\rho_1 = 0.15$. When $r = 10$ microns and $v = 100$ cm per sec, $vr = 0.1$ so that Stokes' law is valid only for the smaller particle sizes and air velocities. When $r = 1$ micron or less, Stokes' law is valid for much higher intensities.

Koenig [27] has shown that, in general, the force depends upon the acceleration as well as the velocity. However, the approximate frequency necessary to obtain the maximum velocity of the particle relative to the air can be obtained by assuming Stokes' law to hold. According to this law, the force of resistance acting on a spherical particle of radius r, moving through a viscous medium with velocity v is $F = 6\pi\eta rv$.

On this assumption St. Clair [26] has derived the following expression for v, the amplitude of the velocity of a particle *relative to the air* in a sound field.

$$v = v_0 \frac{\omega}{\sqrt{k^2 + \omega^2}}. \tag{40}$$

Here v_0 is the velocity amplitude of the sinusoidal air vibration, $\omega = 2\pi$ times the frequency and $k = (9/2)(\eta/r^2\rho)$ where ρ is the density of the particle.

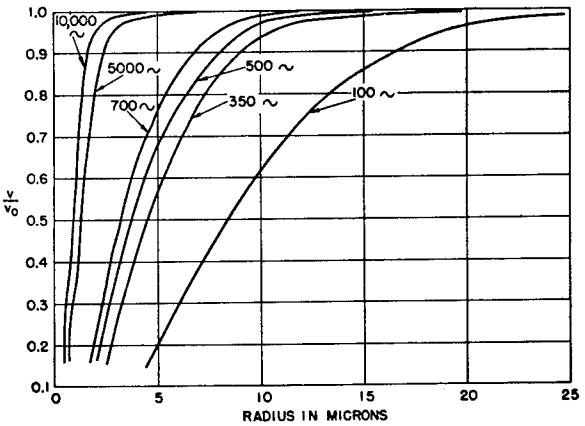

FIGURE 3. Relative velocity v/v_0, as a function of frequency and particle radius, r.

Figure 3 shows v/v_0 plotted against r for several values of the frequency. It is seen that in the neighborhood of 440 c, the relative velocity has nearly reached its maximum at a radius of 10 microns.

Various estimates [28] of the radii of natural fog droplets give the limits to be 4 to 40 microns, the large sizes predominating in radiation fogs. Although the above calculation may give only the order of magnitude of the relative velocity, it is evident that different sized particles will have different amplitudes and phases of vibration, which will increase the rate of coagulation.

It should be pointed out that this particular effect is greatest for comparatively low frequencies. Figure 3 shows that 100 c might be more effective than 440 c in a large droplet radiation fog. Droplets of 5 micron radius would have very low relative velocities and droplets of about 20 microns radius, very large relative velocities. On the other hand, at 5,000 c, all droplets above about 5 microns radius would remain motionless in the vibrating air. Smokes of particle

radii less than 1 micron would require frequencies above 5,000 c to impart different relative velocities to the particles.

2. The increased motion of the particles relative to each other appears to be of secondary importance in causing coagulation when compared to the hydrodynamic forces of attraction between two particles resulting from the motion of the air between them. These forces are greatest when the relative velocity of air and particles is greatest, which does not necessarily mean when the particle is motionless.

Due to the inertia of the particle, its vibrations are more or less out of phase with the vibration of the air. Consequently, when the relative velocity first reaches a maximum, the particle will not be standing still but will be vibrating with considerable amplitude, 180° out of phase with the air. For example, since the actual velocity amplitude u of the particle [26] is:

$$u = v_0 \frac{k}{\sqrt{k^2 + \omega^2}}, \tag{41}$$

a 10-micron particle whose relative velocity amplitude is 0.95 v_0 at 440 c has an actual velocity amplitude of 0.28 v_0.

Koenig [27] derived the following equations for the components of force between two spheres in a sound field. Suppose the particles are stationary and lie in the X–Y plane, their line of centers making an angle θ with the Y axis, and the sound vibration is in the Y direction. The force components are then:

$$X = \frac{-3\pi\rho_1 r_1^3 r_2^3 v_0^2}{2d^4} \sin\theta\,(1\text{–}5\cos^2\theta) \tag{42}$$

$$Y = \frac{-3\pi\rho_1 r_1^3 r_2^3 v_0^2}{2d^4} \cos\theta\,(3\text{–}5\cos^2\theta)\,. \tag{43}$$

Here r_1 and r_2 are the radii of the particles, d is the distance between them, ρ_1 is the density of the air, and v_0 is the velocity amplitude of the sinusoidal air vibration.

The derivation of the above equations is also given by St. Clair.[26] It is interesting to note that the same distribution of forces exists around two magnets when their axes are parallel, at distances large compared to the lengths of the magnets.[29]

For two particles of the same size whose line of centers is perpendicular to the air velocity ($\theta = \pi/2$), the resultant force is an attraction along the line of centers of magnitude:

$$X = \frac{3\pi\rho_1 r^6 v_0^2}{2d^4}\,. \tag{44}$$

When the line of centers is parallel to the air velocity ($\theta = 0$), the resultant force is a repulsion along the line of centers of magnitude:

$$Y = \frac{3\pi\rho_1 r^6 v_0^2}{d^4}\,. \tag{45}$$

These forces have been checked experimentally by Georg Thomas.[30]

Some idea of the rate of coagulation caused by the hydrodynamic forces can be obtained by integrating the equation of motion of two particles attracted by the force X. Assuming that the motion of the particles toward each other obeys Stokes' law, St. Clair [26] obtains the following expression for the time of approach of two particles, separated by a distance d, whose line of centers is perpendicular to v_0:

$$t = \frac{2}{5}\frac{\eta}{\rho_1 v_0^2}\left(\frac{d}{r}\right)^5. \tag{46}$$

If d is the average distance of separation of the droplets in a uniform fog, t is the average time for each pair of droplets to collide once, thus halving the number of droplets. At constant mass concentration, the scattering per unit mass is inversely proportional to the radius for large particles (see Chapter 21). Therefore, halving the number of particles will increase the visibility by 26% since the radius will be increased by the factor $\sqrt[3]{2} = 1.26$.

Expressing d/r in terms of c, the mass concentration in grams per cubic centimeter, we have for an aerosol of spherical particles of unit density:

$$t = \frac{0.66}{v_0^2 c^{5/3}}\,. \tag{47}$$

Thus for a given mass concentration, the time required to halve the number of particles in a uniform aerosol is independent of the particle size, or the distance between them.

This equation is based on the assumption that the concentration remains constant after coagulation, which, of course, it will not do because of precipitation of large coagulated particles. However, as discussed below, the coagulation is quite rapid, particularly for dense aerosols, so that the equation is valid for short times.

Since the average acoustic energy per cubic centimeter of air is $\frac{1}{2}\rho_1 v_0^2$, the intensity of the sound is $\frac{1}{2}\rho_1 v_0^2 V$ where V is the velocity of sound in air and is 3.44×10^4 cm per sec. Thus the time to halve the number of particles is inversely proportional to the sound intensity and to the five-thirds power of the mass concentration.

A dense water fog of 10 microns radius droplets, having a visibility of about 20 ft (99% of light scattered in 20 ft), has a concentration of about 10 g per cu m. For a fog of this concentration, t would be of the order of 300 sec at 160 db and 3×10^4 sec at 140 db.

In experiments on water fog, the observed time required to double the visibility was of the order of one hundredth the time calculated from the above theory. For example, a 4½ micron radius fog of 50 ft visibility ($c = 2$ g per cu m) gave double the visibility in about 1 min at 135 db.

This discrepancy is due in part to the assumption that d is the average distance of separation of the particles in a uniform aerosol. If the aerosol is not uniform the different sized particles will have different amplitudes and phases relative to each other, as already described. Consequently, different sized particles will frequently approach much closer than the distance d (about equal to the amplitude of the sound vibrations). Since the force of attraction varies inversely as the fourth power of the distance, the small values of d will predominate in their effect on coagulation. For instance, if a value of ½d were used in the above calculation, the time would be reduced by a factor of 32.

St. Clair [26] found the same discrepancy between the calculated and observed time in his experiments. He observed the coagulation of 1 micron radius ammonium chloride smoke by sound of 4,000 c to be 30 times faster than calculated according to the above theory.

3. The third cause of coagulation, which has not been taken into account, is the vortex motion of the air around the larger particles which are not vibrating with the air. At the higher intensities, eddy currents are set up in the air around such particles.

Andrade [31] has observed that vortex motion causes neighboring particles to be attracted or repelled depending upon their orientation relative to the sound field and their initial distance apart. He showed that vortex motion occurs around a large spherical particle in air when $vr > 0.35$. Thus 10 microns radius particles would cause vortex motion when the velocity exceeded 350 cm per sec or at about 155 db.

Andrade showed also that vortex motion is the cause of the striations in the large dust particles in a Kundt tube. The distance between the striations is, consequently, not equal to twice the amplitude of the sound vibration as might be expected from the experiments of Koenig [27] and Robinson.[32] Therefore, the sound intensity cannot be obtained from the spacing of the striations. Andrade measured the sound intensity by observing the amplitude of vibration of the 0.25-micron radius particles in tobacco smoke which vibrate with the sound amplitude of the air.

Vortex motion inhibits the hydrodynamic forces so that the Koenig equations for these forces do not apply when $vr > 0.35$. The anomalous experimental results obtained by Gorbatchev and Severnyi [33] are probably due to vortex motion. They observed the forces between two water drops, supported on separate glass threads in a wind tunnel, as well as in a "sound" field of frequency 10^{-3} c. They found the directions of the forces to be just the reverse of those given by the Koenig theory. In the wind tunnel experiments the wind velocity was 15 cm per sec and the droplet radius of the order of 0.5 mm, so that vr was of the order of 0.75. The anomalous results obtained by several other investigators have been shown by Andrade [31] to be due to vortex motion.

The results of the theory may be summarized as follows.

1. No accurate value of the absolute rate of coagulation of an aerosol by sound can be calculated from the present theory.

2. The relative rate of coagulation of uniform aerosols varies directly with the sound intensity, and inversely with the five-thirds power of the mass concentration of the aerosol.

3. Insofar as the coagulation is due to the relative motion of different sized particles, there may be an optimum frequency for which the coagulation rate of a nonuniform aerosol is a maximum.

19.9.2 Experiments

Laboratory experiments at Columbia University and field tests at Lunken Airport, Cincinnati, Ohio, have shown that sound of audible frequency (300 to 700 c) and high but practicable intensities (130 to 160 db) will dissipate natural water fog and artificial sprays having the mass concentration and particle radius found in nature.

In field tests at Lunken Airport, a radiation fog was partially cleared by four Chrysler-Bell victory sirens. The visibility was increased by the sound from 200 ft to 300 or 400 ft.

The clearing occurred in about one minute over a region 300 ft long and 75 ft wide, where the average sound intensity was 140 to 150 db at a frequency of 440 c. The height of the clearing was not measured

879245 O - 50 - 6

but, from the known intensity distribution of the sirens, probably extended about 50 ft upward. The droplet radius of this fog, measured microscopically (see Chapter 22), ranged from 4 to 16 microns and the mass concentration was about 1.0 g per cu m.

In the experiments in a Columbia University tunnel, the visibility of a continuously produced spray of 4½ microns radius droplets was increased from 35 ft to 70 ft by a 2-hp Federal Electric Company siren. The average sound intensity was 135 db at a frequency of 600 c.

In a small-scale laboratory experiment, a spray of the same droplet radius but of much higher concentration was completely dissipated in 15 sec by sound of 150 db intensity and a frequency of 500 c emitted by a loudspeaker.

The details of these and other tests are described elsewhere.[34]

Chapter 6

FORMATION OF AEROSOLS

By *David Sinclair*

20.1 CONDENSATION METHODS

20.1.1 Condensation in Vapor Jets

AEROSOLS OF VERY UNIFORM particle size may be produced in the laboratory by slow and uniform condensation of vapor, well mixed with air, containing condensation nuclei. The size of the particles is determined by the ratio of the mass of condensable vapor to the number of nuclei. When the cooling and other pertinent factors are *carefully controlled*, it is possible to produce aerosols having a particle size which does not vary by more than 10% from the average, as shown by direct microscope measurement of the droplets.

The substance from which the smoke or fog is to be formed is contained in the *boiler*, a 2-l Pyrex flask (see Figure 1). The flask and contents are heated electrically in an asbestos board box to between 100 and 200 degrees C depending upon the substance and the particle size desired.

The condensation nuclei are formed in the *ionizer*, a 1-l Pyrex flask fitted with two electrodes sealed into standard tapered joints. The ionizer is mounted above the heater box and connected to the boiler by a standard tapered joint. The condensation nuclei are formed by a high-voltage electric spark or an electrically heated coil of wire which has been dipped in sodium chloride.

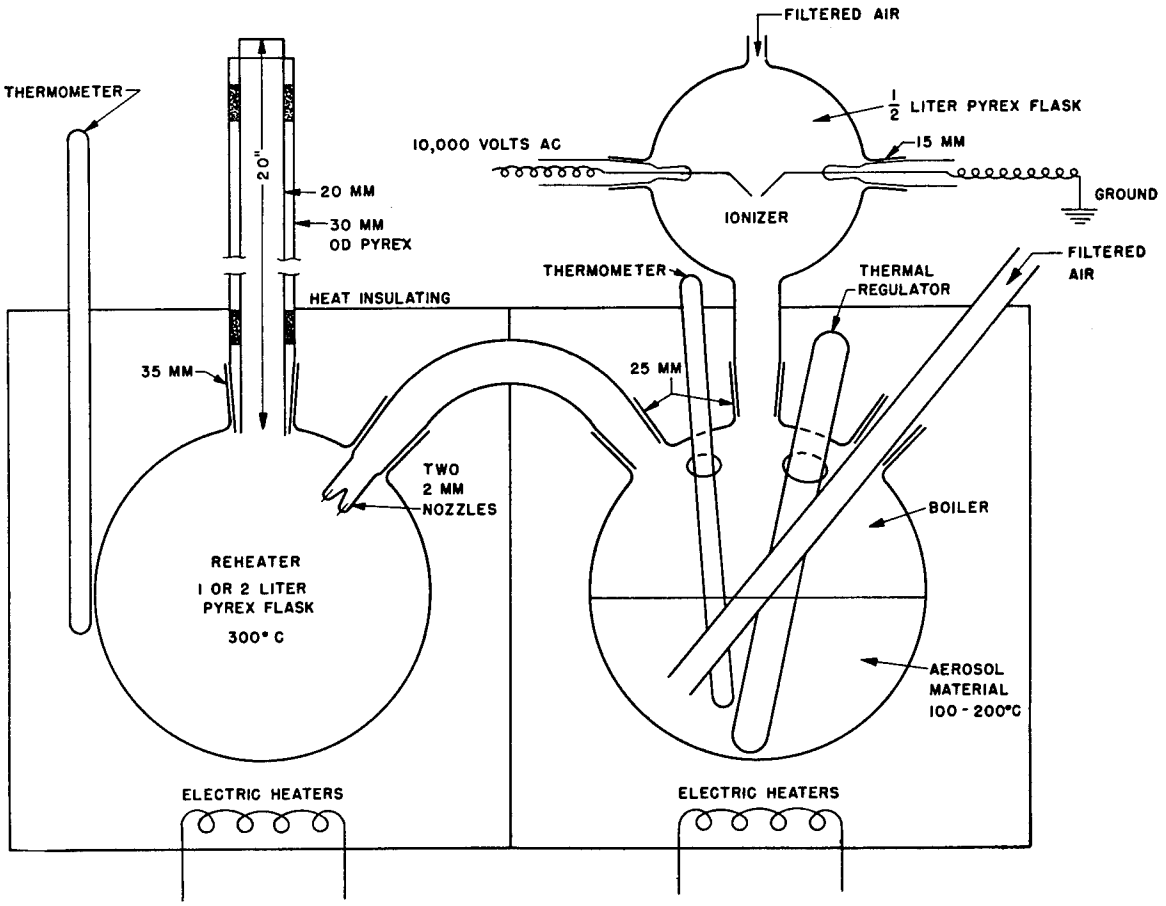

FIGURE 1. Homogeneous aerosol generator.

The *reheater* is a 2-l Pyrex flask in an adjacent asbestos box heated electrically to about 300 C. A double walled Pyrex glass chimney 20 in. long is connected to the reheater by a large standard tapered joint. The boiler and reheater are connected by a Pyrex tube having a standard tapered joint at each end. The outlet of this tube into the reheater consists of a jet having two holes of 2-mm diameter.

Smoke is produced by bubbling air through the hot liquid in the boiler, through the glass tube shown in the diagram. At the same time, air is blown in through the ionizer. The total rate of flow is usually from 1 to 4 lpm. The mixture of nuclei, spray, and vapor-laden air then passes through the two jet holes into the reheater. Here the spray is vaporized and the nuclei well mixed with the vapor.

The mixture then rises through the chimney, the vapor condensing uniformly upon the condensation nuclei. The smoke which issues from the chimney is found to be of quite uniform particle size. When the column of smoke is examined in front of a white light it is seen to be brilliantly colored, the colors varying markedly with the angle of observation.

The smoke has a high mass concentration, about 1 to 10 mg per l, depending upon the particle size. In order to avoid destroying the uniformity of particle size by coagulation, the smoke should be immediately diluted 10 or 100 times with dry, filtered air. Small tubes or jets should not be used for this purpose since turbulent flow destroys the uniformity of size.

The particle size is increased by increasing the temperature of the boiler, or by increasing the flow of air through the liquid relative to that through the ionizer, or by decreasing the rate of production of ions. A little practice with any given piece of apparatus will show the conditions that will yield the most uniform smoke of a given particle size.

The temperature can be automatically maintained constant by a thermal regulator inserted directly into the liquid or into the heater box. *The air must be dried and well filtered.* If it is not, the moisture, dust and oil fog droplets in the air from a compressor, or even a tank, will provide so many condensation nuclei that the control of particle size by the ionizer will be lost.

To produce the larger particle sizes above 1 or 2 microns radius, it is necessary to increase the proportion of vapor by bubbling the air through a porous disk beneath the liquid surface. Care must be taken to avoid decomposition of the material by excessive heating.

A substance having a range of boiling points or an impurity, particularly of higher vapor pressure, is not suitable for producing uniform smoke by this method. The different components condense at different rates in the chimney, causing nonuniformity in the particle size. A volatile impurity sometimes condenses so readily that it forms sufficient nuclei to destroy the control of size by the ionizer.

Uniform aerosols have been produced from oleic and stearic acid, triphenyl and trichresyl phosphate, rosin, menthol, ammonium chloride, lubricating oil and Aroclor. The range of particle radii is from 0.1 to 5.0 microns. Smaller sizes may be produced, but it is difficult to measure the size or uniformity. In general, the large particle aerosols are more uniform in size.

The condensation nuclei may be ionized air molecules or molecules of such compounds as NO_2, H_2, O_2, or NH_3. When a too intense, flaming spark is used, NO_2 is readily detectable by its odor and color.

The construction and operation of this generator is described more fully elsewhere.[1]

20.2 THE DISPERSAL OF PRE-GROUND SOLIDS

20.2.1 Air-Jet Dispersion

Pneumatic dispersion is capable of producing aerosols of solid particles whose size is as small as the primary size of the ground material. This method does not usually break up single particles but does tear apart aggregated particles. The method is very inefficient in that a very large volume of air is required, producing a dilute aerosol.

One form of apparatus,[2] called the *geyser* (see Figure 2) has been used to produce aerosols of lithopone, Kadox (zinc oxide), and egg albumin, of mass concentration up to 30 μg per l. Using Kadox of primary particle size 0.1 to 0.3 micron, the particles dispersed by the geyser are 0.3 to 0.5 micron on the average. Egg albumin was dispersed down to its primary particle size of 0.5 to 10 or 15 microns radius.

It is quite necessary to use well dried and filtered air for the dispersal. The water vapor and oil fog in raw air from an air compressor cause materials such as lithopone to pack into an intractable mass.

The filter and powder chamber are both made of standard 3 in. galvanized iron pipe although they have been drawn to different scales in the diagram. The connections are all made with standard $\frac{1}{4}$-in. pipe fittings, as shown.

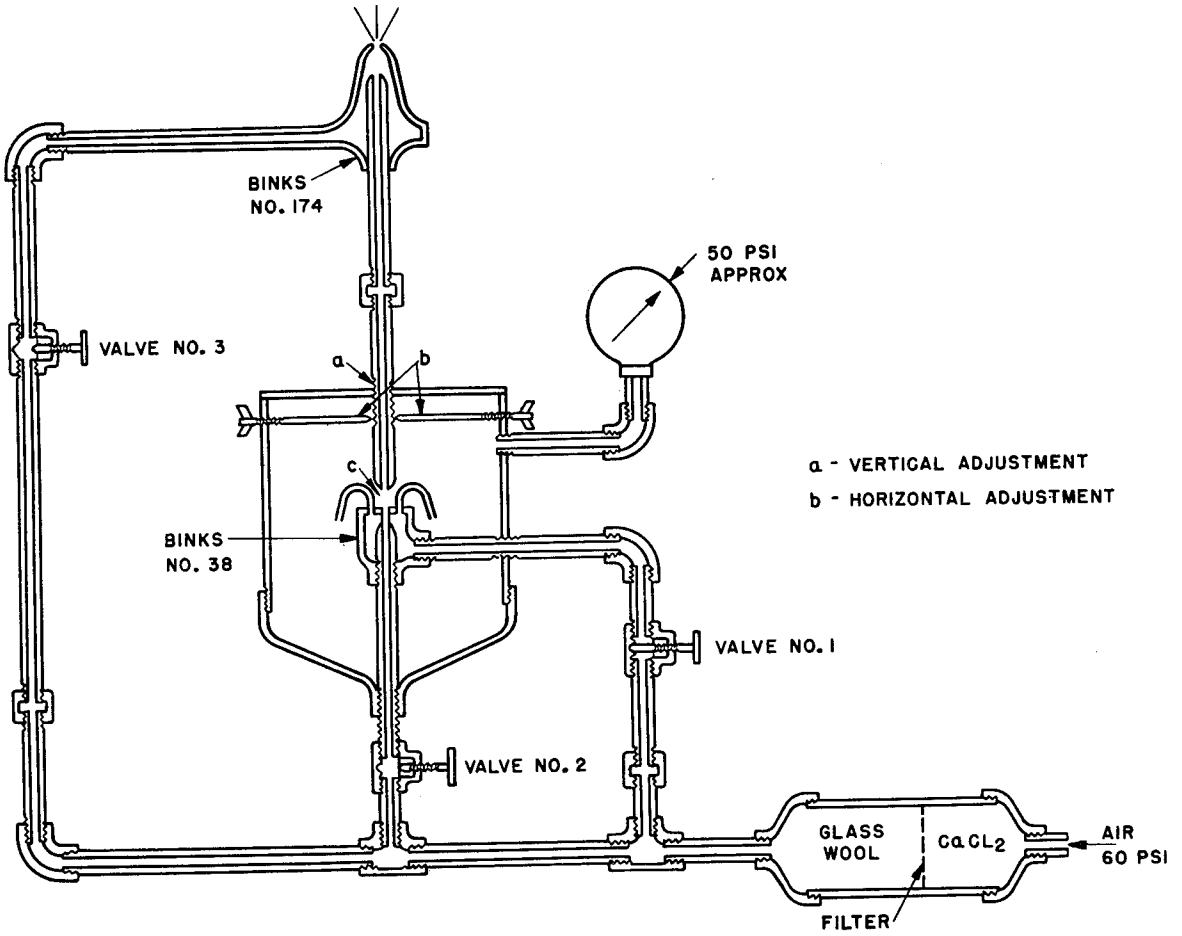

FIGURE 2. The geyser (pneumatic disperser).

Two spray nozzles of different types, made by the Binks Manufacturing Company of Chicago were adapted to this apparatus. The No. 174 nozzle, which gives the final dispersal, was altered by removing the air cap and the needle, and drilling out the central hole to $\frac{1}{16}$ in. diameter.

In order to eliminate a constriction and a right-angle bend, the hole that carried the needle adjustment was enlarged and the pipe from the powder chamber connected to this opening. The regular inlet (stamped WAT on nozzle) is closed off. With this arrangement the powder comes straight from *c* out through the No. 174 nozzle without any turns. This eliminates a tendency of the powder to collect at the turns and then break loose later in large pieces.

The Binks No. 38 nozzle was altered by removing the screw cap and soldering in its place a flat disk having a 1-mm central hole concentric with the central air outlet. All the air from this outlet flows out through the 1-mm hole. In addition, the plate has three symmetrically placed holes to which bent tubes $\frac{1}{16}$ in. ID are attached as shown in the diagram.

The air from these tubes serves to stir up the powder. Air from the central hole of the Binks No. 38 nozzle blows up through the nozzle above at *c*, which should be tapered. This air stream carries more or less of the powder-laden air with it, depending upon the adjustments *a* and *b*. The upper nozzle at *c* is a convex cone having a $\frac{1}{16}$-in. diameter hole.

The top plate of the powder chamber is sealed with a gasket and fastened with screws which are loosened slightly while the adjustments are being made. Three horizontal adjusting screws *b* are used for lateral adjustment, and adjustment at *a* is made by loosening the union directly above it and screwing the pipe up or down a small amount.

The rate of flow out of the No. 174 nozzle is about

140 lpm. Most of this air flows through valve No. 3 and is used to disperse the aggregates blown up from the chamber.

A more convenient, portable form of geyser was made by attaching a Binks 174 nozzle to a DeVilbiss-type GB flock gun. The powder is stirred in the flock gun by a thin stream of air and the concentrated aerosol dispersed by the Binks nozzle as in the above described model.

20.2.2 Gas Ejection Bomb

A bomb of 22 cc capacity was used to disperse Kadox, egg albumin and lycopodium spores in a 22-cu m room. The particle size in the Kadox aerosol was greater than obtained with the geyser. With egg albumin and lycopodium, a primary dispersion was obtained, when using a bursting pressure of 1,800 psi.[3] (See also Chapters 22 and 35.)

Chapter 7

OPTICAL PROPERTIES OF AEROSOLS

By *David Sinclair*

21.1 SCATTERING OF LIGHT BY A SINGLE SPHERICAL PARTICLE

THE SCATTERING OF LIGHT by spheres has been extensively studied, both theoretically and experimentally. In the case of transparent dielectrics, that is, nonabsorbing substances, the scattering properties have been found to provide convenient measures of particle size and size distribution.

The theory of scattering by a spherical particle was originally developed from Maxwell's equations by Gustave Mie [1] in 1908. Since that time, numerous calculations [2] have been made of the total energy, and the angular distribution of the intensity of light scattered by both transparent and absorbing particles. The derivation of the equations is given in a compact form by Stratton.[3]

Since the calculations available in the literature were incomplete, additional calculations on both absorbing and transparent particles were made by the Bureau of Standards. Most of the calculations on transparent particles have already been published.[4] The calculations on absorbing particles and additional calculations on transparent particles are described in following text.

Numerous experimental measurements have amply confirmed the Mie theory, with one exception, described in the discussion that follows.

For transparent, spherical particles that are small compared to the wavelength of light, the Mie theory is in complete agreement with the more elementary theory of Rayleigh,[5] derived to account for the blue of the sky. According to this theory the total amount of light of wavelength λ scattered by a small sphere of radius r per unit intensity of illumination (unit energy per unit area) is

$$S = 24\pi^3\left(\frac{m^2-1}{m^2+2}\right)\frac{V^2}{\lambda^4}\,. \qquad (1)$$

Here V is the volume of a small particle, and m is its refractive index relative to that of air ($= 1$). S is thus the effective scattering area of one particle.

This equation holds for extremely small particles such as air molecules. For such sizes the particles need not be spherical. The equation holds for spherical particles when $r < 0.1\lambda$. It is seen that the total scattered energy varies directly as the sixth power of the radius, and inversely as the fourth power of the wavelength, so that blue light is scattered much more than red.

Consequently, the diffuse light of the sky is blue when free of haze. However, when the sun is near the horizon the sky may exhibit other colors even when free of haze as explained in the following text.

When the particle is illuminated with unpolarized light, the intensity scattered at an angle γ to the incident light is

$$I_\gamma = \frac{9\pi^2}{2R^2}\left(\frac{m^2-1}{m^2+2}\right)\frac{V^2}{\lambda^4}(1+\cos^2\gamma)\,. \qquad (2)$$

R is the distance from the particle to the point of observation. This equation holds only when R is very large compared to the radius of the particle. The angle γ is the angle between the direction of propagation of the scattered light and the *reversed* direction of propagation of the incident light.

When observing at right angles to the incident light, i.e., when $\gamma = 90°$, the scattered light is plane-polarized with the light vibrations perpendicular to the plane of observation. The plane of observation is the plane containing the direction of observation and the incident beam.

If a very small particle is illuminated by polarized light the intensity of light scattered at an angle ψ is [4]

$$I_\psi = \frac{9\pi^2}{R^2}\left(\frac{m^2-1}{m^2+2}\right)^2\frac{V^2}{\lambda^4}\sin^2\psi\,. \qquad (3)$$

Here ψ is the angle between the direction of observation and the direction of the electric vibrations in the incident polarized light. The scattered light is plane-polarized, no matter what the direction of observation.[4]

As the particle radius increases to about the same size as the wavelength of the light, the scattering becomes a very complicated function of the radius, wavelength, and refractive index. The Mie theory shows that the total scattering by one spherical particle per unit intensity, is:

$$S = \frac{\lambda^2}{2\pi}\sum_{\nu=1}^{\infty}\left(\frac{a_\nu^2+p_\nu^2}{2\nu+1}\right) \qquad (4)$$

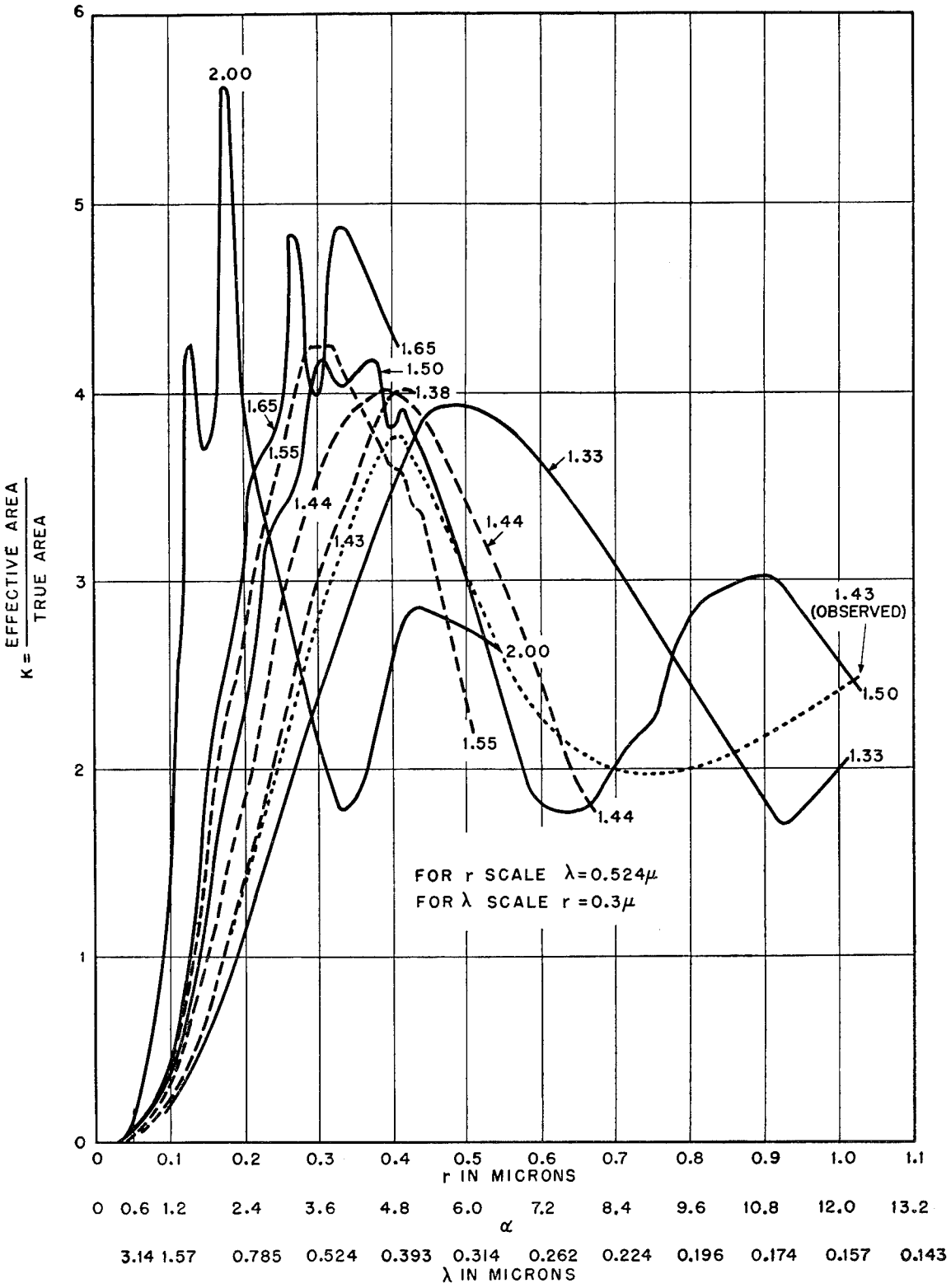

FIGURE 1. Scattering coefficient for spherical particles. K vs α, r and λ.

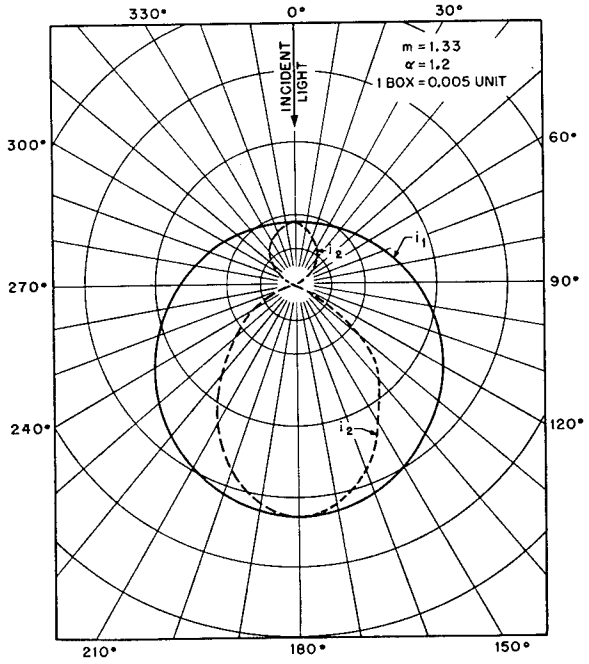

FIGURE 2. Angular distribution of intensity of light scattered by a spherical particle. i_1 and i_2 vs γ.

The a_ν's and p_ν's are functions of $\alpha = 2\pi r/\lambda$ and $\beta = 2\pi rm/\lambda$.

The scattering coefficient K, the scattering per unit cross-sectional area of particle, is obtained by dividing equation (4) by πr^2. Thus:

$$K = \frac{2}{\alpha^2} \sum_{\nu=1}^{\infty} \left(\frac{a_\nu^2 + p_\nu^2}{2\nu + 1} \right). \qquad (5)$$

K is therefore a function of r/λ. This means that once the scattering coefficient is known for a particular value of r and a particular value of λ, it will be known for all values of r and λ which bear the same ratio.

Since the functions are extremely complicated and have already been published,[3, 4] they will not be given here.

The scattering coefficient for particles of different radius and refractive index is shown in Figure 1. The ordinates are the scattering coefficient K, and the abscissas are $\alpha = 2\pi r/\lambda$. The radii corresponding to a wavelength of $\lambda = 0.524$ micron and the wavelengths corresponding to a radius of 0.3 micron have also been given as abscissas, so that these curves show the variation of total scattering with radius at a constant wavelength, and with wavelength at a constant radius.

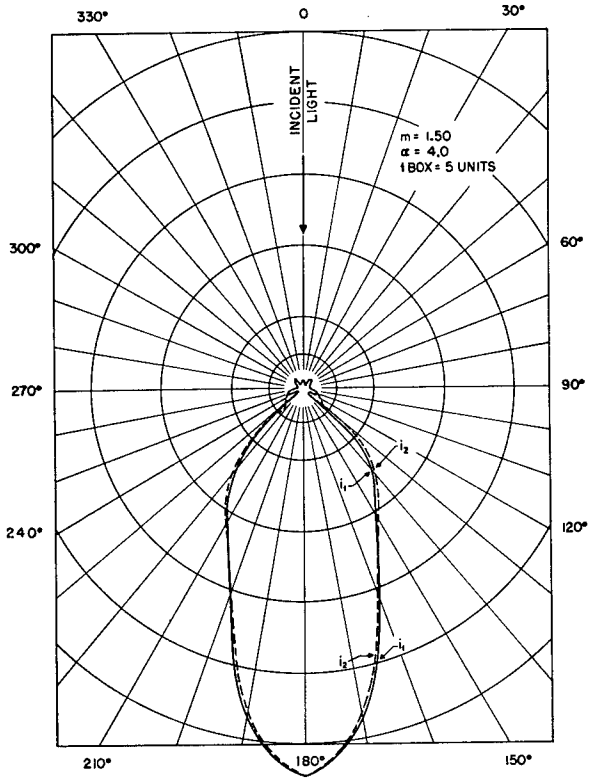

FIGURE 3. Angular distribution of intensity of light scattered by a spherical particle. i_1 and i_2 vs γ.

It is seen that the peak of the curve, and therefore the radius for maximum scattering, moves toward smaller radii as the refractive index increases. There is also a secondary peak in the neighborhood of 1 micron or less.

The angular distribution of intensity varies according to the same function of r/λ. For Rayleigh scattering by small particles, the angular distribution as shown by equation (2) is symmetrical about a plane normal to the incident illuminating beam. That is, as much light is scattered backward as forward. As the particle radius increases, the forward scattering becomes much greater than the backward. For a particle whose radius is equal to or greater than the wavelength of light, the ratio of forward to backward scattering may be 1,000 or more.

The angular distribution of intensity is an extremely complicated function of the scattering angle γ, and the complexity increases markedly with increase in particle size. Numerous equations and angular distribution curves are given in references.[2,3]

The Mie theory predicts, and observations confirm, that the scattered light is partially polarized. That is,

the scattered light is composed of two incoherent plane-polarized components, whose planes of polarization are mutually perpendicular. One of these components, of intensity i_1, has its light vibrations perpendicular to the plane of observation; the other, of intensity i_2, has its light vibrations parallel to the plane of observation.

Figures 2 and 3 show the angular distribution of intensity scattered by spheres of different sizes and materials when illuminated by unpolarized light of $\lambda = 0.524$ micron. Figure 2 is for a 0.1 micron radius water droplet (index 1.33). Figure 3 is for a 0.33 micron radius oil droplet (index 1.50, taken from a paper by Blumer[2]).

The angular distribution of intensity varies with wavelength. For example, a 0.2 micron radius water droplet would have, for a wavelength of 1.048 micron, an intensity distribution like that of Figure 2. This results from the reciprocal relationship between radius and wavelength which states that the intensity distribution is constant when r/λ is constant.

The plane-polarized component, i_1, is the component observed in Rayleigh scattering at an angle $\gamma = 90°$. At this angle, i_2 is zero, as shown by equation (2), since the $\cos^2 \gamma$ term in the brackets is proportional to i_2. The unity term is proportional to i_1, so that i_1 alone is constant for all angles of observation in Rayleigh scattering.

21.2 SCATTERING BY UNIFORM PARTICLE SIZE SPHERICAL AEROSOLS

In aerosols, the particles scatter light independently of one another when the distance between the particles is 10 or preferably 100 times the radius of the particle. In small particle aerosols, of radius 1 micron and number concentration 10^6 per cc, the ratio of distance of separation to radius is $10^{-2}/10^{-4} = 100$. However, for a 10-micron particle aerosol of the same concentration the ratio is reduced to 10. In such an aerosol some interference between the scattering by neighboring particles would be expected, but such high concentrations are not found in practice.

In a water fog of 10 microns radius droplets having a number concentration of 10^3 per cc, the mass concentration would be 4.2 mg per l. This is a concentration found in dense natural fogs. However, the usual concentration found in screening oil fogs and in the laboratory is a few hundred micrograms per liter or less. Consequently, the optical properties of a single spherical particle can be observed by a study of the optical properties of a uniform particle size aerosol.

21.2.1 Angular Distribution of Color

Observations of the scattering were made on a spherical flask of uniform droplet-size fog traversed by a bright and nearly parallel beam of light (called a Tyndall beam), about 1 in. in diameter. The fog was produced in the homogeneous aerosol generator described in Chapter 20.

The angular distribution of color in the scattered light was found [6] to agree closely with the theory. Oleic and stearic acid fogs were illuminated with unpolarized, white light, and the plane-polarized component i_1 was observed as the angle of observation θ (measured from the forward direction, i.e., $\theta = 180° - \gamma$) was varied from near 0 to near 180°. The component i_2 exhibits a different and less distinct series of colors.

As the angle of observation is varied from the forward toward the backward direction, a series of colors is seen which resembles the spectrum of white light. The order of the colors is violet, blue, green, yellow, orange, and red. This series may then be repeated several times, depending on the particle size. Near 90° the order of colors reverses, becoming red, orange, yellow, green, blue, and violet. This reverse series may then be repeated until the backward direction is reached.

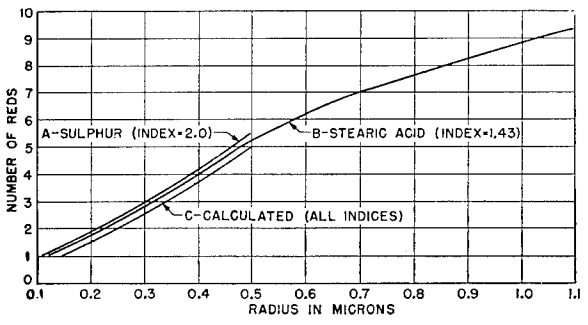

FIGURE 4. Number of reds vs particle radius.

The purity and brightness of the colors increases with the uniformity of particle size. The number of times the color sequence is repeated increases with particle size. This is the basis of a method of particle size measurement, according to which the particle size is given by the number of times red, the most distinctive color, is repeated (see Chapter 22).

In Figure 4, curves A and B are the experimental

curves obtained with oleic acid fogs and sulfur smokes, showing the number of times red is observed as a function of particle size.

Calculations for radii up to 0.5 micron and for indices of refraction 1.33, 1.44, 1.55, and 2.0 show that the number of *reds* corresponding to a given radius is independent of refractive index. Curve C, Figure 4, shows the calculated curve which differs throughout from the experimental curves by about 0.025 micron. Since the curves for all indices of refraction approximately coincide up to 0.5 micron, it seems likely that they will continue to coincide up to 1.0 micron.

The calculated curves were obtained from the Mie theory as follows. A curve was plotted for each particle radius showing the ratio of the intensity i_1 in the red ($\lambda = 0.629$ micron) to the intensity i_1 in the green ($\lambda = 0.524$ micron) for scattering angles from 0 to 180°. The number of maxima of magnitude, greater than 0.45, is taken equal to the number of reds observed visually, for the following reason.

The calculated values of i_1 refer to unit intensity of illumination at all wavelengths in the incident beam. Since, in sunlight (i.e., white light) the intensity ratio of red to green at the above wavelengths is 0.9, it was assumed that the observed scattered light would have a reddish hue when the ratio i_1 (red) to i_1 (green) was greater than 0.9. In the tungsten light used for observation, the intensity

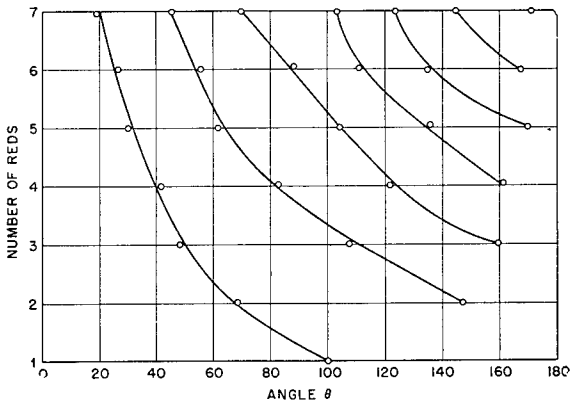

FIGURE 5. Angular position vs number of reds.

ratio of red to green was 2.0. Consequently a calculated ratio i_1 (red) to i_1 (green), greater than 0.45, would correspond to an observed red since the ratio i_1 (red) to i_1 (green) in the observed scattered light would be greater than $2 \times 0.45 = 0.9$.

Figure 5 shows the angular position of the reds seen in i_1 in stearic acid smokes of 1 to 7 spectra. The ordinates show the number of reds and the abscissas their angular position, θ. With the exception of sulfur, most of the calculated points for other indices of refraction lie on the stearic acid curves to within $\pm 5°$.

21.2.2 Polarization

The polarization for various angles θ was found, both experimentally and theoretically, to vary in a regular manner from the Rayleigh region up to about 0.2-micron radius. The relative intensity of i_2 to i_1 was found to vary from a low value up to greater than one. The polarization can thus be used as a measure of particle radii up to 0.2 micron (see Chapter 22). Above 0.2-micron radius, the polarization varies more rapidly with particle radius and is multiply valued.

The polarization may be conveniently measured with a polarization photometer. A Tyndall beam of approximately monochromatic light is observed through a bipartite disk with its dividing line parallel (or perpendicular) to the plane of observation. The bipartite disk is a plane-polarizer having one half of its plane of polarization perpendicular to the dividing line and the other half parallel to the dividing line. One half of the bipartite disk, therefore, transmits i_1 and the other half transmits i_2. Between the observer and the bipartite disk is a plane polarizer, called the analyzer, which can be turned so that its plane of polarization makes a given angle with the plane of observation.

The analyzer is turned so that the intensities of the two halves of the bipartite disk are equal. If the angle between the direction of the light vibrations transmitted by the analyzer and the plane of observation is ϕ, then:

$$\frac{i_2}{i_1} = \tan^2 \phi \cdot \qquad (6)$$

Figure 6 shows the calculated values of ϕ as a function of radius for five different refractive indices when the angle of observation $\theta = 90°$ and $\lambda = 0.524$ micron. Figure 7 shows ϕ as a function of radius for four different values of θ when the index of refraction $m = 1.44$ and $\lambda = 0.524$ micron.

The blue tobacco smoke that rises from the end of a cigarette exhibits Rayleigh scattering approximately when illuminated with white light ($\lambda = 0.4$ to 0.7 micron). If a Tyndall beam is examined in a direction at right angles to the beam through a plane

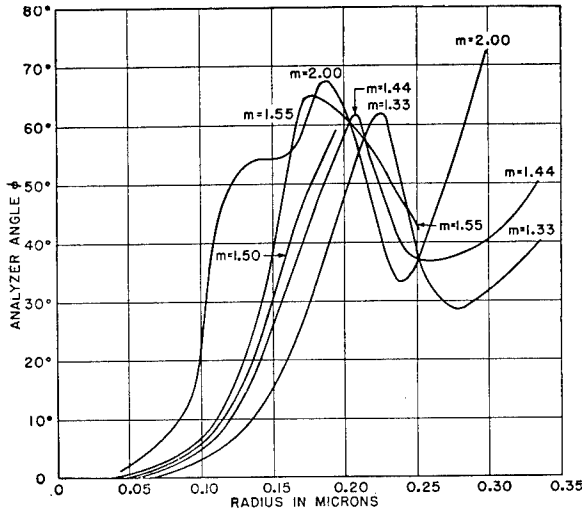

FIGURE 6. Calibration curves for Owl. Analyzer angle ϕ at $\theta = 90°$, vs refractive index.

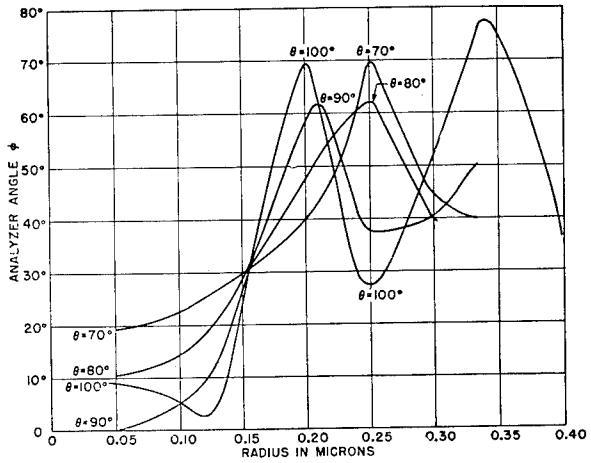

FIGURE 7. Calibration curves for Owl. Analyzer angle ϕ at refractive index 1.44 vs θ.

polarizer, it will be seen to be virtually extinguished when $\phi = 0°$.

When fresh, the particles of tobacco smoke are 0.15-micron radius or less. If this smoke is allowed to age in a flask, or if exhaled smoke is examined, much less polarization will be observed. Aged tobacco smoke particles are 0.2 or 0.25-micron radius, due to the accumulation of moisture. Such smoke may be sufficiently uniform in size to exhibit some color when examined through a polarizer.

21.2.3 Total Scattering

Measurements were made of the angular distribution of intensity of the light scattered by uniform stearic acid and oleic acid fogs. The details of the method of measurement have been given elsewhere.

A fog of known concentration (measured by weighing a known volume of fog collected in a glass wool filter) was observed while streaming out of the generator. A suitable volume was uniformly illuminated and the intensity scattered into a given small solid angle was measured with a photometer. Measurements were made at angles from 3 to 175° at frequent intervals. The intensities were then integrated over all possible directions. In order to obtain the total scattering coefficient, the integrated scattering was compared with that of a diffuse reflector of known reflectivity.

The results are given in Figure 1. The dotted curve shows the experimental measurements made on uniform particle size stearic acid fog, refractive index = 1.43. The agreement with the theoretical curve for index 1.44 is considered to be satisfactory. The discrepancy is due to the difficulties inherent in this type of measurement.

It was found that the theoretical values of both total scattering and angular distribution of intensity are too high by a factor of 2 when the particle is illuminated by unpolarized light. This was due to a mistake made in the original derivation of the theory when transferring from polarized to unpolarized light.[4] The error was made originally by Rayleigh [5] and was first pointed out by Stiles [8] in a paper, which was brought to the author's attention after reference 4 had been distributed. Rayleigh's original error has been propagated unchanged in a number of texts. In the *Handbuch der Physik*, the error is compensated by making an improper integration over the sphere.[9]

The values of the scattering coefficient given in Figure 1 are the correct values. They are equal to the values obtained directly from the Mie theory when derived for polarized light, and to half the values given by the Mie theory for unpolarized light.

The total amount of light scattered by 1 cc of aerosol is equal to the product of the amount of light scattered per particle and the number concentration n. Figure 8 shows S the scattering cross section per particle ($\times 10^8$) as a function of particle size and wavelength for water (index = 1.33), screening oil (Diol, index = 1.50) and sulfur (index = 2.0). These curves may be obtained from equation (4), or they may be obtained from the curves of Figure 1 by multiplying the values of the scattering coefficient K by the cross-sectional area of the particle πr^2. The scattering per cc is then $K\pi r^2 n = Sn$.

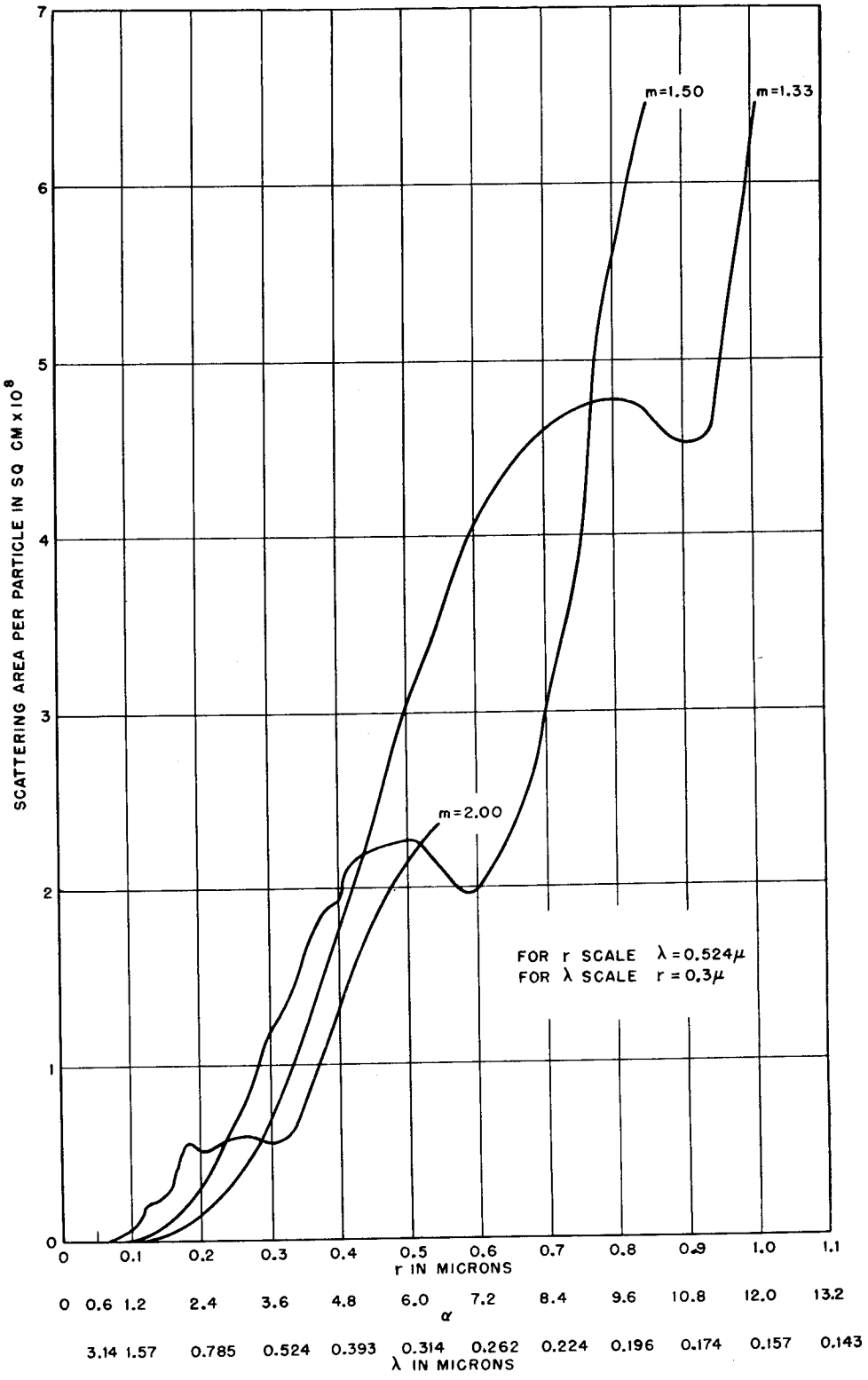

FIGURE 8. Total light scattered per particle. S per particle vs α, r and λ.

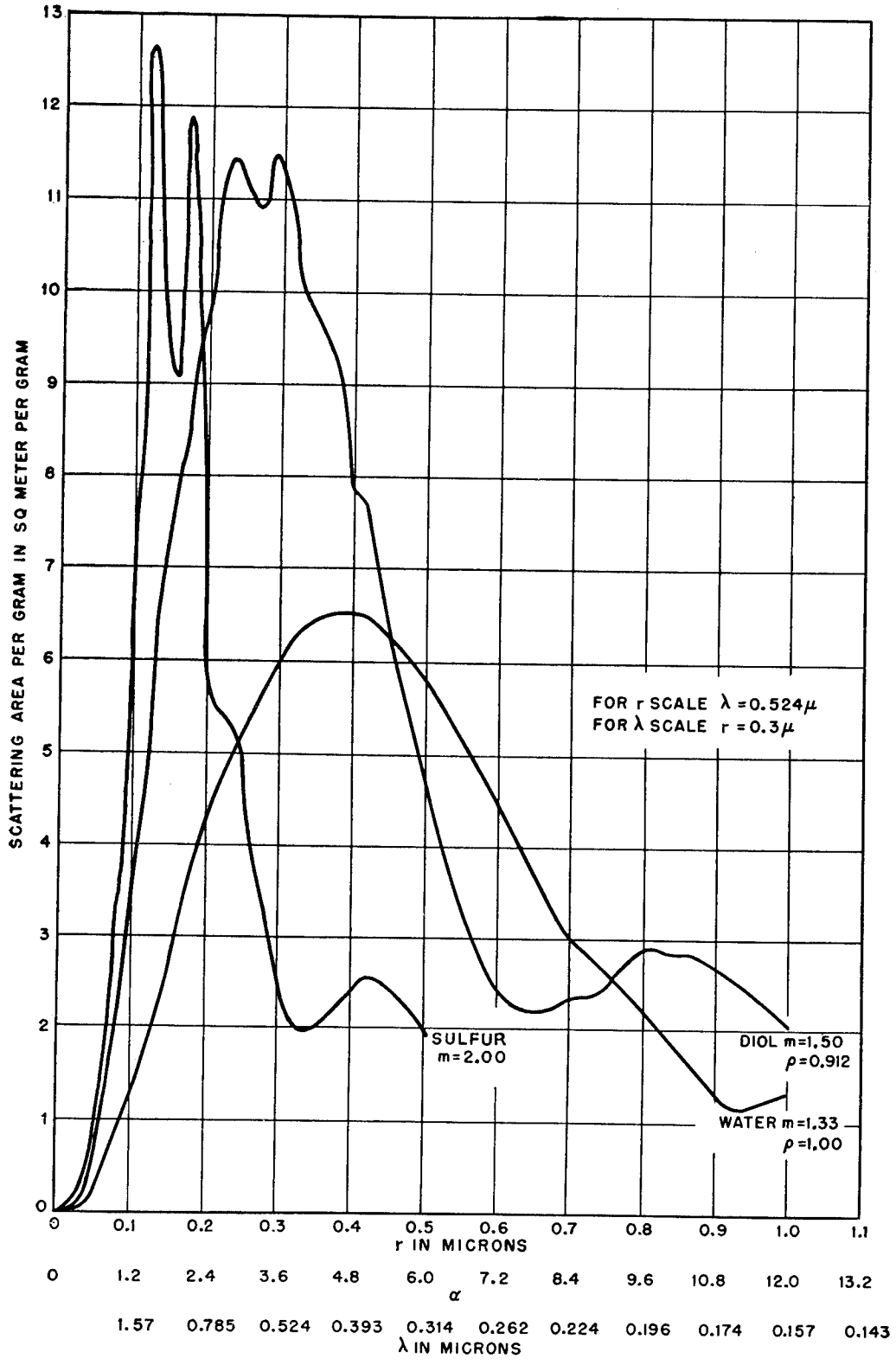

FIGURE 9. Total light scattered per gram of particles. S per gram ($=J$) vs α, r and λ.

The total scattering may also be expressed in terms of the scattering per gram of material. This is the quantity most important in determining the performance of a screening smoke. Figure 9 shows the scattering cross section in square meters per gram for some of the materials of Figure 8. These curves were obtained from Figure 8 by dividing the scattering per particle by the mass of one particle. Thus, the scattering per gram is $J = 3K/4r\rho$, where ρ is the density of the material.

21.2.4 Transmission

The total scattering may be more conveniently obtained by measuring the decrease of intensity of the transmitted beam. For small particles, the intensity of the transmitted beam of wavelength λ decreases exponentially with the distance traversed through the aerosol, that is:

$$I = I_0 e^{-Snl} = I_0 e^{-Jcl}. \tag{7}$$

Here l is the distance, and c is the mass concentration of the aerosol in grams per milliliter. The term Snl ($Snl = Jcl$) is defined as the optical density D.

The intensity I transmitted through a given distance l in a stirred homogeneous aerosol will decrease exponentially with the time, due to the decrease in n, according to equation (2), Chapter 19. Combining equation (2) with equation (7),

$$\log \frac{I_0}{I} = Snl = Snl_0 e^{-(vt/h)}. \tag{8}$$

Thus the optical density $D = Snl$ will decrease exponentially with the time. However, for times short compared to h/v the change will be small. If the concentration n is maintained constant by replenishing the aerosol from a homogeneous generator, the transmitted intensity will be constant.

A beam of monochromatic light was passed into a photocell through a homogeneous aerosol of constant concentration, and the transmission measured as a function of particle size and wavelength. The concentration and distance were also measured and the scattering coefficient then calculated from equation (7). Good agreement was found between experiment and theory for oleic acid [4] (index = 1.46), sulfur [4] (index = 2.0), and Diol (index = 1.5).

In the case of oleic acid and sulfur, it was convenient to plot curves showing the variation of $J\lambda$ [$\propto K(\lambda/r)$] with r/λ. These curves are similar in form to the K vs α curves of Figure 1.

For Diol a series of curves showing the variation of $\log J$ with $\log \lambda$ at constant radius was plotted. It was found that the slope of these curves varied markedly with particle size. For the wavelength 0.65 micron, the slope was -1.9 at $r = 0.3$ micron ($\alpha = 2.9$), reached a maximum of $+2.1$ at $r = 0.7$ micron ($\alpha = 6.8$) and fell to $+1.7$ at $r = 0.76$ micron ($\alpha = 7.3$).

At $r = 0.1$ micron or less the slope should reach the value -4, according to the Rayleigh equation [equation (1)]. The curve of scattering per gram for Diol (Figure 9) shows a variety of slopes of positive and negative values.

A negative slope means that the scattering per gram decreases with increasing wavelength. In other words the transparency of the aerosol increases with increasing wavelength. This is the general situation for aerosols whose particle radii are smaller than the radius (or radii) corresponding to the principal maximum of the scattering curve. Conversely, aerosols whose particles are somewhat larger than this optimum size will be more transparent to shorter wavelengths.

It has been observed that the color of the sun's disk, viewed through a cloud of Diol fog produced in the field, is red when the droplet radii are less than 0.23 micron, and blue or green when the radii are greater than 0.3 micron. Inspection of Figure 9 shows that the optimum radii for Diol are between the above values (for green light, $\lambda = 0.524$ micron).

The observations should be made when the sun's light is nearly extinguished, since the residual rays will exhibit the most distinctive color. The purity of the color will vary with the uniformity of particle size. It is evident that a considerable range of sizes, great enough to span the peak of the curve, would exhibit little or no color. This is a simple criterion for estimating the particle size and size distribution of a fog (see Chapter 22).

If the particles are all considerably smaller than the optimum size, they may have a large range of size and still produce a red color in the transmitted light. The setting sun appears red, usually because of the small particles of haze which exhibit approximately Rayleigh scattering. And the color of the sun deepens as it sets, due to increased selective scattering, until the residual color becomes a deep red just before the sun is extinguished.

Even when free of haze the color of the sky at sunset will differ from the usual blue. The sky color will vary with the color of the transmitted sunlight, which varies with the path length as follows:

Combining equations (1) and (2) into an equation of the form of equation (7),

$$I_\gamma = \frac{9\pi^2}{2R^2}\left(\frac{m^2-1}{m^2+2}\right)\frac{V^2}{\lambda^4}\cdot (1+\cos^2\gamma)\exp\left[-24\pi^3\left(\frac{m^2-1}{m^2+2}\right)^2\frac{V^2}{\lambda^4}nl\right]. \quad (9)$$

This equation is a maximum when

$$\lambda = \sqrt[4]{n\alpha V^2 l}$$

where

$$\alpha = 24\pi^3\left(\frac{m^2-1}{m^2+2}\right)^2 \quad (10)$$

Thus the wavelength of maximum Rayleigh scattering increases with the particle radius, the length of path and the number concentration.

This phenomenon is very striking when observed in a dense homogeneous aerosol exhibiting Mie scattering. The color of the Tyndall beam varies from blue through green and orange to red, before it is extinguished.

The particle radii may be obtained quite accurately by measuring quantitatively the transmission as a function of wavelength. This is the principle of an instrument called the *Slope-o-meter* described in Chapter 22.

21.2.5 Scattering by Large Particles

The Mie equations hold, theoretically, for any value of the radius. However, when α is greater than 10 or 12, the practical difficulties of calculation become excessive. Consequently Figure 1 shows no points beyond $\alpha = 12$.

However, when r is extremely large, approximation methods show [3] that K approaches the value 2. At first sight this appears false since it says that a very large sphere scatters twice as much light as falls on it. Brillouin [11] has recently shown theoretically that the light scattered by a relatively large metallic sphere ($r > 12$ microns) could be divided into two *equal* parts, that scattered into a small solid angle around the forward direction (i.e., into the geometrical shadow), and that scattered in all other directions. This means that although the correct value of the scattering coefficient is 2, the actual value, measured experimentally, will be 1 for very large spheres, since for such spheres the angular divergence of the shadow is extremely small.

This result was confirmed by the following experiment. A cloud of lycopodium spores was allowed to settle on to a glass plate. The radii of these spores were found to be very uniform, 15.0 ± 1 micron. The plate was then placed in a parallel beam of light in front of a photocell, and the transmitted intensity measured at different distances between plate and photocell. The reading of the photocell increased by the factor 2.1 when the distance from the plate to the photocell was decreased from 18 ft to 6 in. Calculation checked this result and showed that at 18 ft the observed scattering cross section was $2\pi r^2$ and at 6 in. it was πr^2. At 6 in., half of the scattered light (i.e., that part scattered into the geometrical shadow) was picked up by the photocell.

This conclusion is further confirmed by a consideration of diffraction by large obstacles. According to the theory of diffraction, the total amount of light diffracted by an opening is equal to the area of the opening (in the case of unit intensity of illumination). For a circular hole of radius r, the amount of light diffracted would be πr^2.

According to Babinet's principle, a circular obstacle of radius r will diffract the same amount of light as a circular hole of radius r. But the obstacle will also intercept an amount of light equal to its area πr^2. Consequently the total amount of light, both intercepted and diffracted, is $2\pi r^2$, and the transmission experiment described above will yield a scattering cross section of $2\pi r^2$, provided the distance from the obstacle to the measuring device is made large enough.

However, for very large obstacles, this condition is not realizable in practice. The diffraction pattern is so small that all the light contained in it is received by the collector. The collector then measures only the amount of light intercepted by the geometric cross section πr^2.

Therefore, it is evident that the total amount of light absorbed and scattered (i.e., diffracted at any angle from its original direction) is $2\pi r^2$, as the Mie-Stratton theory shows. However, any experimental measurement of a very large particle will yield the value πr^2, the amount of light absorbed by an opaque disk, or in the case of a reflecting sphere, light scattered outside of the geometrical shadow.

21.3 SCATTERING BY NONUNIFORM PARTICLE SIZE SPHERICAL AEROSOLS

Ordinary aerosols, having a large range of particle size, exhibit the scattering which would be observed from a mixture of a large number of uniform particle

size aerosols, mixed in varying proportions. The different colors in the scattered light overlap so that the aerosol appears more or less white depending on how much one particle size predominates. The polarization is also a mixture of that from many sizes, the effect of the large particles predominating because of the great increase of intensity with size.

If a nonuniform aerosol, such as tobacco smoke, is allowed to settle in a convection-free chamber, considerable separation of sizes will occur. If the upper layers of the cloud are examined with a beam of white light, various colors will be seen depending upon the height and direction of observation. An approximate idea of the size and size distribution of the smoke particles can be obtained by examining the colors and polarization at different heights and angles.

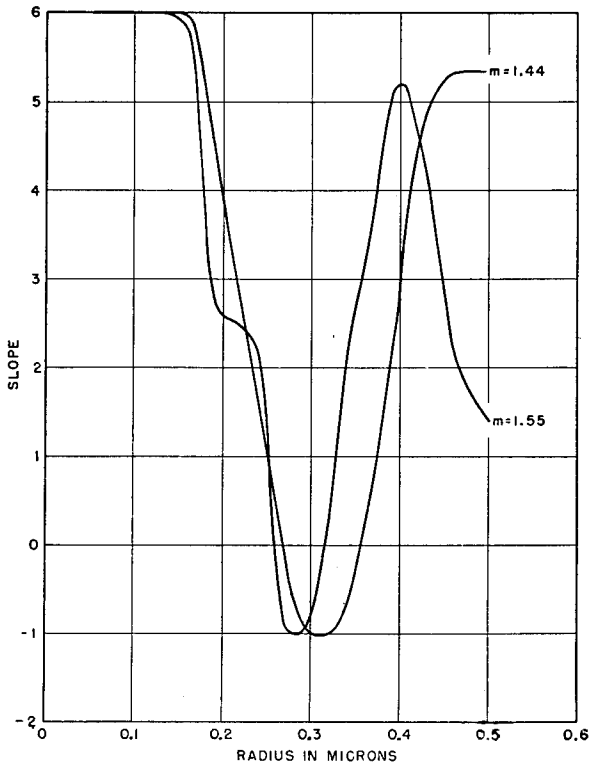

FIGURE 10. Angle scattering as function of particle size. p vs r in eq. $\Delta I = kr^p \Delta n$ at $\theta = 45°$.

21.3.1 Scattered Intensity vs Particle Radius

The intensity scattered at any wavelength by a given volume of smoke at a fixed height will decrease with time since the number of particles in that volume will decrease due to differential settling as explained in Chapter 19. If coagulation is negligible, the rate of decrease of intensity at any time depends upon the particle size and size distribution, and the scattering as a function of size.

The change in the scattered light intensity, ΔI, observed at a given angle and wavelength is proportional to the change in the particle concentration Δn, and the radius raised to some power p, that is

$$\Delta I = kr^p \Delta n. \tag{11}$$

The value of p at a given value of r and angle of observation, θ, is obtained from the calculations of the angular distribution of intensity referred to above.[4] The values of log $(i_1 + i_2)$ vs log r were plotted and the value of the slope p as a function of r was obtained for several angles.

Figure 10 shows the variation of p with r at θ = average of 40°, 45°, 50°, for refractive index 1.44, and 1.55 at the wavelength 0.524 micron. It is seen that p has the value 6 for radii below 0.1 micron as is to be expected in the region of Rayleigh scattering. The region of negative values of p corresponds roughly to the region of the curves of Figure 8 where the slope is negative. Sufficient calculations are not available to carry these curves beyond $r = 0.5$ micron.

Similar curves were drawn showing p as a function of r for total scattering. For Rayleigh scattering, p should again have the value 6, and for very large particles, the value 2. These curves were found to be quite different from those of Figure 10 in the useful range from 0.1 to 1 micron so that they cannot be used to supplement the curves of Figure 10.

The use of these curves in conjunction with the differential settler for the determination of particle size and distribution is described in Chapter 22.

21.3.2 Transmission in Tranquil Settling

The intensity transmitted by an aerosol in tranquil settling will vary in a similar manner. However, the practical difficulties of this measurement were found to be insurmountable. In order to obtain sufficient optical density and avoid coagulation, the smoke chamber must be large in order that the path length may be large since n must be not over 10^5 per cc. It has been found impossible to eliminate convection currents in anything but a chamber so small that the transmission is very nearly 100% when n has a suitable value.

21.3.3 Transmission in Stirred Settling

The optical density $D = Snl$, of a homogeneous aerosol in stirred settling and undergoing coagula-

879245 O - 50 - 7

tion, will vary according to equation (24), Chapter 19, as follows.

$$\frac{1}{n} = \frac{Sl}{D} = -\frac{\mathfrak{K}h}{v} + \left(\frac{\mathfrak{K}h}{v} + \frac{S_0 l}{D_0}\right) e^{-vt/h}. \quad (12)$$

For times short compared to h/v, this becomes

$$\frac{1}{D} = \frac{1}{D_0} + \left(\frac{\mathfrak{K}}{Sl} + \frac{v}{hD_0}\right) t \cdot \quad (13)$$

If $1/D$ is plotted against time a straight line will be obtained, having the slope $\mathfrak{K}/Sl + v/hD_0$. The quantities l, h, D, and D_0 are readily measurable. If the particle radius is known, v, S, and $\mathfrak{K}$ may be calculated, or if $\mathfrak{K}$ is known, then v, S, and r may be calculated. (See Chapter 22.)

This equation neglects the change in particle size (but not the change in number) due to coagulation. As a result of coagulation, v and S would not be quite constant.

21.3.4 Heterogeneous Aerosol without Coagulation

The total scattering cross section of N spherical particles of different sizes can be obtained by measuring the optical density $D = SlN$. In a heterogeneous aerosol, S is the scattering cross section of an average particle. In the range of particle sizes where K is nearly constant and equal to 2 ($r > 1$ micron, see Figure 1), S will be the scattering cross section of the sphere having the average geometrical cross section. Therefore, according to equation (6), Chapter 19, the scattering cross section per cc at zero time is

$$S_0 = \frac{\pi}{4} N_0 K_2 d_2^2, \quad (14)$$

and according to equation (8), Chapter 19, the scattering cross section at time t is:

$$S_t = \frac{\pi}{4} K_2 \int_0^\infty d^2 n_d \exp\left(-\frac{v_d t}{h}\right) \delta \log d. \quad (15)$$

Here K_2 is the scattering coefficient of the sphere of diameter d_2.

Equation (15), Chapter 19, may then be transformed to:

$$-\frac{d}{dt}\log S_t = 1.3 \times 10^5 \frac{\rho}{h} \frac{K_4}{K_2} \frac{d_4^4}{d_2^2}, \quad (16)$$

or

$$-\frac{d}{dt}\log S_t = 1.3 \times 10^5 \frac{\rho}{h} \frac{K_4}{K_2} d_6^2 \cdot \quad (17)$$

Thus d_6 can be obtained by measuring the average scattering cross section provided K_4 and K_2 can be determined.

The scattering per gram at zero time A_0 is obtained by dividing equation (14) by equation (7), Chapter 19.

$$A_0 = \frac{S_0}{M_0} = \frac{\frac{\pi}{4} N_0 K_2 d_2^2}{\frac{\pi}{6} N_0 \rho d_3^3} = \frac{3}{2} \frac{K_2}{\rho d_5}, \quad (18)$$

making use of equation (5), Chapter 19.

A further useful relationship is obtained by dividing equation (16) by equation (14), Chapter 19. Writing $d/dt \log M_t = u_m$ and $d/dt \log S_t = u_s$ we have

$$\frac{u_s}{u_m} = \frac{K_4}{K_2} \frac{d_3^3}{d_5^5} \frac{d_4^4}{d_2^2} \cdot \quad (19)$$

Multiplying equation (19) by A_0 [equation (18)] gives

$$A_0 \frac{u_s}{u_m} = \frac{3}{2} \frac{K_4}{\rho} \frac{d_4^4}{d_5^5} = \frac{3}{2} \frac{K_4}{\rho d_9}, \quad (20)$$

making use of equation (5), Chapter 19.

The use of these equations for particle size measurement is described in Chapter 22.

21.3.5 Complete Analysis of Scattering

The complete analysis of the light scattered or transmitted by a heterogeneous aerosol is extremely difficult. The absence of distinctive color in the scattered light is an indication of heterogeneity, but the distribution curve cannot be obtained by this means. Similarly, the polarization in the range of radii below 0.2 micron, may be used to detect the presence of a distribution of sizes, although it is extremely difficult, if not impossible, to obtain any quantitative results by this means.

The general theory has been discussed elsewhere. The conclusions reached may be summarized as follows.

The determination from scratch of the nonhomogeneity of a smoke is possible only in principle. But if we already know enough about the size and distribution of a heterogeneous smoke, the knowledge of the scattering functions of homogeneous smokes will enable us to find out more. For example, the determination of the proportions of a mixture of two homogeneous smokes of known particle size is relatively easy.

The relative proportions of a mixture of two homo-

geneous smokes of known radii less than about 0.2 micron can be obtained by measuring the polarization at the scattering angle θ. Let x and $1 - x$ be the proportion of particles of radius r_1 and r_2 respectively. Let $i_1(r_1,\theta)$ and $i_2(r_1,\theta)$ be the intensities of the polarized components scattered per particle of radius r_1 at the angle θ, with similar expressions for r_2; and let the wavelength be λ.

Then the ratio of the intensities observed at the angle θ will be according to equation (6)

$$R = \frac{xi_2(r_1,\theta) + (1-x)i_2(r_2,\theta)}{xi_1(r_1,\theta) + (1-x)i_1(r_2,\theta)} = \tan^2\phi. \quad (21)$$

Since the i_2's and the i_1's are known from the Mie theory, this equation may be solved for x.

If the radii were unknown they could be obtained by observing the polarization at three different angles θ.

For radii greater than about 0.2 micron this method would not yield a unique solution since the absolute values as well as the ratio of the intensities are multiple valued.

Usually, however, no such simple distribution of sizes is encountered. Calculations have been made showing the effect of various size distributions on the polarization. The conclusion is that this method cannot be used to obtain the size or size distribution of heterogeneous smokes.

One can merely determine whether or not the smoke is homogeneous by observing the polarization at several angles. If, for example, the polarization of a stearic acid smoke were observed at 90°, 80°, and 70°, and the same size were obtained from each of the corresponding curves of Figure 7, then the smoke would evidently be homogeneous. However, this method would fail for radii near 0.15 micron where the curves cross.

Similarly, the color of the transmitted light serves as an approximate measure of the particle size, and an unsaturated color indicates a distribution of sizes (see preceding text and Chapter 22); but the distribution curve cannot be obtained from the wavelength intensity distribution of the transmitted light.

21.4 THE SCATTERING OF LIGHT BY SOLID PARTICLES

21.4.1 Polarization

The angular distribution of intensity of the light scattered by irregularly shaped particles has not been analyzed in detail. The Rayleigh theory is applicable to extremely small particles no matter what their shape. However, for larger particles near the limit of the Rayleigh region, shape and internal structure have an effect on the scattering. The ratio i_2/i_1, called the *depolarization factor*, is greater than for spherical particles. Lotmar [15] has shown that the internal crystal structure of solid particles has a much greater effect on the polarization than does the external shape of the particle.

When very small particles are illuminated by polarized light the Rayleigh theory shows [equation (3)] that i_2 is zero everywhere. For larger spheres exhibiting Mie scattering, or for irregular particles exhibiting depolarization, i_2 is not zero. Krishnan [16] has shown theoretically and experimentally that the component i_2 (scattered when the incident light is polarized with its electric vibrations perpendicular to the plane of observation) is equal to the component i_1 (scattered when the incident light is polarized with its electric vibrations parallel to the plane of observation). These two components will be referred to as the *rotated* components. This relationship holds for a mass of particles of all shapes and sizes, and for all angles of scattering, provided the orientation of the particles is random.

The Mie theory for spherical particles shows that the rotated components are both equal to zero.[4] Consequently when the incident light is unpolarized, the component i_2, which is observed, is produced by the incident electric vibrations which are parallel to the plane of observation, and the component i_1 is produced by the incident electric vibrations which are perpendicular to the plane of observation.

However, when irregularly shaped particles are illuminated by unpolarized light, the rotated components are no longer equal to zero. Consequently, comparison of the polarization of the light scattered by particles when illuminated with unpolarized and polarized light would provide a measure of the shape or anisotropy of the particles.

It would be expected that the polarization by particles of a given form could be used as a measure of their size, provided a calibration could be obtained. This would require a series of smokes of uniform size. Attempts were made to produce or obtain solid particle smokes sufficiently uniform for this purpose, but they were not successful.

21.4.2 Scintillating Particles

Some useful qualitative information can be obtained by observing the effect of Brownian rotation.

When a bright Tyndall beam is observed in a solid particle smoke, the particles will be observed to scintillate due to random reflections from the crystal faces. Large particles, which are observed to fall rapidly, produce intermittent flashes at a much lower frequency than those from the more slowly falling particles. Stearic acid smokes that have been aged for an hour or more exhibit these scintillations, while fresh smokes do not. This indicates that in the course of time the supercooled stearic acid droplets crystallize.

21.4.3 Transmission in Stirred Settling

The optical density of solid particle smokes in stirred settling may be analyzed according to the methods described in preceding text.

The aerosol, composed of irregularly shaped aggregates of a wide range of sizes, is compared with a hypothetical aerosol of equivalent spherical particles having a logarithmic-probability distribution of sizes. Microscope examination of Kadox (see Figure 1, Chapter 22) and albumin particles has shown them to be fairly compact aggregates that show no tendency to form filamentary particles; particle size exhibits a distribution curve that follows approximately the logarithmic-probability law.

In ground materials it is probable that the number of particles at very small sizes is greater than appears from the measurements, due to the difficulty of observing them. However, since the scattered light decreases with the sixth power of the radius for particles below about 0.1-micron radius, and the contribution to the mass decreases as the third power of the radius, such particles are relatively unimportant so that the approximation appears to be good enough for practical purposes. Bailey has found a logarithmic probability distribution in ground pigments.[17]

Consequently one can calculate various average diameters in a manner similar to that described in Chapter 19. The average scattering cross section and scattering per gram may be expressed as described in preceding text, provided the scattering coefficient is known.

In the case of Kadox and other small particles less than about 2-micron diameter, the Mie theory shows (see Figure 1) that the scattering coefficient usually has a value between 2 and 4 except for extremely small particles exhibiting Rayleigh scattering. It was found empirically by Bailey [17] that if the values of the diameter are multiplied by $(m^2-1)/(m^2+2)$, where m is the refractive index, then all the scattering curves approximately coincide.

It has been found that this relationship is also approximately true for the scattering curves calculated from the Mie theory. Figure 11 shows the average of the curves obtained by plotting the values of K in Figure 1 against the corresponding value of $d(m^2-1)/(m^2+2)$. It is seen that maximum values of the scattering coefficient occur when $d(m^2-1)/(m^2+2) = 0.2$ and 0.5 micron (dashed line in Figure 11). Figure 11 is a universal scattering curve for all

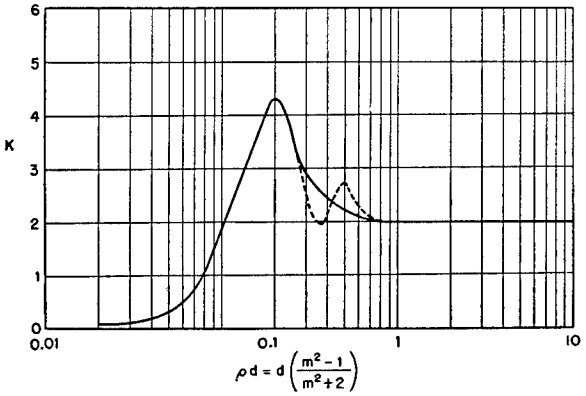

FIGURE 11. Universal scattering curve for all transparent materials of any refractive index.

transparent materials of any refractive index. The heavy line was drawn to average out the trough and minor peak since they are within the precision of measurement. (See Chapter 22.)

Since solid aerosol particles are aggregates of small primary particles, they will have an effective density and an effective refractive index less than the true density and refractive index of the material. The effective density has been found experimentally to be about equal to the density of the powder before dispersal, i.e., the average of the density of the solid particles plus the air in the spaces between the particles. The effective refractive index has been found to be given approximately by the same average.

The author has found that the effective density ρ and effective refractive index m are related according to the Lorenz-Lorentz relation, ρ = Constant $\times$ $(m^2 - 1)/(m^2 + 2)$. The value of the constant for a given aerosol material is found by substituting the true density ρ_0 and the true refractive index m_0 into the equation. The constant is equal to 11 for Kadox and 4 for albumin. It is seen that the factor $(m^2 - 1)/(m^2 + 2)$ is the factor which brings the scattering curves for all materials into approximate coincidence.

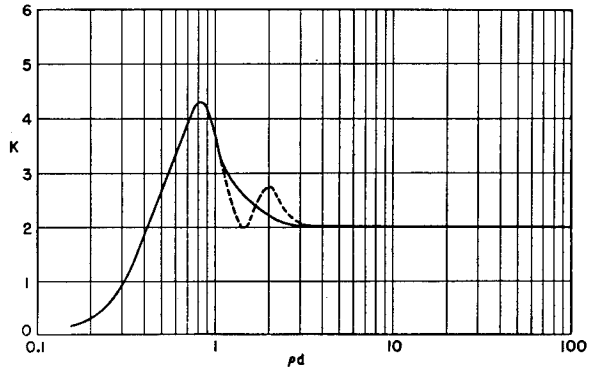

FIGURE 12. Scattering curve for Kadox. K vs ρd.

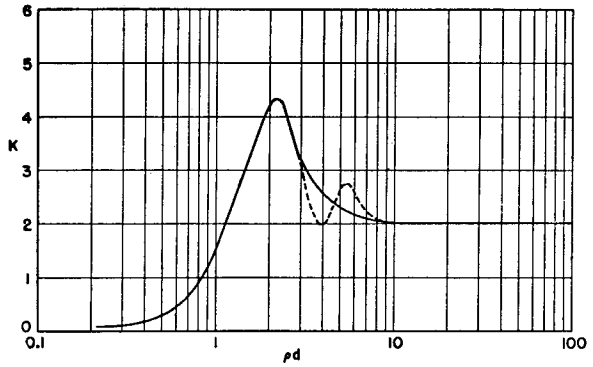

FIGURE 13. Scattering curve for albumin. K vs ρd.

Two curves (Figures 12 and 13), one for Kadox and one for albumin, were plotted, showing the variation of the scattering coefficient K with

$$\rho d = \text{Constant} \times d\left(\frac{m^2 - 1}{m^2 + 2}\right). \qquad (22)$$

Such a curve will yield the scattering coefficient of a loosely aggregated particle of a given material when the product ρd of the diameter and effective density is known.

It has been assumed that the effective density is a constant for all sizes of aggregated particles formed. This means that the packing of the primary particles is the same for all aggregates, which seems probable since most of the aggregates contain large numbers of primary particles, 20 or more.

The assumption that the refractive index of the aggregated particle is a smeared out index appears to be justified since the primary Kadox particles are about one-fifth to one-tenth the wavelength of light. Since the primary particles are packed in contact with each other, they will not individually give rise to Rayleigh scattering but will behave collectively as a single large particle showing Mie scattering. In the case of albumin the particles are all so large that the refractive index has little effect on the scattering, K having the constant value 2 as explained in preceding text.

Figures 12 and 13 may be used to obtain the particle size and size distribution as described in Chapter 22.

21.5 SCATTERING BY LIQUID OR SOLID PARTICLES WHICH ALSO ABSORB

21.5.1 General Characteristics

The scattering of light by colored particles is a combination of the selective scattering by transparent particles having a real refractive index, plus the selective absorption by absorbing particles having a complex refractive index. In selective scattering all the light not scattered is transmitted, but with selective absorption, some of the light not scattered is also not transmitted.

In colored materials the absorption and the refractive index vary markedly with wavelength. For example, solutions of the orange dye (Calco Oil Orange Y-293) used in orange smoke signals have a low value of absorption in the yellow and red, a high value in the green and blue and an intermediate value in the violet. This means that, for the green and blue wavelengths, dye particles and oil droplets containing dye will have complex scattering and absorbing properties, while for the red and yellow wavelengths such particles will exhibit approximately the selective scattering by transparent particles.

At wavelengths of low absorption the optimum particle size of a colored particle will be approximately the same as that of a transparent particle of the same real refractive index. In the case of dye dissolved in oil of real refractive index 1.50, the optimum particle size would be about 0.3 micron for red and yellow. Since the absorption of green and blue is higher, the refractive index at these wavelengths will be higher, and therefore, the optimum particle size will be smaller since it decreases with increasing refractive index. (See Figure 9.)

The exact form of the dispersion curve for pure Y-293 dye is not known. The refractive index of the pure dye for red and yellow is 1.8. For green and blue it is probably higher; for violet, probably lower. In any case, the optimum particle size is lower than for Diol or for dye dissolved in Diol. It is probably near

that of sulfur, index = 2.0, for which the mean optimum particle radius is 0.15 micron. (See Figure 9.)

The observed optical density of pure dye smoke (of unknown particle size), measured with blue light (λ = 0.44 micron) outdoors,[18] was about one-half the observed and calculated optical density of both sulfur and Diol for green light (λ = 0.524 micron) at the optimum particle size. Diol has a scattering cross section of 11 to 12 sq m per g (see Figure 9) for radii between 0.22 and 0.34 micron, and sulfur has about the same scattering cross section for the radii 0.12 to 0.18 micron. The dye smokes should have at least the same scattering cross section at their optimum radius (probably about 0.2 micron). The fact that the observations on the dye smoke were made for blue light and the measurements on sulfur were made with green light does not invalidate this statement since the optical density of sulfur smoke near the optimum particle size (r = 0.12 to 0.18 micron) is practically the same for all visible wavelengths. This can be seen in Figure 9 by dividing the λ scale by 2 to correspond to r = 0.15 micron.

The indications are that the dye smoke particles produced by the orange smoke signals are smaller than the optimum size when produced outdoors and larger when produced indoors. The dye smoke particles produced indoors were examined with a high power microscope of high resolution. They were too small to be measured accurately but appeared to be not greater than 0.3 or 0.4 micron in radius. The particles produced outdoors appeared smaller for the following reasons.

In a dye smoke, the color of the transmitted light is an indication of the size just as it is in the case of transparent particles. For example, the dye smoke produced by burning the orange signals in a 22-cu m room appeared pale green by transmitted light. This occurred because the particles had grown large due to rapid coagulation of the dense smoke. They became somewhat greater than the optimum size so that the transmitted light appeared green as it does through a screening oil fog whose droplets are somewhat greater than the optimum size (green sun's disk). On the other hand, deep red or orange is frequently transmitted by the dye smoke produced outdoors showing that the particles are smaller than the optimum size.

It has been observed frequently that the color of a cloud of dye or other colored smoke becomes paler with dilution. This is a necessary consequence of the absorbing properties of such smokes. A dense cloud of small orange dye particles appears orange by scattered light and deep red or orange by transmitted light. The cloud transmits red and yellow as does an oil solution of the dye, and the color of a cloud becomes paler with dilution, as the color of a solution becomes paler with dilution.

A dense cloud of small orange dye particles appears orange because of *multiple scattering* and *absorption*, and not because of primary scattering, which is practically colorless. At each rescattering, slightly more green than red is abstracted from the light by selective absorption in a particle, so that the light which is finally scattered from the interior of a dense cloud has had much of the blue and green abstracted from it and consequently appears red or orange. In a dilute cloud, however, the multiple scattering is greatly decreased. A great deal of primary scattering is seen, which is practically colorless.

However, in a cloud of large particles, the color decreases less rapidly with dilution. Due to greater selective absorption, larger particles abstract a greater proportion of blue at each scattering process so that less multiple scattering is required to produce a strong orange color. Again, as with the dye smoke produced indoors, if the size is somewhat greater than the optimum, then selective scattering may cause the transmitted light to appear green.

21.5.2 Tables of Calculations

Tables of calculations, based on the Mie theory for absorbing particles, have recently been completed. They can be used to obtain the total scattering by a droplet of transparent oil of real refractive index m_0 = 1.50 containing dye in solution. When the absorption index k of the dye solution is known as a function of wavelength, the total scattering can be calculated for a complex refractive index m, ranging in value from $m = 1.44(1 - ik)$ to $m = 1.55(1 - ik)$ for values of α up to 6.0. The index k can have values up to 0.03, which corresponds to high absorption. These calculations cannot be used for pure dye smokes whose real refractive index is 1.8.

It should be pointed out that these calculations will also yield the total scattering by a transparent particle of refractive index from 1.44 to 1.55 when k is made equal to zero. Approximately correct values will be obtained for refractive indices as small as 1.33 and as large as 1.65.

These tables have been published by the Mathematical Tables Project.[19]

Chapter 8

MEASUREMENT OF PARTICLE SIZE AND SIZE DISTRIBUTION

By *David Sinclair*

22.1 MICROSCOPIC EXAMINATION

22.1.1 Light Microscope

THE LIGHT MICROSCOPE has long been the standard method of observation of the particle size and distribution of smokes. It possesses the advantage that the true shape and size of the particles can be obtained, provided the radii of the primary particles are not less than 0.3 micron. It has the disadvantage that a long and tedious series of measurements is required to obtain a distribution curve.

Solid particles are usually composed of more or less loosely bound aggregates of primary particles too small to be resolved by the light microscope. To reveal the true structure of such particles, the electron microscope is required.

When liquid droplets are observed on slides, the true diameter is not observed since the drop is flattened, more or less, by its weight. The amount of flattening depends to a marked extent on the properties of the surface of the slide as well as the nature of the droplet. If a carefully cleaned slide is used, a definite relationship exists for a given drop material, between the observed diameter of the flattened drop and its focal length.

May [1] has given equations and curves from which the true diameter can be read when the lens diameter and focal length have been measured. The amount of flattening of the drop can be reduced by coating the slide with an oleophobic film.[2]

This method has sometimes been found unreliable. Observation of 4 microns radii droplets (determined by the gravity fall method and also by weighing a known number of droplets) gave results 25% too small when the radius was calculated from microscope measurements of the lens diameter.

Volatile droplets on slides may evaporate so rapidly that the true diameter cannot be obtained. This may be avoided by allowing the drop to settle into a viscous liquid film in which it is insoluble.[1]

This method has been successfully applied to the measurement of the radii of water fog droplets.[3] A small drop of castor oil is placed in a depression slide and spread into a film. The water drops are allowed to settle onto the oil and then immediately covered with a cover glass coated with oil. The water drops are thus imprisoned and may be observed at leisure. The true diameter of the drops is observed, since they assume a spherical form while floating in the oil.

Because the density of castor oil is 4% less than that of water, the droplets will finally sink to contact with the slide. They will usually spread and change their shape. This may occur for large drops before they can be measured. The spreading may be prevented by coating the depression with a thin, transparent film of paraffin.

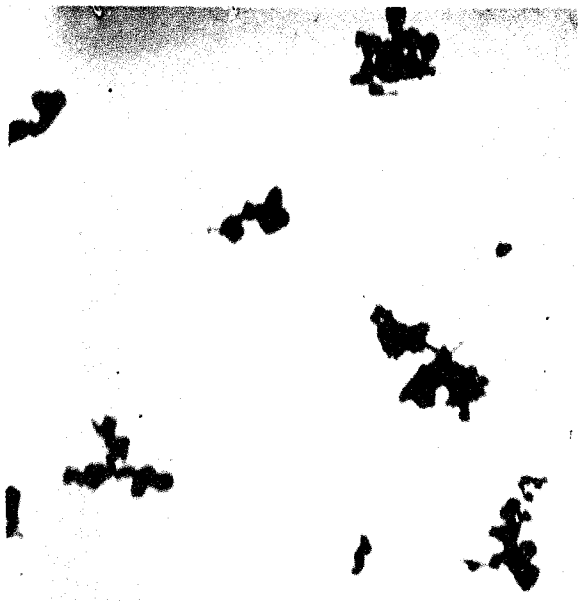

FIGURE 1. Electron microscope photo of ZnO particles.

The light microscope may be used to measure smoke particles in situ. This method has been investigated in greaf detail by Whytlaw-Gray.[4] The difficulties of this method have been analyzed and some of the defects corrected by Stumpf.[5]

In general, the light microscope is most useful as an auxiliary to other methods. These methods, described below, make possible rapid measurements on a mass of particles in their actual state of dispersion, either in the laboratory or in the field.

22.1.2 Electron Microscope

The electron microscope reveals details of the shape, structure, and size of particles completely unobservable by any other method. For example, some magnesium oxide particles of 1 or 2 microns diameter, as seen in the light microscope, are found to be irregular aggregates of a large number of cubical crystals as small as 0.01 micron on a side (see Figure 1, Chapter 18). Carbon particles are found to be long filaments of extremely small spherical particles (see Figure 3, Chapter 18). Similarly, the structure of particles of zinc oxide and lithopone are revealed by such photographs as Figures 1 and 2. Extensive observations of the structure of aerosol particles have recently been made with the electron microscope by Eyring, McGrew,[7] and others.

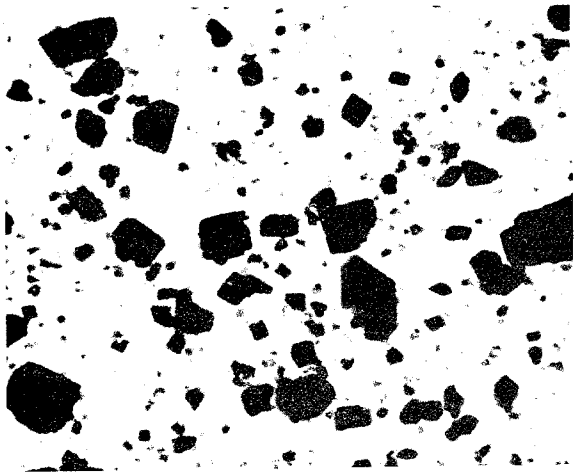

FIGURE 2. Electron microscope photo of lithopone.

The electron microscope has some of the disadvantages suffered by the light microscope. The particles are not observed in the dispersed state and may be altered during or after sampling. This is especially true of fog droplets which are evaporated and distorted by the energy in the electron beam. For this reason, particles must have a vapor pressure at room temperature of not over 10^{-5} cm of Hg, if they are to be observed in the electron microscope. The problems presented by various sampling methods are described in the next section.

The difficulties of obtaining a true particle size distribution curve are even greater with the electron microscope than with the light microscope. Because the magnification is high, the field of view of the electron microscope is so small that a large number of photographs must be taken in order to obtain a representative picture. This greatly increases the time and labor involved in making a count.

Furthermore the details of individual particles observable with the electron microscope are often unimportant, or are averaged out in the mass of particles in an aerosol. For example, the obscuring power of a smoke of solid particles is determined by the average cross section of the particles, their shape and structure being unimportant. For such problems a method of size measurement is desired which will yield the particle area distribution as rapidly as possible.

Similarly, the rate of fall of particles is determined by their geometric cross section and particle density (generally less than the true density of the solid material), so that these quantities can be obtained by suitable measurements of the rate of fall. It would be extremely tedious if not impossible to obtain the particle cross section and density from electron microscope photographs.

In general, the method of measurement should be adapted to obtaining the properties of the aerosol of particular interest.

The electron microscope, even more than the light microscope, is not suitable for measurements in the field. For these reasons the electron microscope, like the light microscope, is most useful as an auxiliary to the methods of measurement of particle size and distribution in the aerosol state, described in following text.

22.2 SAMPLING METHODS

22.2.1 Centrifugal Separation

The cascade impactor is a form of centrifugal separator developed at Porton Experimental Station.[1] It is suitable for particles above 1-micron radius. The aerosol is forced in succession through a series of jets directed at microscope slides perpendicular to their surface. For each succeeding jet the velocity of flow V is increased by decreasing the area of the jet opening; and the radius of curvature R of the path of flow is decreased by placing the jet nearer the surface of the slide.

Particles having a radius equal to or greater than r_1 [given by equation (39), Chapter 19] will be thrown out onto the first slide. Particles having a radius equal to or greater than r_2 will be thrown out onto the second slide, and so on, where $r_1 > r_2 > r_3 \cdots$, $V_1 < V_2 < V_3 \cdots$, $R_1 > R_2 > R_3 \cdots$.

As stated in Chapter 19, the values of $r_1, r_2, r_3, \cdots$

may be determined by the construction of the apparatus, which determines the length of time the particles are in the given centrifugal field, as well as by the values of V and R. The apparatus is usually constructed so that all the particles down to 1 micron radius are collected in four stages. Smaller particles may contribute a large amount to the total number of particles but they contribute a negligible amount to the total mass of large particle aerosols.

In order to obtain a constant range of sizes on each slide the velocity of flow must be kept constant. This can be done by drawing the air through a critical pressure orifice. For example, this may be an opening in a glass tube, adjusted so that the pressure drop across it is appreciably greater than one-half an atmosphere when the flow has the desired value.[8] Under these conditions, moderate changes in the pumping rate have no effect on the flow through the orifice.

The cascade impactor, like the *impinger*,[9] has the disadvantage that the particles are likely to be distorted by the violent impact with the slide. Solid particles are frequently broken, resulting in too high a count of small particles, and droplets are spread out and greatly distorted from their spherical shape. Consequently, only an approximate idea of the true size can be obtained by direct microscope measurement of the impinged particles. An independent measure of size should be made so that the instrument can be calibrated for a given rate of flow and particle density. The cascade impactor has the advantage of compactness, and rapidity and ease of operation in the field.[1]

22.2.2 Thermal Precipitator

The thermal precipitator is particularly suitable for sampling heterogeneous smokes of particle radii less than 1 micron. As described in Chapter 19, aerosol particles will move in a temperature gradient from a hot body toward a colder body with a velocity directly proportional to the temperature gradient. With a high temperature gradient, the force acting on a particle is many times the force of gravity and the particle is deposited quickly. By placing the hot and cold bodies close together, the temperature gradient can be made high when the temperature difference is low (50 to 100 C).

All the particles can be removed quickly from a small volume of smoke in a few minutes so that a true sample can be obtained. Thus, this method is superior to deposition by gravity, which discriminates against small particles because of their lower rate of fall.

This method is superior to centrifugal separation of solid particles since it does not shatter or distort the particles by high velocity impact. It is not suitable for collecting volatile droplets because the hot body causes evaporation.

A type of precipitator that gives 100% precipitation is described by Watson.[10] A similar piece of apparatus was constructed at Columbia University and used to sample both solid and liquid smokes, which were also analyzed with the differential settler.

The apparatus consisted of a heated wire 0.007 in. in diameter, placed midway between two cold microscope cover glasses which were 0.015 in. apart and mounted with their planes vertical and parallel. Each cover glass was supported on one end of two brass plungers which fitted into a brass cylinder. The wire was stretched across the center of the cylinder, perpendicular to the axis. The wire was insulated from the cylinder and was heated to about 100 C by an electric current. The plungers carrying the cover glasses were inserted at opposite ends of the cylinder and held against stops so that each cover glass was at a distance of about 0.004 in. (about 100 microns) from the surface of the wire.

The method of sampling was as follows. The flask of smoke from which a sample was taken for the differential settler was immediately connected by a rubber tube to the thermal precipitator. Smoke was then drawn in between the cover glasses through an inlet tube in the top of the cylinder. The direction of flow was at right angles to the length of the wire. The smoke particles were all deposited on each of the two cover glasses in a strip parallel to the wire and a little ahead of a line opposite the wire.

The rate of flow was kept constant at about 3 cc per min by allowing water to flow slowly out of a reservoir connected to an outlet tube in the bottom of the cylinder. One to three minutes were required to obtain a sample, depending on the particle concentration and size of the smoke.

The efficiency of collection was tested by drawing the air from the precipitator through a spherical flask illuminated by an intense Tyndall beam. Any particles, even extremely small ones, can be readily detected by this method. When the flow was less than about 5 ml per min, no particles could be found in the flask.

The deposits were measured and counted, using a

microscope having an objective of numerical aperture about 0.85 and magnification of 120 diameters. This was used with a micrometer eyepiece, magnification 20 diameters, which was calibrated with a Zeiss stage micrometer. One division on the ocular micrometer = 0.86 micron. The diameter of particles of 0.3 micron radius and larger could be read to ± 0.1 division or about ± 0.1 micron in diameter, i.e., ± 0.05 micron in radius. Particles below 0.3 micron radius could only be estimated.

Distribution curves were obtained by counting about 200 particles. A count of a larger number of particles would be necessary for an accurate distribution curve, but the number counted seemed sufficient for the purpose of testing the performance of the differential settler.

There was some indication of separation of sizes along the direction perpendicular to the hot wire. The smaller particles seemed to be deposited sooner than the larger, in conformity with the theory (Chapter 19). Consequently, in order to obtain as true a count as possible, the counts were made along several lines which completely traversed the deposit.

The particles were deposited in two strips about 1 mm wide and 1 cm long, i.e., over an area of 0.2 sq cm. In 2-min flow at a rate of 3 cc per min, a smoke of 10^5 particles per cc would yield a deposit of 6×10^5 particles. These 6×10^5 particles of 1 micron radius have a total cross-sectional area of 0.002 sq cm, or 1% of the area on which they are deposited. Thus 1% of these particles should be expected to touch and form some sort of double particle. An equal number of smaller particles are less likely to touch, and the time of sampling can be shortened for larger particles.

The normal appearance under the microscope of a deposited smoke prepared from undecomposed stearic acid is that of solid spheres, which are probably supercooled liquids of high viscosity. (The melting point of pure stearic acid is 69 C.) Frequently, however, the particles were not spherical. There were a few doublets which could have been formed either by coagulation in the aerosol or by collision at the time of deposition. Sometimes the slides showed many crystals, either leaves or tetrahedra. These were most numerous when using an old batch of stearic acid which had turned dark brown from the decomposition products.

Crystallization may have occurred in the aerosol, but more probably at the time of deposition on the slide. (It was frequently found that particles, originally deposited as spheres, had changed their shape by the following day.) Scintillating crystal particles are always observed in an aged smoke and only rarely in a freshly made heterogeneous smoke. No scintillating particles were observed in many fresh smokes which, after deposition on the microscope slide, showed leaf or tetrahedral crystals. It seems probable, therefore, that the condition of the surface of the cover glass caused the observed variety of shapes of the particles.

As has already been mentioned, drops will spread when deposited on a hard surface so that the diameter observed in the microscope will be too large.

The thermal precipitator was also used to obtain deposits of lithopone and zinc oxide on electron microscope slides. A brass disk, having a depression cut to fit an electron microscope screen, was used in place of one of the light microscope cover glasses. This method was found to be very unreliable since most of the particles were deposited onto the plastic film on top of the wires where they could not be observed. Furthermore, the heat from the wire tended to break the film on the screen.

A microscopic examination of the plastic film on a new screen revealed the fact that the film sagged between the wires. The center of the film was as much as 20 microns lower than the part touching the wires. This is one-fifth of the distance between the screen and the hot wire of the thermal precipitator. The result is that the thermal gradient is 25% greater over the wires than over the center of the film, so that the particles tend to deposit on top of the wires.

Figure 1 shows one of the few good thermal deposits of ZnO obtained. The sample for Figure 2 was prepared from a liquid dispersion of lithopone. The latter appears to be the only reliable method of preparing electron microscope screens.

22.2.3 Gravity Settling

Gravity settling yields a slide on which the particle number distribution usually differs from that in the aerosol. Unless the slide is left in so long that all the particles settle out, the number of particles of smaller radii which settle out will be less than the true distribution in proportion to the square of the radius. [See equation (1), Chapter 19.] In general, it is impractical to wait for all the smallest particles to settle out.

Consequently, the slide is usually placed in the aerosol for a few minutes and the number distribution corrected by multiplying the observed number of

particles of radius r by r_0^2/r^2. This correction is valid only in tranquil settling, and is applied only to particles of radius $r < r_0$ where r_0 is the radius of the particle for which the distance of fall during the time of exposure of the slide is equal to the distance from the slide to the top of the settling chamber.

According to equation (2), Chapter 19, in stirred settling the fraction f_s of particles having a given velocity v, which settle out during the time t of exposure of the slide is

$$f_s = 1 - e^{-vt/h}. \quad (1)$$

Consequently, the correct number distribution can be obtained by dividing the number of particles of a given size by the corresponding value of f_s.

In general, the type of settling of an aerosol in a closed chamber is somewhere between tranquil and stirred settling, so that an exact correction cannot be applied unless care is taken to maintain either tranquil or stirred settling. For small particles, gravity settling is not suited to obtaining a representative sample because of the length of time required.

22.2.4 Mass Concentration

The mass concentration of an aerosol can usually be readily measured by collecting a known volume in a glass wool filter and weighing. A small drying tube is half-filled with fine fiber glass wool, which should be packed in fairly tightly. The aerosol is drawn through the tube for a given length of time at a rate of about 10 lpm, measured with a flow meter, or a critical pressure orifice.

The efficiency of collection is observed by drawing the filtered air through a spherical flask illuminated with a Tyndall beam. If an appreciable number of particles are observed, more glass wool should be inserted, or the rate of flow decreased. Small particles pass through more readily than large particles.

This method is suitable for aerosol concentrations down to about 10 μg per l. At this concentration and a flow rate of 10 lpm for 30 min, an efficient filter would collect 3 mg, which can be measured with fair accuracy. For lower concentrations a microfilter, developed at Porton,[11] may be used.

22.2.5 Optical Mass-Concentration Meter

The optical mass-concentration meter may be used, when calibrated, to measure concentrations from 200 μg per l down to 10^{-3} μg per l. The instrument is a form of Tyndall meter, modified so that dark field illumination is used. The light scattered forward at angles from about 5 to 30° is observed, instead of that scattered at 90°. As the Mie theory shows, the observed intensity may thus be 100 or even 1,000 times greater. The instrument was developed for measurement of filter penetration.[12]

A schematic diagram of the apparatus is shown in Figure 3. The source S is a 6-v, 32-cp automobile

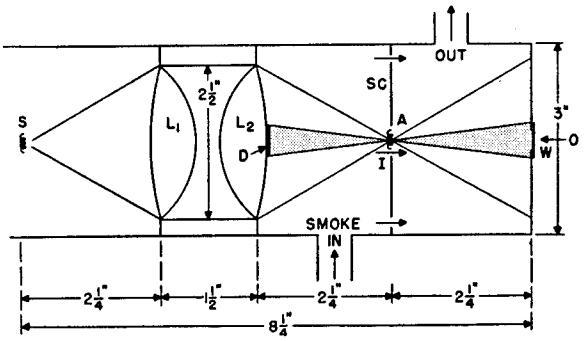

FIGURE 3. Schematic diagram of optical mass-concentration meter.

headlight bulb. L_1 and L_2 are aspheric condenser lenses of about 2¼-in. focal length and 2½-in. diameter. The source is placed at the focal point of L_1. A high intensity image of the source is formed by L_2 at its focal point. At this point the conical beam passes through a 3/16-in. diameter aperture A in the screen S_c. The smoke enters through a glass tube below A, passes through A and several peripheral holes in the screen and leaves the chamber through the tube above A.

A black, opaque disk D of about ½-in. diameter is painted or glued onto the lens L_2. This disk D blocks out a cone of central rays. Observation along the axis of the cone through the window W (about ¼-in. diameter) shows the smoke brilliantly illuminated, but no direct rays reach the eye. The observer sees only the rays which are scattered along or near the axis of the cone, the direct rays from the source being absorbed by the blackened end of the chamber. Stray light is reduced to a minimum by blackening the whole of the interior of the chamber, preferably with soot.

When no smoke or dust particles are present, the observer sees only the black background of the disk D, provided the aperture A is small enough. The aperture A must be so small that no scattered light from the edge of D or from dust particles on the lenses reaches the window. The aperture A must be larger than the image of the source. When the lenses

are not achromatic, violet rays strike the edge of A but are so faint that the resultant stray light is quite weak.

The sensitivity of the apparatus is such that the dust in ordinary room air appears brilliantly illuminated. Consequently, the chamber must be airtight. The zero reading for no smoke in the chamber is made while well filtered air is passing through.

The instrument is calibrated for a given smoke by observing the intensity at several concentrations high enough to be measured by collection in a glass wool filter. The concentration of more dilute smokes is then directly proportional to the intensity.

Because of turbulence the smoke fills the chamber completely. For this reason, a smoke of concentration higher than about 200 μg per l should not be used. At higher concentrations the loss in intensity of the direct beam due to scattering becomes appreciable, so that the linear relationship between observed intensity of scattered light and concentration no longer holds.

The calibration is correct over a wide range of mass concentrations provided the particle size remains unchanged. For this reason the smoke must not be so dense that appreciable coagulation occurs. This sets an upper limit to the mass concentration which decreases with particle size. Because of the short time of flow the maximum allowable number concentration is 10^6 per ml (see Chapter 19). Therefore, a 0.5 micron radius homogeneous smoke will not show appreciable coagulation up to 500 μg per l while a 0.15 micron radius smoke must not be over 14 μg per l (see preceding text).

The measurement or other purpose for which the aerosol is used must not change the particle size appreciably. For example, when using heterogeneous smoke to measure filter penetration, the dilute smoke which issues from the filter usually has a smaller average particle size than the more concentrated smoke entering the filter (see Chapters 19, 23, and 24). Consequently a fairly homogeneous smoke is particularly necessary when measuring filter penetration with the optical mass-concentration meter.

22.3 METHODS BASED UPON GRAVITY SETTLING

22.3.1 Measurement of Individual Particles

The velocity of fall of particles under gravity may be used in a variety of ways to measure their size. The simplest method is to observe with a low power microscope the individual particles when brightly illuminated in a small closed chamber. The radius may be calculated from the observed velocity of fall by means of the Stokes-Cunningham law of fall. (See Chapter 19.)

This method is suitable only for qualitative measurements. In order to obtain quantitative results a large number of particles must be observed and it is difficult to make the measurements representative. The tendency is to select the larger, brighter particles. Furthermore, the smaller particles are difficult to follow because of Brownian movement and the larger particles are likely to fall out before they are observed.

22.3.2 The Homogeneous Smoke Settler

The particle size of a homogeneous smoke may be conveniently measured by observing the rate of fall of the top of the cloud in a settling chamber free from convection currents. (See Chapter 19.) The observation is made with a Tyndall beam from a source which may be held in the hand or mounted so that it can be moved up and down conveniently. If care is taken to shield the chamber from radiation, the top of the smoke cloud will remain quite flat and sharp for an hour or more.

A form of settling chamber, previously described, consisted of a 3-in. diameter Pyrex tube 18 in. long, closed at the bottom with a rubber stopper and at the top with a brass plate cemented to the glass. This chamber is submerged in distilled (dust free) water contained in another glass cylinder and kept at a uniform temperature by stirring.

Smoke is introduced through two brass tubes soldered to holes in the brass top of the settling chamber and extending above the water level. These tubes contain needle valves which are operated from above the water level by wires or strings. This apparatus avoids mechanical and temperature disturbances.

Tranquil settling may best be obtained by placing the chamber in a darkened room free from draughts or other causes of rapid temperature change. A water cell should be used to remove the heat from the Tyndall beam, which is turned on only when a reading is being taken.

The height of the cloud is recorded at suitable time intervals by sighting along the top of the cloud and marking the position on the wall of the water

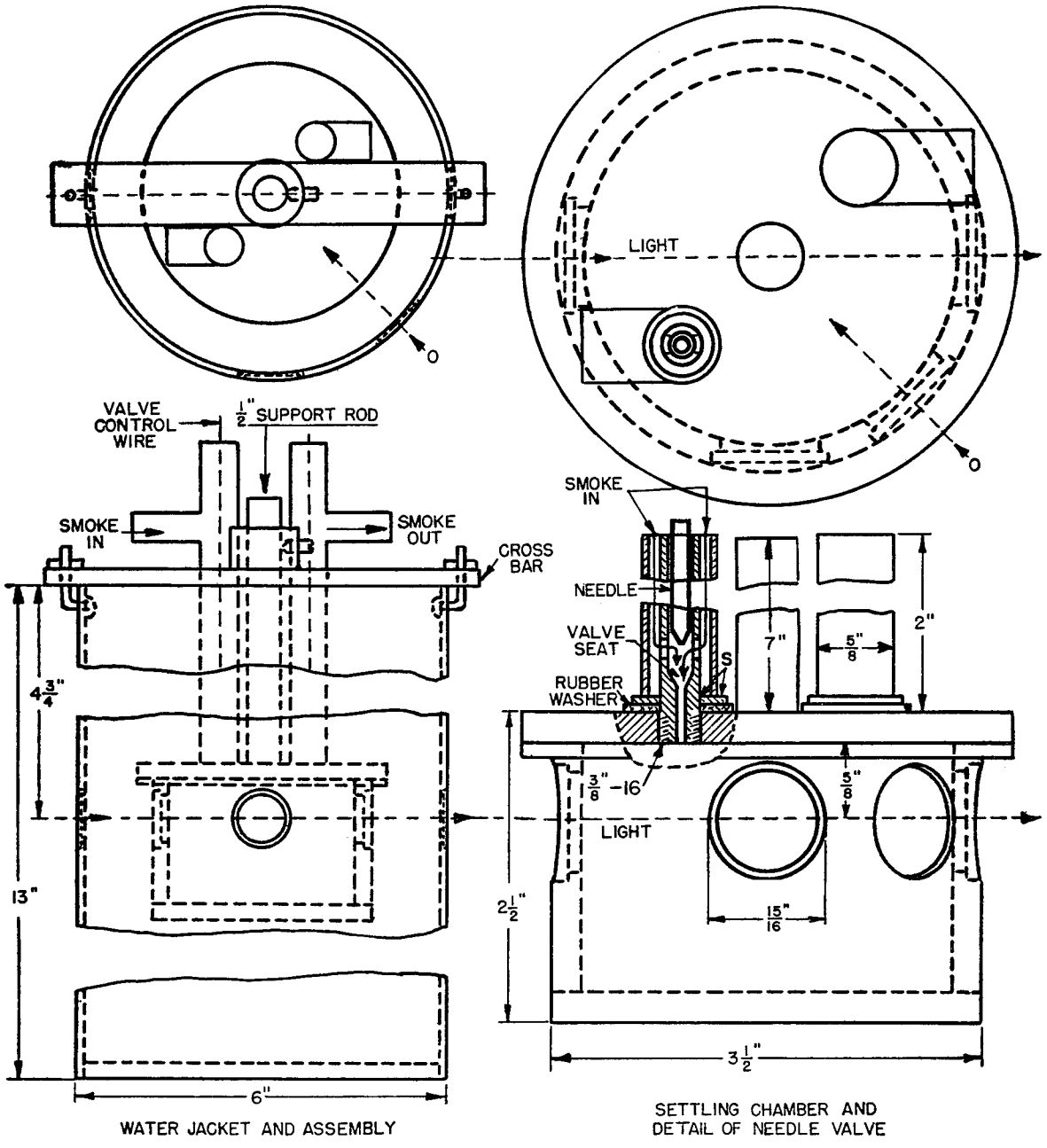

FIGURE 4. Differential settler.

jacket with a wax pencil. A precision of 5% or better can be obtained readily from four successive readings.

This method can be used for rates of fall from about 4 cm per hr up to 160 cm per hr, corresponding to radii from 0.3 to 2 microns for a material of unit density, and radii from 0.2 to 1½ microns for material of density 2 g per cc, such as sulfur.*

Radii down to 0.1 micron may be measured by observation (with a low-power microscope) of the individual droplets in a small chamber. Frequently, the microscope observation can be made on the top of the cloud. Although the top becomes considerably spread due to Brownian movement (see Chapter 19), an average position can be measured with fair accuracy. This method yields sufficiently accurate re-

sults with a few measurements in the case of a homogeneous smoke.

For radii below 0.1 micron the Brownian movement becomes so large that the results are unreliable.

22.3.3 Differential Settler

The differential settler is an instrument designed to measure the size and size distribution of a heterogeneous smoke. As described in Chapters 19 and 21, the rate of change of the number of particles, $\Delta n/\Delta t$, at a fixed height in an aerosol in tranquil settling is proportioned to the rate of change of the scattered light intensity $\Delta I/\Delta t$.

Figure 4 is a diagram of the apparatus constructed and used to measure the size distribution of a variety of smokes having spherical particles.

The settling chamber consists of a hollow brass cylinder closed with brass end plates, 3 in. in diameter and 2 in. high, inside dimensions. The walls of the chamber are ¼ in. thick.

The smoke is illuminated and observed through plane glass windows cemented over circular holes bored in the side of the chamber. The chamber is submerged in distilled (dust free) water contained in a brass water jacket and kept at a uniform temperature by a stirrer (not shown in diagram). The water jacket also carries windows, located opposite the windows in the settling chamber.

Smoke is introduced through two brass tubes soldered to holes in the top of the settling chamber and extending above the water level. These tubes contain needle valves which are operated from above the water level by wires. This apparatus avoids mechanical and temperature disturbances.

In order to make reliable intensity measurements and also to prevent convection currents, it is necessary to reduce stray light to a minimum. For this purpose, clear plane windows consisting of polarimeter tube cover glass 23.7 mm in diameter are used. By means of a slit 2 mm high and 8 mm long, the illuminating beam is made small enough so that it enters one window and leaves by a diametrically opposite window without touching the chamber walls. The light is made roughly monochromatic with a green filter and is completely screened off between readings.

The illuminated smoke is observed at an angle O of 45° ± 5° to the incident beam, as shown in the diagram. The intensity is measured with a Luckiesh-Taylor brightness meter. The 8-mm depth (in the direction of observation) of the illuminated volume of smoke provides sufficient intensity of scattered light for accurate measurement. The smoke should be as dilute as possible in order to prevent coagulation during the time of a run. With fine particle smokes, this time may be as much as an hour or more.

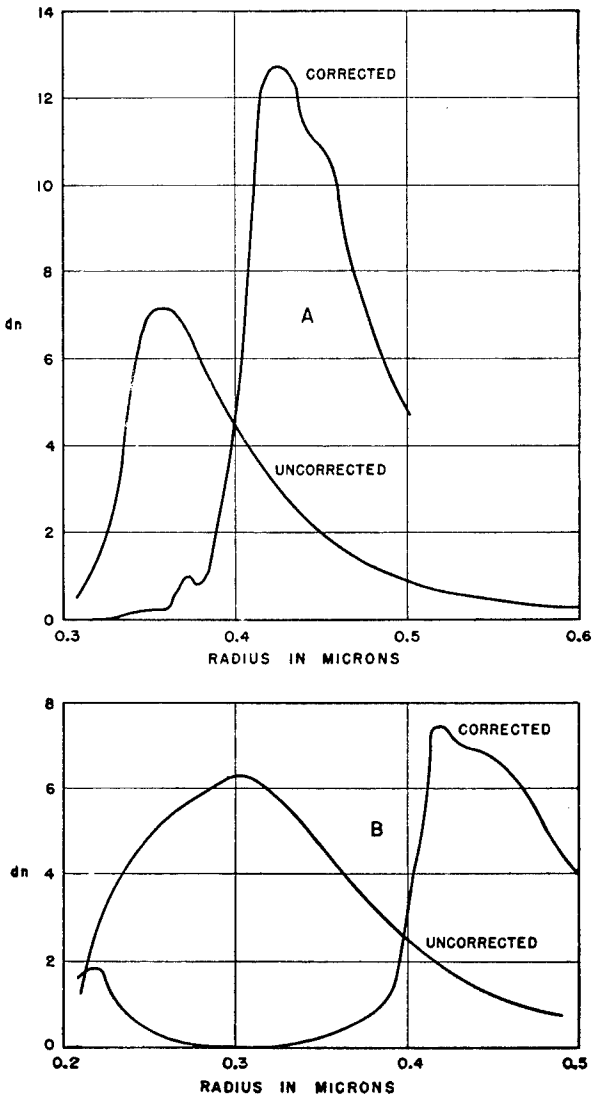

FIGURE 5. Corrected and uncorrected differential settler curves.

The 2-mm thickness (in the vertical direction) of the illuminated volume is the least that will provide a large enough field of view for good matching with the Luckiesh photometer. The thickness of the illuminated region should be kept as small as possible relative to the height of the top of the chamber above the illuminated region. A convenient height is 1.5 cm. A greater height makes the length of some runs exces-

sive, and a smaller height introduces too large an error in the determination of the starting time of a short run. With the above dimensions the intensity observed at any one time is that due to all particles within the region 1.5 ± 0.1 cm from the top. This introduces an error such that a smoke of uniform particle size appears to have a spread in size of about 7%. This is not considered excessive.

When the particle density is known, the particle size can be calculated from the relative intensity at any time provided the law of scattering of light with particle size is known. In the previous measurements described elsewhere, it was assumed that the law of scattering for spherical particles was given with sufficient accuracy by making p [see equation (11), Chapter 21] equal to 3 for all values of the radius. This yielded a distribution curve which was not even approximately correct in some cases.

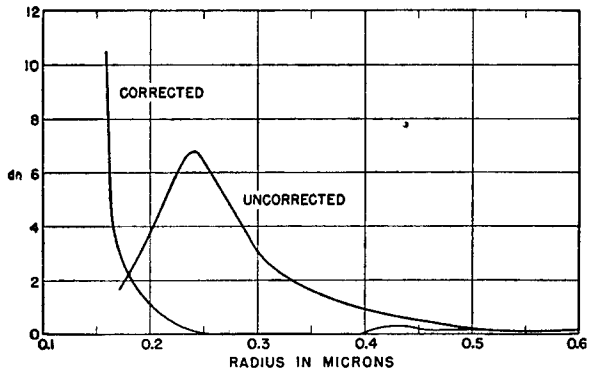

FIGURE 6. Corrected and uncorrected differential settler curves.

The true law of scattering is given in Figure 10, Chapter 21. Some of the distribution curves, previously given, were corrected by means of Figure 10, Chapter 21. The results are shown in Figures 5 to 8 which show the relative number of particles dn of radius r microns.

It will be seen that some of these curves, notably those in Figures 6 and 8, are completely altered. It is not certain that the curves of Figure 10, Chapter 21, are the proper correction curves. In correcting the distribution curves, the observed 7% spread in particle size as well as the 10° spread in angle was taken into account as far as possible.

A more reliable method would be to obtain an experimental calibration curve using very homogeneous smokes. In addition, a type of illumination similar to that used in the optical mass-concentration meter might be used. This would provide a greater angular spread in illumination which would tend to smooth out the calibration curve.

Furthermore, more intense illumination would make it possible to use smokes of low concentration, thus avoiding coagulation which may have been a

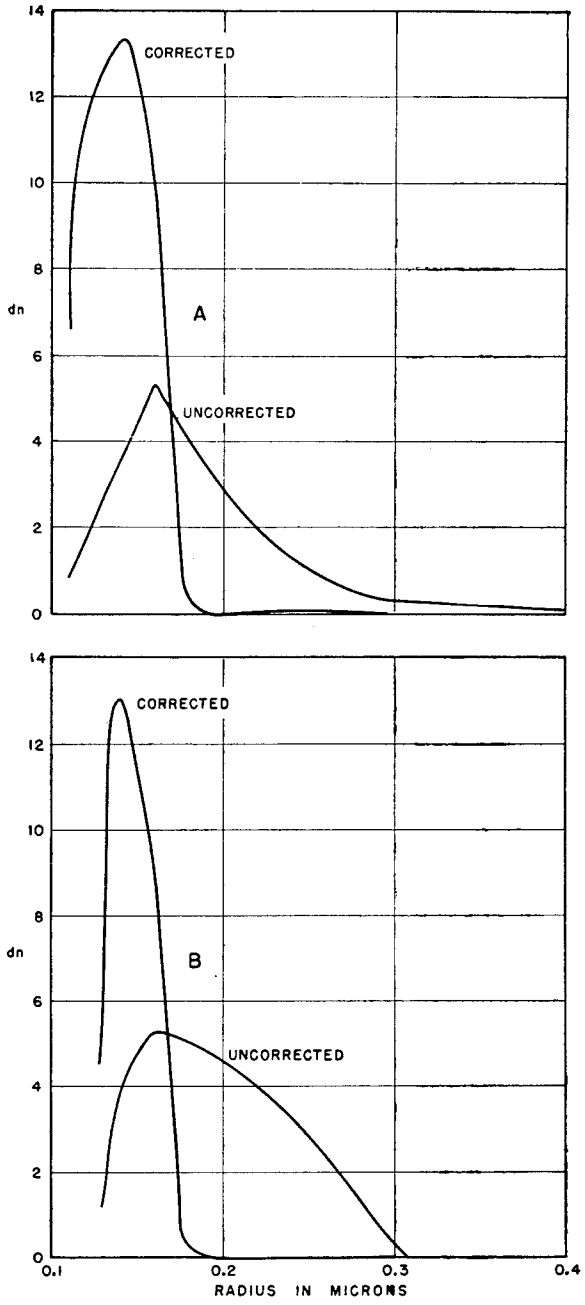

FIGURE 7. Corrected and uncorrected differential settler curves.

disturbing factor in the measurements made with the differential settler thus far.

22.3.4 Stirred Aerosols

The equations to be used in the measurement of particle size and size distribution of uniformly stirred aerosols have been given in Chapter 21.

HOMOGENEOUS AEROSOL WITH SLOW COAGULATION

If the aerosol is initially homogeneous and undergoes slow coagulation, equation (13), Chapter 21, describes the early stages in the life of the aerosol. Some experimental results obtained by this transmission method have been described elsewhere.

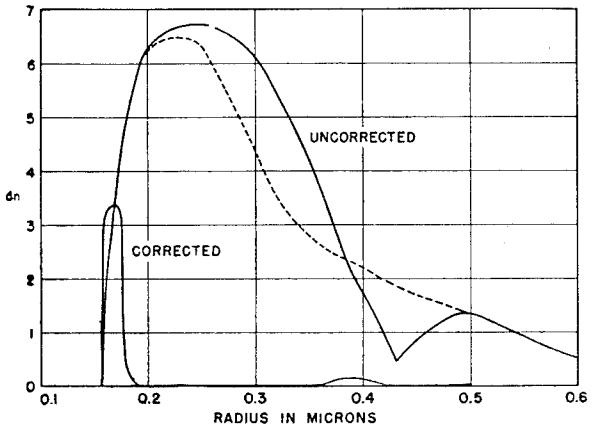

FIGURE 8. Corrected and uncorrected differential settler curves.

HETEROGENEOUS AEROSOL WITHOUT COAGULATION

When a heterogeneous aerosol is sufficiently dilute so that coagulation is negligible, equations (14) to (20), Chapter 21, may be employed. This transmission method has been used [16] to obtain the initial size distribution of aerosols of zinc oxide and egg albumin dispersed with the *geyser* and with the gas ejection bomb described in Chapter 20.

The average diameters of the equivalent spheres (see Chapter 21), that is, spheres having the density, rate of settling, refractive index and scattering cross section of the actual particles, were obtained from measurements of the initial scattering per cc of aerosol, S_t [equation (15), Chapter 21], and the mass concentration, M_t [equation (9), Chapter 19]. The values of S_t and M_t were plotted on semi-log paper.

Extrapolation of these curves to zero time gives the initial scattering per cubic centimeter, S_0, and the initial mass concentration, M_0, from which the initial scattering per gram, $A_0 = S_0/M_0$ [equation (18), Chapter 21], is obtained. The slopes of these two curves at zero time give the initial values of $u_s = d/dt \log S_t$ [equation (17), Chapter 21], and $u_m = d/dt \log M_t$ [equation (16), Chapter 19].

In order to facilitate the analysis of the experimental measurements, figures were drawn from which the values of ρ, d_g and σ_g can be picked off when the experimental quantities u_s, u_m and A_0 are known. These figures were calculated by means of equations (5) and (16), Chapter 19, and (18) and (20), Chapter 21, as described in following text. They are particularly useful when the particles are so small that the scattering coefficient is greater than 2. This is the case for all Kadox particles and for the smaller statistical diameters of egg albumin, although in the latter case K_2 is only a little greater than 2.

Figure 9 shows the values of σ_g and ρd_g corresponding to a set of values of A_0 and R for egg albumin, where $R = u_m/u_s$. To obtain this figure, appropriate values of σ_g and ρd_g were chosen and from these, ρd_2, ρd_4, ρd_5, and ρd_9 were calculated by means of equation (5), Chapter 19. Using Figure 13, Chapter 21, K_2 and K_4 corresponding to ρd_2 and ρd_4 are read off, and these values, together with ρd_5 and ρd_9, are substituted in equations (18) and (20), Chapter 21, to calculate A_0 and $A_0(u_s/u_m)$.

Figure 10 shows the values of ρ corresponding to a set of values of ρd_8 and hu_m calculated by means of equations (5) and (16), Chapter 19.

The figures are used by finding on Figure 9 the value of σ_g and ρd_g corresponding to the experimental values of A_0 and $R = u_m/u_s$. Using the value of σ_g and ρd_g thus obtained, ρd_8 is calculated by means of equation (5), Chapter 19. Using this value of ρd_8 and the experimental value of hu_m, the value of ρ is obtained from Figure 10. The weight median diameter d_6, or other statistical diameter may then be calculated from equation (5), Chapter 19, using the values of σ_g and d_g just found. This calculation of d_6 may be checked by means of equation (17), Chapter 21.

22.4 OPTICAL METHODS

22.4.1 The Owl

As described in Chapter 21, the colors and polarization of the scattered light may be used to determine the particle size of a homogeneous smoke of spherical particles. An instrument, called the *Owl*, has been constructed and used for this purpose.[17] It

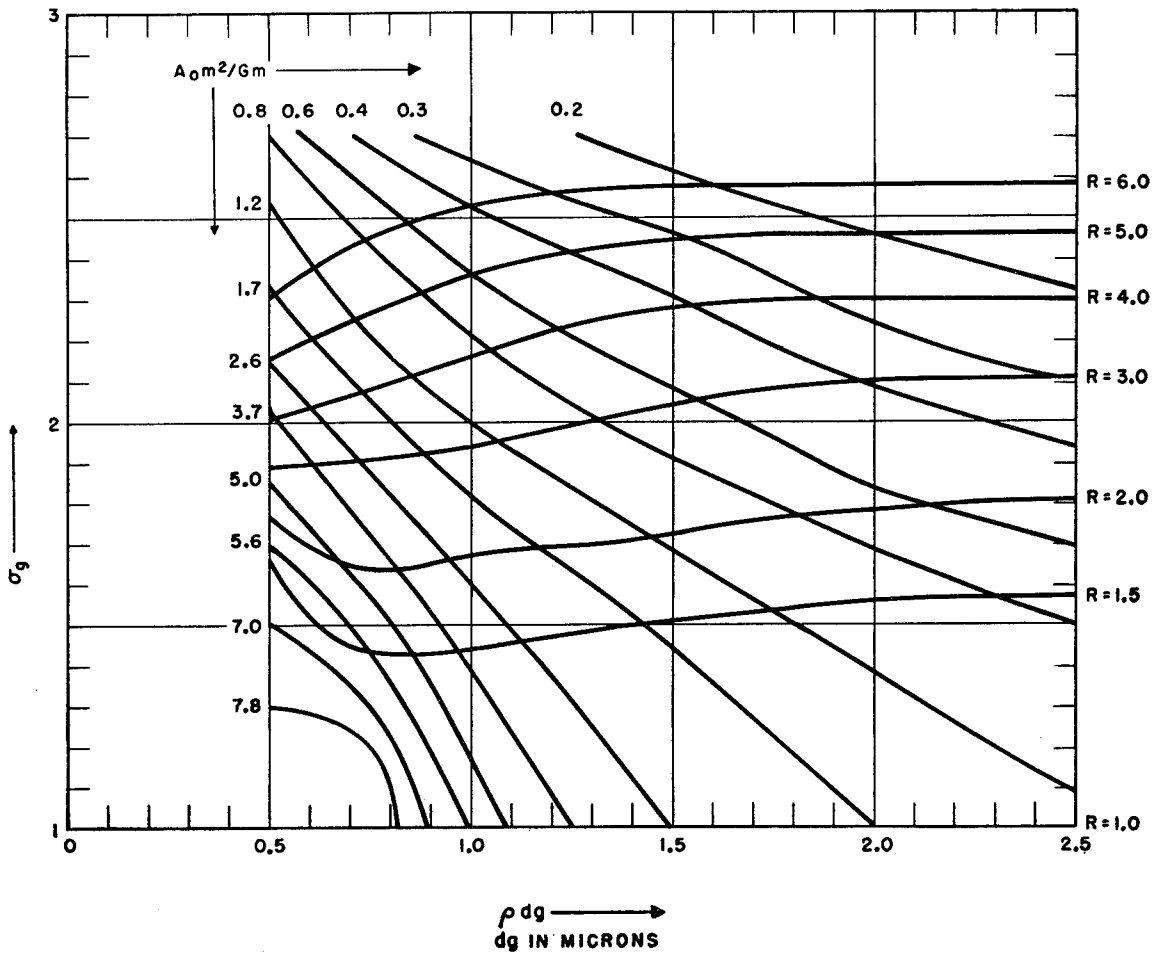

FIGURE 9. Values of σ_g and ρd_g for values of A_0 and R for albumin.

consists of an observation chamber and light source which may be held in the hand and rotated while observing the smoke through a low power microscope.

The observation chamber is a hollow metal cylinder 3 in. in diameter and 1 in. high (ID) having flat end plates, Figures 11 and 12. A window ½ in. high is cut in the side for an angular distance of a little more than 150°. Over this is cemented a section of a cylinder of uniform glass whose inside diameter is equal to the outside diameter of the chamber. This window enables observations to be made at all angles between 15 and 165° by rotating the chamber (and attached illuminator) about an axis through its center. The axis of rotation is perpendicular to the plane of observation.

The illuminator is constructed from microscope eyepieces and an automobile headlight bulb as shown in Figure 11. The arrangement shown provides a sufficiently intense light beam, parallel to ±3°. When the illuminator is properly adjusted, the light beam just clears the open end of the light trap.

On the opposite side of the chamber from the illuminator is a light trap consisting of a ⅝-in. diameter tube 2½ in. long with the far end closed with a metal plate. Except for the window, the inside of the chamber should be blackened with high quality, *dull* black optical lacquer and, preferably, also covered with soot. This can be conveniently done by means of the flame from burning camphor.

A semicircular scale, graduated in degrees, is mounted on the bottom of the chamber as shown in Figure 11. The illuminator should be located at 180° and the light trap at 0° to within 1°. A fiduciary mark should be placed on the supporting bar, extended, for reading the angle of observation, θ. The chamber is rotated by using the light trap as a handle.

By means of an atomizer bulb, smoke is blown in at

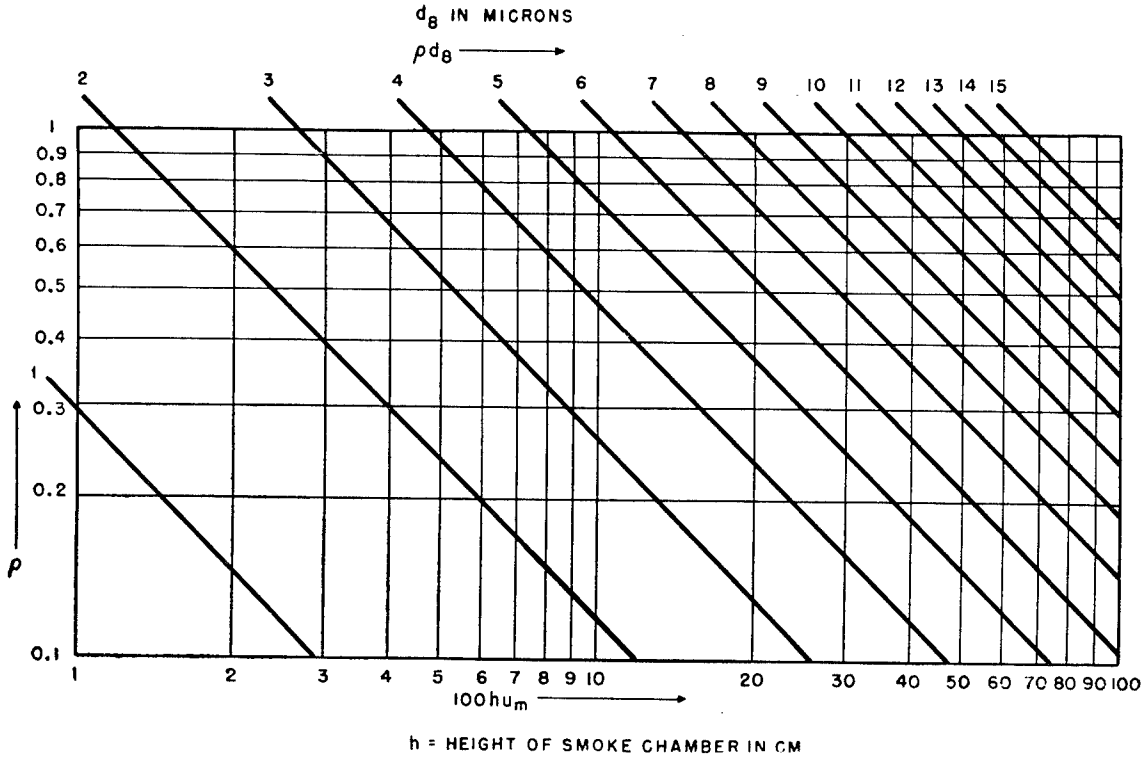

FIGURE 10. ρ vs hu_m for values of ρd_8.

the bottom and out through the top of the chamber. A ball valve is located at the bottom of the bulb, and another at the top of the chamber. A type of valve which does not stick easily is required.

The observations are made through a long focus microscope, of magnification 6×, constructed from ordinary microscope eyepieces as shown in Figure 11. The microscope is focused on the smoke particles in the center of the chamber.

The polarization photometer (see Chapter 21) is made by mounting a bipartite Polaroid disk in the eyepiece of the microscope, in good focus, with the dividing line parallel to the plane of observation to $\pm 1°$. This setting may be made as follows. Remove the chamber and illuminator from their supports and mount the illuminator so that the direct beam can be seen through the photometer and microscope. Mount a Polaroid (hereafter referred to as the *polarizer*) between the illuminator and telescope. The polarizing axis of the polarizer is set parallel (or perpendicular) to the plane of observation and the analyzer (see following paragraph) is set perpendicular (or parallel) thereto. When the polarizer and analyzer are thus *crossed* and the bipartite disk is oriented correctly, no light (except for the residual violet always transmitted by Polaroids) will be transmitted. If any white light is transmitted, rotate the bipartite disk until extinction is obtained, and fix it in this position.

The bipartite disk was made by the Polaroid Corporation (Cambridge, Massachusetts) using their new Polaroid-H laboratory-type film which, they report, gives about 99.99% polarization throughout most of the visible region. The polarizing axes of the bipartite disk are respectively perpendicular and parallel to the dividing line to $\pm 1°$. The dividing line between the two halves should be as inconspicuous as possible.

The analyzer is placed in front of or in the eyepiece *between the bipartite disk and the observer*. It consists of a piece of Polaroid-H laboratory glass mounted so as to be readily rotated about a horizontal axis. The angular setting, ϕ, is read off a quarter circular scale graduated in degrees. The scale is mounted so that the setting of the analyzer is accurate to $\pm 1°$. When $\phi = 0°$ the vibration or polarizing axis of the analyzer lies in the plane of observation.

A piece of Wratten 58B green gelatin filter is also mounted in front of, or in, the eyepiece. This filter should be fastened to the front face of the analyzer. Both the analyzer and filter should be readily removable out of the line of sight.

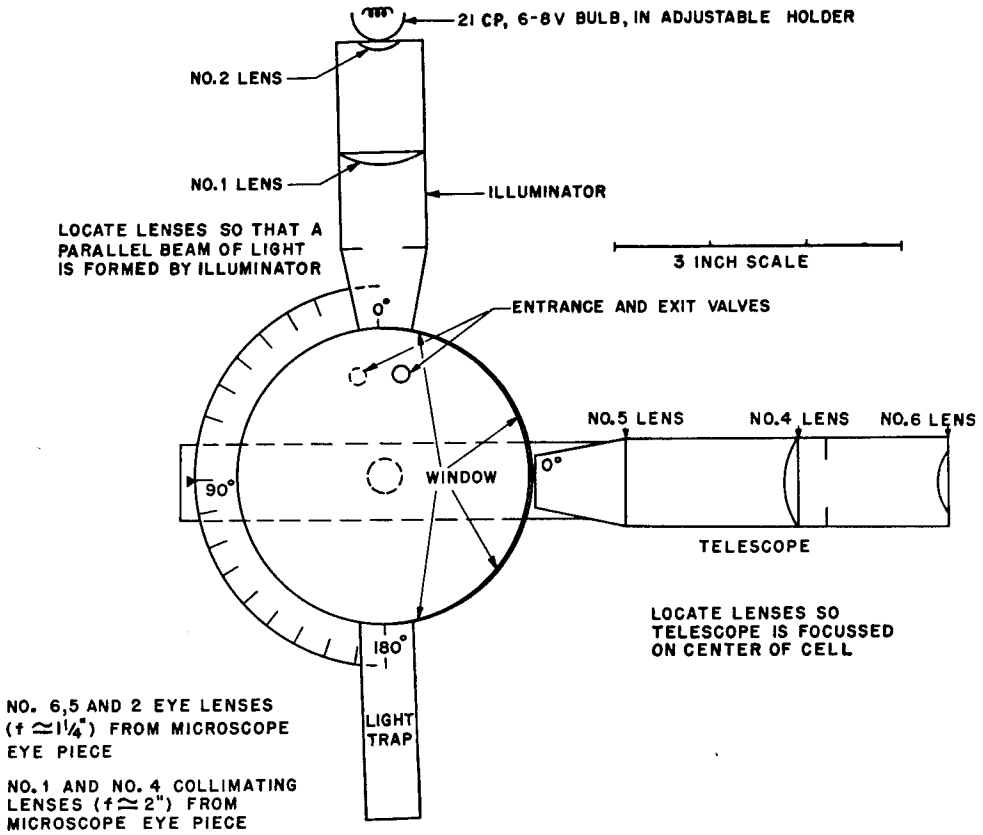

FIGURE 11. Plan of Owl.

In order that observation may be made in daylight, the microscope objective and window should be completely covered. One satisfactory method is to use a conical bag of opaque black cloth open at both ends. The small end fits over the microscope so that it does not interfere with the rotation of the chamber.

A tapered metal sleeve extending to just in front of the window is fitted over the microscope. This prevents the black cloth from obstructing observation. In addition, a black cloth hood is fastened around the eyepiece end of the microscope and thrown over the observer's head.

The foregoing description refers particularly to models made at Columbia University. Another model has been made commercially which is of improved design. Among other features, this model has a fine adjustment for setting the analyzer, and a facepiece which eliminates the need for the black cloth hood.

The particle radius corresponding to the observed angular setting of the analyzer is given in the calculated calibration curves, Figures 6 and 7, Chapter 21. The polarization at a radius of 0.11 micron for sulfur and at 0.17 micron for oleic acid has been checked experimentally by observing the rate of fall of homogeneous smokes under gravity in the small settling chamber described in preceding text.

The calibration curves extend down to 0.05 micron but readings below 0.10 are not reliable. It must be emphasized that these curves can be used *only* for small particle smokes of radii below 0.2 micron (for sulfur and tryphenyl phosphate only below $r = 0.15$ micron). In other words, they should not be used when the number of spectra (reds) observed is two or more.

For measurement of particles of radii from 0.20 up to 1.0 micron, remove the analyzer and green filter and count the number of times red is seen in i_1 as the observation chamber is turned from near 0 to near 180°. The description of the colors observed is given in Chapter 21, and the calibration curve is shown in Figure 4, Chapter 21.

The observations of the number of reds must be made on the scattered component i_1 alone, since the component i_2 exhibits a different series of spectra. The component i_1 is seen when the vibration axis of the analyzer is vertical. In a Polaroid-H disk, this

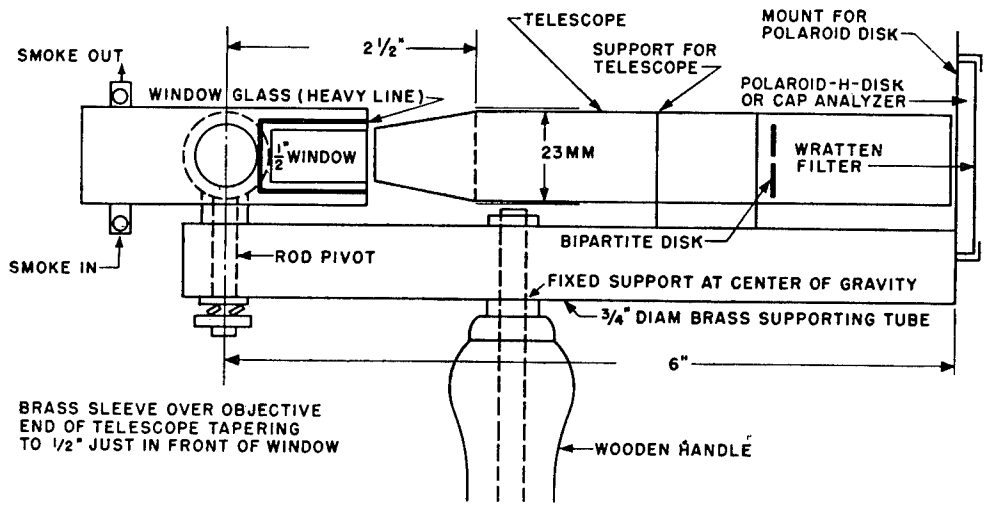

FIGURE 12. Assembly of Owl (vertical projection).

axis is parallel to the diameter through the diamond etched on the disk.

When observing without the analyzer, the two spectral series in i_1 and i_2 are seen simultaneously and adjacent to each other and the contrast between them frequently aids in the analysis of rather heterogeneous smokes.

When observing the spectra, attention should be paid to the angular position of the reds (Figure 5, Chapter 21) as well as their number. It is seen clearly how the position of the first red shifts from 100 to 20° as the number of spectra increases from one to seven, i.e., as the particle radius increases from about 0.1 to 0.7 micron.

22.4.2 Coronae

The radii of transparent fog droplets of 5 or 10 microns and over can be obtained by observing the diffraction rings or *coronae* formed around either a point source of light located in the fog, or, preferably, a beam of light shining through the fog. These diffraction rings are similar in appearance to the colors observed in Mie scattering by smaller droplets, except that the angles at which the colors appear are much smaller.

According to the theory of diffraction for opaque disks, the angular radius θ_1 of the first bright ring is given by $\sin \theta_1 = 0.819\lambda/r$ where λ is the wavelength of the light and r the radius of the droplet.[18] The second bright ring is given by $\sin \theta_2 = 1.346\lambda/r$, the third by $\sin \theta_3 = 1.858\lambda/r$, and the fourth by $\sin \theta_4 = 2.362\lambda/r$. The relative intensity of the first four rings is approximately 1, $\frac{1}{4}$, $\frac{1}{10}$, $\frac{1}{20}$.

The angular radii of the *dark* rings are given simply by $\sin \theta = (n + 0.22)\lambda/2r$ where n is the order of the ring.

The rings are observed most clearly in a fog of uniform droplet size. Experience has shown, however, that the uniformity need not be so great as in the case of Mie scattering. Kohler [19] has used this method for the measurement of the droplet size in water fogs of about 8 microns radius. He found that the rings are usually produced by the predominant size, with the larger sizes being favored since they produce the smallest and brightest rings. The writer has observed several colored rings in water fogs which contained droplets varying in radii from 4 to 16 microns or greater.

It is seen that the size of the rings is independent of the index of refraction of the droplets. This is so because the equations are derived for diffraction by opaque disks. For this reason, Wilson [20] states that the equations are not accurate for radii less than 10 microns and scattering angles θ greater than 10°.

For accurate measurement of radii below 5 or 10 microns, down to 1 micron (below which the Mie scattering can be used) the coronae radii could be calibrated against droplets of known size. However, an approximate value of the radius can be obtained for radii between 2 and 10 microns by the use of the above equations.

For this purpose Humphreys [18] gives a calculated curve showing the angular radii of the first and

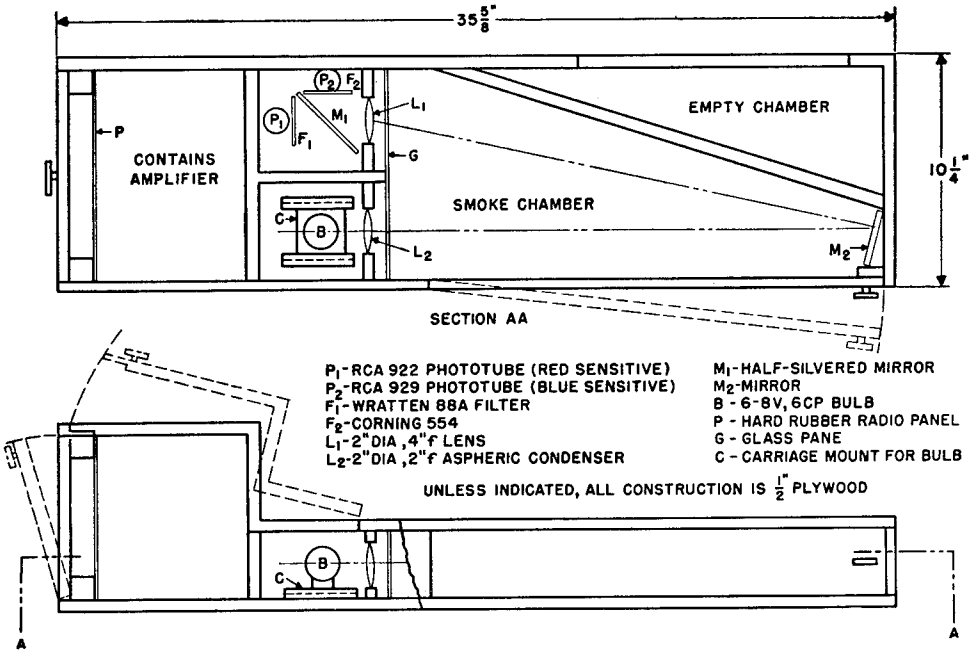

FIGURE 13. Slope-o-meter (layout of parts).

second red rings as a function of the radii of water droplets between 1 and 10 microns. It will be seen that these two curves are roughly extensions of the first two curves of Figure 5, Chapter 21.

The coronae were used to measure the size of lycopodium spores of fairly uniform size. The radius of these spores, as measured in a light microscope, was found to vary from 13.6 to 16.0 microns.

The spores were allowed to settle on a glass plate which was then placed in a beam of light of parallel rays and also in a slightly divergent beam from a point source. Measurements were made of the angular diameter of two orders of both the light and dark diffraction rings in both red and green light. From these measurements the spore radius was calculated to be 15.5 $\pm$ 0.2 microns, in good agreement with the microscope measurements.

Similar measurements were made on a uniform droplet size oil fog in a flask. The radius, as measured by two independent methods was 4.0 $\pm$ 0.1 microns. The agreement here is less good, as is to be expected for such small, transparent spheres.

22.4.3 The Slope-o-Meter

The particle size of a homogeneous smoke, or an average size of heterogeneous smoke, may be obtained by measuring light transmission as a function of wavelength (Chapter 21). An instrument, called the *Slope-o-meter*, has been constructed and used for this purpose.

The instrument is essentially a photoelectric spectrophotometer which compares the intensity of light transmitted at two wavelengths through a sample of smoke. Extensions of the same mechanical and electrical system may be used to compare the transmission at three or more wavelengths. Two types of Slope-o-meter designated as Type I and Type II have been constructed. The following is a description of Type II. Type I is described elsewhere.

METHOD

Photo-emissive photoelectric cells of the vacuum type are used to measure (1) the intensity of blue light (wavelength, 4400 A) transmitted through the aerosol sample, and (2) the difference between the intensities of infrared light (wavelength, 8000 to 9000 A) and blue light transmitted.

CONSTRUCTION

The optical and electrical systems have been assembled in a single box, one compartment of which serves as a smoke chamber (Figure 13). A second box contains three 45-v portable B batteries and an 8-v portable storage battery. Power is transmitted to the optical and electrical systems via a six-wire cable

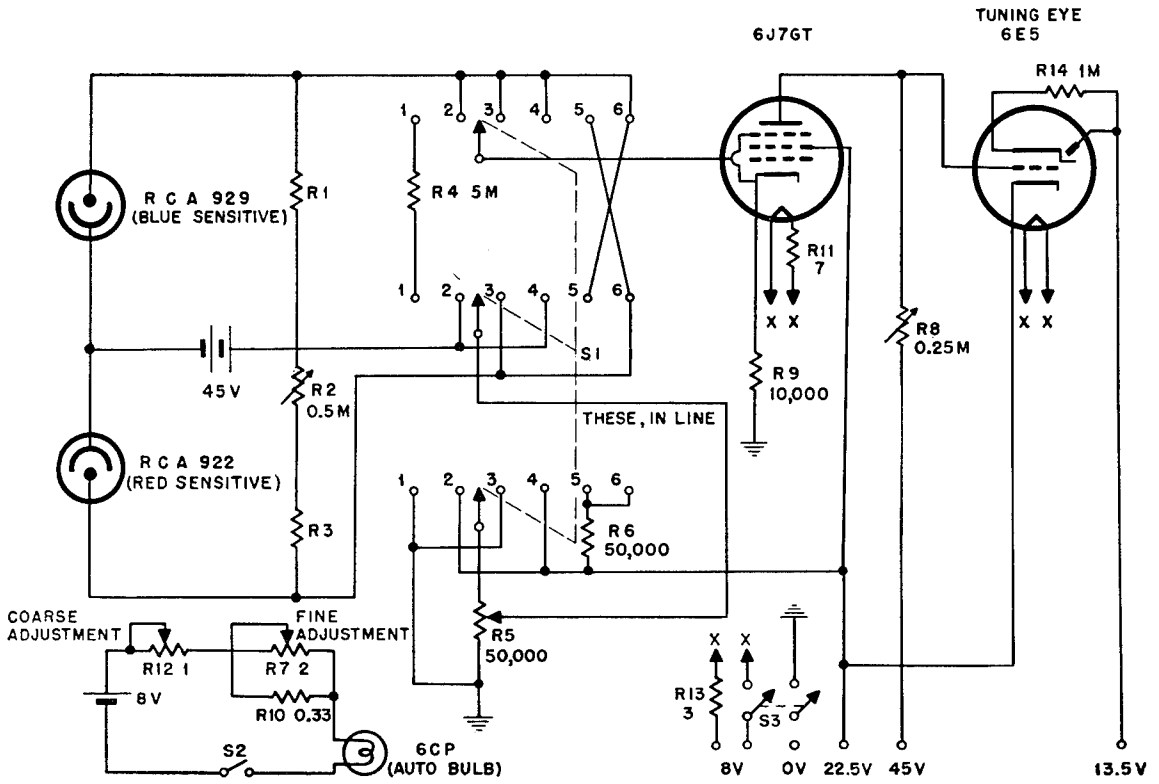

FIGURE 14. Slope-o-meter (wiring diagram).

and suitable plugs and jacks. The optical system consists of a 6-cp automobile bulb (Mazda No. 81), a condensing lens which sends a beam of light through the smoke and a semitransparent mirror directing it finally onto the phototubes. The purpose of the semitransparent mirror is to enable a single beam of light through the smoke to suffice for both phototubes. Color filters are interposed between the semitransparent mirror and the phototubes.

Rigid mounting of all parts of the optical system is necessary for reliable operation. The possibility of warping should be reduced to a minimum, although slight warping is corrected by the normal adjustment of the Slope-o-meter.

The electrical system (Figure 14) consists of suitable resistance loads (R_1, R_2, and R_3) for the phototubes, selector switch S_1 and a slide-back vacuum tube voltmeter. Three 45-v B batteries provide plate and slide-back voltage and an 8-v portable storage battery provides current for the 6-cp lamp and for the heaters of the vacuum tubes.

The resistors, R_1, R_2, and R_3, vary from one machine to the other but are selected so that with no smoke in the chamber, and with the 6-cp bulb operating at its proper current, the emf developed by each photocell is just below 22.5 v, the maximum slide-back voltage. The proper current is selected so that it can be maintained constant for all working voltages of the storage battery through adjustment of R_7.

When the selector switch S_1 is at position 1, the grid of the 6J7 GT is connected through R_4 to ground and the slide-back potential is zero. R_8 may then be adjusted so that the shadow of the tuning eye (6E5) is open to some selected angle near the middle of its range. This angle is marked and used for all subsequent balancing operations and indicates that zero emf is impressed on the grid of the 6J7 GT.

When the selector switch is at position 2 or 4, the emf developed by the blue sensitive phototube (RCA 929) is impressed on the grid of the 6J7 GT and this may be balanced manually by the slide-back emf developed in R_5. The dial reading of R_5 is a measure of the total amount of blue light striking the phototube.

When the selector switch is at position 3 the difference between the emf's developed by the blue and and by the infrared light is impressed on the grid 6J7 GT and the slide-back potential is again zero. The

load resistance ($R_2 + R_3$) of the infrared sensitive phototube may then be adjusted to bring the tuning eye to the balance position. The effect of this operation is to make the response of the instrument to blue light the same as the response to infrared light. This compensates for changes in the color of the light emitted by the lamp as it ages and for other changes in the apparatus such as drift in the value of the phototube load resistors or small amounts of warping.

When the selector switch is at position 5 or 6, the difference between the emf's developed by the infrared and by the blue light may now be balanced by the slide-back potential developed in R_5. With the selector switch in these positions, however, the magnitude of the slide-back voltage corresponding to full scale of R_5 has been reduced by the insertion of R_6. The increase in sensitivity is desirable here because a difference between two quantities is measured which may often be small.

Operation

1. Adjustment: No smoke in smoke chamber.
   a. Switches S_2 and S_3 are thrown to "on" position.
   b. Selector switch on 1. Adjust R_8 to balance.
   c. Selector switch on 2. Set R_5 on preselected value near maximum. Adjust R_7 and R_{12} to balance.
   d. Selector switch on 3. Adjust R_2 to balance.
2. Measurement: Put smoke in smoke chamber. For field use, open the door of the smoke chamber while in the smoke and close it.
   a. Selector switch on 4. Adjust R_5 and note dial reading.
   b. Selector switch on 5. Adjust R_5 and note dial reading. If no balance is possible, turn selector to position 6, balance with R_5 and note dial reading.

The dial readings of R_5 for selector switch positions 4 and 5 (or 4 and 6) fix the particle concentration and the radius (respectively) of the smoke in the chamber. See typical calibration curve in Figure 15.

The concentration lines on the calibration curves were obtained by means of calculations based on the Mie theory. As described in Chapter 21, the Mie theory yields the droplet radius from observations of the color and polarization of the scattered light. The theory also gives the scattering coefficient for a known droplet size and wavelength, so that the concentration can be obtained by observing the decrease of intensity at a known wavelength and known length of light path through the smoke.

Measurement of Particles Below 0.18 Micron Radius

For very fine particles the sensitivity of the Slope-o-meter decreases markedly. For instance, all smokes fine enough to exhibit Rayleigh scattering fall on the same particle size calibration line. Accordingly, for fine particles the Owl described previously should be used to determine the particle size, and the Slope-o-meter used to measure concentration. For this purpose, it is necessary to measure only the transmission of blue light (dial reading of R_5 for selector position 4).

Limitations and Precautions

For particles above 0.5-micron radius, index of refraction 1.50 to 1.55, the particle size calibration curves are duplicates of the curves obtained for smaller particles.

It is apparent that a reading of particle size and concentration will be obtained no matter how inhomogeneous the smoke may be. For a homogeneous smoke, which shows orders in the Owl, the results will be as accurate as the initial calibration. For heterogeneous smokes, a complex weighted average is obtained, where the effect of particles larger than the average tends to cancel the effect of particles smaller than the average, provided there are few particles of 0.5-micron radius or larger. The smoke from large-scale generators of the coil or combustion gas type is apparently homogeneous enough and the particle sizes are within the proper range for use of the Slope-o-meter.

22.4.4 Color of the Transmitted Light

Visual observations of the color of white light transmitted through an aerosol provide a measure of the particle size (Chapter 21). It must be emphasized that this method does not provide an absolute, but only a relative measure of size relative to the optimum size for material of a given refractive index.

If the residual rays transmitted by a Diol fog are blue or green, it indicates that the average radius is greater than 0.33 micron, the optimum radius for Diol. However, a similar observation through sulfur smoke indicates an average particle radius greater than 0.17 micron, the optimum radius for sulfur. If the residual rays are red, it indicates an average radius less than 0.33 micron for Diol fog and less

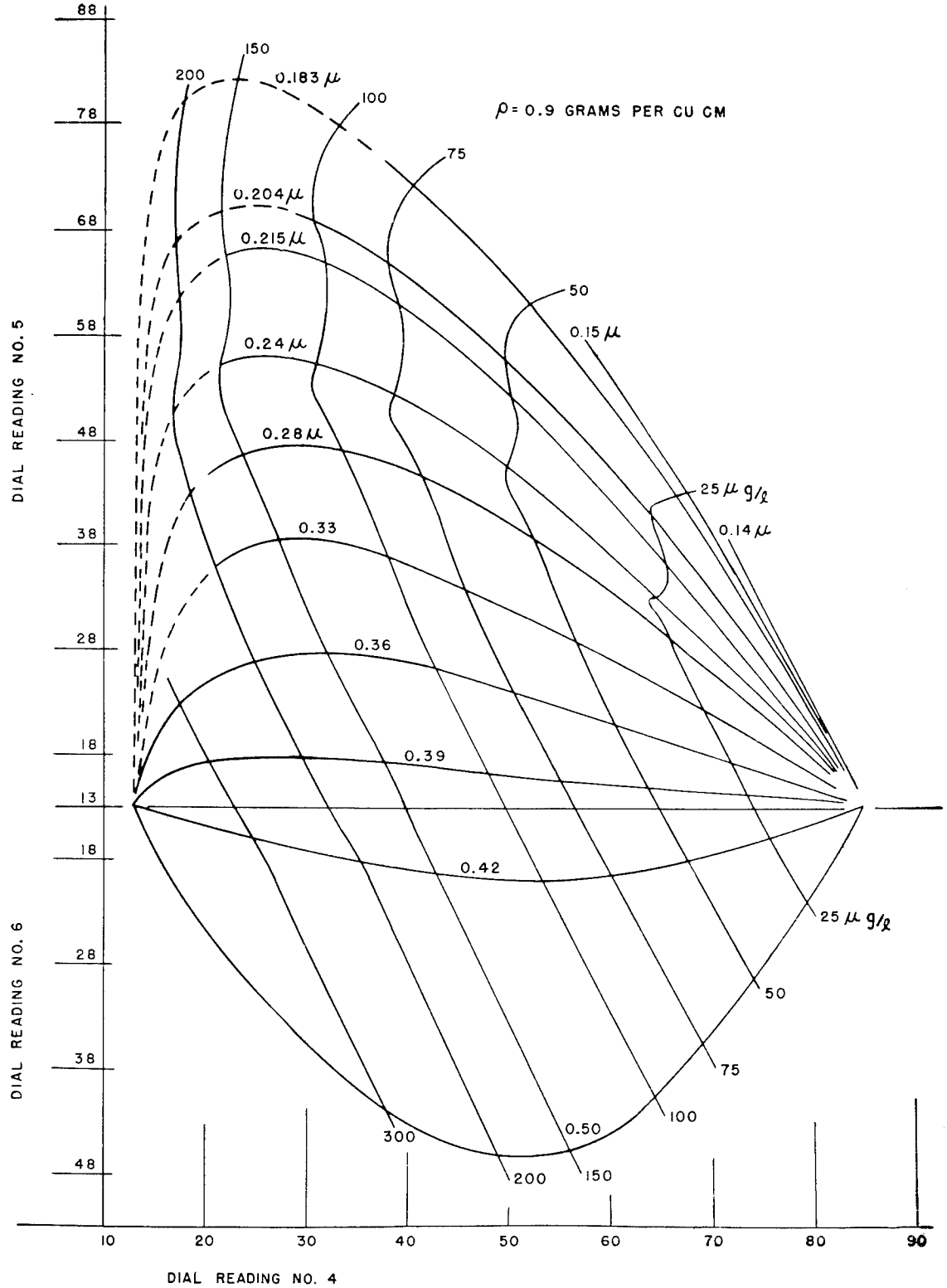

FIGURE 15. Slope-o-meter (calibration curves). Note: Diol $m = 1.50$.

TABLE 1

Date	Generator	Owl radius, microns	Slope-o-meter radius, microns	Sun's disk color	Comments
Nov 10, 1942 am	Esso	0.18	0.15		Fairly homogeneous
		0.16	0.16		
Nov 10, 1942 am	Servel	0.29			Moderately homogeneous
		0.33			
Nov 10, 1942 pm	Servel	0.29	0.28, 0.33, 0.22, 0.33. After turning off and on again: 0.20		
Nov 10, 1942 pm	Haslar	0.5 estimate		Blue	Brownish color, heterogeneous
Nov 23, 1942 pm	Servel 50 gal	0.32		Purple	15 ft from generator
		0.40		Blue	115 ft from generator
Feb 23, 1943 pm	Servel 25 gal	0.22		Red	30 ft from generator, some carbon
Feb 23, 1943	Chrysler			Lavender	Sample unobtainable. Blower
				White	sends smoke 35 ft up
Feb 23, 1943	DeVilbiss	estimate medium size		Lavender	Heterogeneous
				White	
Feb 24, 1943 am	Esso	0.3		Lavender	Owl colors indistinct
				White	
Feb 25, 1943 am	Hickman	0.4 approx	0.5 approx	Blue	Heterogeneous
		0.3 approx			Standard nozzle
Feb 25, 1943 pm	Hickman	0.27	0.30	Lavender-white to red	Multiple-hole nozzle
		0.22	0.26		
Feb 25, 1943 pm	Williams	0.20	0.18	Red	Multiple-hole nozzle
		0.25	0.25	Red	
Feb 25, 1943 pm	Williams	0.32	0.35	Red	Multiple-hole nozzle
		0.35		Blue	
Feb 25, 1943 pm	Hickman	0.29	0.31	Too cloudy	Multiple-hole nozzle
Feb 25, 1943 pm	Hickman	0.35	0.38–0.42	Too cloudy	Standard nozzle
Feb 25, 1943 pm	Esso	0.29	0.25	Reddish white	50 ft from generator
Feb 24, 1943	Esso	0.27	0.24	Red	18 mph wind from propeller
		0.22	0.19	Red	

then 0.17 micron for sulfur smoke. A magenta color indicates the optimum particle size.

Langmuir has developed a set of color filters which enable this measurement to be made more precisely. Several transparent filters, whose colors match the residual colors of the sun when the droplet radius of Diol fog is at or near the optimum, are mounted in a frame and viewed against a white background. The particle size can then be obtained by matching the observed color of the sun with the color of one of the filters.

22.4.5 Field Measurements

During November 1942, and again in February and March 1943, optical methods were used to measure the droplet size of oil fogs from screening smoke generators operated at Edgewood Arsenal, Maryland. The droplet radii in the fog produced by the Esso, Servel, Haslar, Chrysler, DeVilbiss, Hickman, and Williams generators, using Diol 55 as the fog oil, were measured with the Owl and the Slope-o-meter. Observations of the color of the sun's disk were made whenever possible.

TABLE 2. Esso generator.

Owl radius, microns	Sun's disk	Nozzle diameter inches	Diol temperature degrees F	Remarks
0.2	Red	3/16	1,000	Homogeneous
0.2	Red	3/16	950	Homogeneous
0.25	Red	3/16	900	
0.3	Lavender	3/16	850	Indistinct
0.3	Lavender	3/16	800	Indistinct
0.3	Red	1/4	900	
0.3	Lavender		900	
0.3	Lavender-white	5/16	1,020	Homogeneous
0.35	Blue	5/16	1,000	
0.3	Lavender	5/16	900	Homogeneous
0.3	Blue	5/16	800	Homogeneous
0.3	Red	3/8	1,000	Homogeneous
0.35	Lavender-white	3/8	900	Indistinct
0.4	Purple	3/8	800	
0.4	Blue	3/8	825	Indistinct

The results are summarized in Table 1. They represent only the results obtained for the particular

settings of the generators and are not to be taken as the only particle radius that may be obtained from these generators. At the bottom of the table it is shown that an 18 mph wind decreased the droplet radius 0.05 micron.

Special tests were performed on the Esso generator to test the effect of high wind, of nozzle diameter and of oil temperature as shown in Table 2. The standard nozzle diameter in the Esso generator is $\frac{3}{16}$ in. When the diameter was doubled to $\frac{3}{8}$ in. the average droplet radius was increased by 0.1 micron, provided the temperature of the oil was constant. For a given size nozzle, when the Diol temperature was raised from 800 to 1000 F, the average droplet radius was decreased by 0.1 micron. The pressure was not observed. It is seen that the droplet radius could be increased from 0.2 to 0.4 micron by doubling the nozzle size and lowering the temperature simultaneously.

Additional field and laboratory measurements made on various types of smokes are described in an unpublished report.

Chapter 9

FILTRATION OF AEROSOLS

By *W. H. Rodebush*

23.1 INTRODUCTION

As has been pointed out in Chapter 18, aerosol filters do not behave as sieves or screens which stop particles larger than the mesh and let through smaller particles. It is theoretically possible to construct such a filter, but it would offer so much resistance to the flow of air that it would be useless from a practical point of view. Thus, the filter papers used in analytical chemistry for the separation of precipitates are very inefficient as aerosol filters. All mechanical aerosol filters must, in practice, be of open construction, with the openings large compared to the size of the particles to be removed, in order to reduce the resistance offered to the flow of air. The removal of the particles is therefore by chance collision rather than positive action, and the percentage removed is a statistical function of the thickness of the filter; a filter of infinite thickness would be required to remove 100% of the particles from the air stream.

In practice all mechanical filters are made up of fibers, some of which must be of small diameter (i.e., comparable to the diameter of the aerosol particles) if the filter is to be efficient. An efficient filter may be defined as one which offers a low resistance and at the same time a low penetration. These two quantities are mutually interdependent variables, and for a given filter material one can be decreased only at the expense of the other.

It will be obvious from the theory of filtration why an efficient filter must be made up of fibers. The ideal filter would consist of a series of grids of fibers parallel to each other and at right angles to the direction of air flow. In practice it is impossible to obtain any such perfect orientation of the fibers although, in general, they will lie at right angles to the direction of flow.

In theory, the smaller the fiber diameter the better the performance, but it is clear that if the fiber diameter is too small the fiber will not have sufficient mechanical strength to resist the air currents. Furthermore, the forces which cause a particle to adhere to a fiber must depend to some extent upon the area of contact, and a very small fiber would not retain a large particle against the forces exerted by gravity, air currents, etc., which would tend to remove it. In practice, there is a limit to fiber diameter, but fibers of 0.01 micron or less prove to be very effective.

23.2 THE MECHANISM OF THE FILTERING ACTION

It has been pointed out in Chapter 18 that small particles adhere to any surface with which they come in contact, because of van der Waals forces. If electrical charges are present the adhesion forces may be increased; but electrical behavior will be discussed in a separate section. Mechanical filtration depends upon the actual impingement of the particles on the fibers of the filter. In order to consider the mechanism of the filtering action, consider a single fiber placed at right angles to the air stream. Assume in this discussion that the velocity is low enough so that the flow is nonturbulent, since it can be shown that this condition must hold in any filter that operates with a reasonably low pressure drop. There are several different mechanisms which may bring about the impingement of the particle on the fiber.

23.2.1 Direct Interception

Imagine the center of the particle of radius r to lie on a stream line which passes within a distance r of the fiber, in which case the particle will be caught. In the limit of the fiber diameter d, approaching zero, the particle will be removed from a cross-sectional area $= 2r$ per unit length of fiber. For larger fiber diameters the number of particles removed will not be greatly increased and will be independent of velocity, since the stream lines do not change with changes in flow rates. Direct interception is restricted, however, to particles whose centers remain in coincidence with a given stream line. This will occur only if the particles are too large to show appreciable Brownian motion and too small to have an appreciable Stokes' law rate of fall. There is no particle size for which the Brownian motion and the Stokes' law rate of fall are both zero, and simple calculations show that the efficiency of filters is far greater than

could be accounted for by direct interception. These two effects, which prevent particles from following the stream lines around a fiber, evidently play an important role in the mechanism of filtration, and each will be considered in turn.

23.2.2 Stokes' Law Deposition

If a particle is large enough so that it has an appreciable Stokes' law rate-of-fall, its path will no longer coincide with any particular streamline in the air flow. It might be assumed, at first thought, that Stokes' law deposition would not in itself be important, since a particle is likely to fall away from, as well as toward, a fiber of the filter. The following consideration, however, shows that the Stokes' law fall is important in deposition. Suppose that the air flow through a filter be suddenly stopped. Within a short period, all of the larger particles which are present will be deposited on the upper surfaces of the fibers of the filter; and this period will be short because the distances through which the particles must fall are short. Although the same process goes on without interruption when the air is moving through the filter, it appears that it will make no difference whether the direction of flow is horizontal or vertical. The rate of deposition will vary with the particle size and concentration, and the total area that the upper surfaces of the fiber project into a horizontal plane. The flow will maintain the concentration uniform locally, but the concentration will decrease with increasing depth of-penetration of the filter. If the particle is below 0.3-micron radius, the Stokes' law rate of fall is so low that this mechanism of removal is likely to prove unimportant. The rate of deposition is not affected by variation in the rate of flow, but important inertial effects appear at higher velocities (particularly with larger particles), which give rise to another mechanism of filtration.

23.2.3 The Inertial Effect

If a streamline bends sharply around a fiber, a heavy particle at high velocity will not follow the sudden bending but will tend to continue in a direct course and collide with the fiber.

The extent to which a particle may be carried by its own inertia across the stream lines may be measured by the so-called stopping distance. The stopping distance, S, is the distance a particle with a velocity V and a mass m will penetrate a gas which is assumed to be at rest before being brought to rest by the viscous forces. The force resisting the motion of the particle through the gas is $f = 6\pi\eta r V$. Since

$$-\frac{d(mV)}{dt} = f,$$

integration gives

$$V = V_0 e^{-6\pi\eta r t/m},$$

where V is the velocity of the particle at the time t, and V_0 the initial velocity. Integration of

$$S = \int_0^\infty V dt,$$

gives the value

$$S = \frac{mV_0}{6\pi\eta r} = \frac{2r^2\rho V_0}{9\eta},$$

where ρ is the particle density. Substituting the values $\eta = 1.8 \times 10^{-4}$ for the viscosity of air, particle density unity, and a velocity of 3.5 cm per sec (a reasonably high rate of flow), the following table of values in centimeters is obtained:

r, cm	S, cm
0.5×10^{-4}	10^{-5}
5×10^{-4}	10^{-3}

S is the maximum distance that the particle could travel across stream lines if the stream lines bent at right angles. One sees that this distance could have no consequence for impingement if the particles were of 0.5-micron radius, but that with particles of 5-micron radius a considerable increase in the number impinging on a given fiber could be expected. Furthermore, an increase in velocity will increase the number caught.

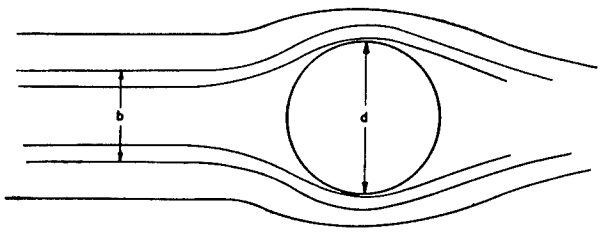

FIGURE 1. Stream lines around fiber and effective diameter b as compared with actual diameter d.

The *effective* diameter of a fiber may be defined as the width b between the bordering stream lines such that particles initially located in them will just clear the fiber (see Figure 1). Particles lying within this boundary will impinge upon the fiber. The ratio b/d is

always less than unity and may approach zero for low velocity of flow, large fiber diameter, or small particle diameter. If the dimensionless ratio, $Vr^2\rho/d\eta$, where V is the velocity of flow, r the particle radius, ρ the particle density, d the fiber diameter, and η the coefficient of viscosity, is plotted against the ratio of the effective diameter b to the actual fiber diameter a curve of the form given in Figure 2 is obtained.

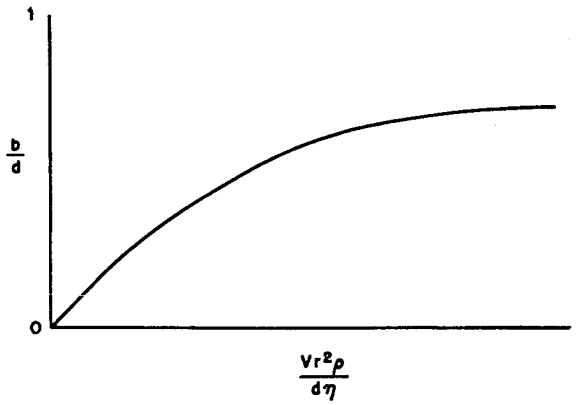

FIGURE 2. Inertial effect for large particles. Ratio of effective diameter to actual diameter, b/d, plotted against dimensionless ratio $(Vr^2\rho)/(d\eta)$.

For particles of large diameter, the effects of direct interception become appreciable and must be superposed on the curve of Figure 2 to give an increased filter efficiency. The effective diameter b is in this case increased by the amount $2r$. When the particle diameter is of the same order of magnitude as the fiber diameter, this correction becomes very important.

23.2.4 Diffusion

THE IMPINGEMENT OF SMALL PARTICLES

For particles of 1 micron diameter or less, inertial effects should not be important, and this is confirmed by the fact that penetration increases rather than decreases with increasing velocity. Similarly, the direct interception effect ($2r$) becomes very small for small particles. Yet, provided the fibers are of small diameter, the filtration efficiency is high and increases with decreasing particle size. The diffusion coefficient D varies inversely as the radius, and this quantity may be combined with the fiber diameter and velocity of flow in a dimensionless ratio D/dV to plot the ratio of effective diameter to actual diameter, as before (Figure 3). The value of b/d now becomes greater than one; but b no longer represents a sharp boundary between particles which impinge and those which escape, since on account of the Brownian motion, the probability of impingement is a matter of chance which decreases with increasing distance measured at right angles to the axis of the fiber and the direction of flow.

Actually, b is a mean distance; the total number of particles impinging on the fiber is equal to the number lying within the limits of b, but many of the particles within these limits do not impinge and many of the particles impinging come from outside these limits. The ratio b/d is of course greater, the greater

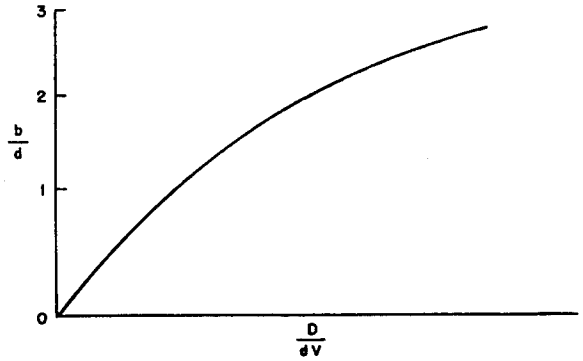

FIGURE 3. Diffusion effect for small particles. Ratio of effective diameter to actual diameter, b/d, plotted against dimensionless ratio D/dV.

the diffusion constant. The number impinging is greater the slower the velocity of flow, since the particles remain in the neighborhood of the fiber for a longer time. The ratio also increases as d approaches zero because b does not approach zero but a finite value which depends upon the mean distance of diffusion.

23.3 THE THEORY OF FILTRATION

It is practically impossible to give an exact mathematical theory of filtration. In the first place the differential equations can be solved only in an approximate manner, either for the inertial or the diffusion mechanism.[2, 3]

Even if satisfactory solutions are obtained for the behavior of a single fiber, a filter is made up of fibers with a random deposition and orientation, which cannot be taken into account in any exact manner. However, certain general considerations can be deduced, and these conclusions have been verified in a general way.

For example, very small particles will be removed

effectively by the diffusion mechanism [4] and very large particles by the inertial effects. It would be expected, therefore, that particles of intermediate size would be most difficult to remove. This prediction has been confirmed by experiment, but the size with a radius of about 0.2 micron [5] turns out to be the most difficult to remove. This maximum of penetration appears to be independent of fiber size. The decrease in penetration for particles above 0.2 micron radius can scarcely be due to the inertial effect, which was shown previously to be unimportant even for particles of 0.5 micron radius. It has been suggested that the effect of direct interception must account for the decreasing penetration of particles of greater than 0.2 to 0.3 micron radius, and it can readily be seen that the direct interception will contribute to the filtering action as the particle size increases. It would not appear however that a sharp maximum of penetration should be found which is apparently quite independent of rate of flow and fiber diameter.

The answer to the question seems to be given by experiments with glass plates, where the filtering action at lower particle size must be entirely due to diffusion and the filtering action for large particles can only take place through Stokes' law deposition. The same sharp maximum of penetration in the neighborhood of 0.2 to 0.3 micron is observed. Hence it must be concluded that the decrease in penetration above 0.2 micron is due to the increasing rate of Stokes' law deposition.

The effect of velocity on filtering efficiency depends upon the particle size. Small particles are removed more effectively at low velocities by diffusion, while large particles are removed more effectively at higher velocities by inertial effects. At some point in the intermediate range, perhaps in the neighborhood of 1 micron radius, the filtering efficiency will not be affected by changes in velocity.

Small fibers are more effective than large fibers in collecting particles from an air stream, because the smaller the diameter of the fiber the closer the stream lines lie to the fiber surface. A fiber may be considered to be surrounded by an envelope of nearly stationary air which is thicker the larger the periphery of the fiber. Also, the stream lines bend more sharply when the fiber diameter is smaller which will make the inertial mechanism of filtration more effective. The correctness of the foregoing statement has been demonstrated experimentally with fibers of 1 micron diameter and particles in the range 0.2 to 0.5 micron radius. It is possible that the statement is not true for very small particles whose diffusion range is very large, but these particles are so readily removed by a filter that they do not constitute a problem.

From the foregoing, one sees that a filter made up of a given number of fibers disposed in a certain way will be more effective when the fiber diameter is smaller, and at the same time the resistance will be less. Actually, a filter made up of smaller fibers will be more closely packed and have a higher resistance. Hence, if very small fibers are used, in order to avoid too high a resistance it is necessary to support the fine fibers on a loose network of coarser fibers.

23.4 FILTER MATERIALS

Most naturally occurring fibers, such as cotton, wool, and silk, are 10 to 20 microns or more in diameter. These fibers are much too large to be effective, and filters made of these materials will have to be very thick and have a high resistance, if the penetration is to be reduced to a low figure.

Paper is a particularly unsuitable material for a filter, since the fibers are flat and ribbon-like and are matted together in such a way as to offer a minimum porosity. Certain fibers obtainable in tropical countries, such as esparto grass, are narrower than the fibers of ordinary paper stock, and papers made of these fibers are more open and have less resistance to the passage of air. In general, however, these fibers can be used only as a supporting grid for finer fibers such as asbestos. There is no apparent limit to the fineness of dispersion which may be obtained with asbestos fibers, and mixtures of asbestos fibers with wool or paper are in use, and make excellent filters. If paper is used, it must be very porous and, hence, of little mechanical strength, but this defect is easily remedied by a backing of gauze.

23.4.1 Glass Wool

Glass fibers of diameter down to 1 micron can be produced by special methods. By coating the glass fibers with a suitable binding, they can be matted into a paper-like web which is very strong and shows excellent filtering characteristics. Such a material is relatively expensive, but is unexcelled in many respects as a filter material.

23.4.2 Rock Wool

Rock wool is composed of glass fibers which are produced from blast furnace slag or special limestone

silica mixtures. The material is fused in a cupola furnace, and the fibers are produced by blowing the molten fluid. The material is produced in carload lots for use as thermal insulation at a cost of a few dollars a ton. By control of the process, it is possible to produce fibers of a few microns diameter, and the material has great possibilities for use as a filter, particularly where bulk is not limited.

23.4.3 Synthetic Fibers

Various types of synthetic textile materials such as cellulose acetate, polyvinyl acetate, or polyvinyl chloride, can be produced in the form of fibers of very small diameter. The methods for producing these fibers are either a modification of the ordinary process of spinning and drawing, or electrostatic spinning. These materials have not been produced on a commercial scale, but experimental samples show the excellent performance that is to be expected. In order to use these very fine synthetic fibers, it is necessary to support them on a gauze backing.

23.4.4 Methods of Testing Bulk Filter Materials

The testing of a material in bulk in order to determine its suitability for use as a filter material is a different process from the testing of a fabricated filter. It is desirable to test the material at varying rates and over long periods of time. In order to detect clogging or breakdown, the penetration and resistance must be recorded as a function of the time.

A filter material may be conveniently tested in the form of layers or pads of uniform thickness arranged in series. The pads are compressed together to a suitable degree by means of metal gauze placed at the front and back of the series of pads. A radioactive smoke such as triphenyl-phosphate is passed through the material for a length of time, after which the pads are separated and each one counted separately with a Geiger counter. During the run, the pressure drop through the series of pads is recorded at intervals.

If the pads are of uniform thickness and homogeneous, and the smoke itself is homogeneous, each layer will remove from the smoke a constant fraction of the number of particles entering the layer. Thus if the number entering the nth layer is N_n, and the number entering the n plus first layer is $N_{(n+1)}$, then their ratio is given by:

$$\frac{N_{(n+1)}}{N_n} = e^{-k\Delta X}, \qquad (1)$$

where k is the stopping coefficient per unit thickness, and ΔX is the thickness of the pad. If the logarithm of the numbers of counts per pad is plotted against the ordinal number of the pad, a straight line results with a slope $S = k\Delta X$. If the pressure drop per pad is p, then the ratio s/p becomes an index for the filtering efficiency of the material; the higher the value of s/p, the better the performance of the material. Since, in general, both s and p will vary with the velocity of flow, it is necessary to test the material at various flow rates.

23.4.5 Clogging and Breakdown

An increase in pressure drop during a run is an indication of clogging. The filtering efficiency may or may not be affected, but the resistance will continue to go up until the filter becomes inoperable.

Breakdown of a filter material is often observed with liquid smokes. It is characterized by the fact that the plot of the logarithm of the counts is no longer a straight line but is a convex upward as shown in Figure 4. This is because the penetration

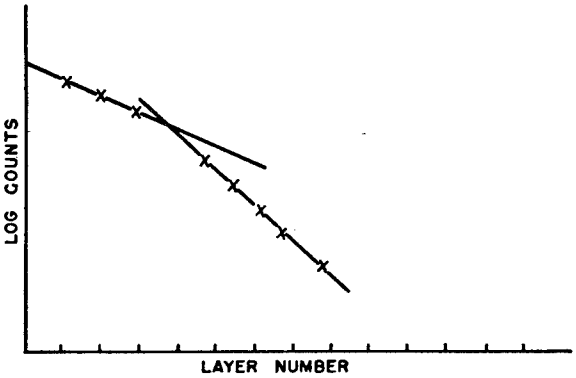

FIGURE 4. Plot of quantities of smoke caught by successive layers of a filter showing evidence of breakdown.

has gone up in the first layers which have become "saturated" with the smoke. This saturation effect is presumably due to the fact that the liquid wets the fine fibers of the filter and draws them together by surface tension forces, thus leaving open passages through the filter.

23.4.6 Electrostatic Filters

It is a matter of common observation that filters show a higher penetration when the relative humidity is high. The explanation of this must be that at low humiditiesstatic charges are accumulated on the filter

fibers and these charges are effective in collecting particles from the air even though the particles may be uncharged. Certain types of materials will retain static charges even at high humidities, and the Canadian wool-resin filter furnishes us with a striking example of this behavior. The wool-resin filter is made by carding various types of naturally occurring or synthetic resins into wool. The resulting material has excellent filtering power with, of course, a very low resistance. It retains this power for long periods of time at high humidities and, if the filtering power is lost, it may be restored by recarding the wool of the filter. There seems to be no question that the action of this filter is electrostatic. Wool and resin are classical materials for the production of static charges by friction, and the carding process undoubtedly produces high static charges on the filaments. In the neighborhood of the filaments the field intensities would rise to thousands of volts per centimeter.

Most of the particles in a smoke are uncharged, but they will be polarized in these strong fields and attracted to the filament. The polarization varies as the cube of the radius of the particle, whereas the resistance to motion through a viscous fluid is inversely proportional to the radius. The situation is the same, therefore, as with the fall due to gravity according to Stokes' law. The velocity with which a particle is drawn toward a filament will be proportional to the square of the radius. Large particles will be removed much more effectively than small particles. The filters are very effective, however, for particles in the ordinary smoke range of 0.2 to 0.5 micron radius (see Figure 4, Chapter 19).

Oil smokes appear to break the filter by dissolving, or perhaps merely wetting the resin. Some resins are more resistant to oil smokes than others.

Methods of testing fabricated filters are described in Chapter 24.

Chapter 10

METHODS OF TESTING SMOKE FILTERS

By *Frank T. Gucker, Jr., Hugh B. Pickard, and Chester T. O'Konski*

24.1 GENERAL PRINCIPLES OF SMOKE FILTER TESTING

The critical evaluation of a smoke filter should include many different considerations. The smoke penetration and pressure drop should be determined over a considerable range of flow rate, including any to which the filter would be subjected in use in the field. The smoke penetration should also be studied over a range of particle size, and correlated with toxicity studies which should indicate both the total number of particles and the total mass of smoke which could be tolerated. Other important characteristics of a filter are its capacity to remove smoke before clogging and its resistance to breakdown due to severe climatic conditions, CW agents, or other factors met in the field.

Once the general characteristics of a filter material are known, routine tests of pressure drop and filtration can be made under a single set of conditions if these are suitably chosen.[1]

Since filter penetration depends on the flow rate, the standard flow rate should be chosen after consideration of actual field conditions. A rate of 32 lpm was used in many of the tests at the beginning of the war. However, studies of breathing rates showed that a man exercising vigorously breathed at an average rate of 50 or 60 lpm, and that the instantaneous rate at the peak of the cycle may be as high as 200.[2] The rate of 85 lpm was taken as a standard for measurement of pressure drop and filter efficiency of canisters, and 320 cm per sec of linear flow for testing filter material, at a pressure drop of 30 mm of water.

The measurement of pressure drop is simple enough, and discussion will be confined to the measurement of smoke penetration. Here the test smoke should be of the most penetrating size. The test apparatus must include a reliable smoke generator and a rapid and sensitive method of measuring inlet and outlet smoke concentration. For poor filters, chemical or other methods of analysis of samples filtered from the smoke are adequate, although the process is extremely slow. Such methods are totally inadequate for the best types of modern filter, which require much more sensitive analytical methods, usually based on the measurement of the light scattered from the smoke. Such methods are more rapid as well as more sensitive. Instead of giving the average penetration integrated over a long period of time, they give instantaneous values of effluent concentration. Unless the instrument is differential and compares inlet and effluent concentration simultaneously, it must be used with a smoke generator which is adjusted to produce a smoke of constant size and constant mass concentration. With any type of instrument the test smoke must be homogeneous or nearly so, otherwise the filtration will cause a change in the particle-size distribution. The particles of the more penetrating sizes will comprise a larger proportion of the effluent than of the original smoke, and the light scattered in the two cases may not be strictly proportional to the respective quantities of smoke.

The actual development of methods of testing smoke filters paralleled the increased understanding of the process of filtration and the improvements in filter material which took place during World War II. The production of test smokes will be taken up first, then the methods of smoke-filter testing designed for laboratory use, and finally those which were adapted to production-line testing.

24.2 CHEMICAL TEST-SMOKE GENERATORS

Most of the generators used for the production of uniform test smokes employed condensation of supersaturated vapors, as described in Chapter 20.

24.2.1 The NDRC Homogeneous Aerosol Generator

This apparatus already has been described in Chapter 20. In the hands of a skilled operator it produces smokes which are beautifully homogeneous as judged by their spectra. However, this generator is temperamental, is not easily adjusted to give fine smokes, and cannot be run for long tests without continuous care and adjustment.

24.2.2 The MIT–E1R7 Smoke Generator

The CWS Development Laboratory perfected a standard test-smoke generator which was widely

879245 O - 50 - 9

used in smoke filter testing. The MIT–E1R7 generator [4] employs a stream of humidified air at 88 lpm. This is divided so that a flow of 17 lpm passes through a heated chamber where it picks up dioctylphthalate vapor from an open cup. The vapor-laden air is mixed with the larger stream of air at a Venturi orifice, under highly turbulent conditions (Reynolds number of 45,000 to 50,000) so that the rapid cooling yields a fine smoke. The mass concentration is adjusted to about 100 μg per l by regulation of the boiler temperature. The particle size is adjusted if necessary by means of a small filament heater in the large air stream, so that the MIT–E1R2 particle-size meter (see The Owl, Chapter 22) gives a reading of 29° ($\pm 1°$). This corresponds to the standard smoke of 0.3 micron diameter. The generator is connected to convenient clamp holders for canisters and sheets of filter paper. The generator furnishes a sample of 3 lpm of raw smoke for the penetrometer and 85 lpm for the filter test.

24.2.3 The NRL Smoke Generator [5]

Work at the Naval Research Laboratory paralleled that at the CWS Development Laboratory. The MIT smoke generators were tested and several basic modifications were made, which added to the stability of operation. The MIT generators were designed to furnish a test smoke under pressure, which was forced through the filter. The insertion of the filter increased the resistance in the line and this changed the concentration and characteristics of the smoke. The NRL generator was designed to furnish smoke to a 5-gal reservoir at a rate somewhat greater than that required for test. Excess smoke escaped to the atmosphere through a vent, while that required for test was *sucked* through the filter by a vacuum connection. Although this arrangement required a tight test system to avoid diluting the test smoke or introducing dust from the room air into the filtered smoke line, the NRL group considered that it stabilized the test smoke by keeping the pressure in the generator constant, and by allowing the smoke to cool to room temperature before it was used.

A propeller stirrer in the reservoir of dioctylphthalate helped improve the control of temperature and rate of evaporation of the liquid. Later, a water jacket was put around the quenching air stream to keep its temperature constant, and this also helped to stabilize the particle size of the smoke.

24.2.4 Smoke Materials

The material for a test smoke should be a liquid with a low vapor pressure at room temperature. It should be stable for long periods of time at the boiler temperature. Triphenyl phosphate [TPP] was used in much of the earlier work. It has the disadvantage of being a solid melting at 50 C. Although it forms a supercooled liquid smoke, this solidifies when it deposits in any cool parts of the generator, and eventually clogs the apparatus. Oleic acid also was used in the early work. It has a lower melting point than TPP and also supercools to form a liquid smoke. It has the disadvantage of decomposing at the temperature of the boiler. Tricresyl phosphate [TCP] has the advantage of being a liquid at room temperature, and was used to some extent, but later was given up because of its tendency to decompose and the fact that it is somewhat toxic. Dioctylphthalate [DOP] was the most useful smoke material, and became a standard test material by the end of the war. It is liquid at room temperature and is fairly stable, although it decomposes somewhat after a considerable time in the boiler.

24.3 LABORATORY TEST METHODS

When the United States entered the war, the CWS at Edgewood Arsenal used two standard laboratory methods of testing smoke filters. The first employed toxic test smokes [DM or DA], the second utilized nontoxic methylene blue [MB] introduced by the British.

24.3.1 DM and DA Smoke Tests [6]

Smokes of DM [7] are produced by dripping a 1% solution of DM in acetone upon a hot plate held at a temperature of about 245 C. The smoke is generated in a closed box, which is kept at a temperature of 45 to 50 C. The resulting smoke particles are solid crystals. Microscopic examination on a thermal-precipitator slide showed a particle-size distribution curve with a peak at 0.2 micron diameter, which is only slightly smaller than the most penetrating size (0.3 micron diameter) and no particles larger than 0.6 micron diameter. The smoke, at a concentration of about 50 μg per l, is passed through the test filter at 32 lpm. The effluent smoke is analyzed for arsenic by a modified Gutzeit method sensitive to 0.01 μg per l, or 0.02% penetration.[8] A charcoal bed is placed between the filter and the analyzer to absorb any

DM vapors which may come from the generator. This arrangement improves the consistency of the results, but removes 20 to 25% of the DM smoke. The test therefore does not yield absolute per cent penetration, although it can be used to grade a series of canisters or samples of paper. Additional disadvantages of this test are the toxicity of the agent, the excessive time required to carry out the chemical analyses, and the fact that solid smokes with irregularly shaped particles are less penetrating than liquid smokes with the same number of spherical particles.

The DA test [9] obviates this difficulty, since this material forms a liquid smoke. The method of production is similar to that for DM smoke. An acetone solution of about 2.6 g per l is dropped at the rate of 80 drops per minute on a hot plate to form the smoke. Experimental tests also were run with DC smoke produced in the same way.

24.3.2 The Methylene Blue Test [10]

In the methylene blue test carried out at Edgewood Arsenal in the EA–E1 meter,[11] the smoke is generated by atomizing a 1% aqueous solution of methylene blue and evaporating the water by mixing the spray with a larger quantity of dried air. Microscopic examination showed that most of the particles were nearly spherical with a diameter of 0.2 micron, and only a few were larger than 0.4. The smoke is drawn through the filter or canister at a rate of 32 lpm and then passes through a strip of filter paper for a definite length of time. The test strip is "developed" by exposing it to steam and the color is compared with a set of standard stains. One disadvantage of this method of comparison is that the rate of drawing off standards is different from the rate used in making a test strip. This may lead to error, since velocity has a considerable effect upon the penetration of smoke through paper, especially the alpha-web paper which is used as the standard strip. The lower limit of the methylene blue test is about 0.005% penetration.

The CWS Development Laboratory at MIT designed the MIT–E2 methylene blue penetration tester [12] to overcome some of these difficulties in the testing of filter paper. The MB smoke, generated as before, is passed through a pad of a number of sheets of the filter paper under test and the stains produced on the single sheets are compared. The penetration per sheet can be calculated from the filtration law. A series of tests at Edgewood Arsenal [13] indicated that the MIT–E2 tester gave less reproducible results than the EA–E1 tester, was not sufficiently sensitive to discriminate closely between filter papers of different filtering qualities, and required 25 min for a test, compared with an average of 4 min per test on the EA–E1. It can be used only for filters in sheet form. An indirect method, which is still less sensitive, must be used when the filter sheet is colored.

24.3.3 The Radioactive Smoke Test [14-16]

Early in the NDRC smoke program (November 1940) a method of testing the filtering power of sheets of paper or bulk material was devised, using radioactive test smokes. The sheets, or bulk material made into pads of uniform thickness, are arranged in series, and the test smoke (e.g., triphenyl phosphate containing radiophosphorus) is passed through these. After a sufficient length of time the sections are tested separately with a Geiger counter which registers counts proportional to the amount of smoke removed by each section. This test served to compare the filtering power of many materials and played an important role in the early NDRC smoke program. It suffers from the disadvantage of requiring radioactive materials and techniques, and later was given up in favor of more rapid, simple, and sensitive optical methods.

24.3.4 Optical Smoke Penetration Meters [17]

The NDRC Optical Mass-Concentration Meter [25]

Before the introduction of photoelectric meters, the NDRC optical mass-concentration meter was developed and used for many of the decisive tests on various filter materials. An appreciation of the advantage of small-angle forward scattering, and thorough familiarity with optical systems led to the design of the instrument already described in Chapter 22. It was operated in a small dark room and, in the hands of a skilled operator, was sensitive to 0.001 μg per l of a 5 order (1 micron diameter) oleic acid test smoke or the standard DOP smoke of 0.3 micron diameter and 100 μg per l. Thus, the instrument was sensitive to 0.001% penetration. The optical comparisons were very tiresome for the operator, and required considerable skill and experience as well as time.

THE MIT–E1R1 OPTICAL MASS-CONCENTRATION METER [18,19]

An optical system nearly identical with that of the NDRC optical meter was developed independently at about the same time at the CWS Development Laboratory and used in the MIT–E1R1 optical meter. This was designed as a rapid, portable, and simple instrument for testing filter papers or canisters with liquid smoke furnished by the MIT–E1R7 generator [4] described in a previous section. It utilized two smoke cells, with identical lamps and identical optical systems, employing small-angle forward scattering. Unfiltered smoke passes through one cell and filtered smoke through the other. The light scattered from the filtered smoke passes directly through a small rectangular hole in the center of the silvered face of a prism forming one half of a photometer cube, while that scattered from the raw smoke is reflected from a single prism and then from the opposite side of the silvered face. Thus the field, viewed by a low-power microscope, consists of the central rectangle of light coming from the filtered smoke, surrounded by the light from the raw smoke. Before measuring smoke penetration, raw smoke first is passed through both smoke cells, and a neutral screen filter in the optical system is adjusted to give uniform illumination of the photometer cube. Then filtered smoke is put into one cell and the intensity of the light scattered from the raw smoke is reduced by means of a calibrated optical gradient until the field is again uniform. The penetration is read directly from a 3-cycle logarithmic scale on the same shaft as the optical gradient. If the filtered smoke concentration is very low, the intensity of the light from the raw smoke can be further reduced by means of optical filters to 0.1, 0.01, or 0.001 of the reading on the gradient.

This instrument is compact, portable, and simple to operate. A small light shield over the eyepiece allows it to be read in the ordinary daylight. It gives absolute penetrations, and has the advantage of any comparative method in that a single reading gives relative light scattering, and gradual changes in the concentration of the test smoke are compensated. Its chief disadvantage is that it requires visual comparison of two fields, which is tedious. It was the experience of the Division with the instrument furnished that under optimum conditions individual readings vary by as much as 10%, and a series of readings are required for 5% accuracy. The limit of sensitivity of this instrument was found to be about 0.05% of a 100 μg DOP smoke, being determined chiefly by stray light in the effluent smoke cell which could not be reduced below this value.

24.3.5 The Australian Ionization Penetrometer [20]

An ionization penetrometer was developed at the Munitions Supply Laboratories, Maribyrnong, Australia. A 1% solution of sucrose is sprayed under a pressure of 30 psi to give a cloud of charged particles. Mobility measurements indicate a mean diameter of 0.03 micron. The spray is diluted to a flow of 1 cu ft per min, yielding a positive ion concentration of about 400,000 per ml. The electrical conductivity of the smoke is measured before and after filtration. The sensitivity of the penetrometer is 0.0002% per mm deflection on the scale, on the highest sensitivity range. Four to five minutes are required per test. The ions are found to be only about one-fifth as penetrating as a carbon smoke at a carbon penetration of 0.1% and only one-hundredth as penetrating as methylene blue. Comparative tests of this method apparently have not been made in this country, but it should be investigated, since it might be useful either for the study of the penetration of very fine smokes, or if larger ions could be produced, as a penetrometer for use with the standard smoke of 0.3 micron diameter.

24.3.6 Photoelectric Smoke Penetrometers

HILL'S PHOTOELECTRIC SMOKE PENETROMETER [21]

At the start of the war, the most sensitive laboratory instrument available was the photoelectric smoke penetrometer developed by A. S. G. Hill for the testing of commercial dust respirators, which is described in the British Journal of Scientific Instruments. Hill's test smoke consisted of carbon particles, which he stated had an average diameter of 0.16 micron. The smoke was made by the carefully controlled incomplete combustion of butane in a bunsen burner. The smoke contained 6.8×10^9 particles per liter, at a mass concentration of about 25 μg per l. The absorption of light by a 50-cm column of this smoke was measured by means of a photocell connected to a triode amplifier, the plate current of which was balanced with a suitable resistor and a highly sensitive galvanometer. Although the total absorption of the raw smoke was only about 9%, penetrations could be read to 0.02% (1 mm galvanometer deflection). This arrangement required careful adjustment of the flame to give a uniform smoke, and

careful regulation of the light current and the batteries, in order to measure the minute changes in the intensity of the transmitted light.

English and Canadian Carbon-Smoke Penetrometers [22, 23]

In the early days of the war, a carbon-smoke penetrometer was developed and used in England for testing gas mask filters, and was employed in Canada as an acceptance test. The English apparatus was sensitive only to 0.5% and was superseded by the MB test. A penetrometer, using carbon smoke also, was developed at the Pulp and Paper Research Institute of Canada. Butane is burned in a bunsen jet with a variable amount of air bled into the gas stream before combustion. The penetrometer consists of two smoke cells separated by a filter holder. The light, scattered by the smoke in either cell, is measured by means of an RCA 929 vacuum phototube and a balanced d-c amplifier of the *cathode follower* type.

It was found that the penetration of rayon-asbestos filters increased markedly as the amount of air bled into the gas stream was increased. Electron microscope photographs showed only a slight increase in the relative number of particles of optimum size as the gas is diluted. This change was not considered great enough to account for the large increase in penetration. It was concluded that the phenomenon was a mass-concentration effect, the carbon smoke forming a *pre-filter* upon the rayon asbestos fibers. The more concentrated the smoke, the greater was the pre-filtering action.

Since the mass concentration must be controlled with care to insure significant penetration data, and since liquid smokes are 50 to 100 times more penetrating than carbon smoke, the carbon penetrometer seems to be of little practical use.

The Kimberley-Clark Nephelometer

This instrument was developed for testing samples of filter paper. A single 50-cp automobile headlight supplied light to two smoke cells set at right angles to each other. In each cell the light was focused by means of a lens system upon a small area where the light, scattered from the smoke at right angles, was viewed by a Type 931 photomultiplier tube. The stray-light current in each cell was balanced out electrically. Raw smoke flowed through one cell and filtered smoke through the other. The current due to the scattered light in each case was read and the ratio of the two gave the smoke penetration. The sensitivity of the instrument was about 0.1% penetration when using the standard 100-μg test smoke.

By 1943, smoke filters were improved to the point where they transmitted only a few hundredths of a per cent of a standard DOP smoke, of 0.3 micron particle diameter (as judged by a 29 degree Owl reading). At a standard concentration of 100 μg per l for the test smoke, the effluent from such a filter could not be measured by means of the MIT–E1R1 optical mass-concentration meter. The NDRC optical mass-concentration meter has the necessary sensitivity only in the hands of a skilled operator. However, a penetrometer for routine testing, sensitive to 0.001%, was evidently needed, and tests in this range are extremely difficult by any visual method. Neither the Kimberley-Clark nephelometer nor any of the photoelectric photometers then in use by the Armed Forces in this country, Great Britain, or Canada, had the desired sensitivity. The only photoelectric penetrometer of sufficient sensitivity was that of Hill to which reference has been made.[21] This instrument, however, measured the *absorption* of light and required extreme control of light intensity as well as an extremely sensitive galvanometer. Since only about 10% of the light was absorbed by the raw smoke, the intensity of the light had to be kept constant to 0.002% in order to obtain Hill's sensitivity of 0.02% in the penetration. If the *scattered* light is measured, however, the variation in light intensity can be of the order of the desired accuracy of measurement, e.g., 1%, provided the background light intensity is kept low. Hill's instrument also required a galvanometer with a sensitivity of 1,500 mm per μa, which cannot be used conveniently except in a research laboratory.

As a result of the need for a sensitive and simple penetrometer for routine tests, several instruments were developed for photoelectric measurement of the intensity of the light *scattered* from the standard test smokes, using electronic amplification and small rugged galvanometers which could be operated anywhere.

The NDRC Balanced Photoelectric Smoke Filter Penetrometer [25]

This apparatus was developed from the NDRC optical mass-concentration meter already described. A single 50-cp bulb supplies light to two of the forward-angle scattering cells placed at 130° to each other. The scattered light falls on two Type 931 photomultiplier tubes. With raw smoke in one cell and filtered smoke in the other, the currents from the

scattered light in the two cells pass through resistors, one of which can be varied so that the IR drops are balanced in a bridge circuit. If the currents are proportional to the smoke concentrations in each case, the ratio is the smoke penetration. Careful tests showed, however, that the Type 931 tubes were far less reliable than had been expected, when appreciable currents were drawn. Individual tubes also varied widely in their characteristics and suffered fatigue so that a current of 0.5 ma would fall off by 25% to 50% in an hour of steady illumination. This meter was studied in some detail at the Central Laboratory of Division 10, but reliable results below 0.05% penetration never could be obtained. Therefore the use of the Type 931 tube in such an arrangement was given up in favor of the more stable vacuum-type phototube in conjunction with suitable amplifying circuits.

The NDRC–E1R2 Smoke Penetrometer [26]

This compact, direct-reading photoelectric penetrometer, designed especially for rapid and accurate readings to 0.001% of the standard DOP smoke, is shown schematically in Figure 1. It was developed between March 1943 and June 1944. The photoelectric current passing through the resistance R produces across it a potential drop E_R which can be balanced by means of the potentiometer so as to bring the galvanometer in the plate circuit of the amplifier tube to zero.

The smoke-cell arrangement is shown in Figure 2. The smoke from any suitable generator can be used. The CWS Development Laboratory MIT–E1R7 generator [4] was widely used for test purposes. The smoke enters at A and leaves the cell at B. The converging beam of light from the aspheric lens system C illuminates the smoke intensely at the focus D where the image of the filament falls. Stray light is reduced to a minimum by use of the light trap E to absorb the diverging beam, the baffles F, G, and the slits H, H, which limit the field of view of the photocell. This reduction of background compensates for the reduction of intensity in using right-angle instead of small-angle forward scattering.

The Type 929 vacuum phototube was removed from its base to reduce leakage currents and connected through a very high resistance to the grid of a Type 38 tube which serves as a single stage of d-c amplification. As the photocurrent is reduced (to 5×10^{-13} a for a smoke concentration of 0.001 μg per l), the potential drop is kept within the range of

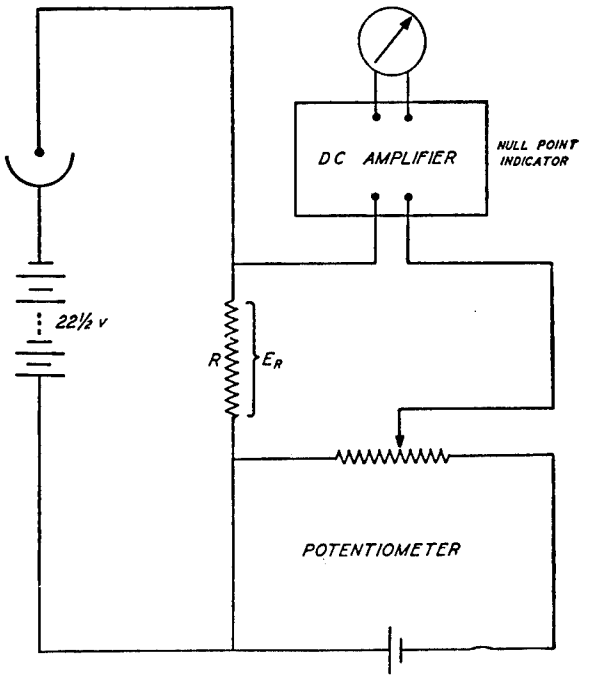

Figure 1. Schematic diagram of penetrometer circuit.

measurement by increasing the high resistance by decimal steps from 10^7 to 10^{10} ohms. A special circuit was introduced, which compensates for any deviation of the high resistors from their nominal values.

A photograph of the instrument is shown in Figure 3. To make a measurement, the switches are turned on, the grid bias is adjusted and the stray light knob is turned to balance the stray light electrically. Then raw smoke is passed through the cell, the scale switch is set on 1 (connecting the 10^7-ohm resistor in the circuit), the per cent penetration dials are turned to 100, and the sensitivity is adjusted to give a zero reading on the galvanometer. Next the filtered smoke is passed through the cell, the scale switch turned to the appropriate value, and the per cent penetration dials adjusted to balance the galvanometer. The resulting readings give the penetration directly. Thus 85% on scale 0.001 (10^{10}-ohm resistor) corresponds to 0.085% penetration. On this scale a change of 0.001% gives a galvanometer deflection of 1 mm, which is significant.

Auxiliary circuits are supplied to check the adjustment of the scale switch to decimal steps, to check the emf of all cells, and to read the stray light, grid, and leakage currents. Arrangements are also made for reading plate currents, so that the characteristics of the Type 38 amplifier tubes can be determined.

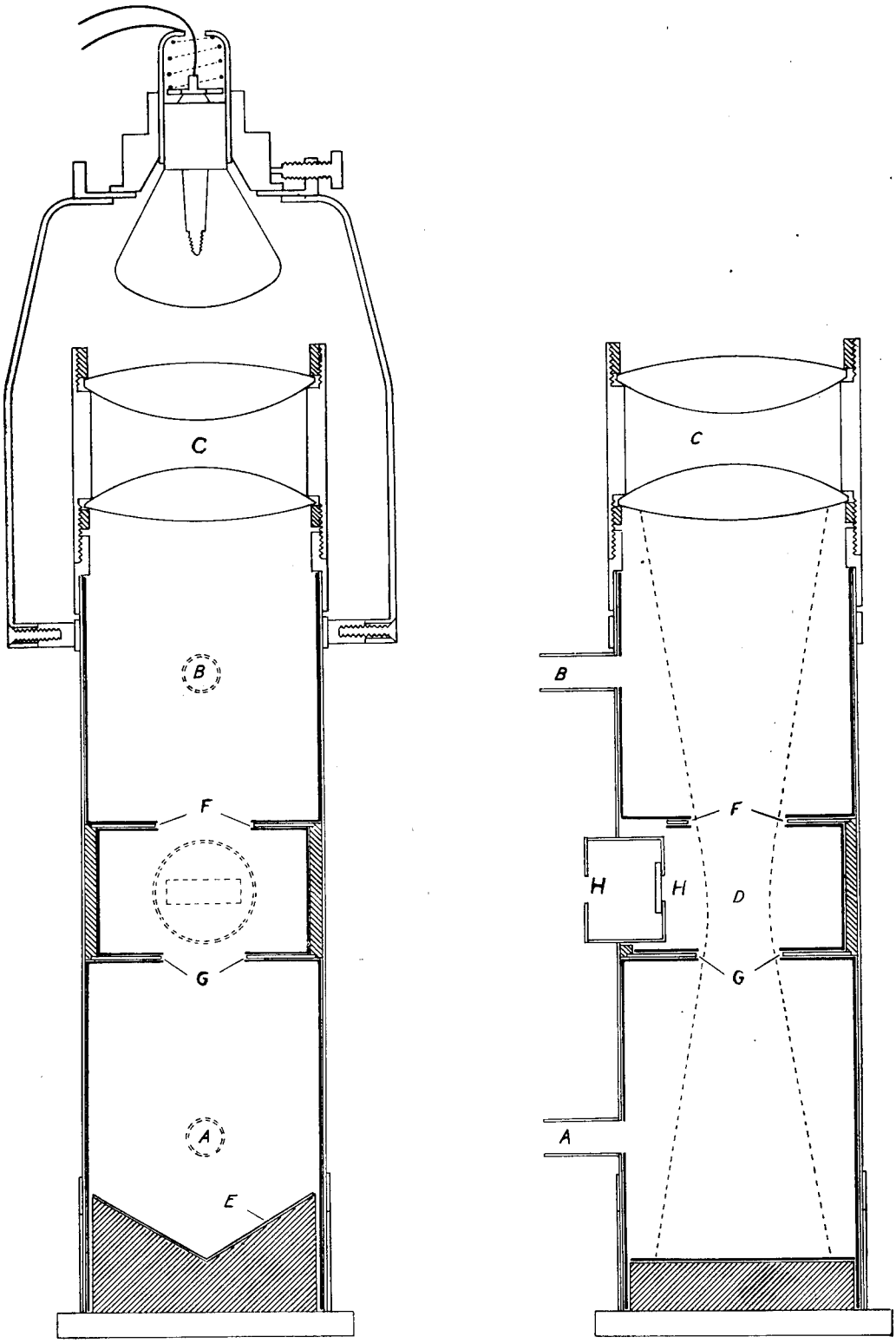

FIGURE 2. Smoke cell arrangement.

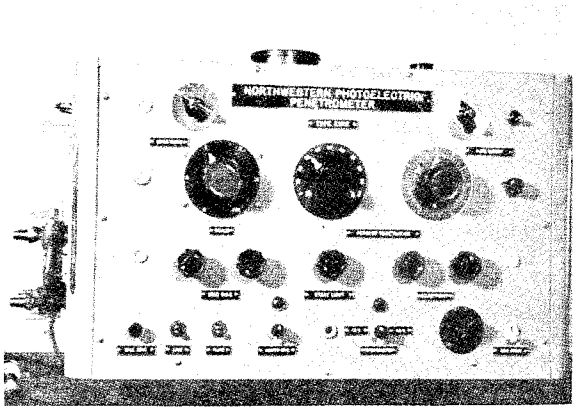

FIGURE 3. NDRC-E1R2 smoke penetrometer.

The unit is self contained, and all these readings are made without auxiliary equipment.

In addition to the NDRC–E1R2 smoke penetrometer built and used in the Central Laboratory of Division 10, at Northwestern University, three instruments were furnished to the Services. The first was sent to the CWS Development Laboratory at MIT, the second to the Naval Research Laboratory, and the third to Edgewood Arsenal.

THE CWS PHOTOELECTRIC SMOKE PENETROMETER, MIT–E2 [27]

This apparatus was developed between June 1942 and August 1945 by adapting the optical system of the MIT–E1R1 optical smoke penetration meter to the measurement of light intensity with an electrical system using a Type 931 photomultiplier tube. It was designed not as a penetrometer but as a versatile instrument for studying the optical properties of smokes at low light intensity. It is sensitive to 0.001% of the standard 100-μg DOP smoke, but is more complicated than the instruments designed as penetration test meters.

The apparatus included two separate smoke cells for measuring forward scattering, with a separate Type 931 tube and associated circuits for each. Great care was taken to supply a regulated constant voltage to the dynodes of each tube, the output of which was kept to 50 μa or less, and amplified by a cathode-follower circuit. Compensation of the stray light and leakage current was accomplished by means of an adjustable compensating lamp and Type 926 phototube. Arrangements were also made to calibrate the intensity of the light falling on the Type 931 tube by means of an incandescent lamp which could be compared with a standard lamp.

In practice, one optical system was used to measure the intensity of the light from the raw smoke. This light was cut to 1% by means of an optical attenuator. The other optical system was used for measuring the intensity of the light from the filtered smoke, and the ratio of the two intensities gave the penetration.

THE NRL SMOKE PENETRATION METER E2 [5]

This meter, developed at the Naval Research Laboratory for laboratory use and factory tests of filter paper, comprised the NRL smoke generator previously described, an Owl particle-size meter, a smoke cell, and an indicator unit. The smoke cell, based on the NDRC optical mass concentration meter, employed small-angle, forward scattering. Careful arrangement of light baffles reduced the stray light to 0.008% of that from the standard 100 μg DOP test smoke. The light was focused upon a Type 931 photomultiplier tube. At first, the output current was measured with a galvanometer sensitive to 0.03 μa per division. Later a vacuum-tube current amplifier was used with a microammeter in a bridge arrangement in the plate circuit, so that the indicator would be immune to the vibrations of factory operation.

In order to insure stable operation of the Type 931 tube by limiting its output photocurrent to 30 μa, the light from the raw smoke was reduced by means of a calibrated optical filter, made from a perforated disk of metal inserted between the condensing lenses so that it was perpendicular to the light beam.

The stray light was compensated electrically. Adjustment of a sensitivity control made the galvanometer read directly in per cent penetration. A scale switch allowed the range to be reduced by factors of 0.01 or 0.001, so that readings could be made to 0.001% penetration of a standard DOP smoke. The whole operation was rapid and convenient.

24.3.7 Comparative Tests of Various Penetrometers

The photoelectric penetrometers are so sensitive that independent tests by other means are difficult. However, careful comparisons were made at the CWS Development Laboratory [27] and at the NRL.[5] Penetrations were measured by collecting standard DOP smoke for a sufficient length of time on a weighed glass-fiber filter, and comparing the penetra-

tions so measured with the readings of the photoelectric meter on the same sheets. In each case, the results agreed within a standard deviation [a] of ±3%, which is less than the experimental uncertainty. These comparisons could not be made with any accuracy for penetrations less than a few per cent.

Each of the penetrometers was tested individually for self-consistency by measuring the penetrations of a series of filter papers singly and in series. Plots of the logarithm of the penetration against the number of sheets showed a straight line as required by the filter law.

In November 1943, two series of measurements were made with the NDRC–E1 penetrometer. This was the original model from which the direct-reading E1R2 was developed. Measurements of 2, 4, 6, 8, and 10 sheets of Brown and Company paper gave penetrations of 33 to 0.4%, with a standard deviation of ±6.6% from the average penetration for 2 sheets. Omitting one result, the standard deviation was ±3.4% for the other 9 sheets. A similar series of experiments on 1 to 12 sheets of paper at MIT gave penetrations of 50 to 0.01%, with a standard deviation of ±5.5% from the mean penetration per sheet. Two series of measurements at the NRL on 1 to 5 sheets gave penetrations of 50 to 2%, with a standard deviation of ±3.7% from the mean penetration per sheet. These results tested simultaneously the smoke generator and the uniformity of the filter paper as well as the penetrometer. The observed deviations include errors due to variations and inhomogeneity in the smoke and paper, as well as experimental errors in the penetrometers.

The self-consistency of the MIT–E2 meter was checked in a series of twenty consecutive tests on a group of canisters over a period of four months. The standard deviation of the results on any one canister averaged ±8% at penetrations of 0.04 to 0.14%. The results for a series of canisters all appeared to vary in the same direction from one day to another, suggesting that a change in the smoke may have caused the differences.

Tests with two different NRL meters showed a standard deviation of ±3% for the penetration of the same canister measured with the same meter over a period of about a month, and ±2% standard deviation for the penetration of a single canister measured with the two meters over a period of seven months. The excellent agreement of this series of results shows the advantage of the close control of the smoke generator which was developed at the NRL.

A series of 27 comparisons of filters and papers, using the same smoke and two different indicator units, gave an average ratio of 1.01 with a standard deviation of ±0.03% over the range from 0.01 to 73% penetration. A comparable series of experiments with two completely separate meters, each including its own smoke generator, cell, and indicator unit, gave an average ratio of 1.02 with a standard deviation of ±0.06%. This indicates that about half of the observed differences were due to difference in the smoke. However, the agreement is very satisfactory, and speaks well for the operation of both NRL smoke generators and indicator units.

A number of comparative tests of the different penetrometers were made. The CWS Development Laboratory [27] made a series of comparisons between their E2 photoelectric meter and their E1R1 optical meter, and NDRC–E1R2 photoelectric penetrometer and an NRL–E2 meter. The results were given in terms of the average value of the ratio of the reading of any meter, referred to the corresponding reading of the MIT–E2 meter. These values are given in Table 1 together with the corresponding standard deviations [SD] of the individual pairs of readings. A series of comparisons was also made at the NRL between their E2 meter and an NDRC–E1R2 meter. The average of these results, most of which are given in the NRL Report,[5] is also given in the table. Since the NRL–E2 meter gives results which are about the average of the others, all of the values have been calculated on the basis of 1.00 for this meter. These results are given in the last column of Table 1.

The Particle-Counting Smoke Penetrometer

By the spring of 1944, work at Camp Detrick had shown that the best canister smoke filters gave almost perfect protection against the BG spores which were being used as simulated BW agents. Many canisters, however, which showed low penetration for the standard DOP smoke, leaked an appreciable number of the BG spores. These spores, which are elliptical in shape with major axis of about 1.2 microns and minor axis of about 0.8 micron, evidently were stopped almost completely by the filter paper but penetrated any cracks due to faulty crimping of the edges of the filter paper, or pinholes in the paper or the metal can.

The method of determining penetration at Camp Detrick was to collect the spores from the effluent

[a] Defined as the square root of the average values of the individual deviations.

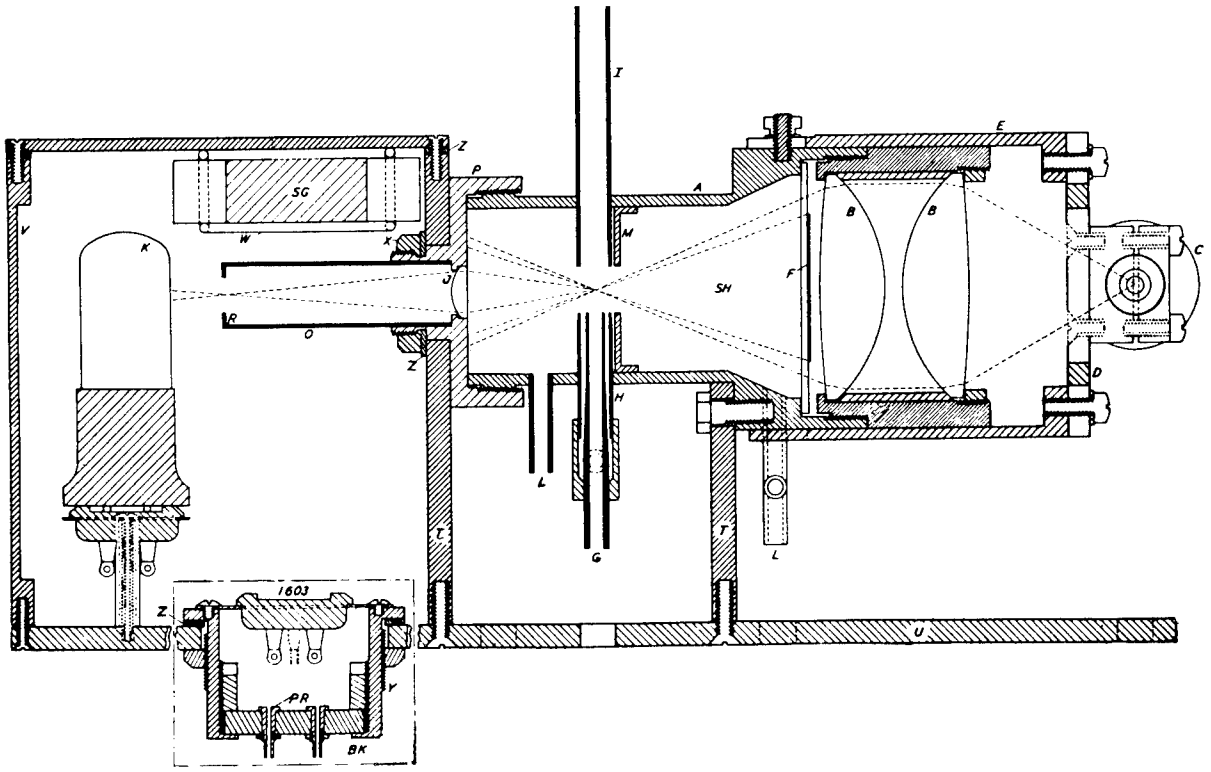

FIGURE 4. General arrangement of particle-counting penetrometer.

TABLE 1. Summary of comparative tests of penetrometers.

Meter	Experiments	Range (%)	Average ratio	SD	Average/NRL
NDRC–E1R2	29	0.07–55	NDRC/NRL 1.05	0.09	1.05
NDRC–E1R2	140	0.002–50	NDRC/MIT 1.05	0.19	1.01
NRL–E2	36	0.01–30	NRL/MIT 1.04	0.07	1.00
MIT–E2	..	.....	... ...	...	0.96
MIT–E1R1 optical	17	0.15–50	MIT–E1R1/MIT–E2 0.97	0.04	0.93

air on a cotton-wad impinger, wash them off onto an agar plate, and count the number of colonies which developed in 24 hours' time. There was urgent need for a rapid method of detecting defective canisters and of comparing the best canisters, which only allow the passage of a few particles per minute. Some indication of defective canisters was obtained by increasing the size of the DOP test smoke and decreasing the flow rate used in production-line tests with the MIT–E1 canister tester. This is because smoke penetration through the filter paper decreases with decreased flow rate much more rapidly than leakage through pinholes. However, a more direct method was needed, comparable both in sensitivity to the biological test and in rapidity to the ordinary photoelectric penetrometer. The problem was solved by developing the photoelectric particle-counting penetrometer described below.

Preliminary tests were made with a uniform DOP smoke of 0.4-micron radius from a generator like that described in Chapter 20. When this smoke was used in the NDRC–E1R2 photoelectric penetrometer described in a previous section, the lower limit of measurement was found to correspond to the light from only about 10 smoke particles. The sensitivity for counting individual particles therefore did not seem unattainable, particularly if the added intensity of small-angle forward scattering were utilized instead of the right-angle scattering of the photoelectric penetrometer. The d-c electronic amplifier of the earlier penetrometer could not be used, but an a-c pulse amplifier and counter had the advantage of

eliminating the effect of any nonfluctuating stray-light background.

The smoke cell contained a dark-field system of illumination similar to that in the NDRC optical smoke penetration meter described in Chapter 22. The general arrangement is shown in Figure 4. The smoke enters the cell A through G, the smaller of the two concentric tubes, while a sheath of filtered air flows through the outer tube H at the same linear rate and prevents the smoke stream from spreading out before it passes into the tube I. The well-defined smoke stream is narrower than the light beam at the focus. Hence every smoke particle is illuminated and scatters light into the conical shadow beyond the focus. Most of this light, indicated in Figure 4 by the inner dashed lines, enters the lens J and is focused on the photosensitive cell K to produce an electrical impulse of about 0.003-sec duration for each particle. The vents L, L, are used to flush the cell with filtered air before use. The cell K, coupling condenser and resistors, and first amplifier tube (Type 1603) are mounted in an airtight brass box, desiccated with silica gel to reduce electrical leakage.

The 50-cp automobile headlamp C was held in a massive clamp. The cell was of heavy construction, mounted on a solid brass plate U which rested on a felt pad. These precautions eliminated mechanical vibrations of the lamp filament which would lead to *optical microphonics* and spurious counts. The appearance of the cell unit is shown in Figure 5.

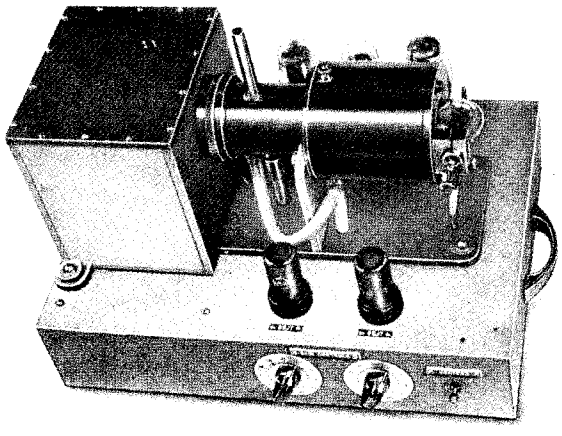

FIGURE 5. Cell unit of particle-counting penetrometer.

In preliminary tests neither vacuum nor gas-filled phototubes were found to give a high enough signal-to-noise ratio to allow successful counting. Even the best available RCA Type 931 electron-multiplier phototube gave a ratio so small that counting was unsatisfactory because of the background. Fortunately a thalofide cell, developed in Division 16 of the NDRC, was made available for this work. This cell gave a high enough signal-to-noise ratio so that background counts could be reduced to one every few minutes and the operation of the counter became practical.

The original pulse was fed into the Type 1603 amplifier, chosen for its low microphonics, followed by two Type 6SJ7 tubes, giving a maximum amplification of about 500,000. The output of the amplifier was fed into a thyratron *trigger* circuit which activated the mechanical recorder. A control of the grid bias of the thyratron regulated the size of the pulse needed to fire the tube. The amplifier and thyratron voltages were taken from a rectifier with a filter and a number of VR (voltage regulator) tubes which gave a closely-regulated, stable power supply. Filters were used to eliminate the feedback between the stages of the amplifier.

The success of the particle counter depended upon three things: (1) the use of the thalofide cell with its high signal-to-noise ratio, (2) the construction of a compact and rigid optical system which eliminated optical microphonics due to vibrations, and (3) the development of a remarkably stable amplifier which eliminated electrical background counts.

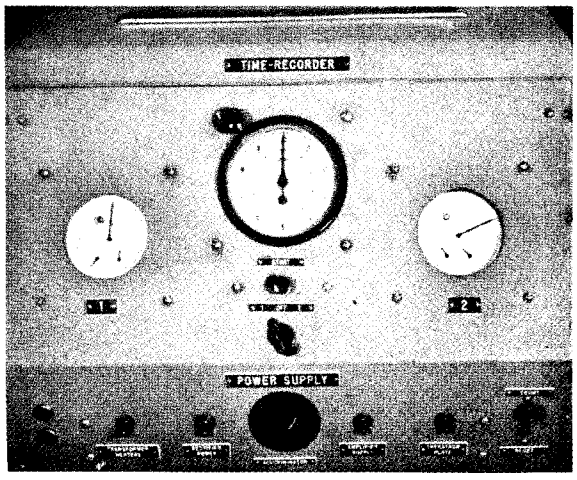

FIGURE 6. Time recorder and power supply unit.

Two mechanical recorders were used, in order to provide a check of their functioning. These and an

electric timer were so arranged that in a normal test a single button started the recorder and timer which were then stopped after 100 counts by a contact on the counter. The time for 100 counts thus recorded was determined with a statistical uncertainty of not over 10% in each experiment. Figures 6 and 7 show the timer, recorder, and power supply units.

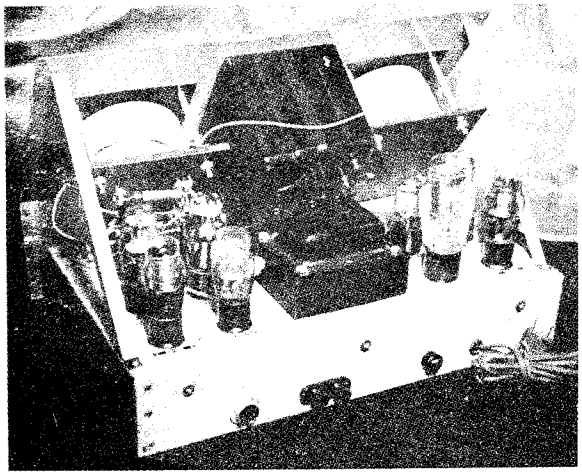

FIGURE 7. Rear view of time recorder and power supply unit.

Although the electrical stray counts were reduced to a negligible quantity, the background due to dust blown from the filter was troublesome unless the filter was blown off for 5 min or more before a test. Then the counts could be reduced to a value of about 1 to 5 per min which is negligible for most tests.

The particle counter was tested by measuring the penetration of the same filter paper, first with smoke of standard concentration and the photoelectric penetrometer, and then with greatly diluted smoke of known dilution and the particle-counting penetrometer. The results agreed up to about 1,000 counts per min, above which an increasing number of the counts were lost.

The range of the instrument is from about 3 to 1,200 counts per min. If the inlet smoke concentration is 10^8 particles per l, which is attainable with BG, one count per min corresponds to 10^{-6} per cent penetration. Hence the sensitivity range of the instrument is 3 micro-per cent to 1.2 milli-per cent.

A particle-counting smoke penetrometer, E1R2, was made for use at Camp Detrick, where it was compared with the BG tester. The work at Northwestern University is being continued under a contract with the War Department and should yield results of considerable interest.

24.4 PRODUCTION-LINE TESTERS

24.4.1 The Edgewood Arsenal E3 Canister Tester [30–33]

The EA–E3 meter, employing an oil smoke, was used extensively at the beginning of the war for production-line filter testing. The oil smoke is produced by spraying amyl stearate into an electrically heated furnace mounted on one side of a large smoke chamber. The furnace is heated to about 450 C, and the smoke is formed by condensation of the oil vapor in the large chamber. The smoke is sucked through the canister at 40 lpm and then through a cell where the light, scattered at right angles from a Tyndall beam, is measured, using a Westinghouse Type SK–60 phototube and a Wheatstone bridge circuit amplifier. The meter is standardized by the use of master standard filters and used as a pass-reject instrument. The mechanical arrangements of the canister holder are well designed for rapid and convenient production-line tests by unskilled operators.

The concentration of the oil smoke originally used in the E3 meter was maintained as uniform as possible, but was not determined accurately. According to the estimate of H. Scherr, it was about 40 mg per l. With this inlet smoke concentration, the sensitivity of the E3 meter was better than 0.02%.[34]

NDRC tests [25] about April 1941 showed that oil smoke caused considerable deterioration of the carbon-impregnated paper then used in the smoke filter. Apparently this is because the liquid smoke wets the fine carbon filaments bridging the openings in the filter paper, causing these fine filaments to coalesce with the coarser cellulose fibers. Later, considerable attention was paid to the harmful effect of oil screening smokes on filters.[35–38]

When the highly concentrated test smokes were shown to be harmful to the filters on the production line, the concentration of the test smoke was reduced to about 2 to 5 mg per l.[39] However, this reduced the sensitivity of the meter to somewhat better than 0.2% penetration.

24.4.2 The CWS Development Laboratory MIT–E1 Canister Tester [40, 41]

The great improvement in Service canisters rendered the EA–E3 meter obsolete, and the much

more sensitive MIT–E1 canister tester was developed to take its place on the production line. This tester is provided with the MIT–E1R1 generator [4] which produces a liquid smoke of DOP. A stream of air is bubbled through the liquid DOP in a boiler maintained at a constant temperature within ±0.5 C by a thermostat. The vapor-laden air is cooled rapidly as it is mixed with a large volume of diluting air in a Venturi tube. By proper adjustment of the temperatures of the boiler and diluting air, the smoke-particle size is maintained at about 0.3-micron diameter, as measured by an Owl reading of 30° (±1°). Originally, the smoke concentration was between 200 and 250 μg per l, at a flow of 85 lpm in the MIT–E1 canister tester. Later, the flow was cut to 32 lpm and the concentration was increased to 750 μg per l in the MIT–E1R1 canister tester. This change was made in order to make the tester more sensitive to pinhole leaks and canister imperfections, as explained in discussing the particle-counting smoke penetrometer.

All the smoke stream put through the canister also traverses the smoke cell. Hence it is flushed out almost instantly. The cell is designed to minimize fouling of the lenses by smoke or by lint blown off from the filters, so as to allow long periods of operation before the background light becomes too high. Since the test-smoke concentration is reduced to avoid damage to the filter, and the scattered light from the smoke cell is viewed at right angles to reduce background scattering as much as possible, the amount of light scattered from the filtered smoke is so minute as to require a very sensitive photoelectric circuit. A Type 929 photocell is employed. A light chopper between the lamp and the smoke cell gives 90-c pulses from the Type 929 tube, which are fed to a 4-stage 90-c amplifier operated at a gain of about 2×10^6. Thus the small current due to the light pulses scattered by the filtered smoke is separated from the much larger d-c leakage current in the Type 929 tube. The background light, scattered by the cell, is compensated by a zero adjustment.

When the instrument has been calibrated against a standard filter, the percentage penetration may be read directly. However, in a production line, it is used as a pass-reject instrument. The rejection limit may be set as low as 0.01% penetration.

Another advantage of the tester is its speed. Since only about 5 sec are required per canister, it is well adapted for use on a production line. The disadvantages are the complicated electronic circuits, which make the initial cost high and require maintenance men who are specialists in electronics to service the meter.

24.4.3 The NRL–E3 Smoke Penetration Meter [5]

This meter employed the smoke generator, small-angle forward scattering cell, and indicator units of the NRL–E2 meter described in an earlier section, adapted to rapid production-line testing. The volume of the smoke cell was reduced by a wooden sleeve, which filled most of the space around the cone of light, so as to reduce the time for equilibration of the cell. With a test smoke of 125 to 150 μg per l, this instrument had a sensitivity of 0.001% and measured absolute penetrations. This was an advantage over the MIT–E1 canister tester, which was calibrated against a standard filter.

The validity of standard filters is always open to some question, due to change of penetration with use. The CWS Development Laboratory supplied standard canisters with filters of glass fiber, which is less affected by DOP smoke than paper filters. The MIT–E1 canister tester, calibrated with such a standard, was found to give results with other glass fiber filters which agreed well with the NRL-E1 meter (the original laboratory model from which the production-line tester NRL–E3 was developed). However, the penetrations of paper filters measured with the MIT–E1 meter were nearly twice as large as those obtained with the NRL–E1 meter. All the measurements were in the range 0.05 to 0.10% penetration. The discrepancy was greatly reduced when the MIT test smoke was used with both indicators. This fact suggested that the test smokes were not equally uniform, and that selective filtration was different with the two filter materials. Even with the same test smoke, unless it were homogeneous, the selective filtration could cause a different reduction of the intensity of the light viewed at right angles in the MIT–E1 meter, and at small forward angles in the NRL–E1 meter.

The complete explanation of all these facts awaits the development of a method of measuring particle size distribution in these fine smokes before and after filtration. If such a method were comparable in ease with the owl reading for average particle size, it would give a tremendous amount of useful information. However, a practical solution in this case was obtained by using paper filters as primary standards for the MIT–E1 meter, and the glass wool filters as

secondary standards which were checked against the primary ones and then used for routine tests the rest of the day. The primary standards were replaced frequently.

24.4.4 The Carbon-Smoke Penetrometer [42]

This instrument, which has been described in a previous paragraph, was used by the British and the Canadians as a production-line tester. The sensitivity of the British apparatus was only 0.5%. The Canadians employed a photoelectric detector sensitive to 0.01% penetration. However, the penetrometer had the disadvantage of using a solid smoke consisting of many chain-like particles made up of small primary carbon nuclei. These particles are less penetrating than spherical liquid particles of the same mass. Also, they tend to clog the filter, decreasing its penetration for the moment by impregnating it with fine carbon filaments. However, this improvement disappears in the presence of oil smokes, which wet the carbon filaments and cause them to coalesce with the larger fibers of the filter, as explained in the discussion of the Edgewood Arsenal E–3 canister tester.

24.4.5 The Sodium-Flame Penetrometer [43]

The sodium-flame apparatus was developed by the British [44, 45] as a 100% filter tester for use in the production of canisters. The smoke is generated by atomizing a 2% solution of salt and diluting the spray with air, allowing the drops to dry to a smoke of solid sodium chloride. As originally designed, the apparatus employed visual comparison of the intensities of sodium light from two hydrogen flames, one burning in the unfiltered smoke, the other in the effluent leaving the test filter. A comparison spectroscope is used so that the *D* lines of the two flames appear to be separated by a dividing line. The intensity of the flame burning in the unfiltered smoke is cut down by means of an optical wedge to match that of the test flame. At balance, the percentage transmission of the wedge is a measure of the concentration of the filtered smoke. Since the intensity of the flame may not be proportional to the concentration of salt in the air about the flame, and since the intensity may change with the alignment of the spectroscope with respect to the flames, the value at balance is not absolute but only relative. Thus, one of the disadvantages of this type of tester is that it yields percentage penetrations only after it is calibrated with filters standardized by some other method such as the methylene blue tester. A second disadvantage is that it requires visual comparisons of intensities, which is rather fatiguing, although the British reported no complaints of eye strain from the observers in their factories.

The advantages of this tester are its high sensitivity, the rapidity with which canisters can be tested (over 400 an hour by one observer), and its simplicity, which reduced the initial cost and required a smaller amount of strategic materials than did more complicated testing apparatus.

The sodium-flame apparatus was later modified by the Canadian Chemical Warfare Laboratories [46] so that visual comparisons are replaced by the use of the RCA Type 931 electron-multiplier type phototube, the output of which is passed through a microammeter. The meter can be made to give absolute penetrations by comparison with a standard filter, the penetration of which has been measured by means of a methylene blue tester. The hydrogen flame is adjusted so that 1 μa corresponds to a penetration of 0.005%. After a careful study of the penetration of wool-resin filters, it was concluded that the sodium-flame penetrometer gave results as consistent as did the methylene blue and DOP penetrometers. The sodium-flame penetrometer might well be adopted as a production-line tester if all canisters were tested against a solid smoke.

24.4.6 Possible Use of a Particle-Counting Canister Tester

The particle-counting smoke penetrometer has definite possibilities as a production-line tester, if the need should arise for such an apparatus. The control of test smoke concentration by a photoelectric device is now under investigation at Northwestern University under a contract with the Army Service Forces at Camp Detrick. The smoke cell and electrical circuits would require little change to arrange for a count of 5 or 10 sec duration. The chief problem would seem to be removal of all dust from the filter, which might be accomplished by blowing filtered air through the canisters on the assembly line before they reached the testing station. The maintenance and servicing of the electronic apparatus probably would be simpler than for the MIT–E1 canister tester.

Chapter 11

TRAVEL AND PERSISTENCE OF AEROSOL CLOUDS

By *W. H. Rodebush*

26.1.1 Thermal Behavior of Smokes

It will be seen from Table 1 that there will be a tendency for smoke to rise in every case, this tendency being especially pronounced for white phosphorus.

When a smoke appears to be "heavy," there is usually a gas of high molecular weight present. For example, even on hot sunshiny days, the black smoke from a factory chimney usually rises at first, but may occasionally fall to the ground after some travel. This happens because the carbon dioxide present loses its heat by radiation and then sinks because it is heavier than air. The carbon dioxide receives no heat directly from the sun because there is sufficient carbon dioxide in the air above to remove all the radiation of the wavelength that is absorbed by carbon dioxide. Particles of soot will, of course, absorb heat and tend to prevent the cooling effect which causes the smoke to fall.

26.1.2 Atmospheric Diffusion

The initial condition of turbulence, which accompanies the generation of smoke, disappears by the time the smoke has traveled a short distance from the generator. The buoyancy effect resulting from the higher temperature of the smoke will continue to be effective, causing the smoke cloud as a whole to rise. As the smoke becomes more and more diluted with the cooler air, this effect will be less and less observable, unless (as in the case of white phosphorus) there is a very great initial rise in temperature when the smoke is formed.

The process by which the smoke is diluted and mixed with air is called *atmospheric diffusion*. This process is often termed *eddy diffusion* to distinguish it from *molecular diffusion*, since eddy-like motions of one to many feet in diameter are commonly observed. Eddy diffusion takes place at the same rate for a gas as for a smoke while molecular diffusion depends upon the size of the molecule or particle. The rate of atmospheric diffusion is measured by the angle of rise and angle of spread of the smoke plume as it travels downwind from the source.

Photographs taken at right angles to the smoke plume, both horizontally and vertically, furnish a convenient method of measuring the angle of rise and angle of spread (see Figures 1 and 2). Such photographs show that the smoke plume usually has initial angles of rise and spread which differ from the angles farther away from the point of generation. It has already been indicated that the initial behavior is a transient effect of the heat and turbulence resulting from the process by which the smoke is generated. Its behavior as the smoke travels farther away from the generator depends upon the meteorological conditions prevailing, and these require detailed discussion.

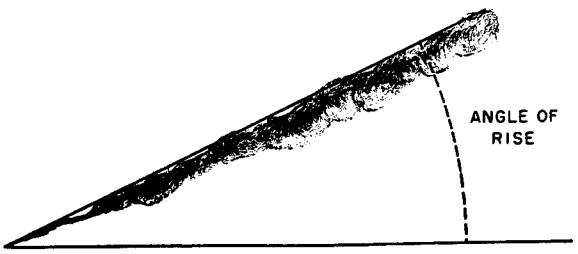

FIGURE 1. Angle of rise of smoke plume (from photograph).

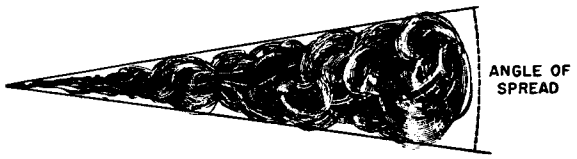

FIGURE 2. Angle of spread of smoke plume (from photograph).

26.1.2 Meteorological Factors

The principal meteorological factors affecting the travel of a smoke cloud are wind speed, direction, and turbulence, in the lower atmosphere.

If it is desired to cover an area with smoke from a limited number of stationary sources, a wind velocity of fixed speed and direction is desirable. Too high a wind speed will require an excessive rate of production of smoke to maintain any sort of coverage. On the other hand, too low a wind speed means that too long a time will be required to develop the screen in the first place.

If there is no wind, the smoke screen can only be

obtained by laying the smoke from a moving vehicle such as a plane or boat, or by projecting smoke munitions into the area. The latter method is usually only feasible in offensive operations.

Conditions of very low wind speed are likely to be accompanied by sudden variations in the wind, which may carry the smoke into areas in which it is not desired.

When smoke is emitted by a stationary generator in a steady wind, the smoke plume travels downwind with the speed of the wind, and the axis of the plume is parallel to the wind direction. The density of the smoke at any point downwind will be, in general, inversely proportional to the wind speed, but this statement is only approximately true because of other factors which must be taken into account.

When smoke is laid from a moving source, the above statements will still be true if one substitutes the relative wind speed and velocity for the true wind speed and velocity. By the relative wind speed and velocity, one means the wind speed and velocity as recorded by an anemometer that is mounted on the vehicle carrying the smoke generator. Thus, if a boat carrying a smoke generator moves due south with a speed of ten knots when the wind is blowing from due east at ten knots, the smoke plume will appear to an observer on the boat to lie exactly downwind, i.e., northwest, and to have a density corresponding to a speed of 14.14 knots. The above statement, however, is not so simple as it sounds, and it only holds for an observer on the boat. To a stationary observer, the smoke plume no longer lies with its axis parallel to the wind (see Figure 3).

If the wind speed and direction are recorded by sensitive instruments, very rapid and violent fluctuations of both quantities will often be observed. Thus, the exact direction of the wind can be established only as an average measurement over a considerable time, and the wind may momentarily veer by as much as 180°. Zero wind may be recorded momentarily. The wind vane records variations only in the horizontal component of wind velocity, but, if a vane is mounted to turn in a vertical plane, vertical components of velocity will be observed. These latter must, of course, approach zero as the measuring instrument approaches the ground surface.

The unsteadiness in wind velocity and direction can be considered, therefore, as being due to pulsations taking place in three directions, namely, in the general direction of the wind, and in horizontal and vertical directions at right angles thereto. The mean

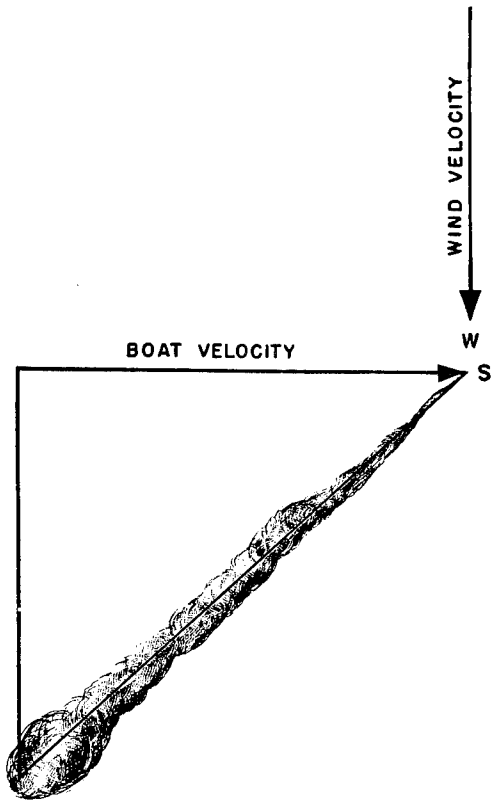

FIGURE 3. Curtain screen laid from a boat.

values of these pulsations in the different directions, measured over a period of time, would be expected to be equal if the motions of the lower air were isotropic, but the vertical direction is unique in this respect. If thermal instability exists, strong vertical gusts may be expected at considerable altitudes. At the ground level, however, the vertical component must fall to zero.

The sum total of the pulsations in the different directions measures the gustiness or turbulence of the atmosphere.

26.1.3 Causes of Turbulence

One obvious cause of turbulence is mechanical. The higher the wind velocity, the greater the turbulence, particularly over a rough terrain. Over a smooth surface of water there will be no turbulence produced by mechanical causes at low wind speeds. Wind speeds greater than 10 to 11 knots, however, will produce waves which in turn will produce mechanical turbulence in the lower air layers.

26.1.4 Thermal Stability

The most important factor in producing turbulence is thermal instability in the lower atmosphere. During the day, in bright sunshine, the ground surface receives a great deal of heat from the sun, and since the earth is a poor conductor, the temperature of the surface will rise many degrees. The layer of air in contact with the ground is heated in turn, and becoming lighter by expansion, it rises. Since the warm lower layer of air cannot rise everywhere uniformly, it must break through the upper cooler layers somewhat as bubbles burst upward through a liquid. The actual driving force is, of course, the weight of the cooler air, which settles toward the ground to be heated in turn. These upward convective currents cause the bumpiness of the air which is noticeable in an airplane, and, if there is sufficient humidity, cumulus cloud formation is likely to take place at moderate altitudes.

On clear nights the ground loses heat by radiation and cools the lower layer of air so that the density is greater near the ground, and a condition of extreme stability prevails. When the sky is overcast, heat is neither received nor lost by the earth, and a neutral condition prevails in which there is no tendency for upward convection

The foregoing statements do not hold for changing weather conditions. The passage of a warm or cold front may completely alter the temperature relation between ground surface and air and produce stability or instability regardless of time of day or sky conditions.

The situation over large bodies of water is also different. Water is a heat reservoir of great capacity, so that there is no significant variation in temperature between day and night. On the other hand, the air is usually not at the same temperature as the water, so that we may expect to find conditions of stability or instability prevailing continuously (throughout the twenty-four hours) for long periods. Changes in stability will usually take place only with changes in wind direction or in seasons. Thus, a wind blowing offshore from the New England coast will probably produce stable air conditions in summer and unstable air conditions in winter, over the ocean. Near the equator the ocean receives so much heat from the sun that a considerable degree of instability is likely to prevail.

26.1.5 Thermal Gradient

Although stability relations have their cause in differences in temperature between the earth's surface and the lower layers of the air, the actual stability conditions are determined by the temperature gradient in the air itself. If the temperature decrease with height is more than 1 C per 100 m, the air will be unstable, that is to say, the lower layer of air will tend to rise and to keep on rising as long as this condition prevails. This is caused by the rising mass of air which, even though it expands and cools as it rises, will be warmer and lighter than the surrounding air at any altitude. On the other hand, if the gradient is less than -1 C per 100 m, i.e., zero or positive, there will be no tendency for the air to rise, because a mass of air carried upward would be colder and heavier than the surrounding air.

It is, of course, not an easy matter to measure the temperature gradient, but it is usually much exaggerated near the ground, so that unless the gradient is near zero a temperature difference of a degree or more will be observed between two thermometers placed a few inches and a few feet, respectively, above the ground.

This critical gradient of -1 C per 100 m is termed by the meteorologist the *adiabatic lapse rate* for dry air, and the degree of stability or instability will depend upon the extent to which the temperature gradient departs in one direction or the other from the critical value. The extreme condition, when the temperature gradient is actually positive, is known as *inversion* and is characterized by extreme stability of the lower atmosphere. (See Figure 4.)

26.1.6 Stability Relations at Land-Water Boundaries

Since a diurnal cycle of stability exists on land and no such variation occurs over water, it might be anticipated that a sharp discontinuity in meteorological conditions might occur at land-water boundaries, which would greatly complicate the use of smoke in landing operations, for example. It turns out, however, that this is not the case, except for discontinuities due to such terrain as high cliffs or other sharp differences in elevation. There is a tendency for the air to be stable over beaches which are bordered by low-lying terrain. This comes about in the following

879245 O - 50 - 10

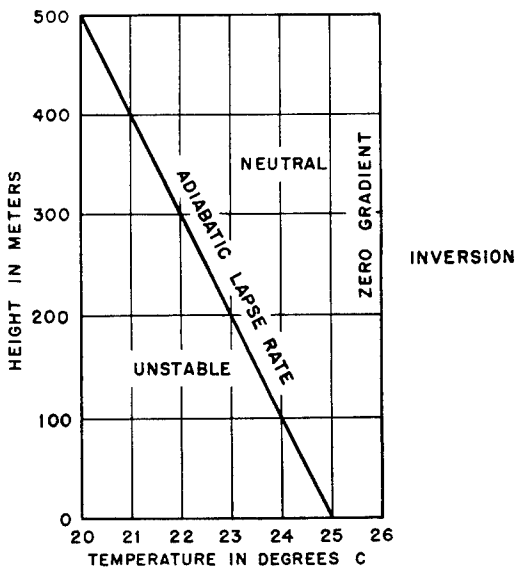

FIGURE 4. Thermal stability and instability. This gradient is 1¼ degrees centigrade per 100 meters.

way. The diurnal variation in stability relations often results in the so-called land and sea breezes. During the day, the air over the land becomes heated and the cooler, stable air from the sea flows in over the beach. This air mass must in turn become heated and unstable by contact with the ground surface, but the instability will not be set up until the air mass has penetrated some distance inland.

On the other hand, at night the land is cooled by radiation, and a cool air mass flows from inland out over the beach. This air mass may be cooler than the water and may, therefore, become unstable as it travels to sea, but the air in the vicinity of the beach will remain stable.

The foregoing generalizations are only statements of tendencies. There will be many departures from this regularity, and the whole situation may be illustrated by a discussion of the stability conditions prevailing over the east coast of Florida in summer. Very few fronts pass through the subtropical regions of the world in summer. This is particularly true in the neighborhood of large water areas where the disturbances due to land areas are at a minimum. Under these conditions the highs and lows are static, and the gradient wind which blows along the isobars maintains a steady velocity day after day. At sea, this wind prevails practically down to the sea surface, where it is known as a trade wind. Off the east coast of Florida a northeasterly wind blows throughout the summer. The warm Gulf Stream lies some distance off the coast, and the air mass becomes unstable over the Stream. This instability is evidenced by the cumulus clouds which can nearly always be seen from the shore.

The water mass between the Gulf Stream and the shore is cooler, so that the air mass may be cooled enough to become stable over this intervening water. When it passes across the beach over the land in the daytime, it will become unstable before it has traveled very far inland. On the other hand, the air at night becomes cooled over the land and flows out to sea as a land breeze. This land breeze is usually strong enough to oppose the gradient wind, but its effect does not extend very far out to sea, nor to a very high altitude. The gradient wind still blows a few hundred or a few thousand feet aloft. At some time during the forenoon, the gradient wind will overcome the land breeze and blow across the beach once more as a sea breeze. The exact time at which this happens depends upon the relative strengths of the two winds, and it cannot be forecast with exactness. Similarly, when the air temperature is near that of the water, the change from stability to instability over the water may take place with slight changes in wind velocity or other variables. The temperature of the water itself is likely to undergo sudden changes such as an offshore wind which may bring up cooler water from below near the beach.

26.2 BEHAVIOR OF SMOKE CLOUDS UNDER VARIOUS METEOROLOGICAL CONDITIONS

26.2.1 Stable Conditions

Under inversion conditions over a smooth terrain such as calm water, the only tendency shown by the smoke cloud to rise and spread is the initial transient effect due to the heat and turbulence produced by the smoke generator. The turbulence is quickly damped out but the heat produced may be sufficient to cause a very pronounced rise as is the case with white phosphorus smoke munitions. In the case of oil smoke where the heat produced is small, the temperature of the smoke at any dilution is only slightly greater than the temperature required to produce a buoyancy sufficient to offset the increase in density caused by the presence of the smoke material. As the smoke rises, the temperature falls because of two effects, namely, further dilution with cool air, and the adiabatic expansion due to the decrease in barometric pressure.

Since, in an inversion, the temperature of the surrounding air increases with increasing altitude, an elevation is soon reached at which the smoke is stable; having the same density as the surrounding air, it has no tendency either to rise or sink.

Oil vapor smoke is often observed to level off (Figure 5) at an elevation of approximately 100 ft under stable air conditions. Certain types of smoke will show an erratic behavior because of abnormal density.

FIGURE 5. Smoke leveling off under inversion conditions.

Since the heat produced in the generation of the smoke will usually cause the smoke cloud to rise, even under the most stable conditions, it may be anticipated that the cloud will lift entirely off the ground after a short distance of travel. If, however, a wind of considerable velocity is blowing, this lifting from the ground will not occur for reasons which will be explained later.

Although the heat produced in the smoke generator produces a rise, it has little effect upon the spread of the smoke cloud. Such spread as takes place is due to the initial turbulence, and this soon damps out. Consequently, if it is desired to produce continuous clouds of smoke from a series of individual generators, it is necessary to place the generators very close together, otherwise the individual plumes may not merge for a long way downwind. This situation holds for smooth terrain. If, however, the terrain is covered with shrubbery, for example, the lateral spread of the cloud is greatly increased as a result of the mechanical turbulence produced by the wind flowing through the shrubbery.

26.2.2 Behavior of Smoke Under Unstable Conditions

When the air current is turbulent because of thermal instability, atmospheric diffusion takes place to such an extent that the initial transient behavior of the cloud due to the heat and turbulence of the generator is of little significance. The smoke cloud continues to rise and spread as it travels downwind until the cloud becomes so thin that its boundaries are no longer distinguishable to the eye. If a time exposure were to be taken of the cloud it would appear as a cone with its apex at the generator and its axis rising at an angle from the horizontal, the angle of rise depending upon the degree of instability and the wind velocity. An instantaneous view of the cloud will show that it is furrowed and broken by variations in wind direction and sudden upward convective currents.

26.2.3 Convective Pattern

As has been stated previously, when the air is thermally unstable, upward convective currents occur. Over a rough terrain these currents are apt to be located at certain points. An upward current may be anchored at the windward brow of a hill, for example. Over a smooth terrain the convective currents are constantly shifting, and the distance between two upward currents depends upon various factors such as wind velocity and degree of instability. (Some idea of the convective pattern may be obtained by observing cumulus clouds.) Between these convective upbursts, the atmosphere is slowly settling over the whole area. Hence, the smoke cloud will appear to hug the ground until it encounters an upward current, when it will appear to change direction suddenly and rise at a considerable angle. The dimension of the convective patterns (distance between up currents) may be as much as ½ mile over a very smooth terrain. Since the convective pattern involves a complete circulation of the air, it might be supposed that, eventually, smoke which has been carried upward would be widely diffused and brought back down with the descending air. This must happen eventually, but whether or not it happens within a short distance from the point of generation depends upon the height of the convective ceiling.

26.2.4 Convective Ceiling

The lower air is thermally unstable when a negative temperature gradient greater than 1 c per 100 m of elevation exists at the ground level. This negative gradient may continue indefinitely upward. Thus, in thunderstorms, cumulus clouds often rise to a height of several miles, and a smoke cloud would be carried to the same height.

Under other circumstances, a current of warmer air may be blowing at an elevation of a few hundred feet, so that the temperature gradient may become zero or even positive, giving an inversion at this elevation. There is no tendency for the lower air to rise through this warmer lighter layer, and a definite ceiling will be established for the convective turbulence. Within this layer the atmosphere turns over and over, and the smoke may become diffused throughout the layer before it has traveled very far. It must be remembered, of course, that eddy diffusion always takes place at the boundaries of the upward convection currents, so that some smoke will become diffused throughout the settling layer of cooler air even with a high convective ceiling.

26.2.5 Angle of Rise

The rate of rise of the convective current increases with the thermal instability. The angle of rise of the smoke cloud (as a statistical average) is inversely proportional to the wind velocity. With zero wind, the convective currents rise directly upward. As the wind increases, the direction of the convective current must incline more and more away from the vertical.

BIBLIOGRAPHY

Abbreviations for Official Titles of Reports

DPGSR	Dugway Proving Ground Special Report
DPGMR	Dugway Proving Ground Memorandum Report
EATR	Edgewood Arsenal Technical Report
FM	Field Manual. War Department publication
FMTR–MIT	Foreign Material Technical Report from MIT laboratory
MIT–MR	Massachusetts Institute of Technology Memorandum Report
MSR	Monthly Summary Report Sections 10.1 and 10.5, NDRC
NDRC	Informal Reports from Division 10 or Section B-6. The latter have Roman serial numbers
OSRD	Formal reports from OSRD
SJPR	San José Project Report
TCIF	Technical Command Informal Report
TDMR	Technical Division Memorandum Report
TM	Technical Manual. War Department publication

Numbers such as Div. 10-200-M5 indicate that the document listed has been microfilmed and that its title appears in the microfilm index printed in a separate volume. For access to the index volume and to the microfilm, consult the Army or Navy agency listed on the reverse of the half-title page.

Chapter 1

1. "Rates of Water Vapor Adsorption from Air by Silica Gel," J. E. Ahlberg, *Ind. Eng. Chem.*, **31,** 1939, p. 988.
2. *The Effect of Tube Diameter and Type of Air Flow on Charcoal Breakdown Times,* J. R. Arthur, E. J. Brockless, and J. W. Linnett, Oxford University, Research Report No. 43.20, (Y. 9896).
3. "Concentration of Dilute Solutions of Electrolytes by Base-Exchange Materials," R. H. Beaton and C. C. Furnas, *Ind. Eng. Chem.*, **33,** 1941, p. 1500.
4. "Some Aspects of the Behavior of Charcoal with Respect to Chlorine," G. S. Bohart and E. Q. Adams, *J. Am. Chem. Soc.*, **42,** 1920, p. 523.
6. G. Damkohler, *Z. Elektrochem.*, **42,** 1936, p. 846; **43,**1937, p. 1.
7. *Some Aspects of the Physical Chemistry of the Respirator,* C. J. Danby, J. G. Davoud, D. H. Everett, C. N. Hinshelwood, and R. M. Lodge, Oxford University.
8. "The Theory of Chromatography," D. De Vault, *J. Am. Chem. Soc.*, **65,** 1943, p. 532.
10. *The Adsorption Wave,* T. B. Drew, F. M. Spooner, and J. Douglas, NDRC 10.5-48, Nov. 17, 1944. Div. 10-202.157-M8
12. "Cation-Exchange Water Softening Rates," J. du Domaine, R. L. Swain, and O. A. Hougen, *Ind. Eng. Chem.*, **35,** 1943, p. 546.
13. "Adsorption Studies of Vapors in Carbon Packed Towers," H. C. Engel and J. Coull, *Trans. Am. Inst. Chem. Eng.*, **38,** 1942, p. 947.
14. "Heat Transfer from a Gas Stream to a Bed of Broken Solids," C. C. Furnas, *Trans. Am. Inst. Chem. Eng.*, **24,** 1930, p. 1942.
15. "Heat, Mass and Momentum Transfer in the Flow of Gases Through Granular Solids," B. W. Gamson, G. Thodos, and O. A. Hougen, *Trans. Am. Inst. Chem. Engrs.*, **39,** 1943, p. 1.
16. "Fluid Flow Through Porous Carbon," M. R. Hatfield, *Ind. Eng. Chem.*, **31,** 1939, p. 1419.
17. *Drying of Gases,* O. A. Hougen and F. W. Dodge, OSRD 123.
18. "Solid Catalysts and Reaction Rates," O. A. Hougen and K. M. Watson, *Ind. Eng. Chem.*, **35,** 1943, p. 529.
19. "Principles of Reactor Design. Gas-Solid Interface Reactions," D. H. Hurt, *Ind. Eng. Chem.*, **35,** 1943, p. 522.
20. *The Nature of Air Flow Through Granular Charcoal Beds,* B. N. P. Hutchesson and K. D. Wadsworth, Porton Report No. 2607, Mar. 17, 1944.
22. *Factors in Canister Design and Tube Testing: Critical Bed Depth and the Nature of Gas Flow Through Charcoal,* I. M. Klotz, OSRD 3774, June 23, 1944. Div. 10-201.1-M26
26. *A Study of Charcoal Adsorption and Methods of Testing Charcoals for Use in Gas Mask Canisters,* R. Macy, EATR 52, Report completed July 1, 1930; issued May 10, 1942.
27. *Gas Mask Canister Design and Charcoal Testing,* D. MacRae, TDMR 942, Dec. 15, 1944.
28. "Layer Filtration, a Contribution to the Theory of Gas Masks," W. Mecklenburg, *Z. Elektrochemie,* **31,** 1925, p. 488; *Kolloid* **52,** 1930, p. 88.
29. *Considerations of the Adsorption Wave in Canister Design,* F. G. Pearce, MIT-MR 132, Apr. 2, 1945.
33. *Design Methods for Adsorbent Section of Canisters,* O. A. Short and F. G. Pearce, MIT-MR 114, Nov. 25, 1944.
34. *A Study of Humidification and Dehumidification of Charcoal in Collective Protector Canisters,* O. A. Short, F. G. Pearce, and K. R. Nickolls, MIT-MR 97, Aug. 25, 1944.
35. "Heterogeneous Ion Exchange in a Flowing System," H. C. Thomas, *J. Am. Chem. Soc.*, **66,** 1944, p. 1664.
36. *A Critical Examination of the Correlation of Tube and Container Gas Test Results,* K. D. Wadsworth, Ptn. 2001 (U. 138), 1943, (Y. 23256).
37. "Studies on Adsorption and Desorption in Beds of Granular Adsorbents," E. Wicke, *Kolloid Zeitschrift,* **93,** 1940, p. 129. Translated by M. Dole NDRC XLVI, 1941; also translated by C. A. MacConkey, National Research Council of Canada, Ottawa, 1942.

Chapter 2

1. "Recording Nocturnal Radiation," A. Angstrom, *Medell. Stat. Meteor. Hydrogr. Anst. Stockholm*, **6**, No. 8, 1936.
2. "Transfer of Heat and Momentum in the Lowest Layers of the Atmosphere," A. C. Best, *Geophysical Memoirs*, **7**, No. 65, 1935.
3. "Notes on Radiation in the Atmosphere," D. Brunt, *Quart. J. Roy. Met. Soc.*, **58**, 1932, p. 389.
4. *Physical and Dynamical Meteorology*, D. Brunt, MacMillan Co., London, 1939.
5. "Professional Note No. 6," E. H. Chapman, M. O. 232, 1919.
6. *Special Report to General Kabrich for Revision of TM 3-240*, R. G. Dickinson, T. S. Gilman, and H. S. Johnston, October 1944.
7. "The Climate of the Layer of Air Near the Ground," R. Geiger, *Die Wissenschaft*, **78**, Braunschweig, 1927.
8. *Physics of the Air*, W. J. Humphreys, McGraw-Hill Book Co., 1940.
9. Jelinek, *Beit. z. Phys. der f. Atm.*, **24**, 1937, p. 3.
10. *Micrometeorology of Woods and Open Areas Within the Withlacoochee Land Use Project, Florida*, H. Johnston assisted by A. Pardee, A. Englander, and W. Ironside, DPGSR 35, Sept. 11, 1944.
12. *Weather Analysis and Forecasting*, S. Petterssen, McGraw-Hill Book Co., 1940, p. 99.
13. "Strahlungsstudien," M. Robitzsch, *Arb. Obs. Lindenberg*, **15**, 1926, p. 194.
14. *Phys. Ocean. and Met.*, C. G. Rossby, MIT, 1935.
15. "Das Massenaustausch bei der ungeordneten Stromung in freier Luft und seine Folgen," Wilh. Schmidt, *Wiener Ber.*, **126**, 1917, p. 757.
16. "Temperatures of the Soil and Air in a Desert," J. G. Sinclair, *M. W. Rev.*, 1922, S. 142.
17. O. G. Sutton, *Proc. Roy. Soc.*, **146**, 1934, p. 701.
18. "Theory of Diffusion," G. I. Taylor, *Proc. Math. Soc.*, **20**, 1929, p. 196.
20. *Evaluation of Meteorological Data of the Lowest Atmosphere, Salt Lake City, Utah*, Mrs. R. Wexler.
21. *Meteorology of Ground Layer*, R. Wexler, Special Report, Dugway Proving Grounds, November 1943.
22. *Résumé of Recent Knowledge on the Technical Aspects of Chemical Warfare in the Field*, Project Coordination Staff, Edgewood Arsenal, Report No. 9, May 17, 1945.
23. SJPR 22, October 1944.

Chapter 3

1. "Transfer of Heat and Momentum in the Lowest Layer of the Atmosphere," A. C. Best, *Geophysical Memoirs*, No. 65, 1935.
5. *Dugway Recording Instruments*, S. W. Grinnell, Special Dugway Report.
6. *Micrometeorology of Woods and Open Areas Within the Withlacoochee Land Use Project, Florida*, H. Johnston assisted by A. Pardee, A. Englander, and W. Ironside, DPGSR 35, Sept. 11, 1944.
8. *Investigation of the Micrometeorology of a Medium Dense, High Canopy Jungle on a Small Tropical Island*, W. W. Stone, R. G. Dickinson, D. L. Kraus, T. S. Gilman, and R. D. Mills, SJPR 22, Oct. 9, 1944.
14. *Meteorological Instruments* (second edition), W. E. K. Middleton, University of Toronto Press, 1943.

Chapter 4

1. *Colloid Chemistry*, A. W. Thomas, McGraw-Hill Book Co., 1934, p. 15.

Chapter 5

1. *Filter Penetration by Aerosols of Very Small Particle Size*, W. H. Rodebush et al, OSRD 2050, Nov. 24, 1943. Div. 10-201.22-M13
2. *Smoke*, Whytlaw-Gray and Patterson, Edward Arnold & Co., London, 1932, p. 184.
3. *The Preparation of Solid Materials for Dispersion as Aerosols*, F. C. McGrew, OSRD 3902, July 17, 1944. Div. 10-504.3-M2
4. "The Removal of Mist by Centrifugal Methods," C. F. Goodeve, *Trans. Faraday Society*, 1936, p. 1218.
5. *Clouds and Smokes*, Wm. E. Gibbs, J. and A. Churchill, 1924, p. 43. *See also* Ref. 1, p. 96.
6. *Hydrodynamics*, H. Lamb, Fifth Edition, p. 567.
7. Reference 1, p. 72.
8. *Micromeritics*, J. M. Dalla Valle, Pitman, New York, 1943.
9. Hatch and Choate, *J. Franklin Institute*, **207**, 1929, p. 371.
10. T. Hatch, *J. Franklin Institute*, **215**, 1933, p. 27.
11. *The Kinetic Theory of Gases*, L. B. Loeb, McGraw-Hill, 1934, p. 402. *See also* Reference 5, p. 48.
12. *Ibid.*, p. 394.
13. See Reference 2, p. 57.
14. Unpublished Report, D. E. Goldman.
15. See Reference 2, p. 67.
16. *Applied Math. Panel, Memo 100.1 M*, NDRC, 1944.
17. "The Motion of a Sphere in a Viscous Fluid," H. S. Allen, *Phil-Mag. (5)*, **50**, 1900, p. 323.
18. *E. A. Progress Report to Col. Fleming*, H. A. Abramson, July 7, 1942.
20. Paranjpe, *Proc. Ind. Acad. Sci.*, **4a**, 1936, p. 423.
23. "The Coagulation of Smoke by Supersonic Vibrations," E. N. deC. Andrade, *Trans. Faraday Soc.*, **42**, 1936, p. 1111.
24. "Experiments on Coagulation by Supersonic Vibrations," R. C. Parker, *Trans. Faraday Soc.*, **42**, 1936, p. 1115.

25. "The Aggregation of Suspended Particles in Gases by Sonic and Supersonic Waves," O. Brandt and E. Hiedemann, *Trans. Faraday Soc.*, **42,** 1936, p. 1101.
26. *Sonic Flocculator as a Fume Settler: Theory and Practice,* H. W. St. Clair, U.S. Bureau of Mines, R. I. 3400, 1936, p. 51.
27. "Hydrodynamisch-Akustische Untersuchung," Walter Koenig, *Ann. Physik,* **42,** 1891, pp. 353 and 549.
28. *Fog Types, etc.,* Meteorological Office, Air Ministry, S. D. T. M. 45.
29. *Electricity and Magnetism,* J. H. Jeans.
30. Georg Thomas, *Ann. d. Physik,* **42,** 1913, p. 1079.
31. "On the Circulations Caused by the Vibration of Air in a Tube," E. N. deC. Andrade, *Proc. Roy. Soc.*, **134,** 1931, p. 445; also "On the Groupings and General Behavior of Solid Particles Under Influences of Air Vibrations in Tubes," *Phil. Trans. Roy. Soc.*, **A230,** 1932, p. 413.
32. J. Robinson, *Proc. Lond. Phys. Soc.*, **25,** 1913, p. 256.
33. "The Action of Sound Waves Upon Droplets of Fog," S. V. Gorbatchev, *Russian Journal Physical Chemistry,* **7,** 1936, p. 536.
34. a. *Dissipation of Water Fog by Intense Sound of Audible Frequency,* V. K. LaMer and D. Sinclair, OSRD 1667, Aug. 17, 1943. Div. 10-503.2-M1
b. *Report of Tests of Sonic Dissipation of Fog in California,* V. K. LaMer, NDRC 10.2-13, Apr. 13, 1944. Div. 10-503.2-M3
35. E. F. Burton et al, Toronto Report, C. E. 42, November 1942, also Reference 6, Chap. 21.

Chapter 6

1. *Portable Optical Instrument for the Measurement of the Particle Size in Smokes, the "Owl", an Improved Homogeneous Aerosol Generator,* V. K. LaMer and D. Sinclair, OSRD 1668, Aug. 3, 1943. Div. 10-501.11-M6
3. *The Optical Characterization of Any Aerosol in the Laboratory or Field. The Production of Aerosols from Powdered Solid Materials,* V. K. LaMer, J. Q. Umberger, D. Sinclair, F. E. Buchwalter, OSRD 4904, Oct. 31, 1944. Div. 10-601.2-M1

Chapter 7

1. G. Mie, *Ann. der Phys.*, **25,** 1908, p. 377.
2. Hans Blumer, *Zeits. f. Phys.*, **32,** 1925, p. 119; **38,** 1926, pp. 304, 920; **39,** 1926, p. 195.
Engelhard and Friess, *Koll. Zeits,* **81,** 1937, p. 129.
R. Ruedy, *Canadian Journal of Research,* **19A,** 1941, p. 117.
3. *Electromagnetic Theory,* J. A. Stratton, McGraw-Hill Book Co., Stratton and Houghton, *Physical Review,* **38,** 1931, p. 159.
4. *Verification of the Mie Theory,* V. K. LaMer, D. Sinclair, et al, OSRD 1857, Sept. 29, 1943. Div. 10-501.1-M2
5. *Scientific Papers,* Lord Rayleigh, Cambridge University Press, 1899, Vol. I, pp. 92–93.
Lord Rayleigh, *Loc. Cit.*, **4,** 1903, p. 400, eq. 13.
6. *Measurement of Particle Size in Smokes, the Owl,* V. K. LaMer and D. Sinclair, OSRD 1668, Aug. 24, 1943. Div. 10-501.11-M6
8. W. S. Stiles, *Phil. Mag.*, **7,** 1929, p. 204.
9. G. Wolfson, *Handbuch der Physik,* **XX,** 314.
11. L. Brillouin, NDRC Applied Math. Panel Report, Nos. 87.1 and 87.2.
15. W. Lotmar, *Helv. Chim. Acta.*, **21,** 1938, p. 792.
16. R. S. Krishnan, *Proc. Ind. Acad. Sci.*, **7A,** 1938, p. 21.
17. Private communication from E. I. DuPont de Nemours Experimental Station, E. D. Bailey.
18. *Testing of Daytime Distress Signals,* V. K. LaMer et al, OSRD 4539, Jan. 5, 1945. Div. 10-501.23-M3
19. *Total Scattering Function for Complex Indices of Refraction,* A. N. Lowan et al, Math. Tables Project, National Bureau of Standards.

Chapter 8

1. K. R. May, Porton Report No. 2463; see also Monthly Progress Reports NDRC Munitions Development Laboratory, 1944–45.
2. V. J. Schaefer, private communication.
3. *Dissipation of Water Fog by Intense Sound of Audible Frequency,* V. K. LaMer et al, OSRD 1667, Aug. 17, 1943. Div. 10-503.2-M1
4. *Smoke,* Whytlaw-Gray and Patterson, Edward Arnold and Co., London, 1932.
5. K. E. Stumpf, *Koll. Zeits,* **86,** 1939, p. 339.
7. *Preparation of Solid Materials for Dispersion as Aerosols,* F. C. McGrew, OSRD 3902, July 17, 1944. Div. 10-504.3-M2
8. *Chemical Engineers Handbook,* J. H. Perry, McGraw-Hill Book Co., 1934, p. 709.
9. E. L. Anderson, *Journal Industrial Hygiene,* **21,** 1939, p. 39.
10. H. H. Watson, *Trans. Faraday Soc.*, **32,** 1936, p. 1073.
11. Porton Report No. 2521.
12. W. H. Rodebush et al, OSRD 865, Sept. 4, 1942. Div. 10-201.22-M5
16. *Optical Characterization of Any Aerosol,* V. K. LaMer et al, OSRD 4904, Oct. 31, 1945. Div. 10-601.2-M1
17. *Measurement of Particle Size in Smoke, the Owl,* V. K. LaMer and D. Sinclair, OSRD 1668, Aug. 24, 1943. Div. 10-501.11-M6
18. *Physics of the Air,* W. J. Humphreys, McGraw-Hill Book Co., 1940, p. 551.
19. Hilding Kohler, *Trans. Faraday Soc.*, **32,** 1936, p. 1153.
20. Wilson, *Cambridge Philos. Soc.*, **32,** 1936, p. 493.

Chapter 9

2. *Filtration of Aerosols and the Development of Filter Materials*, W. H. Rodebush, I. Langmuir, and V. K. LaMer, OSRD 865, Sept. 4, 1942. Div. 10-201.22-M5
3. *Smokes and Filters. Supplement to Section I.*, I. Langmuir and K. Blodgett, OSRD 3460, Apr. 12, 1944. Div. 10-201.22-M14
4. *Filter Penetration of Aerosols of Very Small Particle Size*, W. H. Rodebush, C. E. Holley, Jr., and B. A. Lloyd, OSRD 2050, Nov. 24, 1943. Div. 10-201.22-M13
5. *Final Report on Filtration Efficiency and Particle Size. III-I-2000*, C. E. 42, University of Toronto, November 1944.

Chapter 10

1. *Test Methods Conference, CWS Development Laboratory, MIT. Group VI-Filter Tests*, Sept. 2, 1942, pp. 1–2 and 45–63 deal with general recommendations on smoke testing.
2. Reference 1, pp. 8 and 50–51.
4. *Development of the DOP Smoke Penetration Test for Filter Materials*, J. H. Dinius and A. W. Plummer, MIT-MR-52, Jan. 8, 1944.
5. *Development of Smoke Penetration Meters*, H. W. Knudson and L. White, Naval Research Laboratory Report No. P-2642, Sept. 14, 1945.
6. Reference 1, pp. 12–16 and 41–43.
7. *Canister and Charcoal Test Methods*, CWS Pamphlet No. 2, Part 1, Section C, DM, Apr. 3, 1943.
8. *Gas Mask Filters and Filter Materials, DM Tests January 1934 to September 1941*, P. A. Hartman and E. K. Long, EATR 362, Feb. 24, 1942.
9. Reference 6, Section D, DA.
10. Reference 12, pp. 17–18 and 43–45.
11. *Canister Test Methods Section H — Methylene Blue*, CWS Pamphlet No. 2, Part 1, Jan. 4, 1943.
12. *Methylene Blue Penetration Tester MIT-E2*, A. W. Plummer, MIT-MR-5, May 6, 1942.
13. *Evaluation of the Methylene Blue Penetration Tester MIT-E2*, H. J. Allison, Jr., and E. K. Long, TDMR 440, Sept. 23, 1942.
14. *Report on Aerosols*, W. H. Rodebush, OSRD 14, Sept. 12, 1941.
15. *Design of Apparatus, MIT-E1R1, for Filter Testing Using Radioactive Triphenyl Phosphate Smoke*, B. Vonnegut, MIT-MR-6, July 18, 1942.
16. Reference 1, pp. 40–41.
17. Reference 1, pp. 26–39.
18. *Optical Smoke Penetration Meter*, B. Vonnegut, MIT-MR-2, Mar. 16, 1942.
19. *Optical Smoke Penetration Meter, E1R1*, D. W. Beaumont, MIT-MR-27, Mar. 6, 1943.
20. *Ionization Penetrometer*, A. R. Hogg and A. J. Roennfeldt, C. D. Note No. 14 from Munitions Supply Laboratories, Maribyrong, Australia, Nov. 18, 1943.
21. "A Photoelectric Smoke Penetrometer," A. S. G. Hill, *J. Sci. Inst.*, **14**, 1937, p. 296.
22. Reference 1, pp. 8–11.
23. *Carbon Smoke Penetration*, L. Yaffe, R. L. McIntosh and W. Boyd Campbell, McGill University and the Pulp and Paper Research Institute of Canada, Progress Reports Nos. 1–4, Montreal, 1942.
25. *Filtration of Aerosols and the Development of Filter Materials*, OSRD 865, Sept. 4, 1942. This report contains *The Balanced Photoelectric Smoke Penetrometer* by S. Hochberg. Div. 10-201.22-M5
26. *A Sensitive Photoelectric Smoke Penetrometer*, F. T. Gucker, Jr., H. B. Pickard, and C. T. O'Konski, OSRD 5499, Aug. 28, 1945. Div. 10-201.22-M16
27. *Photoelectric Smoke Penetration Meter MIT-E2*, W. B. Nottingham, D. W. Beaumont, and J. H. Dinius, MIT-MR-203, Oct. 11, 1945.
29. *Development of Stable Thallous Sulfide Photoconductive Cells for Detection of Near Infrared Radiation*, R. J. Cashman, OSRD 5997, Oct. 31, 1945.
30. *Smoke Penetration Meter E3, Engineering Tests*, H. Scherr, EATR 237, Feb. 7, 1938.
31. *Smoke Penetration Meter E3, Final Report on Project D 1.3-1a1*, L. Finkelstein and H. Scherr, EATR 331, Aug. 28, 1940.
32. *Operation of Smoke Penetration Meter E3 for Production Testing of MIXA1 Canister Filters*, CWS Directive No. 40A, June 6, 1942.
33. *Canister Test Methods, Section K — Smoke Penetration*, CWS Pamphlet No. 2, Part I.
34. *Smoke Penetration Tests of Canadian and U. S. Army Canisters*, P. A. Hartmann and E. K. Long, TDMR 332, Nov. 10, 1941.
35. *Effect of Oil Smokes from Esso Jr. and Oil-O-Matic Screening Smoke Generators on Filters as Determined by Field Tests*, MIT-MR-14, Sept. 28, 1942.
36. *The Effect of Oil Smokes and Amyl Stearate Smokes on Filters*, P. A. Hartmann and J. E. Kaufman, TDMR 364, Apr. 28, 1942.
37. *Tests of British Light-Type Respirator Canisters*, J. H. Dinius, TDMR 556, Jan. 31, 1943.
38. *A Note on the Effect of Oil Screening Smokes on Resin-Impregnated Filters and the Stability of These Filters Under Tropical Conditions*, Chemical Defence Experimental Station, Porton, England, May 12, 1943.
39. Reference 1, p. 17.
40. *Development of MIT-E1 Canister Tester*, W. B. Nottingham, F. F. Diwoky, and D. W. Beaumont, MIT-MR-32, May 8, 1943.
41. *Canister and Charcoal Test Methods, Part I, Section M, Installation Operation, and Maintenance of Meter, Smoke Penetration, MIT-E1R1*, CWS Pamphlet No. 2, Jan. 17, 1944.
42. Reference 1, pp. 31–32.
43. Reference 1, pp. 11–12 and 39–40.
44. Porton Report No. 2161; Porton Specification 1206.
45. *Evaluation of the British Sodium Flame Apparatus as a*

Filter Tester, C. A. Rinehart and J. H. Dinius, TDMR 578, Feb. 26, 1943.

46. *Performance of Sodium Flame Penetrometer*, M. W. Lister, Chemical Warfare Laboratories, Ottawa, Canada, Sept. 26, 1944.
47. *Standard Methods of Test (Chemical and Physical) Employed in C. W. Investigations. I(3) Tests on Particulate Filters*, Porton Memorandum No. 17, Mar. 7, 1942.
48. *Aerosols, A Survey and Bibliography of Recent Literature*, D. F. Jurgensen, MIT-MR-8, July 17, 1942.

Chapter 11

1. *Screening Smokes*, T. K. Sherwood, OSRD 436, Mar. 15, 1942. Div. 10-502-M2
2. *Production of Smokes of Controlled Size by the Use of Induction Nozzles*, H. C. Hottel, OSRD 468, Jan. 12, 1942. Div. 10-501.2-M1
5. *The Pancake Effect in Gas Clouds*, W. M. Latimer, OSRD 1176, Feb. 3, 1943. Div. 10-401.123-M1
6. *Practical Considerations Involved in the Use of Screening Smokes*, W. H. Rodebush, OSRD 1321, Apr. 9, 1943. Div. 10-502-M7
7. *Use of a Sulfur Boiler for Smoke Generation*, W. K. Lewis, OSRD 1692, Aug. 9, 1943. Div. 10-501.2-M3
8. *Study of Oil Smoke Plumes by Motion Pictures*, H. F. Johnstone, OSRD 1697, Aug. 6, 1943. Div. 10-502-M8
9. *Smoke Experiments Carried Out at Camp Sibert, Alabama*, T. S. Gilman and P. Hayward, OSRD 1712, Aug. 14, 1943. Div. 10-302.1-M11
13. *Statistical Considerations in the Use of DDT Aerosols*, W. H. Rodebush, OSRD 4757, Mar. 5, 1945. Div. 10-602.21-M2

For sale by the Superintendent of Documents, U. S. Government Printing Office
Washington 25, D. C - Price 60 cents

U. S. GOVERNMENT PRINTING OFFICE : O—1950